THE UNIVERSITY
of EDINBURGH

CELL-LINEAGE-SPECIFIC CHROMOSOMAL INSTABILITY IN CONDENSIN II MUTANT MICE

Jessica Woodward

The University of Edinburgh

Thesis presented for the degree of Doctor of Philosophy

2015

Dedicated to my lovely Grandparents,
Mervyn and Heather Ladbrooke

"I don't know half of you half as well as I should like and I like less than half of you half as well as you deserve."

- *J.R.R Tolkien*

DECLARATION

This dissertation is the result of my own work unless otherwise stated. It has not been previously submitted, in part or whole, to any university of institution for any degree, diploma, or other qualification.

Signed:_____

Date:_____

Jessica Woodward

September 2015

ACKNOWLEDGEMENTS

Firstly, I'd like to thank my supervisors Wendy Bickmore and Andrew Wood, who took on a physicist and somehow managed to produce someone who can do some biology. It was tough, but I couldn't have done it without you, and I am very grateful for the belief you showed in me, especially when I didn't have any in myself.

I'd also like to thank the Bickmore and Wood lab members past and present, including (but not limited to) Liz, Rob, Pierre, Chief Iain, Sehrish, Nezha, Pradeep, Keerthi, Martijn and Irene. Thank you Michael for the experimental bakes you brought to lab meeting and for helping me with coding problems, even when you should have been writing your own thesis. I'd especially like to thank Lady Shelagh and Gillian for all that you've done to help me become a scientist, but mostly for indulging my Lord of the Rings / Harry Potter / Game of Thrones obsessions. Shelagh, I'm sorry for all the drivel you've had to put up with (but secretly I think you'll miss it when it's gone - Gillian will have to keep you up to date on the goings on in the Potter universe).

Thanks to all the students in my year who went through all of this with me, as well as the ones in the years above (the Chromatin Crew) and below me, who have all this to look forward to - Fiona, Ailsa, Katy, Liv, Adam, Christine, Matt, Chris... there's a lot of you - sorry if I missed anyone out. Thank you Hazel and Emma for everything, especially dog-sitting my blond furry baby. Also, thank you to my non-science friends, who pretended to be interested in condensin and section meetings, but who also helped me to remember that failed FACS experiments are not the end of the world.

Finally, thank you to my extremely supportive family. Thank you Nana for teaching me my times tables - you were right, they have been useful. And thank you Pippin, you made my life much, much better.

ABSTRACT

In order to equally segregate their genetic material into daughter cells during mitosis, it is essential that chromosomes undergo major restructuring to facilitate compaction. However, the process of transforming diffuse, entangled interphase chromatin into discrete, highly organised chromosomal structures is extremely complex, and currently not completely understood.

The complexes involved in chromatin compaction and sister chromatid decatenation in preparation for mitosis include condensins I and II. Mutations in condensin subunits have been identified in human tumours, reflecting the importance of accurate cell division in the prevention of aneuploidy and tumour formation. Most mutations described in TCGA (The Cancer Genome Atlas) and COSMIC (Catalogue of Somatic Mutations in Cancer) are missense, and therefore likely to only partially affect condensin function. Most functional genetic studies of condensin, however, have used loss of function systems, which typically cause severe chromosome segregation defects and cell death.

Mice carrying global hypomorphic mutations within the kleisin subunit of the condensin II complex develop T cell lymphomas. The *Caph2*$^{nes/nes}$ mouse model is therefore a good system for understanding how condensin dysfunction can influence tumourigenesis. However, little is known about which cellular processes are affected in mutant cells before transformation. I therefore set out to use the *Caph2*$^{nes/nes}$ mouse model to study the consequences of the condensin II deficiency on cell cycle regulation in several different hematopoietic lineages. The *Caph2*$^{nes/nes}$ mice are viable and fertile, with no obvious abnormalities other than the thymus, which is drastically reduced in size. Previous studies reported greater than a hundred-fold reduction in the number of $CD4^+$ $CD8^+$ thymocytes. I set out to understand why the alteration of a ubiquitously expressed protein which functions in a fundamental cellular process would result in such a cell-type specific block in development. To achieve this, I investigated the possibility that condensin II is involved in interphase processes as well as in mitosis. In addition, I studied the aspects of T cell development that may make this lineage particularly vulnerable to condensin II deficiency. Finally, I carried out a preliminary

investigation into the biochemical properties of the condensin complexes.

During my PhD., I found strong evidence to suggest that the *Caph2*$^{nes/nes}$ T cell-specific phenotype arises due to abnormal cell division. However, I was unable to find any evidence to support the hypothesis that the phenotype is a consequence of abnormal interphase processes. Upon systematic analysis of several stages of hematopoietic differentiation, I found that at a specific stage of T cell development, the mutation results in an increased proportion of cells with abnormal ploidy, followed by a drastic reduction in cell numbers. Erythroid cells revealed a similar increase in the frequency of hyperdiploid cells, but no reduction in cell numbers. B cells and hematopoietic precursors did not reveal an increase in hyperdiploidy, or a reduction in cell numbers in wildtype relative to mutant. Subsequently, I found preliminary evidence to suggest that the T cell-specificity may be due to more rapid progression of CD4+ CD8+ T cells from S phase to M phase, relative to other hematopoietic stages. Finally, a preliminary investigation into the biochemical properties of the condensin complex revealed apparent imbalances in the expression of condensin subunits in T, B and erythroid cells. The sedimentation profile of CAP-H2 from whole-thymus extract did not exclude the possibility that condensin subunits might be forming heavier-weight complexes with non-SMC proteins. Further work must be carried out to determine whether this sedimentation pattern is unique to T cells.

LAY ABSTRACT

Each cell in our bodies has been estimated to contain approximately 2 metres of DNA, which must be compacted into nuclei that can be less than 10 microns in diameter. Before cell division, DNA is compacted still further. This compaction is facilitated by several proteins, including two complexes called condensin I and condensin II. The compaction of chromatin must be carried out correctly before cell division takes place. Mistakes in this process result in abnormal cell division, which can lead to tumour formation. Despite its importance, currently our understanding of the process of chromosome condensation and remodelling is limited. I therefore set out to better understand the role of the condensin complexes in the physical restructuring of DNA using a mouse model which carries a mutation in one of the condensin complexes.

ABBREVIATIONS

2D	Two dimensional
APC	Anaphase Promoting Complex
bp	Base pairs
BSA	Bovine serum Albumin
CTCF	CCCTC-binding factor
DAPI	4,6-diamino-phenylindole
dH2O	Distilled water
DMEM	Dubleco's Modified Eagle's Serum
DMSO	Dimethyl sulpoxide
DNA	Deoxyribonucleic acid
dNTP	Deoxyribonucleotides
ES	Embryonic stem (cells)
FCS	Fetal Calf Serum
FISH	Fluoresence *In Situ* Hybridisation
FITC	Fluorescein isothiocyanate
g	Gram
GTE	Glucose Tris EDTA
HCl	Hydrochloric acid
int.	intermediate
kb	Kilobase
M	Molar
Mb	Megabase
MEF	Mouse Embryonic Fibroblast
mg	Milligram
ml	Millilitre

mM	Millimolar
mRNA	Messenger RNA
NaCl	Sodium chloride
NaOH	Sodium hydroxide
ng	Nanogram
nM	Nanomolar
ORF	Open reading frame
PBS	Phosphate Buffered Saline
PCC	Premature chromosome condensation
PCR	Polymerase Chain Reaction
qPCR	Quantitative PCR
RNA	Ribonucleic acid
RT	Room Temperature
SDS	Sodium Dodecyl Sulphate
SSC	Saline sodium citrate
TAD	Topologically Associated Domain
TAE	Tris acetate buffer
TE	Tris EDTA
TR	Texas Red
TSS	Transcription Start Site
uORF	Upstream ORF
µg	Microgram
µl	Microlitre
µM	Micromolar

TABLE OF CONTENTS

LIST OF FIGURES AND TABLES

Chapter 1: Introduction

Chapter 2: Materials and Methods

Chapter 3: Abnormalities in chromosome Structure in *Caph2* mutant cells

Chapter 4: Cell cycle regulation during haematopoiesis in wildtype and chromosomally unstable (CIN) *Caph2* mutant mice

Tables

CHAPTER 1: INTRODUCTION

1.1 Genome organization and chromosome structure

Each diploid cell in our bodies has been estimated to contain approximately 2 metres of DNA, which must be compacted into nuclei that can be less than 10 microns in diameter. This is achieved through the action of DNA binding proteins that associate with DNA to form chromatin, thereby compacting the genome down to a manageable size while maintaining functionality. This compaction acts to protect the DNA from damage, while also playing a role in transcription and DNA replication. Genomic regions located within more compact chromatin (heterochromatin) tend to be less transcriptionally active than those located on more open chromatin (euchromatin).

The organisation of interphase chromatin shows both commonalities and differences between cell types. During interphase, chromosomes occupy distinct areas within the nucleus: certain areas are preferentially occupied by certain chromosomes. These are known as "chromosome territories". In almost all cells, transcriptionally repressed chromatin is enriched at the nuclear periphery in association with the nuclear lamina (Peric-Hupkes *et al*., 2010). At the molecular level, interphase chromosomes are compartmentalized into discrete domains; loci within the same domain interact more frequently than loci that are located in neighbouring domains (Dixon *et al*., 2012; Lieberman-aiden *et al*., 2010). Within such topologically associated domains (TADs), the linear DNA is thought to be folded to facilitate interactions between gene promoters and distal regulatory elements such as enhancers, which can be separated by many hundreds of kilobases (Lettice, 2003). Conversely, interactions are less frequent between promoters and enhancers that lie on opposite sides of domain boundaries.

1.1.1 The histones

The basic unit of chromatin is the nucleosome, which comprises two copies each of the core histones: H2A, H2B, H3 and H4, around which approximately 147 base pairs of DNA are wrapped. When nucleosomes are subjected to increasing salt concentrations, the DNA dissociates from the histones, indicating that the interactions between core histones and DNA are primarily electrostatic in nature (Andrews & Luger, 2011). Studies that made use of high-salt concentrations and chemical cross-linking revealed that in the absence of DNA, histones H2A and H2B form a stable dimer, while H3 and H4 form a tetramer (Kornberg, 1974).

Histone-histone and histone-DNA interactions occur at the C-terminus of the histone, comprising three alpha-helices. Each histone molecule also has a basic tail region which is exposed to the periphery of the nucleosome, and is targeted by a wide variety of post-translational modifications that can alter nucleosomal biochemistry and affect the functional state of the associated DNA. In addition, acetylation in the globular domain of histones is also very important (Cerbo *et al*., 2014; Tropberger *et al*., 2013). Acetylation of histones H3 and H4 results in decondensed chromatin, while other modifications, such as methylation and ubiquitination, can result in either compaction or decompaction of the chromatin, depending on which residue is modified. Whilst acetylation can alter nucleosome structure directly through alteration of charge, effects of other modifications are indirect: i.e. they rely on the activities of other proteins that "read" the histone modification, such as polycomb or HP1. The amino-acid sequences of both the C-terminal and charged N-terminal are highly conserved, reflecting their crucial roles in higher-order chromatin structure. Histone variants, e.g. H3.3 and the acidic patch on H2A versus H2A.Z (Bönisch & Hake, 2012), are also very important for structure. The histone variant H2A.Z causes chromosome to become more open, and is associated with active transcription (Fan, Gordon, Luger, Hansen, & Tremethick, 2002; Xu *et al*., 2012), whereas chromatin condensation is facilitated by the binding of H4K16 histone tail to the acidic patch on H2A (discussed in Section 1.1.2.4).

Chromatin is further compacted by the linker H1, which binds to the nucleosome and to the linker DNA (Zhou *et al*., 2015) to generate higher order structures. Traditionally,

these structures were thought to comprise a 30nM fibre (Gilbert & Allan, 2001; Greulich, Wachtel, Ausio, Seger, & Eisenberg, 1987), although recent evidence using methods such as electron spectroscopic imaging and tomography, has called into question whether such a structure is prevalent *in vivo* (Fussner *et al.*, 2012; Nishino *et al.*, 2012).

During mitosis, chromosomes undergo dramatic changes in morphology involving further condensation into discrete rod shaped structures. This process serves at least two purposes: to remove entanglements between sister chromatids and to provide the rigidity necessary to withstand forces exerted by the spindle. Mitotic chromosome structure is discussed in more detail in Section 1.1.3.

1.1.2 Chromosome dynamics during the cell cycle

The cell cycle is comprised of events that take place within the cell, including the duplication of DNA, as well as cell division into two daughter cells. The accurate segregation of genetic material into daughter cells during mitosis is essential for normal proliferation. Mistakes in cell division can lead to DNA damage, aneuploidy and cancer. Accurate cell division is also dependant on processes that are carried out in S phase and G2, prior to progression into M phase. These include DNA replication, the establishment and maintenance of sister chromatid cohesion between S phase and anaphase, and centrosome replication. In order for accurate cell division to occur, faithful replication of the genome must first take place. Sources of error in DNA replication, known as replication stress, can result in DNA damage and genetic instability (Mazouzi, Velimezi, & Loizou, 2014).

DNA replication is initiated during early G1 in a process known as “origin licensing” at specific sequences known as replication origins which occur, on average, every 100kb in the mammalian genome.

Origin licensing requires the binding of the Origin recognition complex (ORC), which recruits CDC6 and the hexameric MCM2-7 helicase complex to double-stranded (ds) DNA. During G1 the complex is dormant, but some complexes are activated during

G1-S phase (Symeonidou, Taraviras, & Lygerou, 2012) and begin to unwind the DNA strands in front of the replication fork (Coster, Frigola, Beuron, Morris, & Diffley, 2014) in preparation for DNA synthesis.

Before entry into S phase, the cell must pass through the G1 checkpoint, which ensures genomic integrity before entry into S phase. The p53 tumour suppressor protein is known to have a role at the G1 checkpoint (as well as maintaining a damage-induced G2 arrest). A downstream target of p53, p21, also plays a role at the G1 to S phase transition. This involves the activation of the retinoblastoma protein (pRb) which binds to and inhibits E2F transcription factors (which act to advance the cell into S phase). Once the requirements of the checkpoint have been met, pRb is phosphorylated by the cyclin dependent kinases Cdk2, Cdk4 and Cdk6, thereby liberating the E2F transcription factors. This drives the expression of cyclin E and cyclin A as well as Cdk1 and Cdk2, resulting in the beginning of S phase, and the start of replication (Neganova & Lako, 2008). Different CDKs and cyclins act in different cell types, for example CDK4 and 6 appear to be more important in the thymus in comparison to CDK2. Similarly, cyclin D3 appears to be most important in the thymus (Sicinska *et al*., 2003). The role of cyclin-dependent kinases during S phase is discussed in more detail below. Finally during G2, any remaining S phase replication errors are corrected before the cell enters mitosis. The major cell cycle checkpoints are illustrated in Figure 1.1.

1.1.2.1 S phase

Replication of the genome during S phase requires all sections of DNA to be accurately synthesized exactly once, with no duplications (areas replicated more than once) or omissions. In eukaryotes, once the origins of replication have been licensed in G1, a subset of the replication origins are initiated (this process is also known as "origin firing") by the activation of the Mcm2-7 helicase complex.

Approximately 10% of licensed origins will initiate replication (Ge & Blow, 2010). The excess Mcm2-7 complexes that are loaded but not activated provide additional support should the cell undergo replication stress. The additional origins of replication will then become activated, and replication of the entire genome can take place, even

in the presence of replication stress (Woodward *et al*., 2006).

The number of origins that are licensed in G1, and subsequently, the proportion of these sites that are initiated determines the length of S phase (Sansam, Goins, Siefert, Clowdus, & Sansam, 2015). More activated origins results in an increase in the number of replication forks.

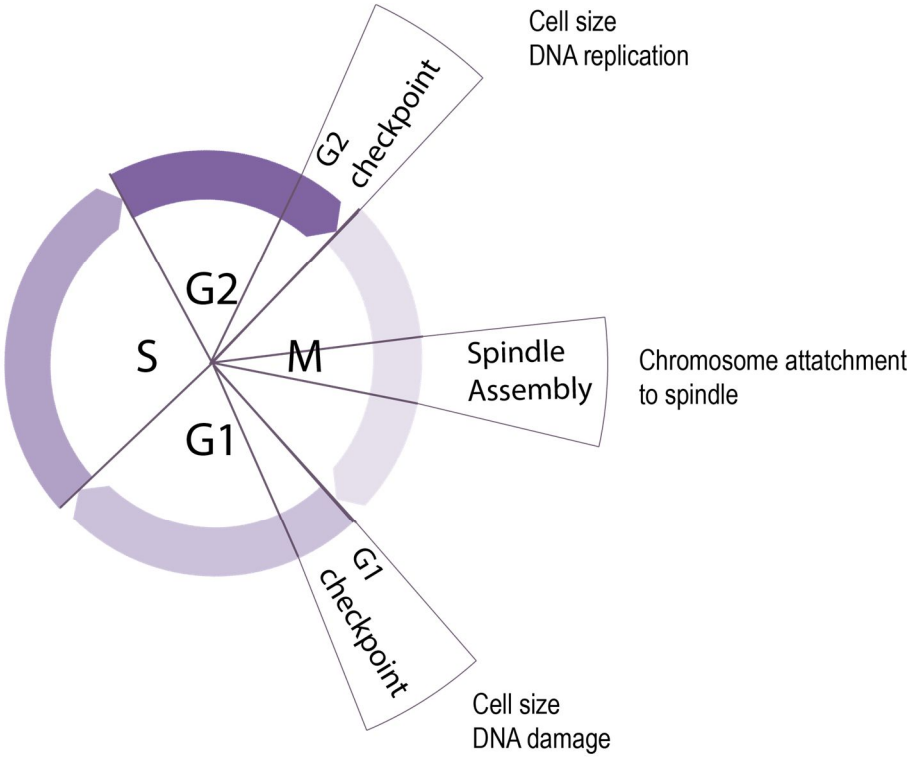

Figure 1.1: Schematic of the cell cycle and major checkpoints

Assuming fork velocity is constant, the increased number of replication forks will replicate the genome more quickly, since each will have less DNA to replicate. Through a combination of RNAi to knockdown regulators of histone assembly together with analysis of DNA replication, it was shown that new histone supply controls replication fork speed (Mejlvang *et al.*, 2014).

The replisome is formed from DNA replication proteins at the replication fork. These proteins are responsible for two main tasks: the helicase complex unwinds the DNA to form separate leading and lagging strand templates (taking the shape of a "fork"), while the DNA polymerase synthesizes new DNA using the template strand. Following initiation and elongation (DNA synthesis), termination takes place. This occurs when two converging replication forks meet. Several processes take place during termination, including the removal of double stranded (ds)DNA catenations and replisome dissassembly. However, due to the difficulty in predicting termination sites, the exact sequence of termination events requires further research. In contrast, a recently published study reveals that the strands of converging replication forks in Xenopus egg extracts freely pass each other, with no evidence of stalling (Dewar, Budzowska, & Walter, 2015).

One of the most important questions in the field of replication is the exact relationship between replication fork progression and genome stability. Since replication and transcription both occur along the same template, collisions between the replication and transcription machinery are inevitable. However, the consequences of these collisions are poorly understood. It is generally considered that the transcription/replication interference is a major cause of DNA damage and replication fork stalling (Mirkin & Mirkin, 2005; Skourti-Stathaki & Proudfoot, 2014). In contrast, a recently published study reveals that the strands of converging replication forks in Xenopus egg extracts freely pass each other, with no evidence of stalling (Dewar *et al.*, 2015).

During S phase, the cohesin complex establishes sister chromatid cohesion at the replication fork by forming a ring structure which entraps both sister chromatids. The role of cohesin is discussed in more detail in Section 1.2.1.

1.1.2.2 M phase

Mitosis is typically broken down into five cytologically distinct stages: prophase, prometaphase, metaphase, anaphase and telophase (Figure 1.2). To facilitate faithful segregation of daughter cells, the interphase chromatin is further compacted at the start of mitosis (prophase) into discrete cylindrical structures. At this stage, the two centrosomes move to opposite sides of the cell, where they will become the poles of the spindle apparatus. Microtubules are nucleated at the centrosomes and begin to spread out into the cell. Sister chromatid cohesion is removed along chromosome arms during prophase (Waizenegger, Hauf, Meinke, & Peters, 2000), when cohesin subunits and associated proteins are phosphorylated by the mitotic kinases PLK1, Aurora B and CDK1 (Dreier, Bekier, & Taylor, 2011; Hauf *et al*., 2005) allowing the removal of cohesin from the chromosome arms by Wapl (Tedeschi *et al*., 2013). Centromeric cohesin is protected by SGO1 (Shugoshin), which recruits PP2A to dephosphorylate sororin, thereby ensuring that sororin remains active at the centromeres. Sororin binds to acetylated SMC3, keeping the cohesin ring closed (Liu, Rankin, & Yu, 2013). Additionally, SGO1 prevents Wapl binding to cohesin by competitive binding (Hara *et al*., 2014).

During prometaphase the nuclear membrane breaks down. Microtubules connect to the kinetochores at the centromeres of each chromatids. Each sister chromatid of a pair will attach to kinetochore microtubules (k fibres) originating from opposite spindle poles in a process called bi-orientation (Walczak, Cai, & Khodjakov, 2010). This ensures that at anaphase sister chromatids are distributed evenly to daughter cells. Uneven distribution of chromatids can result in tumourigenesis, as described in Chapter 3, Section 3.1.1.1.

During metaphase, chromosomes align at the equator of the mitotic spindle (the metaphase plate), which is equidistant from the two spindle poles, and are held there under tension. Sister chromatid cohesion is removed at the centromeres following the cleavage of centromeric cohesin by separase, triggering the onset of anaphase. The kinetochore microtubules separate the sister chromatids, by pulling each of the sister chromatids towards opposite poles (Walczak *et al*., 2010).

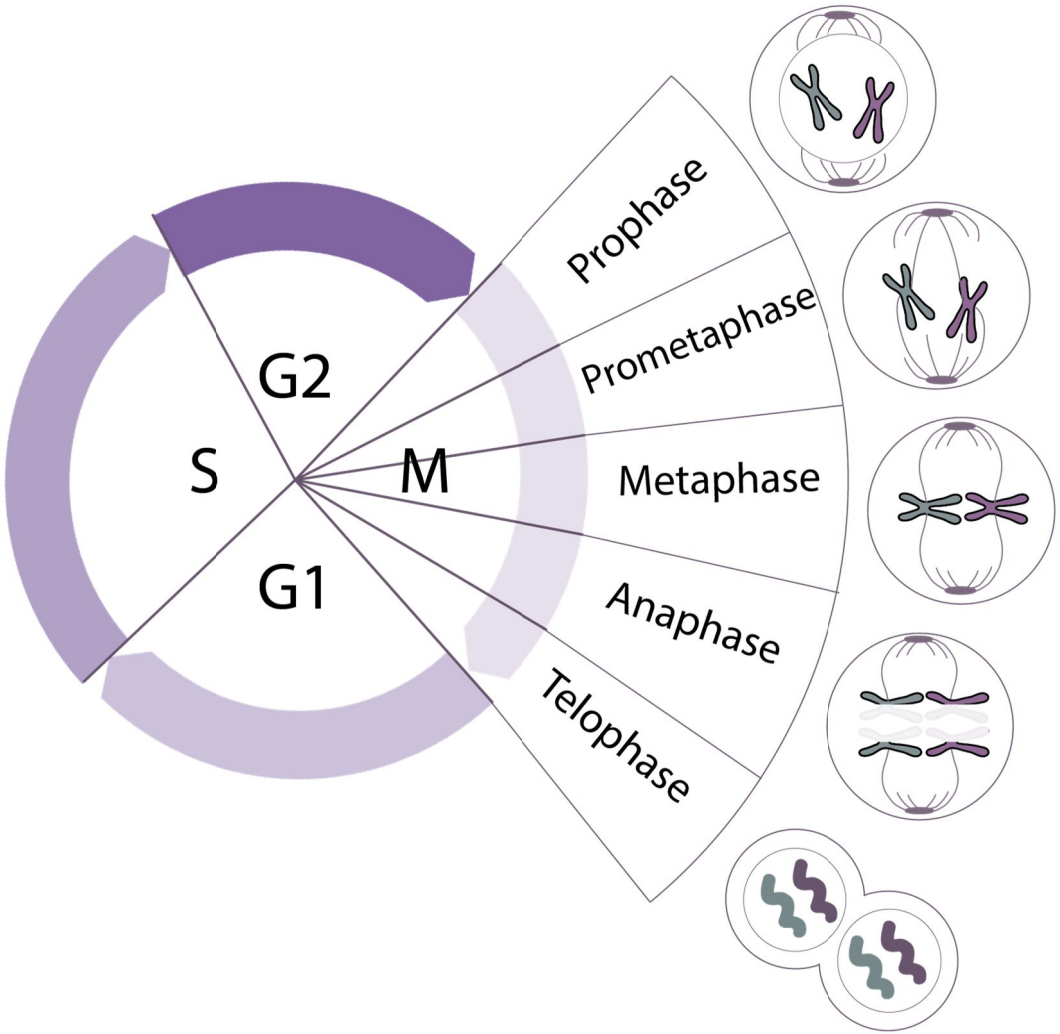

Figure 1.2: Five cytologically distinct stages of mitosis

During telophase the nuclear membrane is reformed, and the spindle apparatus is broken down. Maximum condensation of chromatin occurs in telophase. Finally, cytokinesis occurs. This requires the precise bisection of the metaphase plate by the cleavage furrow: a process controlled by actin and myosin, as well as other cytoskeletal proteins. It is also vital that the daughter cell acquires one centrosome each.

The processes involved in M phase are regulated by different checkpoints to ensure accurate segregation of the sister chromatids.

1.1.2.3 Kinases and cell cycle checkpoints

In order to ensure that the cells maintain a correct chromosome complement, the cell must pass several checkpoints at various stages of the cell cycle. Failure to remove cells with an incorrect number of chromosomes from the cell cycle can lead to the accumulation of further abnormalities and tumourigenesis.

1.1.2.3.1 Cyclin- and Dbf4-dependent kinases during S phase

Cyclin–dependent kinases and Dbf4-dependent kinases (DDKs) are important in the initiation of DNA replication during S phase (Tanaka & Araki, 2013). DDKs activate the replicative helicase by phosphorylating MCM2-7 subunits (Sheu, Kinney, Lengronne, Pasero, & Stillman, 2014). Despite being necessary for initiation of replication, the role of S phase CDKs is less well understood - particularly in vertebrates. In yeast, S phase CDKs phosphorylate Sld2 and Sld3, allowing them to physically interact with the scaffolding protein Dpb11. Sld2 is homologous to the vertebrate DNA helicase RecQL4, which physically interacts with the vertebrate homolog of Dpb11: TopBP1. However, unlike in yeast, this process does not occur as a result of CDK phosphorylation (Matsuno, Kumano, Kubota, Hashimoto, & Takisawa, 2006), and so the necessity for CDKs in vertebrate replication initiation remained unclear.

A screening for TopBP1 interactors revealed TICRR (TopBP1-interacting checkpoint

and replication regulator)/TRESLIN, which is phosphorylated by CDKs and shares some sequence similarity with Sld3 (Kumagai, Shevchenko, Shevchenko, & Dunphy, 2010; C. L. Sansam *et al*., 2010). TRESLIN phosphorylation allows interaction with TopBP1, and this is essential for initiation of replication (Boos *et al*., 2011; Kumagai, Shevchenko, Shevchenko, & Dunphy, 2011). Levels of phosphorylated Treslin control the length of S phase,by altering replication initiation (i.e. the number of replication forks) (Sansam *et al*., 2015).

1.1.2.3.2 DNA structure checkpoints

Entry into M phase is dependent on dephosphorylation of Cdk1. This occurs when Cdc25C (a phosphatase) is more active than the kinases Wee1 and Myt1. DNA structure checkpoints mediate the activity of these enzymes, so that the cell doesn't progress through the cell cycle if its DNA is not replicated faithfully, or if the DNA is damaged (Perry & Kornbluth, 2007). Later during late metaphase, the APC (anaphase promoting complex) ubiquitin ligase targets Cdk1-cyclin B for destruction following satisfaction of the spindle assembly checkpoint, resulting in exit from M phase. However, there are also many other mitotic kinases involved in this process, which has been simplified in the description above (Abrieu, Fisher, Simon, Dorée, & Picard, 1997; Sudakin, Chan, & Yen, 2001).

1.1.2.3.3 The spindle assembly checkpoint (SAC)

The spindle assembly checkpoint (SAC) inhibits sister-chromatid separation (and thus progression to anaphase) until all microtubules are correctly attached to the kinetochores and there is tension across the bi-oriented sister kinetochores. The SAC inhibits progression to anaphase by binding Mad2 and BubR1 directly to Cdc20, thereby preventing the activation of APC/C-Cdc20 (Hwang, 1998; Kim, 1998). Experiments in yeast identified the Mitotic Checkpoint Complex (MCC), which includes BubR1, Bub3, Mad2 and Cdc20 (Hardwick, Johnston, Smith, & Murray, 2000). The complex was later identified in HeLa cells (Sudakin *et al*., 2001). The MCC is produced when kinetochores are unattached during prometaphase. Because Cdc20 is bound in this complex, it is unable to activate APC/C. However, once all

kinetochores are attached correctly, the MCC is no longer produced – allowing Cdc20 to be released to activate APC/C (Kulukian, Seok Han, & Cleveland, 2009). The primary targets of activated APC/C are Cyclin B, degradation of which allows dephosphorylation of Cdk substrates which triggers mitotic exit, (Zachariae, Schwab, Nasmyth, & Seufert, 1998; Sullivan & Morgan, 2007) and securin, degradation of which removes centromeric cohesin to trigger chromosome segregation.

Degradation of Cyclin B in the absence of chromosome segregation leads to a process known as "mitotic slippage", where cells exit mitosis without reducing their DNA content and become tetraploid (Brito, Yang, & Rieder, 2008). The process of "mitotic slippage" is distinct from "mitotic skippage" which occurs when a cell enters G1 without having entered mitosis, and consequently will contain 4N DNA content. The products of these two processes may be distinguished by the presence or absence of sister chromatid cohesion, since cells in G2 (unlike G1), will be subject to sister chromatid cohesion. Additionally, cells that have skipped mitosis can be distinguished from cells that have undergone mitotic slippage, since they accumulate Cdt1 (a DNA replication factor expressed during G1) but lack mitotic regulators, and do not enter mitosis (as determined by the lack of Cdk1 expression). Mitotic skippage can be caused by the transient activation of p53 at G2, and results in senescence, both *in vivo* and *in vitro* (Dikovskaya *et al*., 2015; Johmura *et al*., 2014).

1.1.2.4 Mitotic kinases and chromatin condensation

The most visually dramatic event in the cell cycle is the condensation of chromatin during prophase. The phosphorylation of histone H3 serine 10 by Aurora B kinase is associated with mitotic chromosome condensation. However, how this leads to chromatin condensation is unclear. To investigate the consequences of the phosphorylation of H3S10, Wilkins *et al*. studied protein-protein interactions in yeast (Wilkins *et al*., 2014). They found that histone H3 serine 10 phosphorylation results in the deacetylation of H4 lysine 16, which allows the histone tail to interact with adjacent nucleosomes – thereby encouraging condensation. H4K16 binds to the acidic patch on H2A (discussed previously).

Aurora B - the catalytic subunit of the chromosomal passenger complex (CPC) which

coordinates mitotic processes through phosphorylation of key regulatory proteins - is recruited to centromeric chromatin by the action of another kinase – haspin which phosphorylates H3 on threonine 3. Protein phosphatase 1 (PP1)/Repo-Man acts antagonistically to Haspin, dephosphorylating H3T3ph on chromosome arms. Aurora B phosphorylates Repo-Man at S893, preventing its recruitment. This is counteracted by PP2A - a mitotic interactor of Repo-Man that dephosphorylates S893 and thereby promotes the targeting of Repo-Man to chromosomes and the dephosphorylation of H3T3ph by PP1. Thus, Repo-Man-associated PP1 and PP2A collaborate to oppose the chromosomal targeting of Aurora B (Qian, Beullens, Lesage, & Bollen, 2013).

The Mps1 protein kinase, known to be involved in several mitotic processes including the spindle assembly checkpoint (SAC) and cytokinesis, also facilitates prophase chromatin condensation by associating with the condensin II complex (Kagami *et al*., 2014). Cyclin dependent kinases, particularly Cdk1, have also been shown to induce mitotic chromosome organization by phosphorylating subunits of condensins I and II (Abe *et al*., 2011; Kagami *et al*., 2014; Shintomi, Takahashi, & Hirano, 2015), as well as other mitotic proteins (Olsen *et al*., 2010). However, despite some progress being made, the essential process of transforming diffuse, entangled interphase chromatin into discrete, highly organized chromosomal structures is not currently very well understood.

1.1.2.5 Phosphatases and chromatin decondensation on mitotic exit

The process of chromosome decondensation on exit from mitosis has been visualised in living cells (Müller, Boyle, Singer, Bickmore, & Chubb, 2010). This study revealed through quantitative measurements that the volume and morphology of interphase chromosomes are generated very quickly after mitosis. A key role in chromatin decondensation is carried out by the nuclear protein, Repo-Man, which is involved in the dephosphorylation of histone H3 during mitotic exit (Vagnarelli *et al*., 2011). Repo-Man activity is inhibited by the phosphorylation of the residue threonine 412 (T412) until anaphase onset. At this point, Repo-Man targets protein phosphatase 1 γ (PP1γ) to chromatin, casing the dephosphorylation of Thr3, Ser10 and Ser28 of histone H3 (Vagnarelli *et al*., 2011).

1.1.3 The structure of mitotic chromosomes

The purpose of mitotic chromosome condensation and mitotic chromosome structure is firstly, to ensure chromatin is kept away from the cleavage furrow (failure to do so results in the "cut" phenotype) and secondly, to provide the chromosomes with sufficient structural rigidity to survive the forces of mitosis.

1.1.3.1 The chromosome scaffold

It has been postulated that the increased level of condensation during mitosis is achieved through the "scaffold-and-loop" model whereby the 30nm fibre is organised into loops which are attached to a scaffolding structure (Gasser, Amati, Cardenas, & Hofmann, 1989). In order to identify non-histone stabilizers of mitotic chromosome condensation, Laemmli *et al.* carried out histone depletion experiments, whereby histones were removed from metaphase chromosomes using dextran sulphate and heparin as competitors. They discovered that histone depletion resulted in chromosomes that remained highly folded due to the presence of non-histone proteins (Laemmli *et al*., 1978). These proteins make up the "mitotic chromosome scaffold" – a structure which can be isolated using sucrose gradient sedimentation, illustrated in Figure 1.3 (Adolph, Cheng, & Laemmli, 1977).

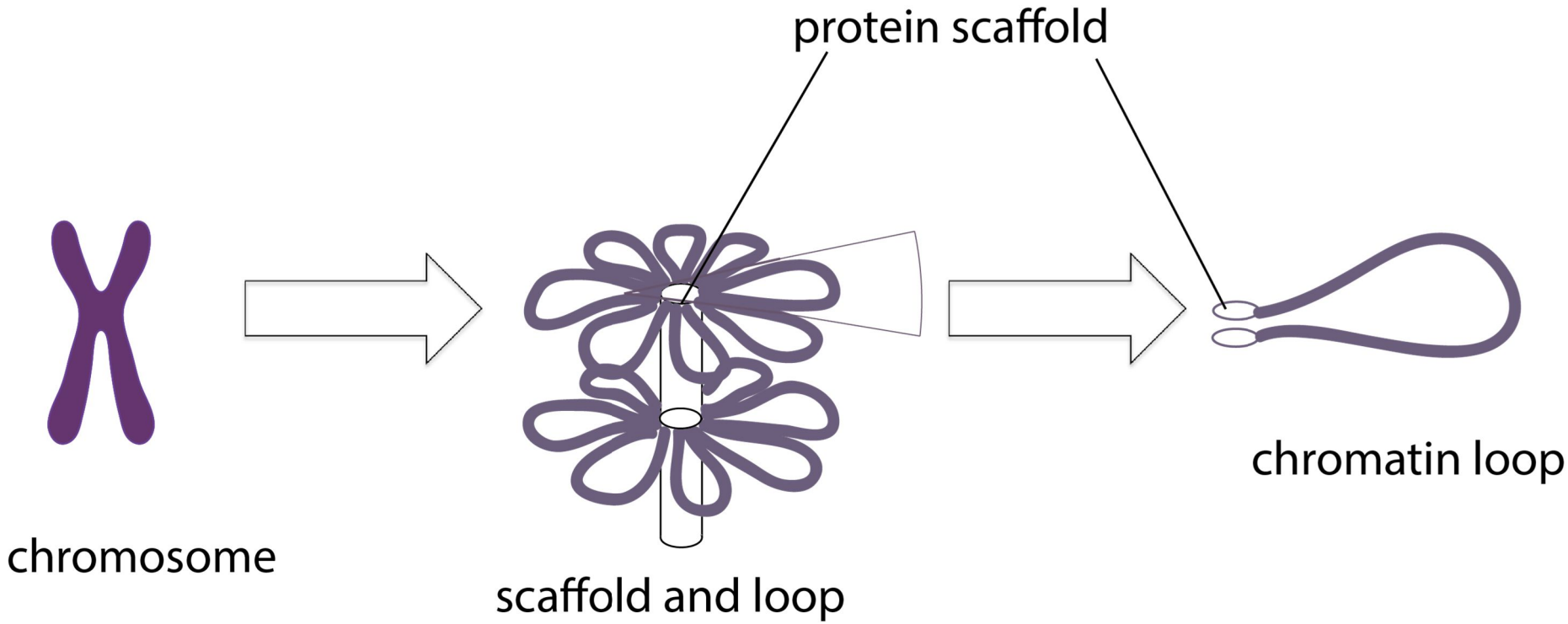

Figure 1.3: Schematic of the mitotic chromosome scaffold model of chromosome condensation

The two major protein components of the mitotic chromosome scaffold were initially thought to be ScI (topoisomerase II) and ScII (a protein belonging to the family of SMC "structural maintenance of chromosomes" protein complexes). Topoisomerase II (topo II) is an enzyme that can relax supercoils through the use of transient double-strand breaks, and it is also required to "untangle" (decatenate) DNA, prior to mitosis. Immunofluorescence on gently centrifuged mitotic chromosomes indicated that topo II was localized towards the centre of the expanded chromatids, specifically on the chromosome axes, rather than in the surrounding chromosome loops (Earnshaw & Heck, 1985). Although these data may not directly relate to the localization of topo II in condensed chromosomes *in vivo*, they suggest that topo II is involved in maintaining the structure of condensed mitotic chromosomes, by anchoring DNA to the mitotic scaffold.

However, inhibiting topo II by either immunodepletion or antibody blocking did not alter chromosome structure once mitotic condensation had taken place. In addition, immunofluorescence indicated that topo II was located throughout the condensed chromosome, rather than being restricted to the chromosomal axis (Hirano & Mitchison, 1993). Finally, extraction of topoisomerase II under mild conditions did not alter the shape of mitotic chromosomes. Together, this evidence suggests that while topo II is vital for successful chromosome condensation in preparation for mitosis, once this has been achieved it is not required to maintain chromosome structure, and therefore does not play an architectural role in maintaining the mitotic chromosome scaffold (Hirano & Mitchison, 1993).

Several studies suggested that certain DNA sequences might directly associate with the axial region of the chromosome, defined as the chromosome scaffold (Cook, 1994; Gasser *et al*., 1989; Razin *et al*., 1993), to form the base of the loops in the "scaffold-and-loop" model of mitotic condensation. Using multicolour fluorescence in situ hybridization (FISH), Bickmore and Oghene provided the first visual evidence for the existence of the scaffold-and-loop model, since their data showed that specific DNA sequences do indeed preferentially bind to the axial region of chromosomes (Bickmore & Oghene, 1996). This data was supported by Saitoh and Laemmli, who suggested that the banding patterns observed in native chromosomes using the AT-specific fluorochrome daunomycin, was a consequence of AT-rich regions of DNA interacting

with the chromosome axis of metaphase chromosomes (Saitoh & Laemmli, 1994). These specific DNA sequences were termed Scaffold Associated Regions (SARs). Originally characterized in *Drosophila* (Mirkovitch, Spierer, & Laemmli, 1986), SARs have since been identified in several other model organisms, often localized near regulatory domains such as enhancers (Cockerill & Garrard, 1986; Gasser & Laemmli, 1986; Kas & Chasin, 1987).

However, this hypothesis remained controversial, as other researchers suggested that the sequences associated with the scaffold were due to artefacts resulting from harsh extraction procedures (Jackson, Dickinson, & Cook, 1990; Okada & Comings, 1980). They argued that the scaffold-associated proteins may not interact *in vivo*, but associate with each other non-specifically after removal of chromatin. Under this assumption, the highly folded structures observed after the removal of the histones is due to the formation of a precipitate consisting of the non-histone proteins. Hudson *et al*. provided the first biochemical evidence that the scaffold components associate with each other as a result of specific interactions. The study revealed that removal of one of the scaffold proteins (SMC2/ScII) resulted in improper localization of other scaffold-associated proteins such as topo II (Hudson, Vagnarelli, Gassmann, & Earnshaw, 2003).

Using the chromosome conformation capture methods 5C and Hi-C, Naumova *et al*. showed that the organisation of metaphase chromatin is dramatically different to that of interphase chromatin. The folding of chromatin into domains (both large-scale compartments and sub-megabase TADs) was lost and loci within 10Mb of each other could come into regular contact. However, metaphase chromatin is linearly organized at distances above 10Mb; i.e. loci more than 10Mb apart rarely come into contact. Their proposed model of mitotic chromosome organization involves linear condensation by the formation of consecutive loops, followed by axial compression – resulting in linear organization above 10Mb (Naumova *et al*., 2013). There is some evidence from Drosophila to suggest the structure of mitotic chromosomes is determined by DNA-protein interaction: using high resolution fluorescence microscopy, actively transcribed, dosage compensated Drosophila genes were shown to be located along the periphery of mitotic chromosomes, indicating that there is an underlying radial organization (Strukov, Sural, Kuroda, & Sedat, 2011).

Chromatin is generally considered to undergo a continuous, smooth condensation in preparation for mitosis. However, new evidence suggests that this might not be the case: instead chromatin may undergo discrete stages of condensation and expansion from mid-prophase to metaphase (Figure 1.4) (Liang *et al*., 2015). Chromosome volumes in HeLa and living muntjac cells were shown to expand from mid- to late-prophase, and then contract into metaphase. Additionally, chromosome density was measured, and found to diminish from mid- to late-prophase, before shifting to considerably higher values during metaphase. This chromosome expansion during late prophase was shown to be a consequence of increased chromosome width, rather than increased length. Chromosome lengths were dramatically reduced during prometaphase, resulting in condensation in metaphase. However, during this compaction phase, chromosome widths continued to increase, indicating that the chromosomes are compressed in a length-wise direction (Liang *et al*., 2015).

During mid-prophase, Liang *et al*. detected a single topoisomerase II signal along the length of the chromosome. However, during the expansion phase at late prophase, this signal was found to split in two, perhaps reflecting sister chromatid individualisation. This occurred concomitantly with loss of cohesin along the chromatid arms. These chromosome morphology changes were sensitive to topoisomerase II inhibition and the phases of expansion and contraction were suggested to be a consequence of the expansion and formation of tethers (either mediated by DNA catenations or proteins), respectively. Removal of linkages by topoisomerase II and release of cohesin during late prophase results in chromosome expansion which allows the chromosome structure to be altered. Unconstrained sister loops are able to expand and push each other apart – causing sister chromatid individualisation. These morphological changes are "locked in" by the subsequent stages of condensation (Liang *et al*., 2015).

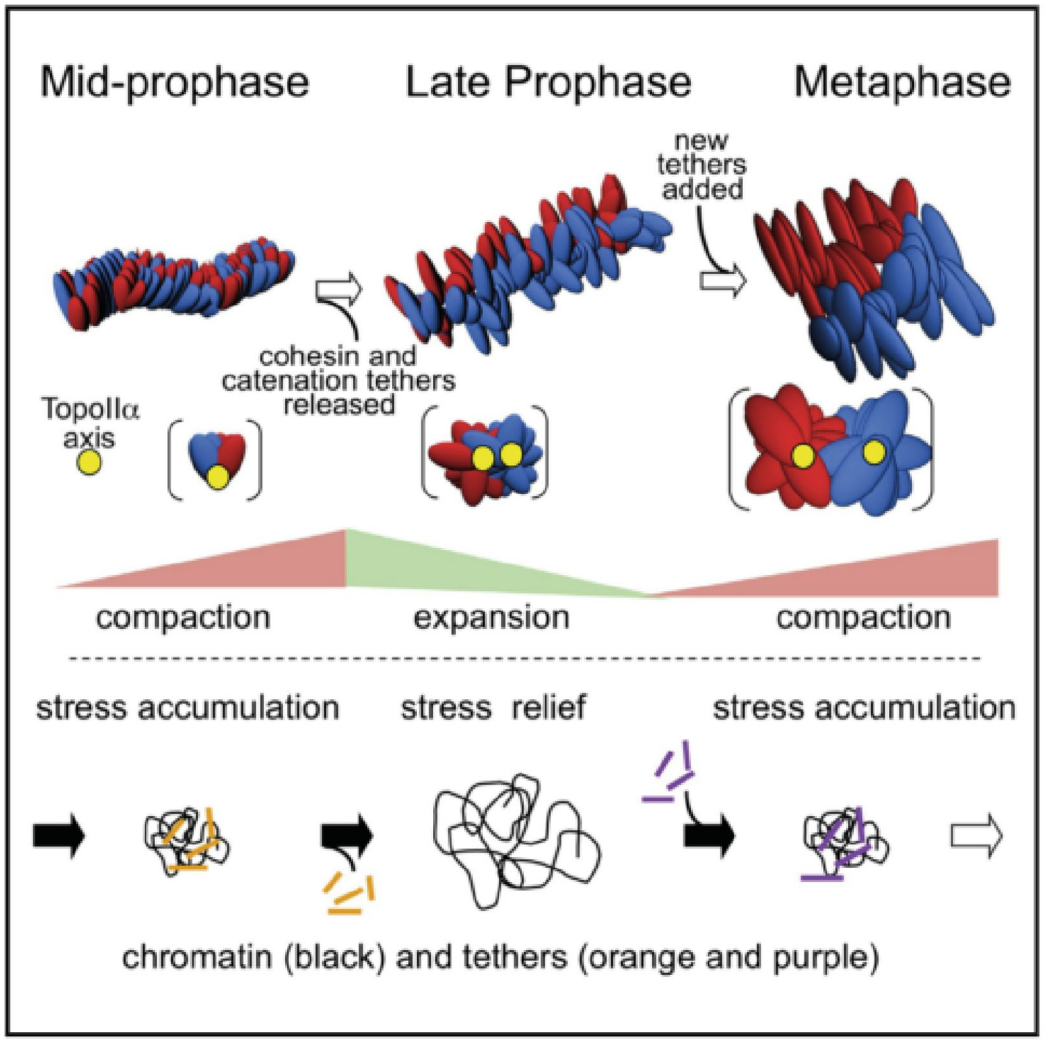

Liang et al., 2015

Figure 1.4
Chromosomes undergo stages of expansion and contraction from mid-prophase to metaphase
Evidence presnted by Liang *et al*. suggests that chromosomes do not become progressively more compact during mitosis, but instead progress to metaphase through a series of contractions and expansions (Liang *et al*. 2015).

1.2 Experiments leading to the discovery of Condensin

In order to better understand the processes involved in restructuring higher-order chromatin during cell division, Hirano *et al*. used a biochemical procedure to isolate proteins from mitotic chromosomes. Two novel polypeptides, XCAP-C (SMC4) and XCAP-E (SMC2), were identified and found to associate with each other, forming a heterodimer. They were subsequently shown to be involved in the condensation of chromatin in *Xenopus* egg mitotic extracts (Hirano & Mitchison, 1994). XCAP-C and XCAP-E are recruited to chromosomes during prophase, at the point when mitotic chromosome structure is being established. By the time the cell has reached telophase, XCAP-C no longer localizes to the chromosomes, but is uniformly distributed throughout the nucleus. Immunodepletion experiments using anti-XCAP-C antibody showed that XCAP-C is necessary for both assembly and maintenance of mitotic chromosomes *in vitro* (Hirano & Mitchison, 1994).

During this time, whilst investigating the protein composition of the mitotic chromosome scaffold in chicken cells, Saitoh *et al*. characterised the second most abundant protein of the scaffold (after topoisomerase II), which they named ScII (now known as SMC2) (Saitoh, Goldberg, Wood, & Earnshaw, 1994). ScII was found to associate only very loosely with interphase nuclei, indicating that it plays a part in mitotic chromosome condensation, perhaps alongside topoisomerase II. Using two different preparation techniques, ScII was found to localize to the axis of the hypotonically swollen mitotic chromosomes (Saitoh *et al*., 1994) in a nearly identical distribution to that of topoisomerase II (Earnshaw & Heck, 1985).

XCAP-C and XCAP-E/ScII are now known to belong to a family of chromosomal ATPases called SMC (structural maintenance of chromosomes) proteins conserved from bacteria to human. In prokaryotes there is only one SMC protein, whereas eukaryotes have six. SMC2 and SMC4 form the core subunits of condensin: a complex that uses energy from ATP hydrolysis to mediate various different aspects of chromosome dynamics. Condensin subunits were also independently identified by members of the Meyer lab, whilst investigating the mechanism of X chromosome dosage compensation in *C. elegans* (Chuang, Albertson, & Meyer, 1994). Condensin is homologous to cohesin (Figure 1.5a), and a third class of complex termed SMC5/6

(not shown). In yeast, a temperature sensitive mutation of *SMC4* was found to result in chromosome segregation errors and chromosome decondensation (Strunnikov, Hogan, & Koshland, 1995).

1.2.1 Cohesin: a homolog of condensin

Considerable research effort has focused on the cohesin complex, which is homologous to condensin. The two complexes are structurally very similar, and both restructure chromatin before cell division. Cohesin maintains sister chromatid cohesion between S phase and anaphase, by entrapping sister chromatids within a ring-like structure (Gruber, Haering, & Nasmyth, 2003). Cohesin is removed from chromosomes via two distinct pathways (as discussed in Section 1.1.2.2). Cohesin is removed from the chromosome arms during prophase by a pathway involving Wapl, but Shugoshin 1 (Sgo1) and PP2A are thought to prevent removal of centromeric cohesin at this stage, by counteracting phosphorylation and preventing binding of Wapl to cohesin located at the centromeres (Hara *et al*., 2014; Kitajima *et al*., 2006). Anaphase begins with the proteolytic cleavage of SCC1, the kleisin subunit of cohesin, by separase (Hauf, Waizenegger, & Peters, 2001). This triggers the release of cohesin from sister chromatid centromeres, enabling the sister chromatids to be separated into daughter cells (Oliveira & Nasmyth, 2010).

Heterozygous mutations in cohesin subunits and in NIPBL (Scc2 in yeast) - a protein implicated in the loading of cohesin (and condensin), have been identified in patients with Cornelia de Lange-like syndromes (Gil-Rodríguez *et al*., 2015; Liu & Krantz, 2010). Cornelia de Lange syndrome is a developmental disorder affecting the physical and intellectual development of patients and is characterized by a number of traits including microcephaly, vision and hearing impairments, and small stature (Gil-Rodríguez et al., 2015). Like condensin, cohesin carries out an important role in cell division (although perhaps to different degrees in different cell types) and it is therefore surprising that reduced cohesin function does not appear to impact all dividing cells. This might indicate that only a small amount of functional cohesin is required to provide cohesion.

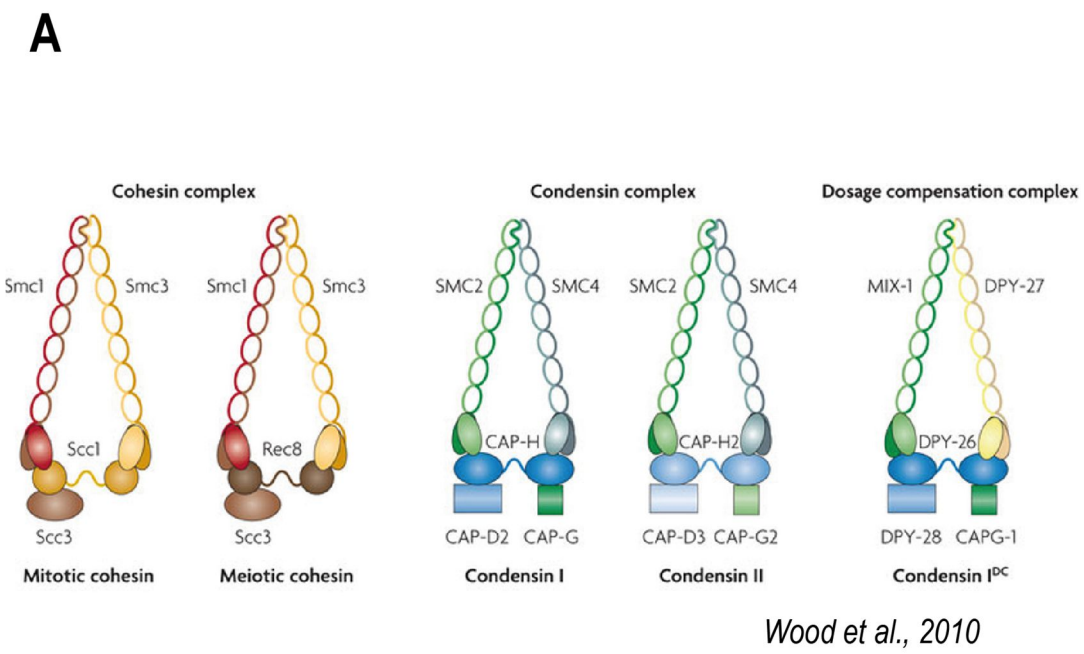

Figure 1.5
Structural maintenance of chromosomes (SMC) complexes
A. Condensins belong to a family of protein complexes that contain a heterodimer of SMC proteins and additional accessory subunits. Each SMC protein contains residues important for ATPase activity at the N and C termini. These are connected to each other via two coiled coil domains, separated by a hinge region. The SMC heterdimers associate with non-SMC proteins, including kleisins, which bridge interaction between the head domains (Wood *et al*. 2010). **B.** Schematic showing the structure of an SMC protein. Walker A and Walker B motifs at the N and C termini, which are connected via a coiled-coil domain. The hinge brings the N and C termini into contact with one another.

Cohesin is implicated in additional processes beyond sister chromatid cohesion, including promoting interactions between enhancers and promoters (Ong & Corces, 2011). Cohesin binding sites often coincide with those of CCCTCF-binding factor (CTCF) in human cells and such sites have been suggested to form the base of chromatin loops and the boundaries of topological domains (TADs) to assist in enhancer-promoter communication (Gil-Rodríguez *et al*., 2015). Thus, accumulating evidence suggests that cohesin is involved in the formation of links between non-homologous sequences in *cis*, as well as between sister chromatids (Wood, Severson, & Meyer, 2010). It is thought that this secondary function is impaired in patients with Cornelia de Lange syndrome, as sister chromatid cohesion is not obviously affected in patient-derived cell lines (Strachan, 2005; Vrouwe *et al*., 2007).

1.2.2 The structure of SMC proteins

Each SMC protein contains motifs - "Walker A" at the amino-terminus and the carboxy terminal "Walker B" motif, which are important for ATPase activity, (Figure 1.5b). These are connected via two coiled-coil domains separated by a central hinge region, which allows the molecule to fold back upon itself bringing N and C termini into contact. All eukaryotic SMC complexes contain a heterodimer of SMC proteins, which interact through the hinge domain to form a V-shape, while prokaryotic complexes are formed from a homodimer. ATP binding, but not hydrolysis is essential for the association of condensin with chromosomes (Hudson *et al*., 2008).

The SMC proteins associate with kleisins, which bridge interactions between the head domains of the different SMC proteins (Figure 1.5a). The kleisin subunit of cohesin is cleaved during anaphase by a protease called separase, allowing chromatid separation. Whether proteolytic cleavage of the condensin-associated kleisin is required to remove condensin from chromosomes is not known.

As well as kleisins, the SMC2/4 heterodimer of condensin also associates with two different HEAT repeat-containing proteins (*Capg/Capg2* and *Capd2/Capd3*) to the

complex. HEAT repeats form rod-like helical structures which, in other contexts, have been shown to mediate protein-protein interactions (Nasmyth & Haering, 2005). The subunit composition of condensin is highly conserved from yeast to humans, indicating its fundamental role in the physiology of eukaryotic cells.

1.2.3 Two distinct complexes: condensin I and II

There are at least two different condensin complexes in most eukaryotes. Evidence for a second condensin complex was identified (Schleiffer *et al*., 2003), through searches to identify homologs of the *B. subtilis* SMC-interacting protein ScpA. Schleiffer *et al*. characterized a superfamily of SMC-interacting proteins, called kleisins. This family included the Barren/CAP-H-kleisin (a known subunit of condensin I) and a novel protein, which was termed kleisin-β (Schleiffer *et al*., 2003). In addition to condensin I and condensin II, a third distinct condensin I-like complex binds specifically to X chromosomes in *C. elegans*. This complex is known as the dosage compensation complex (DCC), as it is involved in the regulation of transcription levels in hermaphrodites (Csankovszki *et al*., 2009).

Vertebrate condensin II was discovered through searches for homologs of condensin I subunits (Ono *et al*., 2003). Condensin II contains the same SMC subunits as condensin I (SMC2 and SMC4), but is comprised of different non-SMC subunits (Ono *et al*., 2003; Ono, Fang, Spector, & Hirano, 2004). While the SMC2/SMC4 dimer in condensin I associates with a Barren/CAP-H-kleisin, the condensin II dimer associates with the kleisin identified by Schleiffer *et al*., - Kle-2/CAP-H2-kleisin (Schleiffer *et al*., 2003). Different pairs of HEAT repeat-containing proteins associate with condensin I (CAP-D2 and CAP-G) and condensin II (CAP-D3 and CAP-G2) (Nasmyth & Haering, 2005) (Figure 1.5a). The gene duplications that gave rise to these paralogs apparently predate the radiation of modern day eukaryotes (Tatsuya Hirano, 2012).

Despite their conserved subunit composition, condensin I and condensin II exhibit different cell cycle localization patterns. Immunostaining of a condensin I subunit shows it to be cytoplasmic during interphase, and only associated with chromosomes after breakdown of the nuclear membrane during prometaphase. In contrast, the

condensin II complex is both nuclear and cytoplasmic throughout the cell cycle (Ono *et al*., 2004). Fluorescence recovery after photobleaching (FRAP) was used to assess the association of the condensin complexes with chromatin and revealed that condensin II binding to mitotic chromatin is stable, whereas condensin I binding is dynamic (Gerlich, Hirota, Koch, Peters, & Ellenberg, 2006). Given their different spatial localization and binding affinities, it seemed likely that the functions of condensin II would be distinct from those of its condensin I counterpart.

1.2.3.1 Functions of condensin I and II

It is becoming apparent that different cell types, species, and experimental systems have different degrees of requirement for condensins I and II - the reasons for which are not yet known. Using gene disruption, Fujiwara *et al.* demonstrated that condensin II is not essential for mitosis in the model organism *Cyanidioschyzon merolae*, which was chosen because the localization of the condensin complexes throughout the cell cycle is similar to that of vertebrate cells, and also because it is one of the most basal eukaryotes known to have two condensin complexes (Fujiwara, Tanaka, Kuroiwa, & Hirano, 2013). Using immunodepletion experiments, Shintomi and Hirano showed that *Xenopus* egg extract chromosomes were less severely impacted by depletion of condensin II compared to condensin I. They found that the ratio of condensin I to condensin II in *Xenopus* egg extracts is 5:1, which implies that the contribution of condensin II to chromosomal architecture is far less important than that of condensin I in this organism (Shintomi & Hirano, 2011). In DT40 chicken cells, the ratio of condensin I to II is even more extreme at 10:1 (Green *et al*., 2012; S. Ohta *et al*., 2010). Finally, condensin II is known to function during interphase in several organisms (Bauer, Hartl, & Bosco, 2012; Haeusler, Pratt-hyatt, Good, Gipson, & Engelke, 2008; Hartl, Smith, & Bosco, 2008; Wood *et al*., 2010). Taken together, this data suggests that the role of condensin II may not be as vital as that of condensin I in mitosis.

Despite this, there is increasing evidence to suggest that condensins I and II have distinct, as well as overlapping functions in some model systems. A recent study investigated the roles of condensins I and II using mouse strains containing floxed alleles of *Caph1* (condensin I) and *Caph2* (condensin II). *Caph1* and *Caph2* were inactivated specifically in meiosis using Cre recombinase (Houlard *et al*., 2015) which

revealed that condensin II, but not condensin I, is essential for meiosis since *Caph1* deletion did not result in a pronounced effect, while *Caph2* deletion caused sterility. In addition, condensin II depletion was shown to affect chromosome morphology, with stretching of pericentric sequences occurring during spindle attachment, and delayed bi-orientation of chromosomes. No such effect was observed as a consequence of *Caph1* deletion. However, deletion of both *Caph1* and *Caph2* resulted in failure to form pericentric foci, and stretching of the pericentric sequences was more severe than that observed for the *Caph2* single mutant (Houlard *et al*., 2015), indicating that some of the functions of condensins I and II overlap.

Nishide and Hirano (Nishide & Hirano, 2014) found that condensin I and II are both essential for accurate chromosome segregation in mouse neuronal stem cells (NSCs), and contribute to chromosome re-structuring and maintenance in distinct, as well as overlapping ways. Using strains of conditional knockout (cKO) mice that were depleted for condensin subunits, they found that defects in cortical development were most severe in animals depleted of both CAP-H and CAP-H2 (i.e. both condensins I and II) or depleted of SMC2 (a subunit common to both condensin complexes), supporting the hypothesis that condensins I and II carry out overlapping functions. However, NSC numbers were also significantly reduced in strains depleted of both CAP-H (condensin I) and CAP-H2 (condensin II) individually, indicating that both complexes also perform distinct roles that are essential for cortical development (Nishide & Hirano, 2014).

Conditional knockouts of the genes encoding CAP-H (condensin I subunit) and CAP-D3 (condensin II subunit) in chicken cells showed that condensin I depleted mitotic chromosomes were wider and shorter, whereas condensin II depleted chromosomes seemed to lack axial rigidity, as indicated in Figure 1.6. The results suggested that condensin II plays a vital role in the construction of an initial chromosome axis, thereby providing rigidity. Interestingly, the results indicate that condensin I deficient cells are better able to condense and divide appropriately than condensin II depleted cells. Anaphase bridges were observed in both condensin mutants, but were considerably more severe for cells that were depleted of condensin II. Additionally, condensin I depleted cells were considerably more successful in maintaining chromosome rigidity (Green *et al*., 2012). The main consequence of condensin

depletion (through the conditional knock out of SMC2) in chicken DT40 cells was revealed to be loss of rigidity, or stiffness (Ribeiro *et al*., 2009).

Consistent with this, Hudson *et al*. found that altering the ratio of condensin I and II in DT40 cells via disruption of a conserved Cdk1 phosphorylation site within CAP-D3 changed the shape of mitotic chromosomes (Bakhrebah, Zhang, Mann, Kalitsis, & Hudson, 2015). This was the first evidence indicating that manipulation of the ratio of condensin I to II alters mitotic chromosome shape *in vivo*. This is also supported by the fact that chromosomes formed in *Xenopus* egg extract are long and thin, with a ratio of condensin I to condensin II of approximately 5:1. In HeLa cells however, where the ratio is closer to 1:1, the chromosomes are generally shorter and thicker. Indeed, Shintomi and Hirano found that when the ratio of condensin I to condensin II in *Xenopus* egg extracts was experimentally manipulated by quantitative immunodepletion to give a 1:1 ratio, the chromosomes became shorter and thicker (Shintomi & Hirano, 2011). However, the molecular mechanisms through which condensins impact chromosome morphology still remain poorly understood.

Ono *et al.,* using siRNAs to knockdown CAP-G (condensin I) and CAP-G2 (condensin II) in HeLa cells, reported dramatic differences in the structure of mitotic chromosomes depleted of condensin I relative to condensin II (Ono *et al*., 2004). Depletion of CAP-G resulted in localisation of SMC2 away from the central chromosome axis, and a slight swelling of the chromosomes. Depletion of CAP-H2, however, resulted in dramatic morphological changes, with SMC signal localised along a "wavy" central chromatid axis. The sister chromatid arms were also often no longer positioned close to one another, but became splayed (Ono *et al*., 2003). These data support the hypothesis that condensin II contributes to the structural rigidity of metaphase chromosomes, in a role that is distinct from that of condensin I.

In their study, Nishide and Hirano found that depletion of SMC2 and simultaneous depletion of condensin I and II subunits in mNSCs resulted in severe chromosomal abnormalities and apoptosis as a result of p53 accumulation (Nishide & Hirano, 2014).

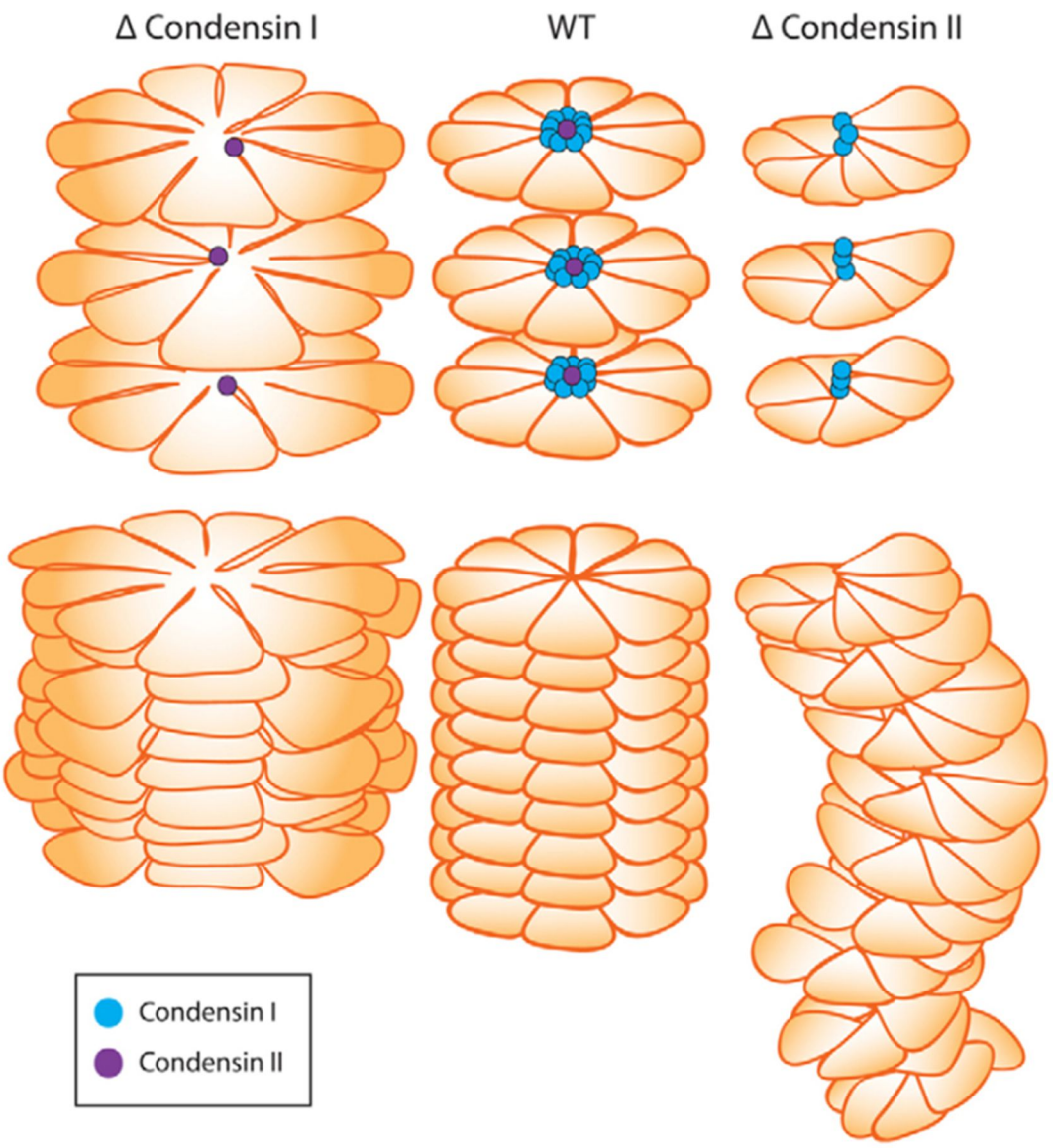

Figure 1.6
Contrasting roles of condensin I and condensin II
Schematic illustrating the consequences of deleting condensin I and condensin II in chicken DT40 cells (Green *et al.*, 2012). Condensin I depleted chromosomes are shorter and thicker, whereas condensin II depleted chromosomes lack axial rigidity.

However, RNAi-mediated depletion of SMC2 in mouse embryonic stem cells (mESCs) was reported to result in cell cycle arrest during metaphase (Fazzio & Panning, 2010). These differences may indicate that the response to condensin-deficient mitosis is cell type dependent. Nishide and Hirano further investigated a possible cell type-dependent consequence of condensin depletion using an alternative cell line – the human retinal pigment epithelial cell line (RPE-1) – and demonstrated that unlike mouse NSCs, abnormal RPE-1 cells accumulate nuclear p21 and became senescent, rather than either undergoing G1/S phase arrest, or p53 nuclear accumulation leading to apoptosis (Nishide & Hirano, 2014).

1.2.4 The role of condensins in organising chromosome structure

Hirano and Mitchison carried out some of the earliest investigations relating condensins to mitotic chromosome structure, using *Xenopus* egg extracts to demonstrate that a heterodimeric coiled-coil protein (later shown to be condensin) is essential for proper condensation of chromatin into typical rod-shaped chromosomes (Hirano & Mitchison, 1994). As well as being required for the final stages of *Xenopus* chromatin condensation, condensin is also essential for the maintenance of condensation, unlike topoisomerase IIa, which can be extracted without altering the chromosome structure (Ono *et al*., 2003).

DNA condensation is necessary before mitosis for two main reasons. Firstly, uncondensed chromosomes are larger than the diameter of the mitotic cell and so would be broken by the cleavage furrow at cytokinesis (a so-called cut phenotype). Secondly, the condensed chromosomes are structurally rigid, and are therefore less likely to be damaged when they are subjected to the opposing forces which separate the sister chromatids during anaphase. Homologs of condensin subunits are important for chromosome condensation in many model organisms, including *S. cerevisiae* (Alexander, Hogan, & Koshland, 1995), and *Drosophila* (Bhat, Philp, Glover, & Bellen, 1996).

However, other studies have indicated that condensin depletion has only a very subtle effect on chromosome condensation (Charbin, Bouchoux, & Uhlmann, 2014; Coelho, Queiroz-Machado, & Sunkel, 2003; Steffensen *et al*., 2001). This has been most

extensively characterised in chicken DT40 cells in which knockout of SMC2 results in cells that are able to form mitotic chromosomes, albeit not entirely normal ones (Hudson et al., 2003). This could indicate that the role of condensin in the formation of condensed mitotic chromosomes is not universal, and may vary between cell types or organisms. In fact, rather than chromosome decondensation, loss of condensin is most commonly associated with anaphase defects such as the presence of anaphase bridges, leading to abnormal chromosome segregation.

1.2.4.1 Mechanisms of condensin

Very little is known about the mechanism by which condensin might condense chromatin. Given the structural similarity of condensin and cohesin, it has been suggested that condensin might encircle DNA, causing distal DNA segments to be brought into close proximity, in the same way that cohesin is thought to encircle sister chromatids during S phase. This hypothesis is supported by experiments showing that either linearization of circular mini chromosomes, or opening the ring structure of condensin using engineered protease cleavage sites, results in disassociation of condensin from chromosomes (Cuylen, Metz, & Haering, 2011).

This mechanism would facilitate the condensation of chromosomes, but could also inhibit the formation of sister chromatid catenations formed during replication by contracting the newly replicated DNA away from their sister DNA (Gruber *et al*., 2014). However, unlike in bacterial cells where replication and segregation occur concomitantly, metazoan chromosome condensation does not begin until long after replication has finished. In the presence of topoisomerase, condensin is known to be involved in DNA supercoiling (Kimura, Rybenkov, Crisona, Hirano, & Cozzarelli, 1999), which is thought to play a significant role in the restructuring of chromatin in preparation for mitosis.

1.2.4.2 Supercoiling

During replication or transcription, the double-stranded DNA must be unwound at a certain location, in order that polymerases can gain access to single-stranded DNA and begin replication or transcription. This unwinding causes the DNA to become overwound (positively supercoiled) in front of the polymerase, and underwound (negatively supercoiled) behind it (Gilbert & Allan, 2013; Liu & Wang, 1987). Supercoiling arises due to an inability to rotate "free ends" of the DNA around one another, and the inability of the polymerase to turn with the pitch of the helix, due to its size. This restriction of DNA can occur in several ways. For example, ends of the DNA may attach to one another forming a closed circle: a shape that is representative of bacterial circular plasmids. Supercoiling can also occur in linear DNA perhaps due to restriction of free rotation at supercoil boundaries (discussed below) or due to the rapid introduction and slow dissipation of torsion (Kouzine, Liu, Sanford, Chung, & Levens, 2004).

Positive supercoiling is the process of over-winding a DNA strand, which imposes strain on the strand, and alters its shape. The level of supercoiling is determined by the number of twists relative to a relaxed strand, and the number of times the strand crosses over itself, which is known as writhe. Writhe can form two types of supercoils: solenoidal supercoiling involves the curving of DNA into spirals around a ring (for example when DNA wraps around a protein, Figure 1.7a, left and Figure1.7b), while plectoneme supercoiling occurs when the strand crosses above and below itself: Figure 1.7a, right and Figure 1.7b (Calladine, Drew, Luisi, & Travers, 1994). Topoisomerase enzymes have the ability to relieve helical stress by cutting one or both DNA strands thereby introducing "free ends" and allowing the strands to unwind and relieve tension, before topoisomerase repairs the breaks. Topoisomerase I enzymes cleave single stranded DNA, while topoisomerase II cleaves double stranded DNA. It is likely that topoisomerase II works on most DNA strand crossovers during plectonemic writhe, and has been shown to be involved in sister chromatid separation and decatenation of circular chromosomes (Baxter *et al.*, 2011). However, the different roles of topoisomerases I and II in relieving supercoils generated by polymerases are somewhat unclear.

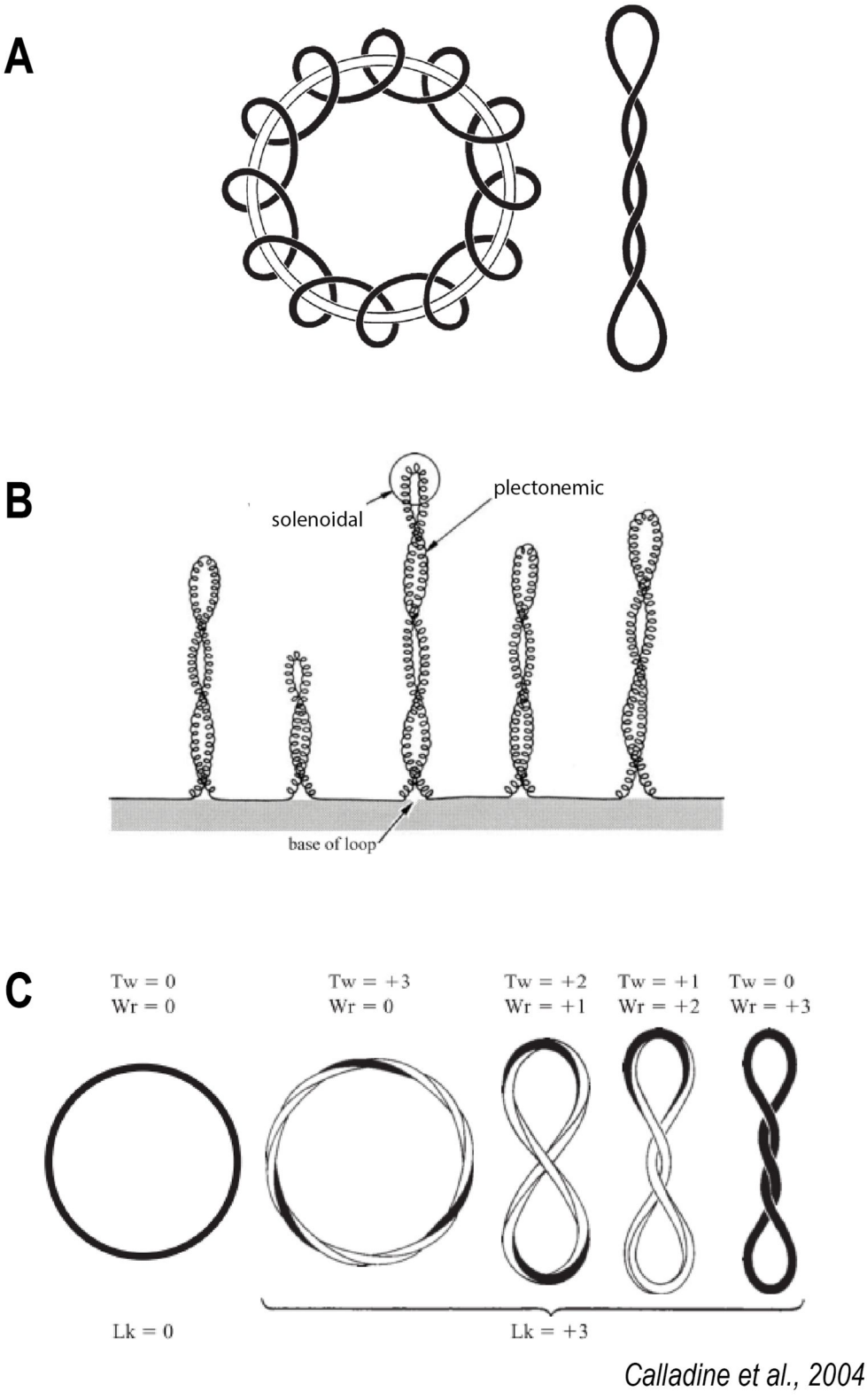

Figure 1.7
Chromosomes are supercoiled to facilitate condensation
A. Two types of supercoil within circular DNA: solenoidal (left) and plectonemic (right). **B.** Two types of supercoil within linear DNA. **C.** Five circular DNA molecules, each with different degrees of twist and writhe (Calladine *et al.*, 2004).

The linking number (Lk) is the sum of twist (Tw) and writhe (Wr). The Lk remains constant – unless the strand is cut by, for example, topoisomerase (Figure 1.7c). DNA in its relaxed state has a linking number of zero. By convention, if the DNA is overwound it is assigned a positive value for Lk, and underwound DNA is assigned a negative value.

Generally, DNA that is not being replicated (relaxed) is underwound, i.e. it has a negative Lk_0 (Champoux, 2001). *In vitro* studies have demonstrated that, in the presence of bacterial or eukaryotic topoisomerase I, condensins can alter DNA topology by forming positive supercoils (Kimura & Hirano, 1997). This change in DNA structure requires mitotic condensin, specifically. In contrast, condensin purified from interphase extracts does not introduce positive supercoils into the circular DNA (K Kimura, Hirano, Kobayashi, & Hirano, 1998).

Following the discovery that condensin acts in concert with bacterial or eukaryotic topoisomerase I to introduce positive supercoils into *Xenopus* DNA (Kimura & Hirano, 1997), work was carried out to determine how condensin might achieve this topological change. The structure of condensin provided some clues: the anti-parallel confirmation of SMC proteins (Figure 1.5a) results in the ability of condensins to bind both ATP via the C terminus, and DNA via the N terminus. ATP hydrolysis could power the complex to alter the DNA structure between the bound globular heads (Lammens, Schele, & Hopfner, 2004) thereby resulting in a more compact chromatin configuration.

Xenopus 13S condensin restructures DNA by introducing global positive writhe into a circular plasmid in the presence of topoisomerase I. This might occur when multiple condensin complexes bind to DNA and introduce a right-handed bend - Figure 1.8a (Kimura *et al*., 1999). This hypothesis is supported by the fact that proteins that bend DNA often preferentially bind to four-way junctions (Bhattacharyya *et al*., 1991): a property shared by condensin (Kimura & Hirano, 1997).

A

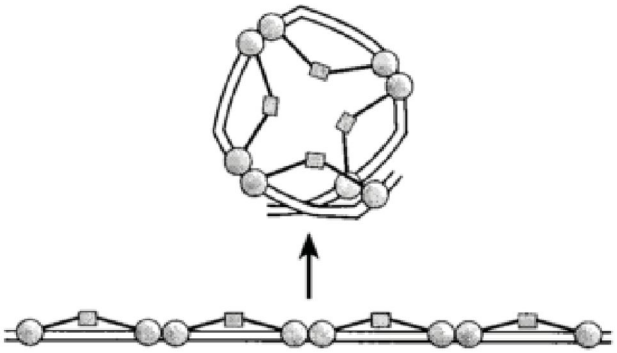

Kimura et al., 1999

B

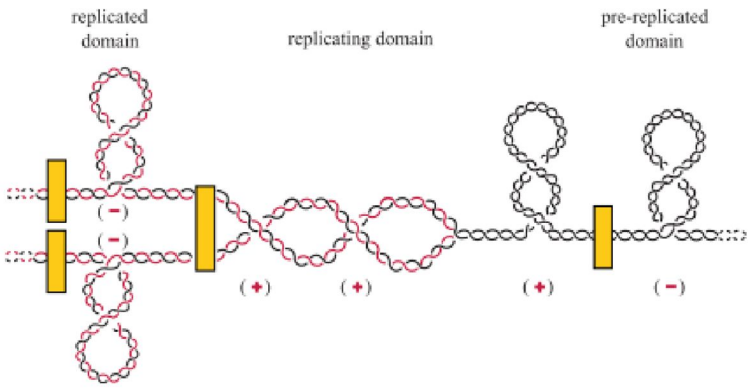

Hardy et al., 2004

Figure 1.8
Positive supercoils are introduced to facilitate condensation, but also arise as a consequence of transcription
A. Model of chromosome condensation. Condensin introduces right-hand bends into chromosomes (Kimura *et al*., 1999). **B.** Linear DNA may be constrained by barriers (shown in yellow), resulting in the introduction of positive supercoils and positive precatenanes during replication (Hardy *et al*., 2004).

The introduction of global positive writhe by condensin is an efficient way of compacting chromosomes since it causes chromosome structure to alter directly, rather than relying on the introduction of compensatory negative supercoils to bring about condensation. Therefore, it seems likely that condensin induces chromosome condensation via the introduction of global positive writhe, rather than positive supercoiling on a more local level (Kimura *et al*., 1999).

In agreement with previous studies (Kimura *et al*., 1998), mitotic condensin was found to be able to introduce topological changes to *Xenopus* DNA (supercoiling and knotting), while interphase condensin was not (Kimura *et al*., 1999). This stage specific nature of condensin mediated supercoiling is phosphorylation dependent, since the ability of interphase condensin to introduce positive supercoils and knots is greatly enhanced by Cdc2-cyclin B (Kimura *et al*., 1998; Kimura *et al*., 1999).

There are Cdc2 phosphorylation sites in the C-terminus of the condensin II subunit CAP-D2 in *Xenopus*, leading Kimura *et al*. to speculate that Cdc2 induces chromatin condensation by phosphorylating (and thereby activating) condensin (Kimura *et al*., 1998). However, inhibiting protein phosphatase 1 from localizing to mitotic chromosomes rescues condensation defects in cells depleted of condensin subunits (Vagnarelli *et al*., 2006), which may indicate that Cdc2-cyclin B and condensin reconfigure chromatin via distinct mechanisms. Vagnarelli *et al*. suggest that since chromosomes can undergo condensation and mitosis until the onset of anaphase in the absence of condensin in some model organisms (Charbin *et al*., 2014; Coelho *et al*., 2003; Steffensen *et al*., 2001), a system other than condensin must exist to compact chromosomes. This system was termed the "regulator of chromosome architecture" (RCA). It was hypothesised that the RCA system may be regulated by CDK1 phosphorylation, which induces chromosome condensation. Subsequently, condensin maintains and stabilizes the condensed state (Vagnarelli *et al*., 2006).

1.2.4.3 Disentangling DNA catenations

In order for supercoiling to have any impact on the structure of DNA, it was thought that the ends of the strands must be constrained, such that the tension produced as a consequence of unravelling the sister strands does not dissipate, i.e. the DNA strands

must be prevented from rotating relative to each other. DNA rotation might be prevented by physical barriers, which would bind to the DNA strands and constrain them. As mentioned above, however, some evidence exists to suggest that transient supercoiling might arise in linear DNA without the presence of barriers due to the rapid introduction and slow dissipation of torsion (Kouzine *et al.*, 2004), or alternatively as a consequence of increased friction due to higher order chromatin organisation (Kouzine, Levens, & Baranello, 2014).

DNA is organized into topological supercoiling domains (Worcel & Burgi, 1972). Supercoiling domains were initially investigated in prokaryotes (Hardy, Crisona, Stone, & Cozzarelli, 2004), but have also been characterised in higher eukaryotes (Naughton *et al.*, 2013). Supercoiling domains of higher eukaryotes are large areas (approximately 100kb) of overwound and underwound DNA, and are distinct from TADs (Gilbert & Allan, 2013). Experiments using psoralen, which preferentially binds to underwound DNA, indicates that supercoiling domains are approximately a tenth of the size of TADs (Bermúdez, García-Martínez, Pérez-Ortín, & Roca, 2010; Pezzulo *et al.*, 2013) – i.e. approximately the size of a replicon.

In order to carry out semi-conservative DNA replication, the linking number must be reduced to zero (Hardy *et al.*, 2004). Division of the genome into domains allows this reduction of linking number to occur across the smaller DNA segments: something that would be impossible across whole genomes. In addition, the barriers isolate the production of supercoils and precatenanes to limited areas. This may result in the ability to decondense and replicate a single domain followed by topoisomerase mediated removal of some of the resulting supercoils and precatenanes before progressing to the next domain in a systematic manner - Figure 1.8b (Hardy *et al.*, 2004). This hypothesis is only applicable when chromosome condensation occurs concomitantly with DNA replication.

If topoisomerase enzymes do not relieve the tension almost immediately, the positive supercoiling in front of the fork will increase as the fork progresses along the strand. As the fork approaches the place at which the strands are constrained (e.g. the domain barrier), less space will be available to contain the supercoils. Additionally, less space will be available for topoisomerases to act to remove the supercoils (Postow, Crisona,

Peter, Hardy, & Cozzarelli, 2001). However, the tension caused by the fork progression may be dissipated along the DNA strand if the fork is able to rotate. This rotation would result in the introduction of precatenanes between daughter strands (J. Champoux & Been, 1980). Convincing evidence exists indicating that precatenanes arise in circular plasmids both *in vitro* and *in vivo* (Adams, Shekhtman, Zechiedrich, Schmid, & Cozzarelli, 1992; Khodursky, Zechiedrich, & Cozzarelli, 1995; Peter, Ullsperger, Hiasa, Marians, & Cozzarelli, 1998; Sundin & Varshavsky, 1981). Due to the difficulty in observing catenations in linear DNA, however, there is no direct evidence for the presence of inter-strand catenations. However, the high incidence of anaphase bridges in topoisomerase mutants indicates that sister catenations may also arise in higher eukaryotes (DiNardo, Voelkel, & Sternglanz, 1984; Sundin & Varshavsky, 1980).

Processes other than fork rotation may also introduce precatenanes into sisters, including aberrant topoisomerase activity or perhaps replication fork collisions, as has been shown in SV40 cells (Sundin & Varshavsky, 1980).

Studies in the yeast *S. cerevisiae* have shown that the complete removal of catenations by topoisomerase II is dependent on the presence of mitotic spindles (Baxter *et al*., 2011; Holm, Goto, Wang, & Botstein, 1985; Uemura *et al*., 1987). Additionally, topoisomerase II activity is required as late as anaphase in budding yeast (Baxter & Diffley, 2008), implying that the cell must progress through M phase for all catenations to be resolved. However, the process of decatenation is known to begin during replication, very quickly after the catenations are introduced (Charbin *et al*., 2014; DiNardo *et al*., 1984; Sundin & Varshavsky, 1981) and several studies have concluded that sister DNA molecules are completely decatenated before the sisters are separated by the spindle (Baxter *et al*., 2011; Oliveira, Hamilton, Pauli, Davis, & Nasmyth, 2010). As discussed previously, however, investigations into sister catenations have generally been carried out using circular chromosomes, and therefore the relevance of these results to open-ended eukaryotic chromosomes is unclear.

Depletion of condensin in yeast resembles the phenotype of topoisomerase II depletion (Bhalla, Biggins, & Murray, 2002; Uemura *et al*., 1987), suggesting that the two proteins act in concert to resolve catenations. This is supported by the direct interaction

of the *E.coli* condensin homolog MukB with topoisomerase IV (Li *et al*., 2010), which is a homolog of eukaryotic topoisomerase II. Using electrophoresis assays, it was also shown that MukB can stimulate topoisomerase IV to relax plasmid DNA in a dose dependent manner (Li *et al*., 2010). However, the magnitude of the effects was not large.

Several studies have been carried out to investigate the role of supercoiling in the decatenation of prokaryotic chromosomes, and concluded that sister chromatid catenations are reduced by the introduction of intra-chromosomal supercoils (Hardy *et al*., 2004; Martínez-Robles *et al*., 2009; Zechiedrich, Khodursky, & Cozzarelli, 1997). Consequently, Baxter *et al.* set out to investigate whether decatenation of eukaryotic sister chromosomes is also facilitated by the introduction of positive supercoils. Using circular yeast plasmids depleted of functional topoisomerase II, they demonstrated that the conformation of eukaryotic circular chromosomes changes from being negatively supercoiled before mitosis, to being positively supercoiled during mitosis. Usually, however, topoisomerase II rapidly relaxes the positive supercoils. The transition from negative to positive supercoils is dependent on the presence of mitotic spindles, since it does not take place when the cells are treated with nocodazole, a microtubule-depolymerizing drug (Baxter *et al*., 2011).

It was hypothesised that the conformational changes to DNA during mitosis (i.e. the introduction of positive supercoils) might be necessary for topoisomerase II mediated decatenation. Interestingly, it was found that DNA enriched for positive supercoils was more easily decatenated by topoisomerase II than negatively supercoiled DNA (Baxter *et al*., 2011). In agreement with previous results (Kimura & Hirano, 1997; Kimura *et al*., 1999), condensin was found to be necessary for the formation of positive supercoils (Baxter *et al*., 2011). This indicates that condensin, alongside topoisomerase II, plays an important role in decatenation of sister-strands, at least in *S. cerevisiae* minichromosomes. Indeed, it has been suggested that positive supercoiling of DNA by condensin might be necessary to provide directionality to the decatenating activity of topoisomerases and thereby minimize inter-chromosomal bridging (Baxter & Aragón, 2012). Without the ability to direct topoisomerases to introduce breaks in the appropriate places, topoisomerases might introduce as many catenations as they resolve. Condensin depletion has been shown to affect the

localisation of topoisomerase II on mitotic chromosomes (Coelho et al., 2003; Hudson et al., 2003), further indicating that topoisomerase II binding is influenced by the presence of positive supercoils introduced into the DNA by condensin. However, work carried out by Vagnarelli *et al*. in chicken DT40 cells using an SMC2 conditional knock out did not reveal differential topoisomerase II activity as a consequence of condensin depletion (Vagnarelli *et al*., 2006).

In budding yeast, a recent study addressing the process of sister chromatid decatenation on circular chromosomes of different sizes, discovered that most catenanes were resolved quickly, while S phase was ongoing. However, condensin was required to complete the process of decatenation and remove all remaining catenanes. This was most evident in the largest chromosomes (Charbin *et al*., 2014).

The vast majority of studies into whether condensin acts to resolve catenations have been carried out in prokaryotes, or on circular mini-chromosomes in yeast, because catenations between linear DNA strands is lost after DNA extraction. A major challenge facing the field is to ascertain the extent to which these findings are applicable to the linear chromosomes found in eukaryotes, which can be hundreds of megabases in size and subject to a distinct set of topological constraints.

1.2.5 Condensin's role in organizing the interphase genome in preparation for mitosis

While condensin I is cytoplasmic during interphase, condensin II is nuclear (Gerlich *et al*., 2006; Tatsuya Hirano, 2012; Ono *et al*., 2004). This differential localization might indicate that condensin II-mediated condensation begins before prometaphase, when condensin I gains access to the chromosomes. This implies that chromosome condensation is a carefully timed process: first condensation by condensin II provides rigidity, and only then do chromosomes undergo lateral condensation by condensin I after breakdown of the nuclear membrane.

Consistent with the prediction that condensin II begins to restructure chromosomes prior to breakdown of the nuclear membrane during prometaphase, siRNA knockdown

studies of CAP-G or CAP-G2 levels suggested that condensin II could be important during the early stages of chromosome assembly, during prophase or prometaphase (Ono *et al*., 2004), or perhaps even as early as S phase (Ono, Yamashita, & Hirano, 2013). Most CAP-H2 was found to be detergent extractable from G1/S phase HeLa cells, but became increasingly detergent resistant as cells progressed through S to G2. This data was used to support the hypothesis that condensin II begins to associate with chromatin during S/G2, before chromosome compaction becomes evident.

Next, Ono *et al.* artificially induced chromosome condensation of early, mid and late S phase cells (determined using EdU incorporation) (Ono *et al*., 2013). G1 and G2 (EdU negative) stage cells were determined on the basis of their appearance, and number of chromosomes. The prematurely condensed early S phase chromosomes were "pulverised" into a number of small fragments, whereas the structure of the late S phase chromosomes were drastically different: in fact, discernible paired sister chromatids were observed in the early replicating regions (as judged by EdU). The researchers then carried out premature chromosome condensation in HeLa cells depleted of condensin subunits. When CAP-G (a condensin I subunit) was depleted, only minor changes to the structure of the prematurely condensed chromosomes were observed. However, drastic morphological changes were observed in the cells depleted of CAP-G2 (a condensin II subunit): the sister chromatids were no longer easily discernible, and interestingly, the chromosomes were "wavy" in appearance. The researchers inferred from this data that condensin II, rather than condensin I is crucial for PCC-driven chromosome condensation.

In addition, the researchers used FISH as an independent method to investigate the role of condensin II in the resolution of sister chromatids during S phase. To achieve this, the distance between FISH probes situated on sister chromatids was measured in late S phase cells depleted of either a condensin I (CAP-G2), condensin II (CAP-G) or a cohesin (Rad21) subunit. The cells depleted of condensin I showed no change in the distance between probes with respect to wildtype. However, the distance between probes increased in cells depleted of cohesin (as expected due to a loss of sister chromatid cohesion) and significantly decreased in cells depleted of condensin II. These data provide additional support to the theory that condensin II plays a role in the individualisation of sister chromatids during late S phase, before entry into mitosis

(Ono *et al*., 2013).

1.2.5.1 Condensin as a regulator of gene expression

An alternate explanation for the location of condensin II in the nucleus could be that it also functions during processes that are completely independent of cell division, such as transcription (Bauer *et al*., 2012; Fazzio & Panning, 2010; Haeusler *et al*., 2008; Kruesi, Core, Waters, Lis, & Meyer, 2013; Li *et al*., 2015). The possibility that condensin could be a regulator of gene expression was originally suggested by studies on *Caenorhabditis elegans* dosage compensation: a process that controls gene expression across a whole chromosome. The purpose of dosage compensation is to ensure that the genes located on the X-chromosome are equally expressed in males (XO) and hermaphrodites (XX). In *C. elegans*, this occurs by the condensin I-like dosage compensation complex (DCC) binding to both X chromosomes and reducing transcriptional output to half the level of the single male X-chromosome.

The mechanism by which the DCC controls transcription is not completely understood, but is thought to involve the reduction of RNA Pol II recruitment to promoters (Kruesi *et al*., 2013). *C. elegans* have three, rather than two condensin complexes, of which two are orthologues of condensin I (Csankovszki *et al*., 2009). As discussed previously, the DCC is almost identical in structure to condensin I, and only differs by one subunit: SMC4 is replaced by DPY-27 (Csankovszki *et al*., 2009). The DCC is involved in the restructuring of the X chromosome with the formation of a series of regularly spaced topologically associated domain (TAD) boundaries (Crane *et al*., 2015). The conformation of the X chromosome is distinct from that of autosomes since X chromosomes consist of more pronounced and more regularly spaced TAD boundaries. Interestingly, the boundaries were shown to be enriched within areas of high-affinity DCC binding sites. DCC-defective mutants caused a reduction in the number of TAD boundaries, resulting in chromosome topology that closely resembled that of autosomes (Crane *et al*., 2015).

Condensins have also been implicated in other interphase processes. Condensin promotes physical clustering of tRNA genes in the yeast nucleus, despite their being

encoded on different chromosomes (Haeusler *et al*., 2008). It has also been demonstrated that condensin II acts to inhibit transvection in flies: an interaction between homologous alleles, resulting in either gene activation or repression. The same study also demonstrated that polytene chromosomes fail to disassemble during Drosophila nurse cell development in condensin mutants (Hartl, Smith, et al., 2008). Thus, condensin complexes may serve to prevent associations between different chromosomes during both interphase and mitosis (Hartl *et al*., 2008; Wood *et al*., 2010).

The possibility that condensin may be important for the formation or maintenance of interphase chromosome territories is supported by a study of polytene chromosomes in condensin-deficient nurse cells in Drosophila. This study revealed that condensin II promotes the axial compaction of interphase chromosomes, thereby sequestering chromatin into discrete areas or "territories" (Bauer *et al*., 2012). However, mammalian chromosomes don't generally exist in a polytene configuration, so whether these findings would apply to mammals is not currently clear. Since the majority of the work into the roles of condensins in regulating gene expression had thus far focused on simpler eukaryotes, Heale *et al*. used HeLa cells to better understand the interphase roles of condensin I in higher eukaryotes (Heale *et al*., 2006). While the vast majority of condensin I is sequestered within the cytoplasm during interphase (Ono *et al*., 2003), evidence exists to suggest that a subpopulation of condensin I associates with chromatin during interphase (Li *et al*., 2015; Schmiesing, Gregson, Zhou, & Yokomori, 2000). Heale *et al*. discovered that mammalian condensin I interacts with DNA nick-sensor poly(ADP-ribose) polymerase 1 (PARP-1) and base excision repair (BER) machinery to rapidly repair single stranded breaks. Additionally, it was shown using conditional knockout DT40 cells that condensin I depletion compromises single strand, but not double strand break repair (Heale *et al*., 2006).

The diversity of the roles of condensin complexes in both chromosome segregation and interphase gene regulation indicate their adaptability: altering one subunit results in multiple complexes that are able to carry out diverse biological functions.

1.2.6 Genome instability and chromosome missegregation as a consequence of condensin mutation

Mutations in condensin can impede both chromosome resolution and condensation. Failures in either of these processes could lead to abnormal mitosis with an increased incidence of anaphase bridges (Vagnarelli *et al*., 2006; Hartl, Sweeney, Knepler, & Bosco, 2008), abnormal ploidy (Cobbe & Heck, 2000; Green *et al.,* 2012; Hardy *et al*., 2004), and ultimately, cancer. An investigation into the potential causes of lymphoma revealed mutations in condensin subunits in multiple leukaemia-lymphoma patient-derived cell lines (Ham *et al*., 2007). Three of the eight pyothorax-associated lymphoma (PAL) cell lines tested revealed either SMC2 or SMC4 heterozygous missense mutations, suggesting that mutations in condensin are reasonably frequent in PAL. Additionally, condensin I or condensin II subunit mutations have been detected in 4.2% of tumours tested by Leiserson *et al*. This represents a statistical enrichment, and therefore supports the hypothesis that these complexes play an important role in preventing chromosomal instability and tumourigenesis (Leiserson *et al*., 2015).

1.2.6.1 Interlinked sister chromatids as a consequence of the absence of condensin I in B. subtilis

A study into the importance of condensin for accurate sister chromatid segregation in *B. subtilis* found that condensin deficient bacterial cells did not undergo successful chromosome segregation when grown in rich medium. This was investigated by labelling the origin of replication, *oriC*, with GFP during spore outgrowth. A second GFP signal quickly appeared in control cells, followed by a third and a fourth, until multiple GFP signals were observed uniformly throughout the cell. Multiple GFP signals were generally absent in condensin mutant cells. However, the intensity of the signal gradually increased, leading the researchers to conclude that multiple *oriC* regions are generated, but are unable to segregate efficiently from one another (Gruber *et al*., 2014).

Using small-molecule inhibitors to slow the growth rate of *B subtilis*, and treatment with either chloramphenicol or streptolydigin (which inhibit translation and transcription respectively), the researchers investigated the possibility that rapid cell

growth rates were the cause of the condensin deficient lethality. However, under slow cell growth conditions, condensin depleted cells were still unable to grow and divide accurately. Further investigation revealed that lowering replication fork velocity, specifically, by the addition of either hydroxyurea (HU) or arginine hydroxamate (Rhx) rescued the phenotype of condensin deficient cells. The researchers concluded that condensin is essential in rapidly dividing bacterial cells with replication forks that progress quickly, but that chromosome segregation occurs almost normally in condensin mutants when the replication fork velocity is artificially slowed (Gruber *et al*., 2014).

This suggested that fast DNA replication might result in more pressure being placed on topoisomerase to untangle chromosomes, resulting in an increase in chromosomal bridging. However, Rudner *et al.* have shown that inactivation of topoisomerase IV does not hinder segregation at replication origins in *B. subtilis* (Wang, Tang, Riley, & Rudner, 2014). This implies that fast DNA replication may result in long swathes of replicated DNA situated alongside its sister DNA. Nucleoid-associated proteins may more readily bridge these sisters, resulting in an inability to separate efficiently during segregation. Gruber *et al.* suggest that condensin may be involved in contracting the newly replicated DNA away from its sister, thereby minimizing the potential for catenations. Whether these findings also apply to mammals is, as yet, unknown. However, this study does provide further support for a possible role of condensin in the restructuring of chromatin during genome duplication, specifically during rapid fork progression, as well as during segregation.

1.3 Chromosomal Instability (CIN)

Chromosomal instability is an increased likelihood of the duplication or loss of either whole or subsections of chromosomes. Mistakes in chromosome segregation can lead to chromosomal instability, resulting in the production of aneuploid cells. There is a consensus that the acquisition of an aneuploid karyotype is an early event in cancer formation, likely due to loss of chromosomes carrying tumour suppressor genes or gain of chromosomes carrying growth promoting genes, providing a selective advantage. Genome instability may also arise as a consequence of incorrect chromosome segregation resulting in lagging chromosomes, which may eventually

form micronuclei. These micronuclei undergo inefficient defective replication, leading to chromosome rearrangement in the following cell division (Crasta *et al*., 2012; Ganem & Pellman, 2012). In support of these hypotheses, Van Deursen *et al.* showed that defects in SAC genes accelerate thymic lymphomas in heterozygous p53 mutant mice, and colonic tumours in Apc mutant mice (Baker, Jin, Jeganathan, & Van Deursen, 2009). In almost all cases, the non-mutated tumour suppressor allele was absent in these tumours and had been replaced by a second copy of the mutant allele due to a mitotic non-disjunction event promoted by the CIN phenotype.

1.3.1 Mouse models of CIN

Model systems to study the consequences of CIN during development have been hampered by the essential role of mitotic genes in cell division, meaning that animals in which the function of these genes is perturbed typically die early in gestation. This has also been shown to be true in available mouse models of condensin mutation (Houlard *et al*., 2015; Nishide & Hirano, 2014). SAC and other mouse models of chromosomal instability have generally used reduction- or gain-, rather than loss-of-function systems. A recent study has indicated that haploinsufficiency for a cohesin subunit can cause defective telomere replication resulting in CIN – with accelerated tumourigenesis and high levels of aneuploidy (Remeseiro *et al*., 2012). This is further evidence of the crucial role of chromosome structure in chromosomal stability.

Many studies have shown that reducing levels of mitotic checkpoint proteins (Mad1, Mad2, Bub1, BubR1 etc.) results in a higher rate of chromosome missegregation in murine embryonic fibroblasts - "MEFs" (Baker *et al*., 2004; Weaver, Silk, Montagna, Verdier-Pinard, & Cleveland, 2007). However, the consequences of these mutations in terms of tumour formation were inconsistent. Li *et al*. expressed a dominant mutation in Cdc20, which prevents it being repressed by the mitotic checkpoint. The experiments showed that these mice exhibit high levels of aneuploidy and tumours (Li, Fang, Wei, York, & Zhang, 2009). However, other mouse models of CIN have shown that, in some cases, high levels of aneuploidy can result in decreased levels of tumour formation. For example, Rao *et al*. (2005) showed that mice carrying mutations in the Apc tumour suppressor displayed reduced levels of tumour formation in the small intestine when BubR1 was reduced (Rao *et al*., 2005). In addition, Jeganathan *et al*.

showed that reducing BubR1 further resulted in fewer spontaneous liver tumours (Jeganathan, Malureanu, Baker, Abraham, & van Deursen, 2007).

One hypothesis is that low levels of CIN – a low but still elevated frequency of chromosome missegregations per cell division – provides the increased mutation rate associated with tumourigenesis, whereas higher CIN often causes apoptosis and tumour suppression due to the more severe perturbation of cellular physiology. Highly aneuploid tumour cells may be the consequence of a gradual accumulation of missegregations over multiple cell divisions (Holland & Cleveland, 2009).

Several studies have also implicated condensin II in maintaining a stable karyotype to suppress tumourigenesis; however the current available evidence is indirect. Longworth *et al.* investigated the Drosophila retinoblastoma protein RBF1. Mutations or loss of pRB, the human ortholog of RBF1, are known to result in a variety of cancers including non-small-cell lung cancer, T cell acute lymphoblastic leukaemia and pancreatic and breast cancers. In their study Longworth *et al.* showed using biochemical techniques that RBF1 interacts with a subunit of condensin II (CAP-D3), and is involved in directing condensin II to DNA (Longworth, Herr, Ji, & Dyson, 2008). Another study revealed that depletion of the retinoblastoma protein (pRB) results in an increase in lagging chromosomes, delayed mitosis and whole-chromosome gains and losses (Manning, Longworth, & Dyson, 2010). In addition, Coschi *et al*. used gene targeted mutant mice to show that mutations in Rb1 crossed into a *Tp53*$^{-/-}$ background result in the development of tumours more quickly than *Tp53*$^{-/-}$ controls. The double mutant mice also developed more aggressive tumours, with more frequent metastases (Coschi *et al*., 2010). Although there are numerous examples of CIN influencing aging-associated phenotypes such as cancer, there are few, if any examples in the literature of CIN inducing developmental phenotypes in non-aged mice other than embryonic lethality.

Previous studies have, for the most part, utilised loss of function alleles in order to understand the roles of the condensin complexes (Green et al., 2012; Houlard et al., 2015; D. F. Hudson et al., 2003; Nishide & Hirano, 2014). There is an enrichment of condensin mutations in the COSMIC (Catalogue of Somatic Mutations in Cancer) (Forbes *et al*., 2014) and TCGA (The C ancer Genome Atlas) (Leiserson *et al*., 2015)

datasets, and the majority of these are missense (Figure 1.9). Therefore, a missense or partial loss of function mouse model may be a more relevant model of human disease.

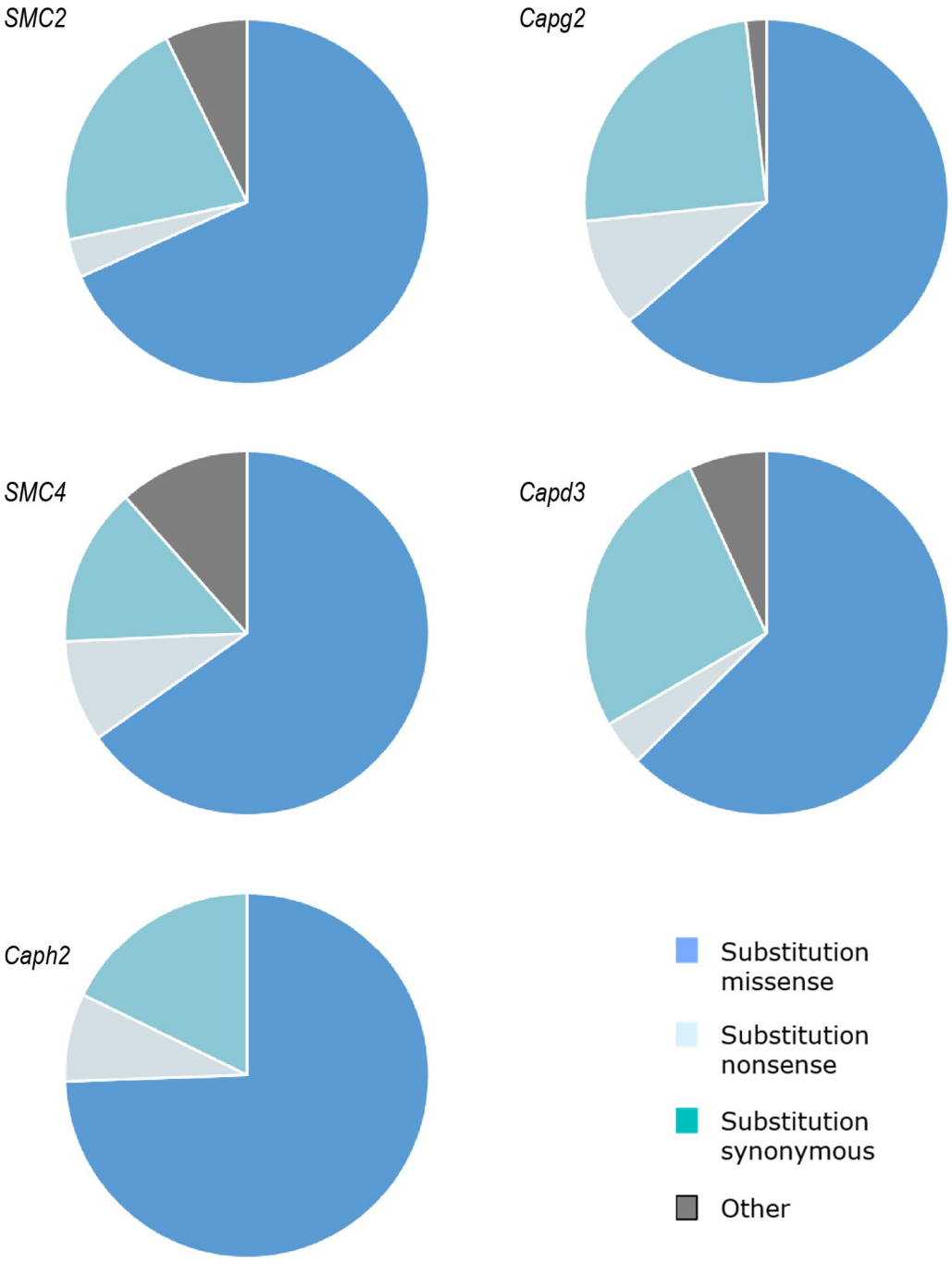

Figure 1.9
Pie charts showing the distribution of mutation types for the indicated genes
Data reveals that the majority of mutations within condensin II subunits are missense. Data was obtained from the Catalogue of Somatic Mutations in Cance, Cosmic (cancer.sanger.ac.uk): *Forbes, et al, COSMIC: exploring the world's knowledge of somatic mutations in human cancer, Nucleic Acids Research. 2015.*

1.3.1.1 The "nessy" mouse model

The nessy mutation originated from a forward genetic screen and arises due to a single nucleotide change (a T to A substitution) within the evolutionarily conserved N-terminus of the kleisin-β subunit (CAP-H2) of condensin II (Figure 1.10), a ~1Mb region on Chromosome 15 containing no previously identified T cell differentiation genes (Gosling *et al*., 2007; Bürmann *et al*., 2013; Piazza *et al*., 2014). The mutation results in an Ile to Asn amino acid substitution within the long isoform of *Caph2*, i.e. a conserved hydrophobic amino acid is substituted for a polar residue.

The mutation results in a developmental block: peripheral T cell numbers are reduced by approximately two to threefold in *Caph2*$^{nes/nes}$ mutants, but the most pronounced defects occur in the thymus where the developmental block results in a more than one hundred-fold decrease of $CD4^+$ $CD8^+$ double positive (DP) thymocytes.

Since forward genetic screens can result in the introduction of multiple point mutations, it was necessary to determine that the identified nucleotide change within the condensin II complex was the cause of the nessy phenotype. This was achieved by transducing haematopoietic stem cells with wildtype *Caph2* long isoform cDNA. The researchers showed that untransduced nessy cells exhibited the nessy developmental phenotype, while cells successfully transduced with the wildtype allele did not, thereby proving that the T cell specific block in development is caused by the mutation to condensin II (Gosling *et al*., 2007).

The Ile to Asn substitution is not present in either the short or intermediate isoforms. A different substitution is encoded in the intermediate isoform. However the long isoform is thought to be the most important because it is highly conserved, and because cDNA encoding the long form was sufficient to rescue the developmental phenotype.

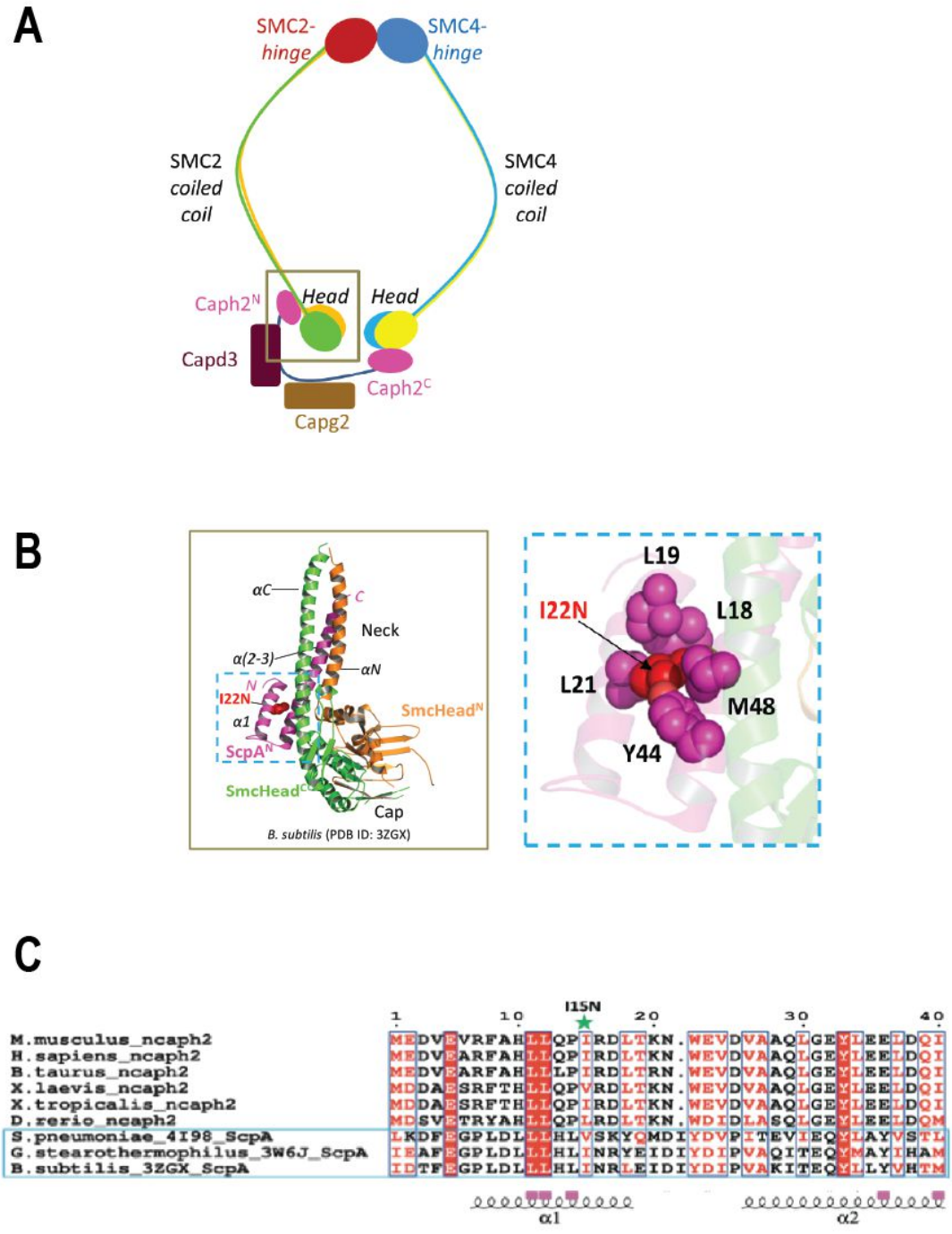

Figure 1.10
Position of the *Caph2* mutation
A. Schematic of condensin II (Burmann *et al.* 2013, Piazza *et al.* 2014). The region within the box is expanded in figure B. **B.** (Left) 3D structure of the SMC head and ScpA N-terminal domains in *B. subtilis* (Burmann *et al.*, 2013). The region within the dashed box is expanded (right). The residue equivalent to I15 in *B. subtilis* is indicated. **C.** Multi-species amino acid alignment of the conserved N terminal region. *Caph2*$^{nes/nes}$ mutation is indicated by the green star (Burmann *et al.* 2013).

Caph2$^{nes/nes}$ homozygotes are viable and fertile, with no major morphological abnormalities, with the exception of the thymus: there is a noticeable reduction in the size of the *Caph2*$^{nes/nes}$ thymus, and a reduction in cellularity within the cortex. Since the cortex contains mostly CD4$^+$ CD8$^+$ double positive (DP) thymocytes, this decrease in cellularity is to be expected given the reduction in DP *Caph2*$^{nes/nes}$ thymocytes. The observable phenotype is highly T cell specific, with B cell numbers apparently unaffected. This is somewhat surprising, considering T cells and B cells undergo similar processes (i.e. stages of proliferation interspersed with stages of VDJ recombination) during development. In addition, since the condensin complexes are thought to be ubiquitous and perform vital roles in all dividing cells, the T cell specific phenotype is highly unexpected.

Several potential causes for the reduction in numbers of *Caph2*$^{nes/nes}$ DP thymocytes were considered. The mutant CD4$^+$ CD8$^+$ DP thymocytes showed high levels of annexin V staining, causing the researchers to question whether the nessy mutation affects expression of IL-7Rα (an essential protein, necessary for T cell survival) resulting in increased apoptosis of the *Caph2*$^{nes/nes}$ thymocytes. IL-7Rα was, however, found to be expressed on the mutant thymocytes, ruling out deficiency of the interleukin as a possible cause of the reduction in cell numbers.

Pre-rearranged TCR transgenes (which eliminate the requirement for VDJ recombination) were used to test whether defective VDJ recombination could be the cause of the T cell specific developmental block in *nessy*. Abnormal VDJ recombination could prevent the expression of functional T cell receptor subunits that are necessary to receive signals that facilitate developmental progression. It was found that the transgenes failed to rescue the block in development in *Caph2*$^{nes/nes}$ cells, suggesting that VDJ recombination is not the primary cause of the nessy phenotype, and that the block occurs after the β selection checkpoint, during the proliferative expansion of β-selected cells (Figure 1.12, Table 1.1).

Finally, in order to test the hypothesis that the *Caph2*$^{nes/nes}$ thymocytes are less able to proliferate resulting in an overall reduction in numbers, the researchers used BrdU incorporation to study the rates of proliferation of *Caph2*$^{nes/nes}$ cells relative to wildtype at various stages of T cell differentiation. However, Gosling *et al.* did not find reduced

levels of *Caph2*$^{nes/nes}$ proliferation at the CD4^{+} CD8^{+} DP stage of development: the stage at which the block in nessy development becomes apparent.

Given the cell lineage-specific phenotype of the nessy condensin mutant mice, the researchers concluded that the T cell specific defect in *Caph2*$^{nes/nes}$ mice is most likely caused by a separation of function allele of kleisin β. This mutation was suggested to alter the proposed role of condensins in transcriptional regulation, (known to take place in yeast and *Drosophila* through interactions with either a histone deacetylase or a polycomb group protein (Hirano, 2005)), rather than its well-known role in mitosis (Gosling *et al*., 2007). However, neither possibility was tested empirically.

Further analysis into the *Caph2*$^{nes/nes}$ mouse was carried out by Rawlings *et al*. who deduced the degree of chromatin compaction using several techniques, including the ability of antibodies to access the histones (Rawlings, Gatzka, Thomas, & Ihle, 2011). The researchers discovered that the histones of wildtype mouse T cells were readily detectable at the CD4^{-} CD8^{-} double negative (DN) stage (implying that the chromatin was decondensed at this stage) whereas they were unable to detect the histones at either the CD4^{+} CD8^{+} double positive (DP) or CD4^{+}/CD8^{+} single positive (SP) stages (indicating a more condensed chromatin state). Further evidence of decompaction at specific stages of development was inferred from flow cytometry forward scatter data (a marker for cell size) and electron micrograph images. The researchers inferred from this evidence that chromatin decompaction occurs at a very specific stage of T cell development to allow activation of naïve T cells. Prior to this, the cells must remain in a compact state, in order to avoid premature activation. The researchers concluded that the compaction of chromatin is dependent on condensin II, since *Caph2*$^{nes/nes}$ mutants revealed a decompacted chromatin state, according to their assays (Rawlings *et al*., 2011). In agreement with the previous study into the *Caph2*$^{nes/nes}$ mutation, Rawlings *et al*. concluded that the mutation within condensin II most likely impacts epigenetic processes: specifically, the compaction of interphase chromatin.

1.4 The haematopoietic system

I have used various haematopoietic populations to investigate the consequences of condensin II deficiency on cell cycle regulation. There are many advantages to using this system: haematopoiesis is a paradigm for the differentiation of multiple cell types from a single stem cell precursor – as a result, the consequences of condensin perturbation may be investigated in many different, but related cell types. Haematopoietic development generates a diverse range of functionally specialised cell types, many of which undergo extensive cellular proliferation during the differentiation process. In addition, this system offers convenient cellular phenotyping using flow cytometry to assess developmental stage and cell cycle parameters in individual cells in a high throughput manner. Throughout this thesis, I have focused on early haematopoietic progenitors, T cells, B cells and erythroid cells. I will therefore introduce only these lineages here.

In adult mice, haematopoietic stem cells reside in the bone marrow, where they differentiate into multipotent progenitor cells that divide and give rise to all mature blood cell types (Figure 1.11). The concept of self-renewing multipotential haematopoietic precursors was initially put forward when it was discovered that mice that had undergone lethal levels of irradiation could be saved when they were injected with healthy bone marrow (Micklem & Loutit, 1966). These haematopoietic progenitors do not express the lineage markers characteristic of the later stages of differentiation: B220 (B cells), CD4 and CD8 (T cells), Ter119 (erythroid cells), Gr-1 (granulocytes) and Mac-1 (myelomonocytic cells). It was discovered that the haematopoietic stem cell population can be further purified based on the expression of Sca-1 (stem cell antigen-1) (Spangrude, Heimfeld, & Weissman, 1989) and the mouse receptor, c-kit, also known as CD117 (Ikuta & Weissman, 1992). It should be noted, however, that Sca-1 can only be used as a stem cell marker in certain mouse strains, such as C57BL/6 (Wognum & Szilvassy, 2013). This population of haematopoietic progenitor cells are known as LSK ($Lin^{-}Sca\text{-}1^{+}c\text{-}kit^{+}$) cells, which contains both the true haematopoietic stem cells and their direct derivatives. The LSK population can thus generate all haematopoietic cell types.

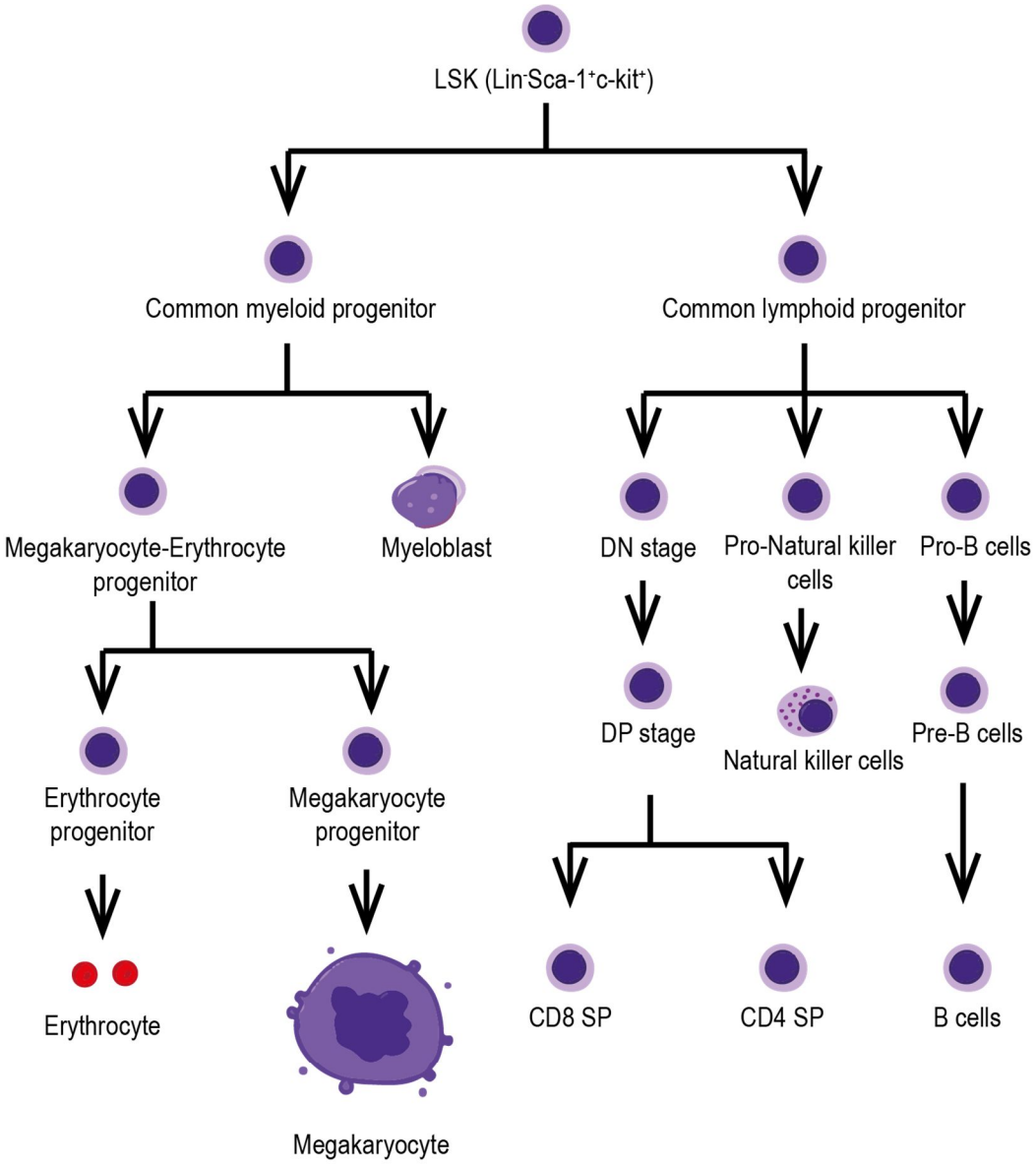

Figure 1.11: Schematic showing several stages of haematopoietic differentiation

Blood cells can be divided into two major lineages: myeloid (including erythrocytes, megakaryocytes and macrophages), and lymphoid (including T and B cells). Once the lymphoid and myeloid progenitors have been formed in the bone marrow, they migrate to other locations (for example, the liver, the thymus or the spleen) to proliferate and differentiate further.

1.4.1 αβ-T cell development

The adult thymus consists primarily of two cell types, lymphoid and epithelial. Thymic epithelial cells develop first, and play a role in the generation and subsequent selection (self-antigen presentation) of developing T cells (Anderson & Takahama, 2012). From approximately embryonic day E15.5 onwards, small numbers of lymphoid progenitors seed the thymus where they mature and commit to the T cell lineage (Koch & Radtke, 2011). At this stage, the cells are double negative (DN) for the major T cell lineage markers, CD4 and CD8. The cells then begin to undergo VDJ recombination, and rearrange their T cell receptor genes. The α/β T cell receptor comprises two variable chains: α and β, encoded by two distinct loci. The β locus is the first to rearrange, and at this point the cells exit the cell cycle. Alternatively, cells may rearrange their gamma and delta chains and differentiate along the TCRγδ, rather than the TCRαβ lineage.

Cells which generate out-of-frame rearrangements at the T cell receptor β locus are unable to assemble pre-T cell receptor complexes, and thus do not proliferate, but instead undergo apoptosis. TCR-β rearrangements that have occurred in-frame, however, pass the β selection checkpoint, proliferate rapidly in response to signalling via the pre-T cell receptor and downregulate CD25 expression to progress from DN3 to DN4 stage cells (Ho, Tai, & Pai, 2009). Later, these cells upregulate the CD4 and CD8 cell surface markers to become $CD4^+$ $CD8^+$ double positive (DP) and relocate to the thymic cortex. There are two major signalling pathways responsible for driving αβ-T cell development to the DP stage. Notch is important in early thymic T cell precursors for T cell lineage commitment. At the DN3 stage, pre-TCR signalling plays a more prominent role and is responsible for the selective expansion of cells that have undergone successful VDJ recombination.

Upon cell cycle exit, $CD4^+CD8^+$ (DP) cells downregulate the transferrin receptor

CD71 and rearrange the α-chain locus. The cells that successfully rearrange their α-chains then undergo two rounds of selection. In the first round, T cells are tested for their ability to bind the major histocompability complex (MHC – "positive selection"), which is essential for their function in an adaptive immune response. This process is termed "positive selection". The cells that have successfully passed positive selection proceed to downregulate either CD4 or CD8 to become single positive thymocytes. Next, T cells are tested for their ability to interact with self-peptides, and those which do so too strongly are removed by apoptosis, in order to prevent autoimmune responses.

Of the approximately 50 million $CD4^+$ $CD8^+$ DP thymocytes generated in the mouse thymus each day, approximately 90% - 95% will fail to progress past positive and negative selection (Kyewski & Klein, 2006). The expression of cell surface markers used to determine stages of T cell development is illustrated in Figure 1.12 and the relationship between stage of development and VDJ recombination is presented in Table 1.1.

The single positive cells then relocate to the periphery, where they remain in a G0, quiescent state, with reduced transcription levels until they are stimulated to proliferate when they are presented with their cognate antigen by the MHC complex on dendritic cells. The cells proliferate rapidly, and facilitate the destruction of the invading pathogen.

TCR activation is a tightly controlled process, in order to prevent premature activation of T cells and so autoimmunity does not occur. Stimulation via the TCR of naïve single positive CD4 cells results in the upregulation of the transcription factor GATA-3, which binds to loci encoding T Helper 2 (Th2) cytokines (Yamane & Paul, 2012). In addition to this, stimulation via the TCR generates production of interleukin 2 (IL-2) in both CD4 and CD8 T cells, which causes Stat5 proteins to be phosphorylated. The phosphorylated Stat5 protein dimerizes and translocates to the nucleus where it is bound to DNA and promotes transcription of genes that promote proliferation and differentiation into Helper ($CD4^+$) or cytotoxic ($CD8^+$) T cells.

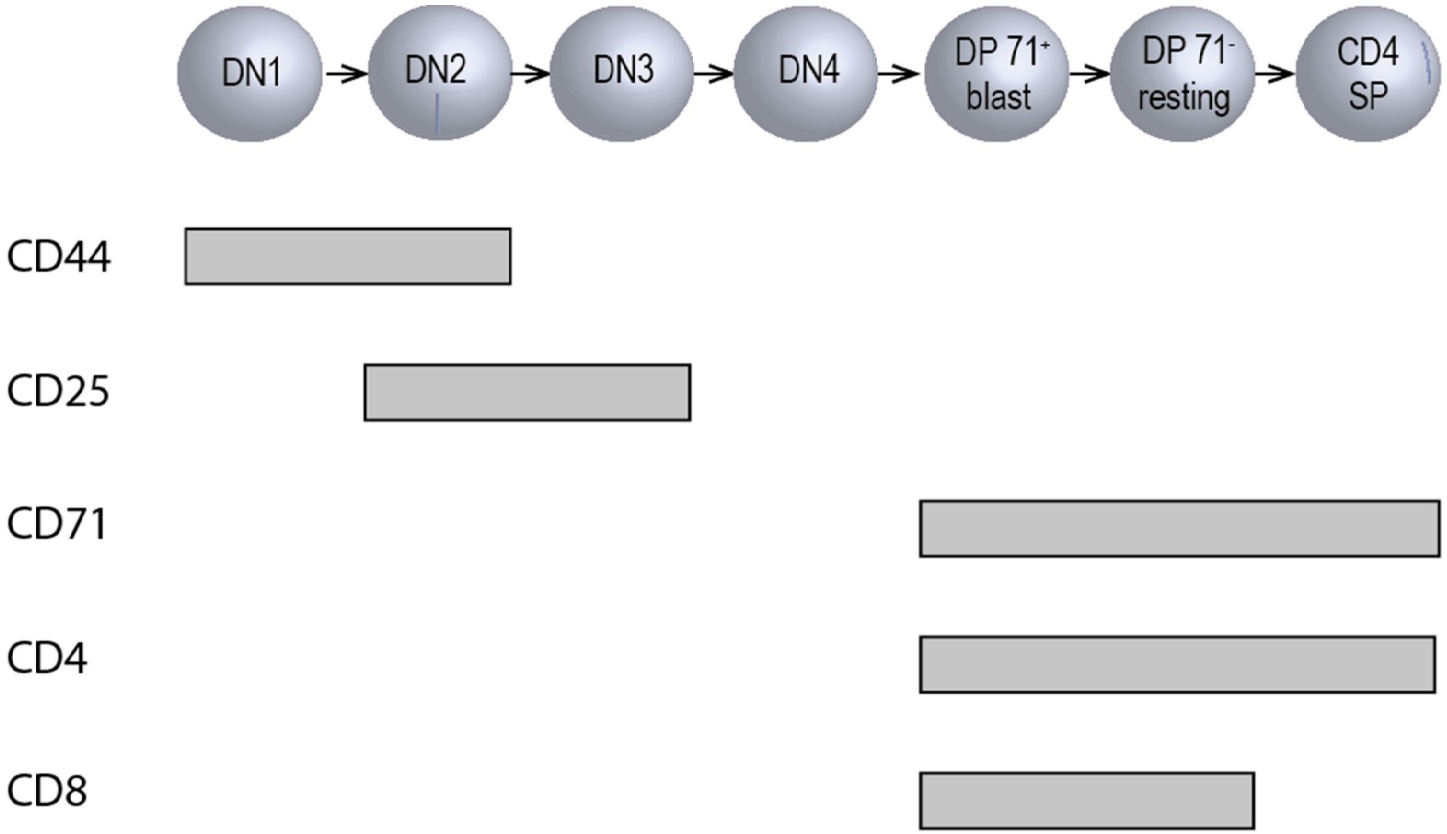

Figure 1.12
Schematic showing the stages of thymic T cell differentiation, in relation to expression of cell surface markers.

Developmental stage	Beta (β) Chain	Alpha (α) Chain
$CD4^-$ $CD8^-$ DN1	germline	germline
$CD4^-$ $CD8^-$ DN2	D-J	germline
$CD4^-$ $CD8^-$ DN3	V-DJ	germline
$CD4^-$ $CD8^-$ DN4	VDJ rearranged	germline
$CD8^+$ Intermediate Single Positive	VDJ rearranged	germline
$CD4^+$ $CD8^+$ DP 71^+ blast	VDJ rearranged	V-J
$CD4^+$ $CD8^+$ DP 71^- quiescent	VDJ rearranged	VJ rearranged

Table 1.1
Stages of VDJ recombination in developing T cell
During T cell development D-to-J rearrangement occurs first, in the beta-chain of the TCR. DNA between these two segments is deleted during the DN2 stage of development. Subsequently, the rearranged D-J segment joins to an upstream V segment, and the intervening DNA is deleted. VDJ rearrangement of the beta locus is completed during the DN3 stage of development. Successful completion of beta rearrangment is followed by a burst in proliferation.
Rearangement of the alpha chain occurs at the DP stage of development. The D segment is absent from the alphas chain, but V-J rearrangement takes place, as described for the beta chain. The cells which have undergone successful alpha rearrangment undergo rapid proliferation at the DP 71^+ blast stage of T cell development.

The block in thymic development in *Caph2*$^{nes/nes}$ mice is first apparent by reduced numbers of rapidly proliferating cells that have undergone β-selection (i.e. DP cells – Figure 1.12, Table 1.1). The block occurs after the expression of TCRβ protein, indicating that faulty VDJ recombination is unlikely to be the principle cause. This is further supported by the finding that pre-rearranged T cell receptor transgenes fail to rescue block in T cell development (Gosling *et al*., 2007). This does not rule out the possibility that condensin plays a role in VDJ recombination, as has been shown for cohesin (Seitan *et al*., 2011). Rather, the data suggests that the process is not majorly affected by the single amino acid change in *Caph2* present in the nessy mouse.

1.4.2 B cell development

B cell development occurs in the fetal liver before birth, and continues in the bone marrow afterwards. The bone marrow, therefore, contains B cells at various stages of development. Cells committed to the B cell lineage can be identified by the expression of B220, a cell surface lineage marker. The earliest cells lack the surface marker CD19, which is expressed at all later stages of B cell development. The earliest stages of B cell development are characterised by the accumulation of CD24, followed by BP-1 upregulation, and finally loss of CD43 expression. These individual stages were determined using flow cytometry, and named Fraction A ($B220^+$ $CD43^+$ $CD24^-$ BP-1), Fraction B ($B220^+$ $CD43^+$ $CD24^+$ BP-1^-), and Fraction C ($B220^+$ $CD43^+$ $CD24^+$ BP-1^+) (Hardy, Carmack, Shinton, Kemp, & Hayakawa, 1991). The gating strategy used to determine each of the Hardy stages of B cell development by flow cytometry is shown in Figure 1.13 (Hardy *et al*., 1991).

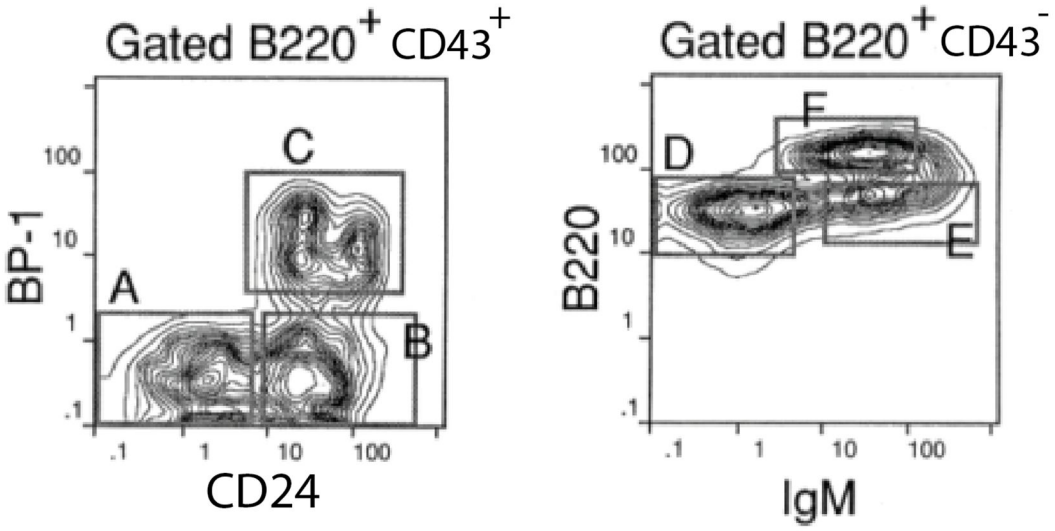

Figure 1.13
Gating strategy to determine stages of B cell development
Schematic showing the different stages of B cell development, as determined by expression of cell surface markers (Modified from Hardy *et al*., 1991).

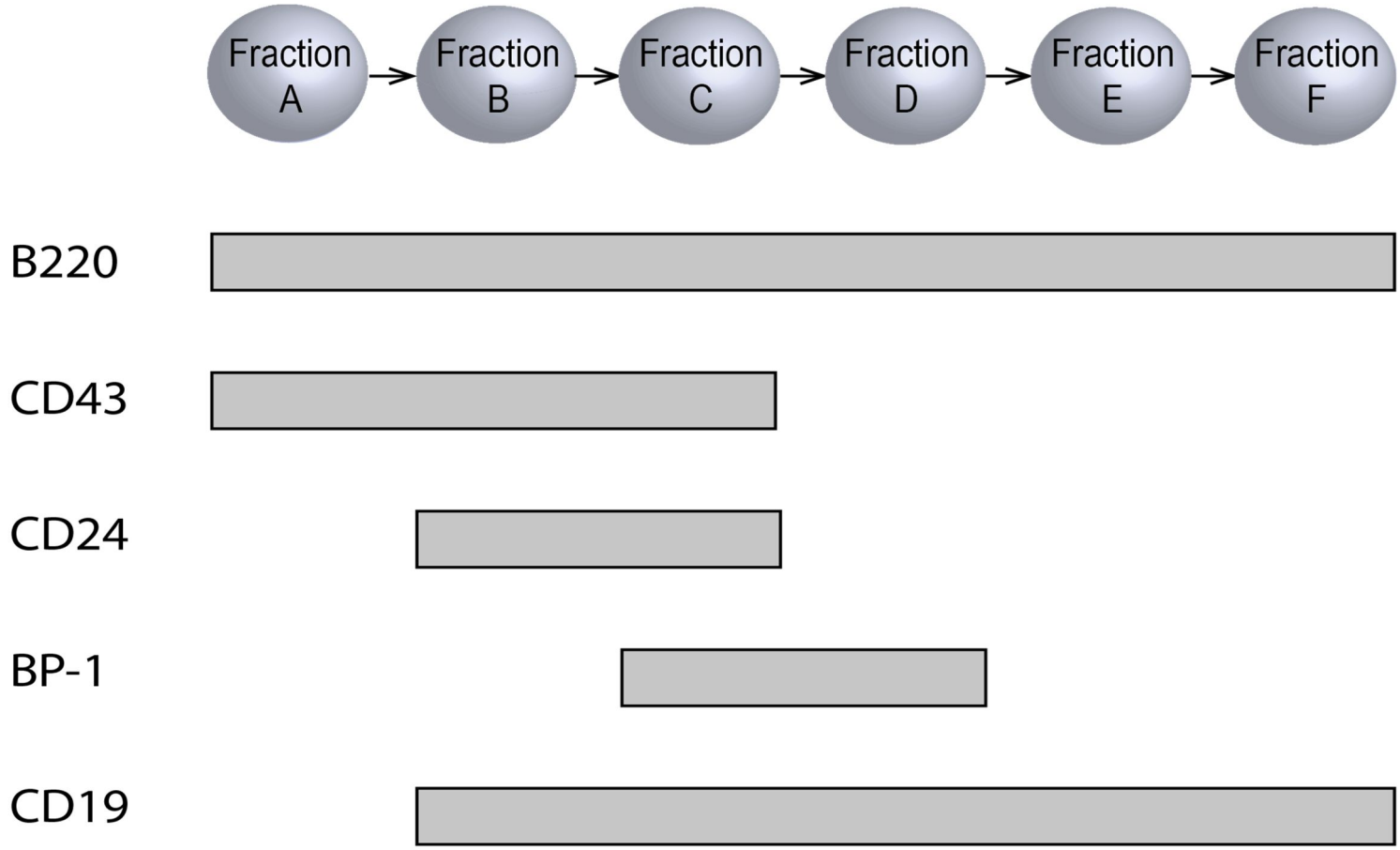

Figure 1.14
Schematic showing the stages of B cell differentiation, in relation to expression of cell surface markers.

There are many parallels in the development of T and B cells: for example, both undergo successive rounds of VDJ recombination, followed by stages of rapid proliferation. In the B cells, D-J rearrangement of the Heavy (H) chain genes begins at the Fraction B stage and V-DJ rearrangement is completed in cells of Fraction C. If rearrangement is successful, the H chain forms part of a pre-B cell receptor, which drives massive proliferation in response to signalling. This stage is known as Fraction C, and is loosely equivalent to the rapidly proliferating β-selected T cells (DP blast cells). In the absence of Ig rearrangement, cells cannot progress to later stages of development: for example, SCID mice are unable to rejoin DNA effectively during rearrangement of the H chain, and are therefore blocked at Fraction C in development (Reichman-Fried, Hardy, & Bosma, 1990). Similarly, inhibition of double strand break formation during Ig rearrangement in RAG-2-deficient mice results in a similar block in development (Mombaerts *et al*., 1992; Shinkai *et al*., 1992).

After the burst of proliferation, the cells downregulate CD43 and exit the cell cycle. The subsequent stages of development are classified based on IgM and B220 expression: Fraction D ($B220^{+}$ $CD43^{-}$ IgM^{-}), Fraction E ($B220^{+}$ $CD43^{-}$ IgM^{+}) and ($B220^{++}$ $CD43^{-}$ IgM^{+}) (Hardy *et al*., 1991). The expression of markers used to determine individual stages of B cell development are presented in Figure 1.14.

Rearrangement of the Light (L) chain genes begins during Fraction E, and is completed by Fraction F. The relationship between stage of development and VDJ recombination is presented in Table 1.2. Like the T cells, B cells that fail to produce functional H or L chains undergo apoptosis. Cells that succeed go on to undergo positive and negative selection, which ensures that the cells recognise antigens derived from pathogens, but do not recognise self-pathogens. Mistakes in this process can lead to autoimmunity (Hardy & Hayakawa, 2001).

Hardy Fraction	Developmental stage	Heavy Chain	Light Chain
Fraction A	Progenitor pre-pro B	germline	germline
Fraction B	Early pro (pre-pre) B	D-J	germline
Fraction C	Late pro (pre-pre) B	V-DJ	germline
Fraction D	Pre B	VDJ rearranged	germline
Fraction E	Immature B	VDJ rearranged	V-J
Fraction F	Mature B	VDJ rearranged	VJ rearranged

Table 1.2
Stages of VDJ recombination in developing B cell
During B cell development D-to-J rearrangement occurs first, in the heavy chain locus. Subsequently, the rearranged D-J segment joins to an upstream V segment. VDJ rearrangement of the heavy chain is completed by the stage of development called Fraction C. Following successful rearrangement, the cell undergoes a burst of proliferation.
Rearangement of the light chain occurs during Fraction E. The D segment is absent from the light chain, but V-J rearrangement takes place, as described for the heavy chain. Again, successful rearrangment is followed by a proliferative burst.

1.4.3 Erythroid development

Erythroid cells are responsible for oxygen transport and are produced in massive numbers. Therefore, like lymphocyte development, erythropoiesis requires extensive cellular proliferation. During fetal development, erythropoiesis occurs in the liver and spleen. During the final stages of gestation, the primary site of production is transferred to the bone marrow.

The major regulator of the production of erythroid cells is the cytokine erythropoietin (EPO). The committed erythroid progenitor cells experience a proliferative burst in response to erythropoietin stimulation, during which time they condense their nuclei and ultimately undergo enucleation to become immature erythrocytes (reticulocyte) (Ji, Murata-Hori, & Lodish, 2011). The process of enucleation is not well understood. The main model of enucleation is asymmetric cytokinesis and is based on the hypothesis that nuclear extrusion occurs as a consequence of a particular type of cell division. According to this model, the process of enucleation produces a small cell with almost no cytoplasm called the pyrenocyte (this is the expelled nucleus) and an anucleate reticulocyte that will form the mature erythrocyte (Giger & Kalfa, 2015). This model is supported by several pieces of evidence, including the presence of a structure resembling a cleavage furrow (Koury, Koury, & Bondurant, 1989; Repasky & Eckert, 1981; Skutelsky & Danon, 1970). In addition, the process of enucleation is dependent on actin: a protein which forms microfilaments which are essential for successful cytokinesis. The depolymerizing agent cytochalasin D inhibits enucleation *in vitro*. (Koury *et al*., 1989; Repasky & Eckert, 1981), further supporting the hypothesis that cell division is the mechanism by which enucleation takes place.

Stages of erythroid development can be determined through the expression of cell surface markers, specifically CD71 and Ter119 (Figure 1.15). Five sequential stages of erythroid differentiation: R1, R2, R3, R4 and R5, can be isolated from the population using the main cell surface markers (Zhang, Socolovsky, Gross, & Lodish, 2003).

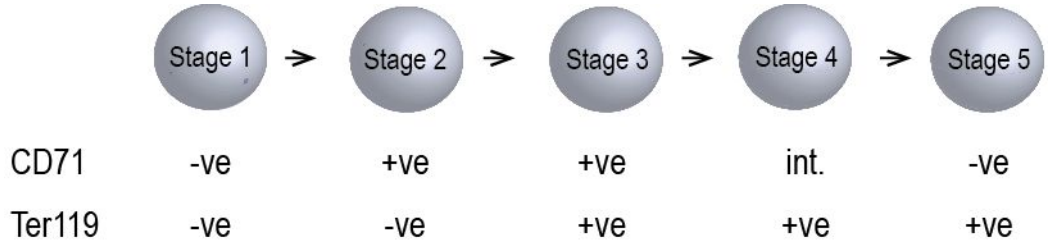

Figure 1.15
Schematic showing the stages of erythroid differentiation, in relation to expression of cell surface markers CD71 and Ter119. Intermediate levels of cell surface markers are indicated by "int."

1.5 Thesis Aims

The core aim of this thesis is to understand why a mutation to a ubiquitously expressed protein which functions in a fundamental cellular process would result in such a cell-type specific block in development. To achieve this, I investigated the possibility that condensin II is involved in interphase processes, and that this function is affected most severely by the mutation to condensin II. I also investigated the possibility that the mutation impacts the best-known role of condensin II in mitosis. In addition, I studied the aspects of T cell development that may make this lineage particularly vulnerable to condensin II deficiency. Finally, I carried out a preliminary investigation into the biochemical properties of the condensin complexes.

CHAPTER 2: MATERIALS AND METHODS

2.1 Stock solutions, reagents and buffers

Water used in solutions is deisonised, and solutions were stored at room temperature unless otherwise stated.

Table 2.1	Commonly used buffers
Acetate buffer	5M potassium acetate, 11.5% glacial acetic acid
Antibiotic Stock solution:	
Chloramphenicol	25µg/µL in ethanol, aliquoted and stored at -20°C
Blocking buffer (FISH)	4x SSC, 5% Marvel
Blocking buffer (Western)	5% Marvel or 3% BSA in TBS with 0.2% Tween 20
DNA loading buffer	50% glycerol, 5mM EDTA pH8, 0.3% Orange G (v/v)
FISH Hybridisation Mix	50% deionised formamide (v/v), 10% dextran sulphate (v/v), 1% Tween 20 (v/v), prepared in 2x SSC
Gradient Buffer (Sucrose gradients)	50mM Tris HCl pH 7.5, 150mM NaCl, 1mM EDTA
GTE buffer	50mM glucose, 25mM Tris-HCl pH8, 10mM EDTA, stored at 4°C. Approximately 10mg lysozyme/mL was added prior to use
Hypotonic	0.5% sodium citrate, 0.25% potassium chloride, prepared in deionised

buffer (metaphase spreads)	water
LDS loading buffer **Reducing agent**	NuPage LDS Sample Buffer (4x) (Life Technologies cat#1606369) NuPage Reducing agent (10x) (Life Technologies cat#1413173)
Luria agar*	Per litre: 10g tryptone, 5g yeast extract, 10g NaCl, 15g agar
Luria - Bertani (LB) broth*	Per litre: 10g tryptone, 5g yeast extract, 10g NaCl, 1g glucose
Lysis buffer (fosmid miniprep)	0.2M NaOH, 1% SDS (v/v), made fresh prior to each use
Lysis buffer (Sucrose gradients)	50mM Tris HCl pH 7.5, 150mM NaCl, 1mM EDTA, 1% DNAse, 1% RNAse, 1% Triton X, protease inhibitors
Nick Translation Salts	Made as a 10x solution, which was aliquoted and stored at -20°C. 0.5M Tris pH7.5, 0.1M $MgSO_4$, 1mM DTT, 0.5mg/mL BSA fraction V (Sigma)
NP-40 Lysis buffer	50mM Tris HCl pH8, 150mM KCl, 1.5mM $MgCl_2$ 0.1M DTT, 0.2mM EDTA, 1% NP-40. Aliquoted and stored at -20°C. Protease inhibitor cocktail (Calbiochem) was added immediately prior to use.
Phosphate Buffered Saline (PBS)*	160mM NaCl, 3mM KCl, 8mM Na_2HPO_4, 1mM KH_2PO_4 from tablets (Oxoid, Thermoscientific, cat#BR0014)
RIPA buffer	1% NP-40 (v/v), 0.5% sodium deoxycholate (v/v), 0.1% SDS in 1x PBS. Protease inhibitor Cocktail added immediately prior to use. Buffer made fresh each use, and passed through a 0.2 micron filter.
Saline Sodium Citrate Buffer (SSC)*	Per litre for 20x solution: NaCl 175.3g, $Na_3C_6H_5O_7$ 88.2g
Tris-Acetate	40mM Tris base, 20mM acetic acid, 1mM EDTA. Prepared as 50x

EDTA (TAE) Buffer	stock.
TE buffer*	10mM Tris-HCl pH7.6, 1mM EDTA
Tris Buffered Saline (TBS)	50mM Tris-HCl pH7.4, 150mM NaCl. Made as 10x stock
MOPS Running buffer	NuPage MOPS SDS Running Buffer (20x) (Life Technologies cat#NP0001)
Western Transfer Buffer	25mM Tris base, 200mM glycine, 20% methanol (v/v), 0.02% SDS (v/v). Made fresh prior to use.

*Prepared by Technical Services at MRC HGU IGMM.

2.2 Methods

Centrifugation steps were performed at room temperature unless otherwise stated.

2.2.1 Cell culture

All cells were incubated under the same growth conditions at 5% CO_2 levels.

2.2.1.1 MEFs:

Cells were maintained in DMEM medium + L-Glutamine (Invitrogen cat#41965-039) supplemented with 15% FCS, 1% Penicillin Streptomycin, 1% β-mercaptoethanol (50μM/0.00035%), 1% Non-Essential Amino Acids and 1% sodium pyruvate (NaPyr). Cells were passaged at approximately 80% confluence.

2.2.1.2 OP9 in vitro Proliferation and Differentiation System:

Cells were maintained in αMEM medium (+nucleosides) (Invitrogen cat#22571020) supplemented with 20% FCS, 1% Penicillin Streptomycin and β-mercaptoethanol (50μM/0.00035%).

Passaging

The OP9/DL1 cells (OP9 cells expressing the notch ligand DL1) were passaged every 3 days seeding $2x10^5$ cells into a fresh T75 flask. The cells were passaged by incubating the cells at 37°C in 3mL TrypLE Express (1x) (Life Technologies) for 3 to 5 minutes. The TrypLE Express was neutralised by adding 15mL media and transferring to a 50mL Falcon Tube to be centrifuged and re-suspended in fresh medium.

Seeding OP9/DL1 cells for Primary T cell culture

OP9/DL1 cells were seeded 24 hours before the thymocytes were added to the culture. The OP9/DL1 cells were dissociated, neutralised (as above) and counted on a haemocytometer. The cells were seeded at a concentration of $20x10^3$ cells per mL of media. 3mL of media was added to each well of a 6-well plate.

Primary T cell cultures

Primary T cells were cultured on OP9/DL1 monolayers (de Pooter and Zúñiga-

Pflücker, 2007). Primary T cells were MACS purified (according to manufacturer's instructions) to deplete CD4 positive cells using CD4 (L3T4) MicroBeads (Miltenyi Biotec cat#130-049-201). The cells were counted using a haemocytometer. $250x10^3$ *Caph2*$^{+/+}$ cells were seeded per well of a 6-well plate, and $250x10^3$ *Caph2*$^{nes/nes}$ cells were seeded per well of a separate 6-well plate. IL-7 was added to each well at a concentration of 1ng/mL. The cells were cultured for 4 days before being treated and analysed.

The T cells were removed by mechanical dissociation (gentle agitation of the media using a p1000 pipette), without removing the adherent monolayer of OP9 DL1 cells. The media was allowed to pass through a 40µm nylon mesh cell culture strainer (Corning B.V Life Sciences cat#352340). This prevents any OP9 DL1 cells that have been removed with the T cells to pass into the sample.

2.2.2 Nucleic Acid methods

2.2.2.1 Spectrophotometric quantification of nucleic acids

The concentration of nucleic acids was determined by measuring the optical density at 260nM using a NanoDrop 1000 UV-Vis Spectrophotometer (Thermo FisherScientific). 1µL of each sample was used for each measurement. The purity of the nucleic acid sample was determined by the absorbance at 230nM, 260nM and 280nM. The 260/280 ratio of a sample free of protein contamination should be 1.8-2.2 and 230/260 ratio ≥ 1.7 indicates a sample free of carbohydrates and lipids.

2.2.2.2 Agarose gel electrophoresis

Nucleic acid samples were analysed in 2% agarose gels. Gels were prepared by dissolving agarose (Hi-Pure Low EEO agarose, Biogene) in TAE buffer by boiling and adding ethidium bromide to a final concentration of 0.5µg/mL. The samples were mixed with 5x DNA loading buffer resulting in a final 1x concentration, loaded on to the gel and subjected to a voltage of 80-150 volts to resolve the nucleic acid fragments by size. The nucleic acids were visualized using a UV transilluminator (BioDoc-It System, UVP). For reference, markers containing DNA fragments of known sizes were included (New England Biolabs).

2.2.2.3 Preparation of RNA and cDNA for Expression Analysis

RNA extraction

Total RNA was isolated from cells using Trizol reagent (Ambion) according to manufacturer instructions. For purposes of practicality, a minimum of 100µL of Trizol was added directly to the cells at a concentration of 0.75mL of Trizol per 0.25mL of sample (5–10x10^6 cells), before lysing the cells by pipetting up and down several times. The sample was incubated in the Trizol for 10 minutes at room temperature, allowing the nucleoprotein complex to dissociate. 200µL chloroform was added to the sample per 1mL Trizol used, and then shaken vigorously. The sample was transferred to a Phase-Lock tube (5 Prime) and incubated at room temperature for 2 – 3 minutes, before being centrifuged at 12,000g for 15 minutes at 4^{o}C. The aqueous phase was

removed, transferred to a new tube, and incubated for 10 minutes at room temperature with 5-10µg Glycoblue (Ambien) and 500µL isopropanol per 1mL of Trizol used previously. The sample was centrifuged at 12,000g for 10 minutes at 4ºC, the supernatant was removed, and the pellet washed in 1mL 75% ethanol per 1mL Trizol used. The sample was centrifuged as described previously, the supernatant was removed and the pellet allowed to air-dry before being resuspended in 20-50µL (based on the size of the RNA pellet) of RNase-free water.

RNA was DNAse treated to remove trace amounts of contaminating DNA using a DNA-free kit (Ambion), according to manufacturer's instructions. Briefly, this involved adding 10x DNase1 Buffer at 0.1x total volume of sample and 1µL rDNase1 to the RNA, mixing gently, and incubating at 37ºC for 20-30 minutes. The resuspended DNase Inactivation Reagent was added at 0.1x total volume of sample, and mixed well by inversion. This was incubated for 2 minutes at room temperature, mixing occasionally, and centrifuged at 10,000g for 1.5 minutes. The RNA was transferred to a fresh tube and stored at -80ºC or used to synthesise first strand cDNA. Concentration of RNA was determined using spectrophotometry with a Nanodrop ND-1000 (Nanodrop Technologies) or a Nanodrop 8000 (Thermoscientific) according to manufacturer instructions (A_{260} of 1 equals 40µg/mL concentration of RNA).

2.2.2.4 cDNA Preparation

cDNA was prepared using a First Strand cDNA Synthesis Kit (Promega). 500ng of RNA was placed in a sterile RNase-free tube. The primer was added at a concentration of 0.5µg per microgram of the mRNA sample. RNase-free water was added to the sample to give a final volume of 13µL (or less). The tube was heated to 70ºC in a heat block for 5 minutes to melt the secondary structure within the template, and was then immediately cooled on ice to prevent reformation of the secondary structure. The sample was centrifuged briefly in order to collect the solution at the bottom of the tube, before the following components were added to the annealed primer/template:

M-MLV 5X Reaction buffer	5µL	(Promega)
dATP 10mM	1.25µL	(Invitrogen)
dCTP 10mM	1.25µL	(Invitrogen)
dGTP 10mM	1.25µL	(Invitrogen)

dTTP 10mM	1.25µL (Invitrogen)
Recombinant RNasin Ribonuclease Inhibitor	25 units (40 units per microliter)
M-MLV Reverse Transcriptase	200 units (200 units per microliter)
Nuclease-free water to final volume	25µL

The sample was mixed gently by flicking the tube, and incubated for 60 minutes at 37°C, and stored at 4°C.

2.2.2.5 Expression Analysis

Real-time-PCR:

cDNA generated using First Strand kit (above) was amplified by PCR using primers for the gene of interest, *Caph2* (Table 2.2) with Gotaq 2x green taq polymerase (Promega) according to manufacturer instruction. *Actin* primers were used as a loading control.

PCR reaction was incubated at 95°C for two minutes, followed by 30 cycles of amplification (95°C for 30 seconds, 56°C for 35 seconds, 72°C for 45 seconds), and products were checked for size by electrophoresis (see Section 2.2.2.2).

Quantitative-PCR:

Quantitative measurements of gene expression were obtained using qPCR on cDNA. In brief, PCR was used to amplify specific cDNA sequences and the amount of PCR product at each stage of PCR cycle was measured using the double stranded DNA (dsDNA) binding dye SYBR Green as a reporter.

The reaction consisted of 50ng template cDNA, 1x Brilliant II Sybr Green qPCR Master Mix (Life Technologies), 0.2µM of each oligonucleotide primer (Table 2.2) in a 20µL volume. The themo-cycling reactions were performed in 96 well PCR plates (Roche) with optically clear plate seals (Roche) using a LightCycler 480 (Roche).

The LightCycler continuously detected the fluorescence of each well in the plate in real time, producing a cycle threshold (C_T) value for each well. This indicates the cycle number at which the amount of fluorescence detected reaches a fixed threshold. The C_T values for each target gene were normalised to the housekeeping gene, *Actin*. Primer efficiency had been previously calculated and found to be 100%. The relative expression of target genes to a calibrator was calculated using the comparative C_T ($2^{-\Delta\Delta CT}$) method.

Table 2.2	**Primers**	
Primer Set Name	Forward Sequence	Reverse Sequence
Caph2	TCCTTGCAACTGGCTAATGACTAC	TGCTGTCCACTCAAGGCTGG
Actin	ACTGCCGCATCCTCTTCCTC	GATTCCATACCCAAGAAGGAAGG

2.2.3 Protein handling and preparation

2.2.3.1 Whole cell protein preparations

A single cell suspension was obtained from the thymus, or bone marrow (as described previously). $CD4^+$ T cells, $Ter119^+$ erythroid cells and $B220^+$ B cells were MACS purified according to manufacturer's instructions (MACS Miltenyi Biotec). Cells were washed in PBS and pelleted at 400g. Cell pellet volume (in µL) was estimated by eye. The cell pellet was re-suspended in 5x its volume of NP-40 lysis buffer and incubated on ice for 30 minutes with intermittent vortexing. Lysed cells were centrifuged at 15,000g for 10 minutes at 4°C, and supernatant collected and stored in the short term at -20°C.

2.2.3.2 Protein quantification

To determine the concentration of proteins in cell extracts or purified recombinant protein the Bradford assay was performed with the Bio-Rad Protein Assay kit. Initially, a standard curve was drawn using a BSA concentration range of 0.1, 0.2, 0.4, 0.6, 0.8 and 1.0mg/mL. To measure unknown concentrations, 10µL of each solution was added to 200µL 1x Bradfords dye reagent and A595 was measured after 5 minutes. The absorbance reading was compared to the BSA standard curve to calculate protein concentration.

2.2.3.3 SDS-PAGE Resolution of Proteins

Protein samples were separated according to their molecular weight by SDS-PAGE using the NuPage Novex (Invitrogen) gel system. 4-12% Bis-Tris gels (Invitrogen cat#15030984) were used to separate proteins.

Protein samples were denatured by heating at 70°C for 10 minutes in 1x protein sample loading buffer (Table 2.1) and loaded onto the gel.

Gels were run in a Novex minicell X-Cell Sure Lock (Invitrogen) electrophoresis tank in 1x MOPS running buffer for Bis-Tris gels (Invitrogen) at a constant voltage of 130V for approximately 90 minutes, until the desired separation was achieved. A prestained protein size ladder of standard molecular weights was loaded alongside all gels

(PageRuler Plus 10-250kDa, Thermoscientific cat#26619).

2.2.3.4 Western blotting

Stacking gel was removed from SDS-PAGE gel, and samples were transferred to polyvinylidene difluoride (PVDF) membrane. PVDF membrane was soaked in methanol and then transferred to western transfer buffer for 2 minutes before being used in transfer on a Genie Blotter (Idea Scientific). Gel and membrane were sandwiched between two sheets of 3mm filter paper soaked in western transfer buffer, and transfer proceeded for 90 minutes.

Alternatively, the samples were transferred via iBlot 7-minute transfer (Life Technologies) using iBlot 2 NC Regular Stacks (Life Technologies cat#IB23001) according to manufacturer's instructions.

After transfer, the membrane was blocked to prevent non-specific protein binding. To block, the membrane was incubated with either 5% milk-powder (Premier Foods) or 3% BSA (Roche) in TBS with 0.2% Tween 20 for 1 hour at room temperature or overnight at 4^{o}C with constant agitation. Primary antibodies were added to the blocking solution at the appropriate dilution (Table 2.5) and then the appropriate HRP labelled secondary antibody (Table 2.5) diluted in appropriate blocking solution, was added to the membrane for 1 hour.

To detect horse radish peroxidase (HRP) immobilised onto membrane, ECL detection kit (Amersham Biosciences) was used according to manufacturer's instructions. For a 20cm^2 nitrocellulose membrane, 2mL of ECL solution (1:1 mixture of solutions A and B) was added to the protein side of the nitrocellulose membrane and incubated for 30 seconds at room temperature. The membrane was blotted to remove any excess liquid, and signal was detected using the Image Quant.

2.2.4 Fluorescence In-Situ Hybridization (3D FISH)

2.2.4.1 Preparation of FISH probes

Genomic Clones used for FISH

The UCSC browser was used to identify genomic clones flanking regions of interest for FISH experiments. Fosmids were obtained from the BACPAC Resources Centre at the Children's Hospital Oakland Research Institute (http://bacpac.chori.org/). All fosmid clones were provided as bacterial stab cultures in agar. A full list of all fosmids used in this thesis is provided in Table 2.3.

2.2.4.2 Bacterial culture and stocks

Fosmids were streaked out onto LB-agar plates containing chloramphenicol (25µg/ml-made up in Ethanol) and incubated overnight at 37ºC. Single colonies were picked using a sterile pipette tip and transferred to a universal tube (Sarstedt Ltd cat# 60.9922.241) containing 5mL L-Broth supplemented with chloramphenicol (25µg/mL) (Sigma cat#C1200000-1EA). These were grown overnight in a 37ºC incubator with agitation. Bacterial stocks were made of all fosmid clones taking a 1:1 mixture of the overnight culture of L-Broth: 80% Glycerol. This mixture was stored at -80ºC.

Table 2.3	**Fosmid probes**							
Locus	Chromosome	Probe Type	Probe 1 ID	Probe 2 ID	Coordinate P1	Coordinate P2	Separation (bp)	
CD8	6	Fosmid	WI1-1250E21	WI1-1141E17	71,240,174 - 71,271,898	71,395,924 - 71,439,943	124026	~100kb
HoxA	6	Fosmid	WI1-571D3	WI1-2733I21	52,113,628 - 52,155,199	52,270,657 - 52,308,704	115458	~100kb
CD8 to Igkv	6	Fosmid	G135P68104F4	WI1-1141E17	70,041,587 - 70,083,551	71,395,924 - 71,439,943	1312373	~1Mb
CD8 to Mad2L1	6	Fosmid	G135P600867C1	WI1-1141E17	66,449,639 - 66,484,514	71,395,924 - 71,439,943	4911410	~5Mb

2.2.4.3 Fosmid minipreps

L-Broth cultures were pelleted by centrifugation at 16,000g for 30 seconds and resuspended in 200µL GTE buffer (50mM glucose, 25mM Tris pH8, 10mM EDTA) containing freshly added lysozyme (Sigma cat#L-6876) for 5 minutes at room temperature. Subsequently, 400µL of ice-cold lysis buffer (0.2M NaOH, 1% SDS) was added and mixed by inversion before being incubated on ice for 5 minutes. Following this, 300µL of acetate buffer (5M potassium acetate, 11.5% glacial acetic acid) was added to precipitate out cell debris, and the sample was mixed by inversion before being incubated for 5 minutes on ice. At this stage white flocculent precipitate formed in the tube.

The precipitate was pelleted by centrifugation at 16,000g for 5 minutes at 4ºC, the supernatant was transferred to a fresh tube, and combined with an equal volume of phenol: chloroform (Sigma cat#P2069-100ML). The samples were mixed by inversion and centrifuged at 16,000g for 5 minutes at 4ºC (as described above). The aqueous top layer was removed to a fresh tube and was combined with an equal volume of chloroform (Fisher cat#BP1145-1). The samples were mixed and centrifuged (as above) and again, the aqueous top layer was removed to a fresh tube. An equal volume of isopropanol (Sigma cat#24137-2.5L-R) was added, the sample was mixed by inversion, and incubated at -20ºC for a minimum of one hour. The samples were centrifuged for 15 minutes at 16,000g at 4ºC, causing the DNA to form a pellet, which was washed in 70% ethanol and air-dried. The pellet was then re-suspended in 20-30µL (depending on the pellet size) of TE (technical services). 20µg of RnaseA (Roche cat#10109169001) was added to the re-suspended DNA and incubated for 5 minutes at 37ºC. All fosmid DNA preparations were stored at -20ºC.

2.2.4.4 Labelling of probes by nick translation

DNA probes for FISH were labelled by nick translation to incorporate either biotin-16-dUTP (cat#11095070910) or digoxigenin-11-dUTP (cat#11093088910) (both Roche). This was achieved by adding 500ng–1µg of DNA to 2µL of nick translation salts (0.5M Tris-HCl pH7.5, 0.1M $MgSO_4$, 1mM DT, 500µg/mL BSA) with 2.5µL of each of 0.5mM dATP, dCTP and dGTP. Then either 2.5µL of 1mM biotin-16-dUTP was added to the mixture for biotin labelling or 1µL 0.5mM dTTP and 1.5µL digoxigenin-11-dUTP to label with dig. DNaseI (Roche cat#04716728001) was

diluted 1:20 for a final concentration of (500U/mL) and added to the mixture with 1µL of 5U DNA polymerase1 (Invitrogen cat# 18010). The reaction was made up to 20µL with deionised water, and was incubated at 16ºC for 90 minutes. The nick translation was stopped by the addition of 2µL 20% SDS and 3µL of EDTA. Quick Spin sephadex Columns (Roche cat#11273965001) were used according to manufacturer instructions to remove any unincorporated nucleotides and enzymes.

2.2.4.5 Quantitation of labelled FISH probes

Labelling was detected using Streptavidin alkaline phosphatase or anti-DIG alkaline phosphatase on nitrocellulose filters. These filters were prepared by soaking in 20xSSC for 10 minutes, and then drying at room temperature. Probes were spotted onto the nitrocellulose filters at dilutions of 1:500; 1:1000; 1:5000 and 1:10000 and allowed to dry at room temperature. Standards were also spotted onto the filter at concentrations of 20, 10, 2 and 1pg. Following this, the DNA was exposed to UV irradiation (150mJ) in a UVC500 Crosslinker (Hoefer) in order to facilitate cross-linking of the DNA to the filter. The filter was immersed in 0.1M Tris-HCl pH 7.5, 0.15M NaCl for 5 minutes at room temperature followed an incubation in the buffer described above, with the addition of 3% BSA (w/v) for 60 minutes at 60ºC.

Following this, the membrane was incubated for 15 minutes with gentle agitation at room temperature in 10mL of 0.1M Tris pH7.5 and 0.15M NaCl with 1% streptavidin-alkaline phosphatase (Roche cat#11093266910) and 1% anti-DIG alkaline phosphatase (Roche cat#11093274910). The filter was washed twice in 0.1M Tris pH7.5 and 0.15M NaCl for 15 minutes per wash. Following this, the filter was sealed in a polythene bag containing 5mL of 0.1M Tris pH9.5 and two drops of each of the solutions in the alkaline phosphatase substrate kit VI (Vector laboratories). The filter was removed from the polythene bag when a blue reaction product formed by 5-bromo-4-chloro-3-idolyl phosphate and nitroblue tetrazoilum. This allowed the biotin/DIG to be detected, and the concentration of the fosmid probes estimated by comparison to known standards.

2.2.4.6 Preparation of cells for 3D FISH

T cells were obtained from the thymus, and B cells were obtained from bone marrow

from the tibia and femur. Cells were prepared for flow cytometry cell sorting (as described in Section 2.2.7) with the appropriate cell surface antibodies. Cells were collected in tubes containing 0.5mL FCS.

2.2.4.7 Preparation of slides for 3D FISH

Cells were re-suspended in PBS at a concentration of $1x10^6$ cells per mL of PBS. To preserve three-dimensional nuclear structure, cells were seeded onto Polyprep slides (Sigma cat# P0425-72EA) within a circle drawn with hydrophobic pen. Approximately $1x10^5$ cells (100µL) were added to each of the slides. The slides were placed in a humidified chamber and incubated at 37ºC for 20 minutes. Following this, the cells were fixed in 4% PFA in PBS for 10 minutes in a 37ºC waterbath before being washed three times in PBS and then permeabilised in 0.5% Triton X (Sigma cat#T9284-500ML) for 10 minutes. The cells were washed in PBS a further three times and the slides were left to dry at room temperature, before being stored at -80ºC. Slides were rinsed in 2xSSC before use.

2.2.4.8 Hybridisation of labelled FISH probes

The slides were incubated in 2x SSC, 100µg/mL RNaseA (Roche cat#10109169001) at 37ºC for 1 hour. The slides were then washed in 2xSSC before being dehydrated through a series of two-minute ethanol washes (70%, 90% and 100%) before being air dried. The slides were then heated in a 70ºC oven for five minutes and denatured for 30 minutes at 80ºC in 70% formamide/2x SSC pH7.5 before being transferred to ice-cold 70% EtOH for two minutes, before further dehydration in 90% and 100% ethanol at room temperature, for two minutes each.

To prepare for hybridisation, one of the fosmid pairs was labelled with biotin-16-dUTP and the other fosmid was labelled with digoxigenin-11-dUTP by nick translation (see above). Approximately 70-100ng of fosmid was used per slide, together with 18µg mouse Cot1 (Invitrogen cat#18440-016) DNA and 5µg of salmon sperm DNA (Sigma cat#31149-10G-F). Twice the volume of ethanol was added, and the probes were spun under high heat, resulting in a white pellet of DNA. This was resuspended in 15µL hybridisation mix (50% deionised formamide, 10% dextran sulphate and 1% Tween 200 in 2x SSC). Probes were denatured at 70ºC for five minutes and then transferred

to a 37ºC waterbath to allow re-annealing before being pipetted onto a pre-warmed coverslip and picked up by a slide. The coverslips were sealed using TipTop rubber solution (BRAND cat#) and the slides were incubated in a covered tray for 48 hours in a 37ºC waterbath.

2.2.4.9 Washing and detection of FISH probes

Following the 48-hour incubation, the rubber sealing solution was removed from the edges of the coverslips and the slides were washed four times in 2x SSC at 45ºC for three minutes per wash. The slides were transferred to 0.1x SSC at 60ºC and were washed four times for three minutes each. Slides were then transferred to 4xSSC/0.1% Tween at room temperature before being incubated for 5 minutes with blocking buffer (4x SSC, 5% Marvel) under a 22x40mm coverslip. Biotinylated probes were detected using Texas Red (TR)-conjugated avidin (1mg/mL stock diluted 1:500 in blocking buffer), followed by biotinylated antiavidin (BAA) (0.5mg/μL diluted 1:100) and a final layer of TR-conjugated avidin (1mg/mL diluted 1:500). Digoxigenin-labeled probes were detected with sequential layers of Fluorsecein isothiocyanate (FITC)-conjugated antidigoxigenin (200μg/mL diluted 1:20) and FITC-conjugated anti–sheep (1.5mg/mL diluted 1:100). All antibodies were obtained from Vector Laboratories with the exception of FITC-conjugated anti-digoxigenin, which was obtained from Roche.

Each antibody incubation was carried out in a humidity chamber at 37ºC for 30-60 minutes, and was followed by 3x 2 minutes washes in 4xSSC/0.1% Tween at 37ºC before the addition of the next layer of antibody.

After the last antibody incubation, slides were washed as described above, and were incubated in 4xSSC/0.1% Tween with 50ng/mL DAPI (Sigma cat#D9542) for 2 minutes before mounting in Vectashield (Vector). Coverslips were then sealed onto the slides using super glue (the brand used was Super Solution F).

2.2.4.10 Image Capture

3 colour imaging with single emission filters

The imaging system comprises a Photometrics Coolsnap HQ2 CCD camera (Photometrics Ltd, Tucson, AZ), Zeiss Axioskop II MOT fluorescence microscope with Plan-neofluar or Plan apochromat objectives, a Lumen 200W metal halide light source (Prior Scientific Instruments, Cambridge, UK) and Chroma #89014ET single excitation and emission filters (Chroma Technology Corp., Rockingham, VT) with the excitation and emission filters installed in Prior motorised filter wheels. A piezoelectrically driven objective mount (PIFOC model P-721, Physik Instrumente GmbH & Co, Karlsruhe) was used to control movement in the z dimension. Hardware control, image capture and analysis were performed using Volocity (Perkinelmer Inc, Waltham, MA).

Deconvolution of 3D data:

FITC and Texas Red signals were deconvolved using a calculated PSF with the Fast Restoration, nearest neighbour algorithm of Volocity (Perkinelmer Inc, Waltham MA). DAPI signals were deconvolved using a calculated PSF with the constrained iterative algorithm of Volocity (Perkinelmer Inc, Waltham, MA).

Image Quantitation

Image analysis was carried out using the Quantitation module of Volocity (Perkinelmer Inc, Waltham, MA).

2.2.4.11 Scripts for Image Analysis

All scripts for image analysis of 3D FISH images were written for Volocity by Shelagh Boyle (Research Assistant, Bickmore Lab) using packages set up for Volocity by Matthew Pearson (Microscopy and Imaging Department).

Inter-probe distances were calculated by taking the centroid of each probe in the pair and calculating the pixel with the highest intensity. The distance was then calculated between the highest intensity pixels within the centroid of each probe pair. All inter-probe distances from 3D FISH were converted from pixels to microns by multiplication by 0.134μm.

The inter-probe distances (d) were squared. The difference between the distributions of squared inter-probe distances between datasets was assessed statistically using the Wilcox test with a cut-off of $p < 0.05$.

To determine the radial positioning of probe pairs a nuclear erosion script was used in IPLab for analysis of FISH images. The 3D images were collapsed and the script eroded the nuclei into five concentric shells of equal area. It was then possible to count the distribution of probe hybridisation signals across the erosion shells in 50-60 nuclei. The number of hybridisation signals in each shell in the dataset were calculated as a percentage of the total number of signals and plotted as a histogram. Significance of changes in radial positioning of probes between wildtype and mutant was assessed using the Mann-Whitney test with a cut off of $p < 0.05$.

Table 2.4	**FISH experiments**						
Locus	Mouse Model	Probe 1 ID	Probe 2 ID	Separation (bp)	Mean d^2	Median d	Median d^2
CD8	WT	WI1-1250E21	WI1-1141E17	124026	0.055940685	0.19	0.0361
	Nessy				0.048162355	0.19	0.0361
CD8 to Igkv	WT	G135P68104F4	WI1-1141E17	1312373	1.107510015	0.7025	0.4938865
	Nessy				1.489036106	0.966	0.933156
CD8 to MadL1	WT	G135P600867C1	WI1-1141E17	4911410	1.974506456	1.26	1.5876
	Nessy				3.144608446	1.32	1.7424
CD8	WT	WI1-1250E21	WI1-1141E17	124026	0.083570769	0.268	0.071824
	Nessy				0.081358473	0.19	0.0361
HoxA	WT	WI1-571D3	WI1-2733I21	115458	0.098523732	0.268	0.071824
	Nessy				0.104106556	0.268	0.071824

Locus	Median d/Mean d	Median d^2/Mean d^2	St. Dev. d	St Dev d^2	St.Dev. d/Mean d	St.Dev d^2/Mean d^2	p-value Wilcox test
CD8	0.865036797	0.645326385	0.088341253	0.048207403	0.402202286	0.861759252	0.1615
	0.935960591	0.749548068	0.084067498	0.043024909	0.414125607	0.893330675	
CD8 to Igkv	0.77191376	0.445943146	0.53251162	1.393427714	0.585128892	1.25816263	0.4022
	0.936692867	0.626684602	0.657287825	1.833000612	0.637346602	1.230998096	
CD8 to MadL1	1.039814681	0.80404903	0.717771757	2.339465465	0.592340961	1.184835561	0.1722
	0.885622568	0.554091242	0.968251115	4.376403917	0.64962503	1.391716645	
CD8	1.014625938	0.859439259	0.117989546	0.078803577	0.446698707	0.942956223	0.5388
	0.737663856	0.443715309	0.123204884	0.08388285	0.478335736	1.031027831	
HoxA	0.946361667	0.729002022	0.135608221	0.097464654	0.478859785	0.989250528	0.9588
	0.932545745	0.68990852	0.14704312	0.122543785	0.511658343	1.17709959	

WT shown in white, nessy in grey

2.2.5 Preparation of metaphase spreads

The cells were treated with hypotonic solution (0.5% sodium citrate, 0.25% potassium chloride in deionised water) and incubated at 37ºC for 10 minutes. The sample was then centrifuged at 12000 rpm for 5 minutes before being fixed in 10mL of 3:1 methanol: acetic acid. The fix was added drop-wise, whilst vortexing the sample. The samples were incubated at room temperature for 30 minutes, before being centrifuged (as above), re-suspended in 10mL fix, and stored at -20ºC overnight. Following this, the cell suspension was dropped onto Poly-Prep (Sigma) slides (cleaned in 95% EtOH and 1% conc. HCl) to make metaphase spreads. Slides were stained in 50mL PBS with with 50ng/mL DAPI (Sigma cat#D9542) for 2 minutes before mounting in Vectashield (Vector). Coverslips were then sealed onto the slides using Super Solution F.

The spreads were imaged using a confocal microscope. The imaging system comprises a Photometrics Coolsnap HQ2 CCD camera (Photometrics Ltd, Tucson, AZ), Zeiss Axioskop II MOT fluorescence microscope with Plan-neofluar or Plan apochromat objectives, a Lumen 200W metal halide light source (Prior Scientific Instruments, Cambridge, UK) and Chroma #89014ET single excitation and emission filters (Chroma Technology Corp., Rockingham, VT) with the excitation and emission filters installed in Prior motorised filter wheels. A piezoelectrically driven objective mount (PIFOC model P-721, Physik Instrumente GmbH & Co, Karlsruhe) was used to control movement in the z dimension. Hardware control, image capture and analysis were performed using Volocity (Perkinelmer Inc, Waltham, MA).

2.2.5.1 Preparation of metaphase spreads for Super-Resolution image capture

Super-resolution images were acquired using structured illumination microscopy. Cells were treated with hypotonic solution and fixed in 3:1 methanol: acetic acid, as

above. The cell suspension was dropped on to high precision cover-glass (Marienfelt, Germany) and mounted in Prolong Gold (Life Technologies). 3D SIM images were acquired on a N-SIM (Nikon Instruments, UK) using a 100x 1.49NA lens and refractive index matched immersion oil (Nikon Instruments). SIM images were reconstructed using NiS Elements software (Nikon Instruments) from a z stack comprising of no less than 1um of optical sections. In all SIM image reconstructions, the Wiener and Apodization filter parameters were kept constant.

2.2.6 Sucrose gradients

2.2.6.1 Preparation of 5% - 20% Sucrose gradients

The relevant quantity of sucrose was dissolved in Gradient buffer (50mM Tris HCl pH7.5, 150mM NaCl, 1mM EDTA). Seton tubes (Beckman Coulter cat#344059) were placed in a marker block, and a line was drawn around the tubes to indicate 6mL. The rubber stoppers were sprayed with 70% EtOH to ensure that they were free of dust, and allowed to dry. A 7-gauge needle was attached to a 20mL syringe, and rinsed with deionised H_2O. Following this, the needle was air-dried by vigorously pumping air through the needle with a fresh syringe.

Using a fresh syringe, the Seton tube was filled (Beckman Coulter cat#344059) up to the 6mL mark with 5% sucrose solution, without allowing the needle to touch the sides of the tube. The needle was rinsed and dried (as above). Following this, a further 6mL of 20% sucrose solution was added to the Seton tube, by placing the needle at the bottom of the tube, and raising the needle in time with the meniscus. The needle was then removed quickly, to avoid disturbing the layers. The rubber cap was slowly lowered onto the tube, whilst avoiding air bubbles forming under the rubber cap. A linear gradient of 5% - 20% sucrose was obtained using a gradient maker. Following this, the gradients were incubated at 4^{o}C for a minimum of one hour. During this time, the Seton tubes were covered with foil to prevent contamination.

2.2.6.2 Sample Preparation

A single cell suspension was prepared from three wildtype thymuses (~3x10^8 cells) by

passing the thymus through a cell culture strainer, as described previously. The cells were washed twice in ice-cold PBS, re-suspended in 200µL Lysis buffer (Gradient buffer, supplemented with protease inhibitor (Roche cat#04693159001), 1% DNAse (Promega cat#0000128463), 1% RNAse (Roche cat#10109169001) and 1% Triton X (Sigma cat#053K00262V)). The sample was incubated at 4ºC for 30 minutes, before being pelleted by centrifugation.

2.2.6.3 Loading of cell lysate

100µL was removed from the top of the sucrose gradient. Following this, 200µL of cell lysate sample was added to the top of the gradient. The gradient was weighed in order to ensure that the centrifuge was appropriately balanced. Gradients were placed in pre-cooled cradles and loaded onto an SW41 TI rotor. The rotor was lowered into the centrifuge (Beckman Coulter Optima L-90K Ultracentrifuge), and the sample was centrifuged for 15 hours at 32.4k RPM, 4ºC.

2.2.6.4 Protein Precipitation

Following centrifugation, 24 fractions were removed manually and placed in pre-cooled eppendorfs. One volume of 100% TCA stock was added to four volumes of protein sample. The samples were vortexed and incubated at 4ºC for 10 minutes. Samples were pelleted by centrifugation at 14,000 rpm for 20 minutes at 4ºC. The supernatant was then removed leaving the protein pellet intact, before the pellet was washed in 200µL of ice-cold acetone. The samples were centrifuged (as above), and the pellets were dried at room temperature for 5 – 10 minutes. Samples were re-suspended in loading buffer, according to manufacturer's instructions.

2.2.7 Flow Cytometry

2.2.7.1 The fundamental concept of flow cytometry

Flow cytometry is the measurement of certain properties of individual cells, which are usually fluorescently labelled. These properties include the relative size and granularity of the cell, as well as the relative fluorescence intensity. The flow cytometer is designed to focus the cell suspension into a single cell stream (called the sheath fluid) so that only single cells pass through the light beam in the flow chamber at any given time. This is achieved by ensuring the flow rate (the speed at which cells pass through the laser beam) is low, i.e. no greater than 400 events per second. More than one cell passing through the laser beam at any given time can result in loss of data, as well as consequences for the analysis of the acquired data.

Components of the flow cytometer

The flow cytometer consists of three main parts: fluidics (i.e. the Flow Chamber), optics and electronics. The fluidics system (the Flow Chamber) is designed to transport a single cell stream to the light beam (usually a laser). The cells are focussed into the centre of the sheath fluid, called the sample core. The degree to which the cells are focussed at the centre of the sheath fluid has an impact on the flow rate: decreasing the width of the sample core results in fewer cells entering the stream at any one time, making it less likely that more than one cell will enter simultaneously. This also makes it more likely that all the cells will pass through the centre of the light beam, resulting in more uniform emission of light.

Once the cells have passed through the laser beam, they emit light at certain angles (depending on the size and granularity of the cell), and the fluorescent particles emit fluorescent light of specific wavelengths. This scattered and fluorescent light is directed towards the relevant detectors via a series of filters and mirrors called the optical system.

The detected light must then be converted into electronic pulses, which the software is able to process. The data is stored and analysed to obtain information about the cell populations.

2.2.7.2 Generation of Forward- and Side- Scatter

Forward Scatter (FSC)

When the cell passes into the laser beam, the cell becomes an obstacle to the path of light. Due to the wave-like nature of light, however, the light is able to diffract (bend) around the edges of the obstacle. This bending is due to Huygen's principle, which states that all points along a wave front act as if they were point sources. The light that is diffracted around the edges of the cell is called forward scatter and is detected by a photodiode located a small increment away from the axis of the incident laser light, in the forward direction.

Usually, this diffraction of light is not noticeable: when we observe light encountering an object, we generally see the formation of a shadow, rather than an interference pattern caused by diffraction. This is because a diffraction pattern is only noticeable if the incident light is a narrow monochromatic beam (such as a laser beam) and the object is approximately the same size, or smaller, than the wavelength of the light. Since the wavelength of light is small ($\sim x10^{-7}$ m) compared to, for example, the wavelength of sound, diffraction of light will only be noticeable around very small objects, such as cells. The level of diffraction provides information (independent of fluorescence intensity) about the size of the cell: larger cells will diffract light by a smaller angle than smaller cells.

Side Scatter (SSC)

Side Scatter of light is generated as a result of reflection of light by a barrier (such as a cell membrane) and refraction of light due to a change in refractive index at various interfaces within the cell. Reflection and refraction both result in a change in direction of the light beam. When light is reflected by a barrier, the angle of incidence (the angle at which the light hits the barrier) is equal to the angle of reflection. Since the cell passes through the centre of the laser beam, a large proportion of light will encounter the cell membrane at an angle of 90 degrees, causing the reflected light to bounce back towards the light source. However, due to the curvature of the cell, some light rays will hit the barrier at an angle of approximately 45 degrees, and be reflected in a

direction approximately 90 degrees to the laser beam.

The speed of a wave is dependent on the medium through which the wave is travelling. Refraction of light occurs when the light wave moves from one medium to another with a different refractive index (or density). This causes the speed of the light wave to change. For example, when light moves from a low-density medium to a medium of higher density, the light wave will slow down, and the direction of propagation of the wave will be bent towards the perpendicular of the boundary between the two media.

When a laser beam is incident on a cell, the light travels into a higher density medium (within the cell) and is refracted towards the normal (the perpendicular) of the boundary. When the light beam emerges from the cell, it is refracted away from the normal. Given that cells are approximately spherical in shape, a large proportion of the refracted light will emerge at an angle of approximately 90 degrees to the laser beam, along with the reflected light.

The same is true at any interface with a difference in density within the cell, for example when the light beam encounters the nucleus, or mitochondria. At each interface, some light will be reflected, and some refracted, to be collected by photodiodes situated at approximately 90 degrees to the light source. Therefore side scatter provides information about the cell granularity and the internal composition of the cell.

Forward scatter can be plotted against side scatter, in order to gate out cell debris (e.g. dead cells) from the data to be analysed, as shown in Figure 2.1a. The dead cells and debris will not share the same forward/side scatter parameters as live cells (i.e. they might be smaller and more granular).

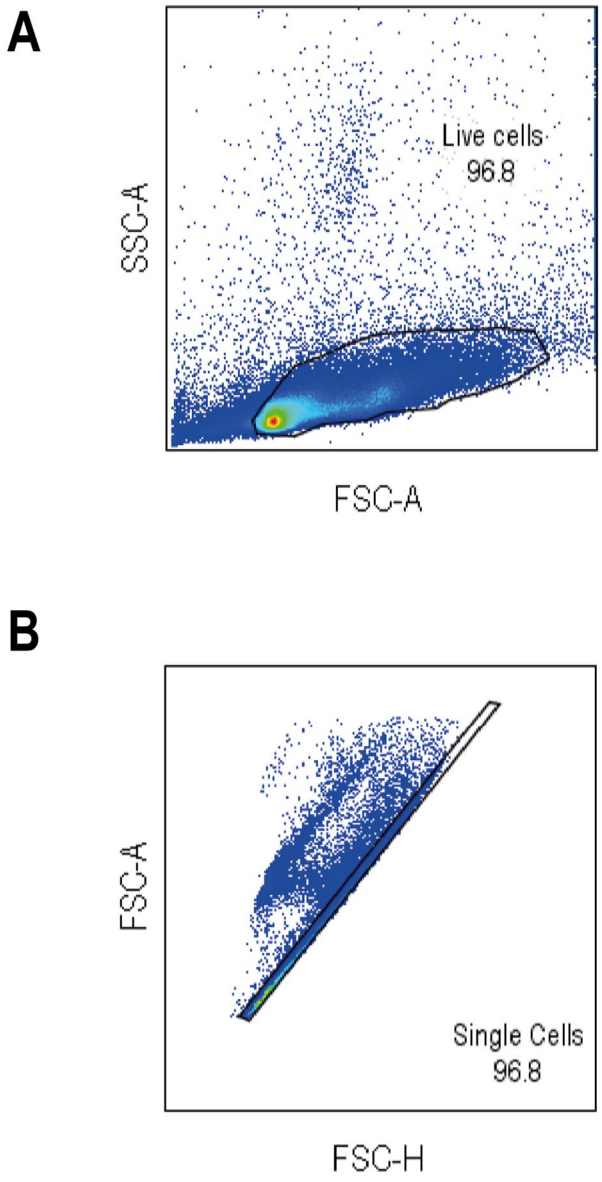

Figure 2.1
Population of interest selected based on Forward- and Side-scatter
A. Flow cytometer dot plot showing the gating used to discriminate dead cells and debris. **B.** Flow cytometer dot plot showing the gating used for doublet discrimination.

2.2.7.3 Fluorescence

A fluorescent particle absorbs light at a specific wavelength. This light energy (in the form of a photon) can be absorbed by an electron in the outer orbit of the fluorescent particle, which raises the electron to a higher energy level. This absorption can only occur when the photon is of exactly the right energy according to the Planck-Einstein relation: $E = hf$ (where E is energy of the photon, which is equal to the difference in energy levels of the electron; h is Planck's constant and f is the frequency of the photon). The electrons of different fluorescent particles will be excited by different wavelengths of incident light: these wavelengths are characteristic for that particle. The range of wavelengths that can excite a fluorescent particle is known as its absorption spectrum.

Once the electron has been raised to a higher energy level, the electron may lose some of the energy gained from the photon through collisions or other interactions. The electron will then return to its original energy level, releasing a photon with lower energy and a longer wavelength than the original photon. The range of wavelengths that are emitted by a fluorescent particle is called its emission spectrum. A particle can be labelled by more than one fluorochrome, provided that the emission wavelengths are far enough apart that they can be distinguished from one another. The amount of signal detected from the fluorescent particles indicates the fraction of fluorescent particles within the sample.

2.2.7.4 Compensation

When multiple fluorescent antibodies are expressed on a single cell, the fluorescence expression signal from one antibody may “spill” into the expression signal of another. If this is not compensated, the data may not be interpretable. All flow cytometry data presented in this thesis has been compensated.

2.2.7.5 Doublet Discrimination

For many flow cytometry experiments, including ploidy experiments, it is essential to be able to exclude doublets (two cells passing through the laser beam together) from the analysis. This is because when analysing the DNA content of cells, two diploid cells that are attached to each other could be misinterpreted as a cell with 4N ploidy.

Doublets can be excluded based on properties of the cell or doublet, such as forward and side scatter.

2.2.7.6 Pulse Processing

As an object passes through the laser beam, a signal is generated. This signal is recorded, and can be analysed to obtain information about the object. The width of the signal provides information about the length of time the object took to pass through the beam. The height (or peak) of the signal directly correlates with the maximum fluorescence of the cell. The signal can be integrated to find the area, which directly correlates with the total fluorescence of the cell.

If the forward (or side) scatter area signal is plotted against the forward (or side) scatter height signal then single cells will lie along the diagonal x=y. This is because a single cell with 4N DNA content will be twice as bright as a single cell with 2N DNA content, since it has twice as much DNA. Therefore, the forward-scatter area signal will be double that of a 2N cell. Since the 4N cell does not double its membrane or cytoplasmic size, the maximum fluorescence (forward-scatter height) signal will also be twice that of a 2N cell. Therefore, these single cells will lie along the diagonal of the area versus height plot. When we compare a doublet (two 2N cells that are stuck together) with a single cell with 4N DNA content, the doublet will show the same level of total fluorescence (the area value), however the maximum fluorescence (signal height) will be half that of the single 4N cell. Therefore, the doublet will not lie along the diagonal of forward versus side scatter, and can be gated out from the population to be analysed. Clumps of cells (more than two cells stuck together) will also be excluded in this way. Unless otherwise stated, forward scatter-area versus forward scatter-height doublet exclusion was used in every flow cytometry experiment performed. A figure of a typical forward-scatter area (FSC-A) versus forward-scatter height (FSC-H) doublet exclusion step is shown below (Figure 2.1b).

Alternatively, the signal width data can be used in a similar way, since a doublet will take twice as long to pass through the beam than a single cell with either 2N or 4N DNA content. For this technique, forward-scatter width is plotted against forward-scatter area. It is possible to use both techniques (FSC-A vs FSC-H followed by FSC-W vs FSC-A, or vice versa) to ensure that no doublets are included in the analysis.

2.2.8 Cell Sorting

2.2.8.1 Simultaneous Staining of Cell Surface Proteins

This protocol was carried out to sort specific populations of differentiated cells for FISH experiments. To obtain $CD4^-CD8^-$ DN, $CD4^+CD8^+$ DP $CD71^+$ T cells, a single-cell suspension was made from a mouse thymus by passing the thymus through a cell culture strainer with 40µm nylon mesh (Corning B.V Life Sciences cat#352340).

To obtain Fraction C B cell populations, the bone marrow from a tibia and femur was flushed out of the bone, and (as above) passed through a 40µm nylon mesh. The cells were counted using a haemocytometer and approximately $2x10^7$ cells were resuspended in PBS at a concentration of approximately $1x10^8$ cells/mL. Cell surface antibodies were added at the relevant concentrations (see Table 2.5). The cells were incubated in the dark with cell surface antibodies for 10 minutes at 4ºC, before being washed in 5mL of PBS. Following this, the samples were centrifuged for 5 minutes at 1300K, the supernatant was aspirated and the pellets were resuspended in 500µL PBS. Cell sorting of fluorescent cells was performed on a BD FACS AriaII SORP (Beckton Dickinson) by Elizabeth Freyer (FACS technician, MRC HGU). Cells were collected in FACS-tubes containing 0.5mL of FCS (diluted by the PBS cell suspension). The cells were re-suspended in the appropriate amount of PBS and seeded onto Superfrost + slides.

2.2.9 Analysis

2.2.9.1 Simultaneous Staining of Cell Surface Proteins for DNA content analysis

This protocol was carried out to acquire data for the proportion of hyperdiploid cells and total cell numbers at various stages of haematopoietic differentiation.

To analyse the T cell population, a single-cell suspension was made from a mouse thymus by passing the thymus through a cell culture strainer with 40µm nylon mesh (Corning B.V Life Sciences cat#352340). To obtain both B cell and Erythroid

populations, the bone marrow from a tibia and femur was flushed out of the bone, and (as above) passed through a 40um nylon mesh.

The cells were counted using the Moxi Z mini automated cell counter OS 4.0 (Orflo), which provides accurate cell numbers. Approximately 5 to 10 million cells of each cell type were transferred to a fresh tube and re-suspended in 100µL PBS. Cell surface antibodies were added at the relevant concentrations (see Table 2.5).

The cells were incubated in the dark with cell surface antibodies for 10 minutes at 4ºC, before being washed in 2mL of PBS. Following this, the samples were centrifuged for 5 minutes at 1300K, the supernatant was aspirated and the pellets were re-suspended in 100µL Cytofix/Cytoperm Fixation and Permeabilization Solution (BD cat#51-2090KZ) and incubated in the dark for a further 15 minutes at 4ºC. Each sample was washed in 2mL of 1x Perm/Wash buffer (BD cat#51-2091KZ), centrifuged (as described above) and re-suspended in 300µL 70% ice-cold ethanol drop-wise, while vortexing. The samples were incubated in the dark at 4ºC for a minimum of 10 minutes, and were then washed in 2mL of diluted Perm/Wash (BD cat# 51-2091KZ) before being centrifuged (as described above). The supernatant was aspirated, and unless otherwise stated, the pellet was re-suspended in 200µL 1X DAPI (Sigma cat#081M4005V) staining solution (diluted 1:100 in diluted Perm/Wash (BD)). The cells were left at 4ºC in the dark for a maximum of 24 hours before being analysed.

In addition to the labelled cells, an aliquot of unlabelled cells were DAPI stained, providing a negative control. Single-stains were prepared using OneComp eBeads according to manufacturer's instructions (cat#01-1111-42).

The cells were analysed on either the BD FACS AriaII SORP (Beckton Dickinson) or the BD LSR Fortessa X-20 SORP. Once the cell exits the laser beam, it is sent to the waste collector.

The data was analysed using FlowJo Version 10. The gating strategies used to determine each of the stages of interest of T cells, B cells and erythroid cells are shown in Figures 2.2, and 2.3. The same gating strategies were used to determine individual

stages of T, B and erythroid development for every experiment. The gating strategies used to determine the haematopoietic progenitor populations are indicated in Figure 2.4. Progenitor cell DNA content was analysed using propidium iodide (PI).

2.2.9.2 In vivo BrdU incorporation studies

BrdU incorporation studies were undertaken in animals 2 hours following IP injection of 1-2 mg of BrdU, and detection was carried out using the FITC BrdU Flow kit (BD cat# 51-2354AK) according to manufacturer's instructions.

A single cell suspension was prepared from the thymus. The cells were counted using a haemocytometer and $1x10^7$ cells were transferred to a Falcon tube labelled T cells. A single cell suspension was also prepared from the bone marrow and $1x10^7$ cells were transferred to a new tube labelled B cells, and another $1x10^7$ cells were transferred to a tube labelled erythroid cells. All samples were re-suspended in 100µL PBS and fluorescent cell surface antibodies were added at the relevant concentrations (see Table 2.5).

The cells were incubated in the dark with cell surface antibodies for 10 minutes at 4ºC, before being washed in 1 mL of PBS. Following this, the samples were centrifuged for 5 minutes at 1300K, the supernatant was aspirated and the pellets were re-suspended in 100µL Cytofix/Cytoperm Fixation and Permeabilization Solution (BD cat# 51-2090KZ) and incubated in the dark for a further 15 minutes at 4ºC.

Each sample was then washed in 1mL of 1x Perm/Wash buffer (BD cat# 51-2091KZ), centrifuged (as described above) and re-suspended in 100µL of BD Cytoperm Permeabilization Buffer Plus (BD cat#559619). The cells were then incubated at on ice in the dark for 10 minutes before being washed in 1mL of 1xBD Perm/Wash Buffer, centrifuged (as above) and re-suspended in 100µL Cytofix/Cytoperm Buffer (BD cat# 51-2090KZ).

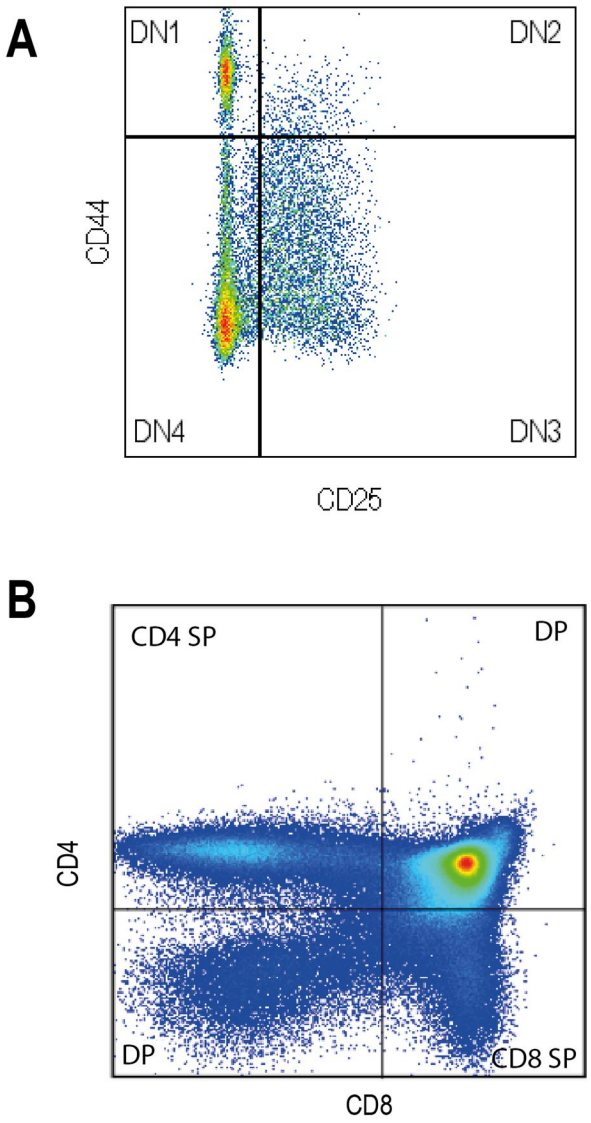

Figure 2.2
Gating strategies used to determine T cell stages of differentiation
A. Flow cytometer dot plot showing the gating used to determine DN stages of T cell development. **B.** Flow cytometer dot plot showing the gating used to determine later stages of development.

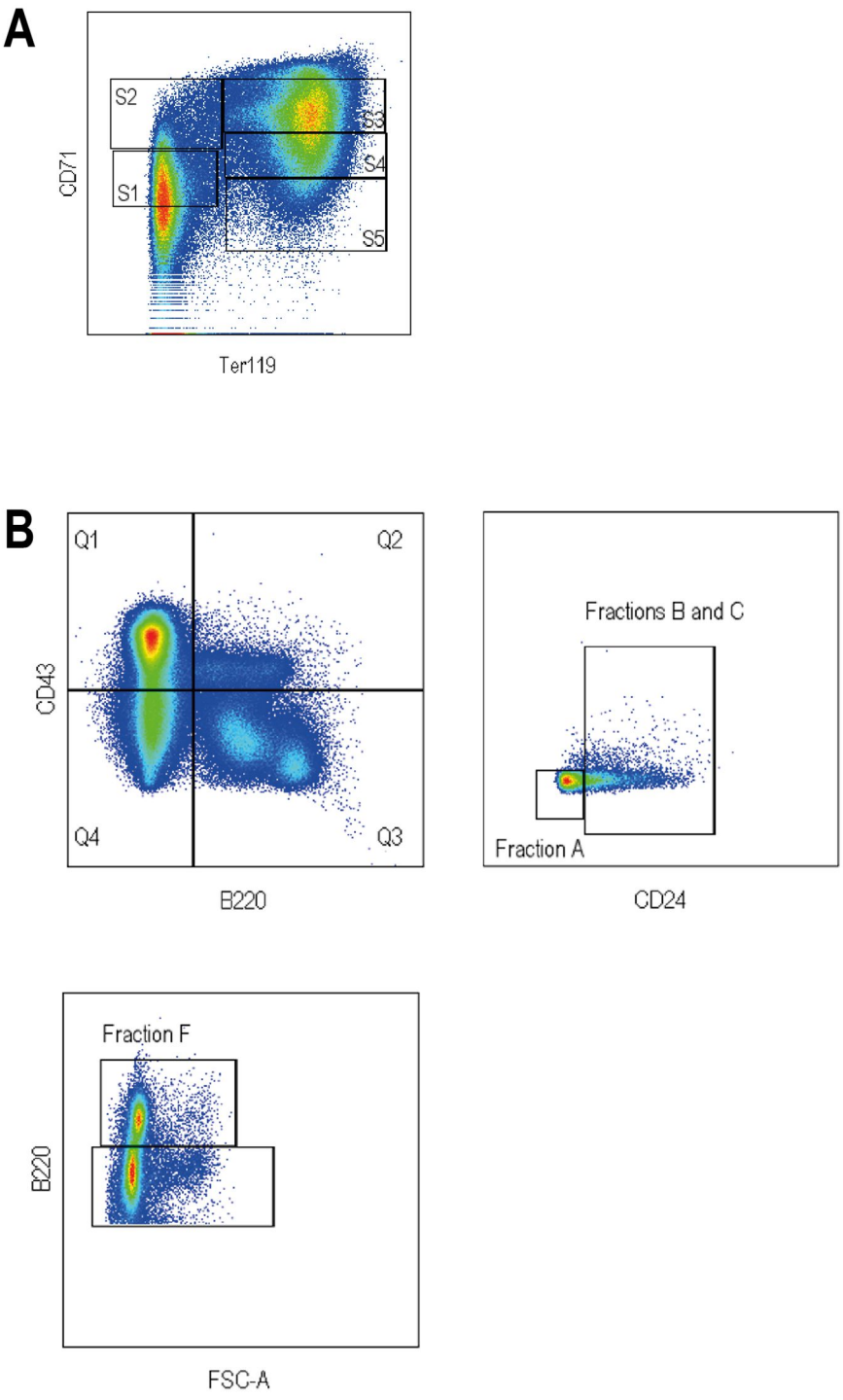

Figure 2.3
Gating strategies used to determine stages of erythroid and B cell differentiation
A. Flow cytometer dot plot showing the gating used to determine stages of erythroid differentiation. **B.** Flow cytometer dot plot showing the gating used to determine stages of B cell differentiation.

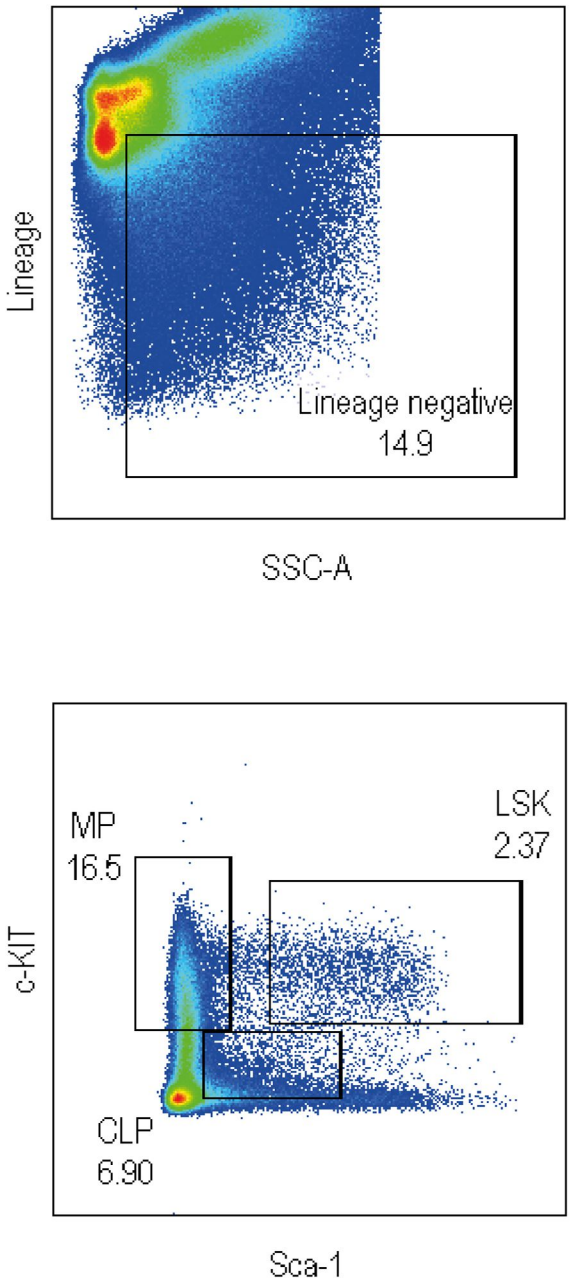

Figure 2.4
Gating strategies used to determine haematopoietic populations
Flow cytometer dot plots showing the gating used to determine common myeloid, common lymphoid and LSK populations

Following this, the cells were incubated in the dark for 5 minutes at room temperature, washed in 1mL of 1x Perm/Wash Buffer, centrifuged (as above) and re-suspended in 100µL of DNase (BD cat#559619) diluted to a concentration of 300µg/mL in PBS. The cells were incubated for an hour at 37ºC.

Next, the cells were washed in 1 mL of 1X BD Perm/Wash Buffer (BD cat# 51-2091KZ) per sample, centrifuged (as above) and re-suspended in 50µL of BD Perm/Wash Buffer (BD cat# 51-2091KZ) containing fluorescent anti-BrdU-APC (BD cat# 552598) at the relevant concentration. The samples were incubated for 20 minutes at room temperature, washed and centrifuged (as above) and re-suspended in 0.5mL Perm/Wash buffer.

In addition to the fluorescently-labelled cells, an aliquot of unlabelled BrdU-treated cells were DAPI stained, providing a negative control. Single-stains were prepared using OneComp eBeads according to manufacturer's instructions (cat# 01-1111-42).

Cell analysis was performed on a BD FACS AriaII SORP (Beckton Dickinson).

2.2.9.3 DNA content analysis of MEFs

Mouse Embryonic fibroblasts were prepared from *Caph2*$^{+/+}$ and *Caph2*$^{nes/nes}$ E14.5 embryos on the C57 Black 6 outbred strain (as described in Section X). Cells were trypsonised to dissociate, neutralised with media, and pelleted by centrifugation. Pellet was washed in PBS. The cells were fixed and re-suspended in DAPI as above. Cells were analysed on the BD LSR Fortessa X-20 SORP.

2.2.9.4 DNA content analysis of Primary T cells cultured ex vivo

Primary T cells were obtained from *Caph2*$^{+/+}$ or *Caph2*$^{nes/nes}$ thymuses. A single cell suspension was obtained by passing the cells through a 40µm nylon mesh (Corning B.V Life Sciences cat#352340), and purified using CD4 (L3T4) MicroBeads (Miltenyi Biotec cat#130-049-201) according to manufacturer's instructions. CD4 negative cells were counted and seeded onto an OP9/DL1 monolayer at a concentration of $20x10^3$ cells per mL. The cells were kept in culture for 4 days and were then disassociated from the OP9/DL1 monolayer by gently pipetting the media up and down using a p1000 pipette. The media was then passed through a 40µm nylon mesh (Corning B.V

Life Sciences cat#352340) to remove any OP9/DL1 cells that had been disassociated along with the cultured T cells. The cells were washed in PBS, incubated with anti-CD4-PECy7 (eBiosciences cat#25-0042) anti-CD8-PE (eBiosciences cat#12-0081-81) fluorescent antibodies, fixed in 100µL Cytofix/Cytoperm Fixation and Permeabilization Solution (BD cat# 51-2090KZ) and re-suspended in 200µL 1X DAPI (Sigma cat# 081M4005V) staining solution (diluted 1:100 in diluted Perm/Wash (BD)) as described above. The cells were kept at 4°C in the dark before being analysed on either the BD FACS AriaII SORP (Beckton Dickinson) or the BD LSR Fortessa X-20 SORP.

2.2.9.5 Ex vivo BrdU incorporation studies

Primary T cells were cultured on OP9/DL1 monolayers. After 4 days, the cells were treated with Bromodeoxyuridine (BrdU) from the FITC BrdU Flow kit (BD cat# 559619) at a concentration of 10µM (i.e. 10µL of 1mM BrdU per mL of culture medium) at 0 hour, 1 hour, 2 hour 3 hour and 4 hour time points. Nocodazole was added at the same time points as BrdU, at a concentration 300ng per mL of culture medium. The cultured T cells were dissociated from the OP9/DL1 monolayer as described above, passed through a 40um nylon mesh (Corning B.V Life Sciences cat#352340) to remove any OP9/DL1 cells that had been disassociated along with the cultured T cells and washed in PBS. The cells were re-suspended in 100µL PBS and CD4 PECy7 (eBiosciences cat#25-0042) CD8 PE (eBiosciences cat#12-0081-81) fluorescent antibodies were added at the relevant concentration (see Table 2.5).

The cells were incubated with the antibodies for 10 minutes at 4°C in the dark before being washed in 1mL of PBS. The samples were centrifuged at 1300K for 5 minutes, the supernatant was aspirated and the pellets were re-suspended in 100µL Cytofix/Cytoperm Fixation and Permeabilization Solution (BD cat# 51-2090KZ) and incubated in the dark for a further 15 minutes at 4°C.

The cells were then washed in 1 mL of 1x Perm/Wash buffer (BD cat# 51-2091KZ), centrifuged (as described above) and re-suspended in 100µL of BD Cytoperm Permeabilization Buffer Plus. After being incubated at on ice in the dark for 10 minutes the cells were washed in 1mL of 1xBD Perm/Wash Buffer, centrifuged (as above) and re-suspended in 100µL Cytofix/Cytoperm Buffer.

The cells were kept in the dark for a further 5 minutes at room temperature, washed in 1mL of 1x Perm/Wash Buffer (BD cat# 51-2091KZ), centrifuged (as above) and re-suspended in 100µL of DNase diluted to a concentration of 300µg/mL in PBS. The cells were incubated for an hour at 37ºC.

Following this, the cells were washed in 1mL of 1X BD Perm/Wash Buffer (BD cat# 51-2090KZ) per sample, centrifuged (as above) and re-suspended in 50µL of BD Perm/Wash Buffer (BD cat# 51-2090KZ) containing fluorescent anti-BrdU-FITC (BD cat# 552598) and anti-PH3S10-APC (New England Biolabs cat#9716s) at the relevant concentrations (see Table 2.5). The samples were incubated for 20 minutes at room temperature, washed and centrifuged (as above) and resuspended in 0.5mL Perm/Wash buffer (BD cat# 51-2090KZ).

For this experiment, the 0 hour time point provided the no-stain control. Single-stains were prepared using OneComp eBeads according to manufacturer's instructions (cat# 01-1111-42).

Cell analysis was performed on a BD FACS AriaII SORP (Beckton Dickinson).

Table 2.5	Antibodies				
Experiment	**Antigen**	**Conjugate**	**Dilution**	**Company**	**Catalogue Number**
Cell Sorting					
T cell	CD4	FITC	1 in 200	BioLegend	100509
	CD8	PE	1 in 200	eBioscience	12-0081-82
	CD71	APC	1 in 100	eBioscience	17-0711-82
B cell	B220	PECy7	1 in 200	eBioscience	25-0452-81
	CD43	PE	1 in 200	eBioscience	12-0431-82
	CD24	APC780	1 in 200	eBioscience	47-0242-80
***In vivo* DNA content**					
T cell DP	CD4	FITC	1 in 200	BioLegend	100509
	CD8	PE	1 in 200	eBioscience	12-0081-82
	CD71	APC	1 in 100	eBioscience	17-0711-82
T cell DN	CD4	FITC	1 in 200	BioLegend	100509
	CD8	FITC	1 in 200	eBioscience	11-0081-81
	TCRγδ	FITC	1 in 100	eBioscience	11-5711-81
	CD25	APC780	1 in 100	eBioscience	47-0251-80
	CD44	PE	1 in 100	eBioscience	12-0441-81
	CD90	PECy7	1 in 200	eBioscience	25-0902-81
B cell	B220	PECy7	1 in 200	eBioscience	25-0452-81
	CD43	PE	1 in 200	eBioscience	12-0431-82
	CD24	APC780	1 in 200	eBioscience	47-0242-80
Erythro	Ter119	PE	1 in 200	eBioscience	12-5921-81
	CD71	APC	1 in 100	eBioscience	17-0711-82
	Streptavidin	FITC	1 in 100	eBioscience	11-4317-87
	CD3e	Biotin	1 in 25	eBioscience	13-0031-75
	B220	Biotin	1 in 25	eBioscience	13-0452-75
	Ly-6G (Gr-1)	Biotin	1 in 25	eBioscience	13-5931-75

***In vivo* BrdU**					
T cell DP	CD4	e450	1 in 200	eBioscience	48-0042-80
	CD8	PE	1 in 200	eBioscience	12-0081-82
	CD71	PECy7	1 in 100		
	BrdU	FITC	1 in 100	BD Biosciences	51-9000019AK
T cell DN	CD4	FITC	1 in 200	BioLegend	100509
	CD8	FITC	1 in 200	eBioscience	11-0081-81
	TCRγδ	FITC	1 in 100	eBioscience	11-5711-81
	CD25	APC780	1 in 100	eBioscience	47-0251-80
	CD44	PE	1 in 100	eBioscience	12-0441-81
	CD90	PECy7	1 in 200	eBioscience	25-0902-81
	BrdU	FITC	1 in 100	BD Biosciences	51-2354AK
B cell	B220	PECy7	1 in 200	eBioscience	25-0452-81
	CD43	PE	1 in 200	eBioscience	12-0431-82
	CD24	APC780	1 in 200	eBioscience	47-0242-80
	BrdU	FITC	1 in 100	BD Biosciences	51-2354AK
Erythro	Ter119	PE	1 in 200	eBioscience	12-5921-81
	CD71	APC	1 in 100	eBioscience	17-0711-82
	Streptavidin	FITC	1 in 100	eBioscience	11-4317-87
	CD3e	Biotin	1 in 25	eBioscience	13-0031-75
	B220	Biotin	1 in 25	eBioscience	13-0452-75
	Ly-6G (Gr-1)	Biotin	1 in 25	eBioscience	13-5931-75
	BrdU	FITC	1 in 100	BD Biosciences	51-2354AK
***Ex vivo* BrdU**					
T cell DP	CD4	e450	1 in 200	eBioscience	48-0042-80
	CD8	PE	1 in 200	eBioscience	12-0081-82
	BrdU	FITC	1 in 100	BD	51-2354AK

				Biosciences	
	PH3S10	APC	1 in 250	Cell Signalling Tech	9716s
B cell	IGM	PerCPCy5.5	1 in 100	eBioscience	46-5790-80
	BrdU	FITC	1 in 100	BD Biosciences	51-2354AK
	PH3S10	APC	1 in 250	Cell Signalling Tech	9716s
***Ex vivo* DNA content**					
T cell	CD4	PECy7	1 in 200	eBioscience	25-0042
	CD8	PE	1 in 200	eBioscience	12-0081-82
Westerns					
Whole cell lysis	SMC4		1 in 4000	Bethyl labs	A300-064A
	CAP-H		1 in 2000	Bethyl labs	A300-603A
	CAP-H2		1 in 2000	Bethyl labs	A302-276A
	PCNA		1 in 3000	Santa Cruz	sc56
	α rabbit IgG	HRP	1 in 10000	Sigma	A0545
Sucrose gradients	SMC4		1 in 4000	Bethyl labs	A300-064A
	CAP-H		1 in 2000	Bethyl labs	A300-603A
	CAP-H2		1 in 2000	Bethyl labs	A302-276A
	α rabbit IgG	HRP	1 in 10000	Sigma	A0545

CHAPTER 3: ABNORMALITIES IN CHROMOSOME STRUCTURE IN CAPH2 MUTANT CELLS

3.1 Analysis of mitotic abnormalities in Caph2$^{nes/nes}$ mutant cells

3.1.1 Introduction

The role of condensins both in the process of condensation and in the removal of catenations between sister-chromatids in preparation for mitosis is well-established (Baxter & Aragón, 2012; Hagstrom, Holmes, Cozzarelli, & Meyer, 2002; Hirano & Mitchison, 1993, 1994; Hudson, Vagnarelli, Gassmann & Earnshaw, 2003; Ono *et al*., 2004). Mistakes in mitosis can lead to aneuploidy, chromosomal instability, and cancer, but mutations in genes encoding individual condensin subunits are not found in a large proportion of cancers.

3.1.1.1 Aneuploidy Defined

The term "aneuploidy" is often used to describe cells with an incorrect number of chromosomes. Strictly, however, the term should be reserved for cells with an abnormal number of chromosomes that is not an integer multiple of the haploid chromosomal complement. This definition therefore includes cells that have lost or gained whole chromosomes. Partial aneuploidies arise when sub-chromosomal regions are multiplied or deleted. In contrast, cells containing an integer multiple of chromosomes are referred to as "polyploid". Polyploid cells contain a balanced number of chromosomes, and are therefore less deleterious to the cell in comparison to an unbalanced chromosome complement (Guo, Davis, & Birchler, 1996; Papp, Pál, & Hurst, 2003). If the daughter cell, for example, loses part of a chromosome encoding a tumour suppressor gene, or gains a copy of an oncogene, this may result in inappropriate and extensive cellular division (Torres, Williams, & Amon, 2008).

Specifically, cells that undergo failed cytokinesis and therefore contain a 4*n* DNA complement (the haploid complement multiplied by four) are referred to as

"tetraploid". In the absence of cell cycle arrest, tetraploid cells have a strong tendency to assemble multipolar spindles due to the presence of supernumerary centrosomes, which then have an increased tendency to generate aneuploid cells via the missegregation of individual chromosomes (Figure 3.1) (Ganem, Storchova, & Pellman, 2007; Pfau & Amon, 2012).

Often, the assays used in this thesis are unable to distinguish between whole genome duplications (polyploidy) and either whole chromosome or partial aneuploidy. Therefore, throughout this thesis I have referred to cells with more than 4N DNA content as being "hyperdiploid", since these cells may be either polyploid or aneuploid.

Cells with 4N DNA content may arise as a consequence of failed cytokinesis, in which case they are termed "tetraploid" (as discussed above). Alternatively, a cell with 4N DNA content may represent a diploid cell in G2. Strictly, these cells should not be labelled tetraploid. However, the assay I have used most frequently in this thesis (flow cytometry) is unable to distinguish between these two possibilities. Therefore, I refer to cells with 4N DNA content as being "tetraploid", regardless of their stage in the cell cycle.

3.1.1.2 Condensins and tumourigenesis

Cancers tend to exhibit mutational heterogeneity, where a small number of "gatekeeper" genes, often direct regulators of the cell cycle, are frequently mutated. However, there are very many infrequently mutated genes, often with "caretaker" functions in the cell (Vogelstein *et al*., 2013). Condensin and cohesins belong to this second group of 'caretakers'. Interestingly, recent pan-cancer analysis revealed that the genes encoding subunits of condensin I, condensin II and cohesin are mutated in a small number of cancers. When the subunits were analysed separately, only the *SMC4* mutation was found to be significant. However, when the condensin II complex subunits were analysed as a unit, it was discovered that this complex was significantly mutated in lung adenocarcinoma (LUAD) (Leiserson *et al*., 2015). These mutations were missense. In addition, somatic point mutations in *SMC2* and *SMC4* have been observed in gastric and colorectal cancers (Je, Yoo, & Lee, 2014) and human

pyothorax-associated lymphomas (Ham *et al*., 2007), reaffirming the importance of condensins in maintaining chromosomal stability.

Although previous studies concluded that the *Caph2*$^{nes/nes}$ phenotype most likely arises due to interphase abnormalities (Gosling *et al*., 2007; Rawlings *et al*., 2011), I first decided to investigate the consequences of condensin II depletion on its well-established role in mitosis. In this section of Chapter 3, I describe the experiments carried out to determine whether the mutant cells exhibit abnormalities consistent with aberrant mitosis, as well as experiments that set out to investigate the morphology of mutant metaphase chromosomes in comparison to wildtype.

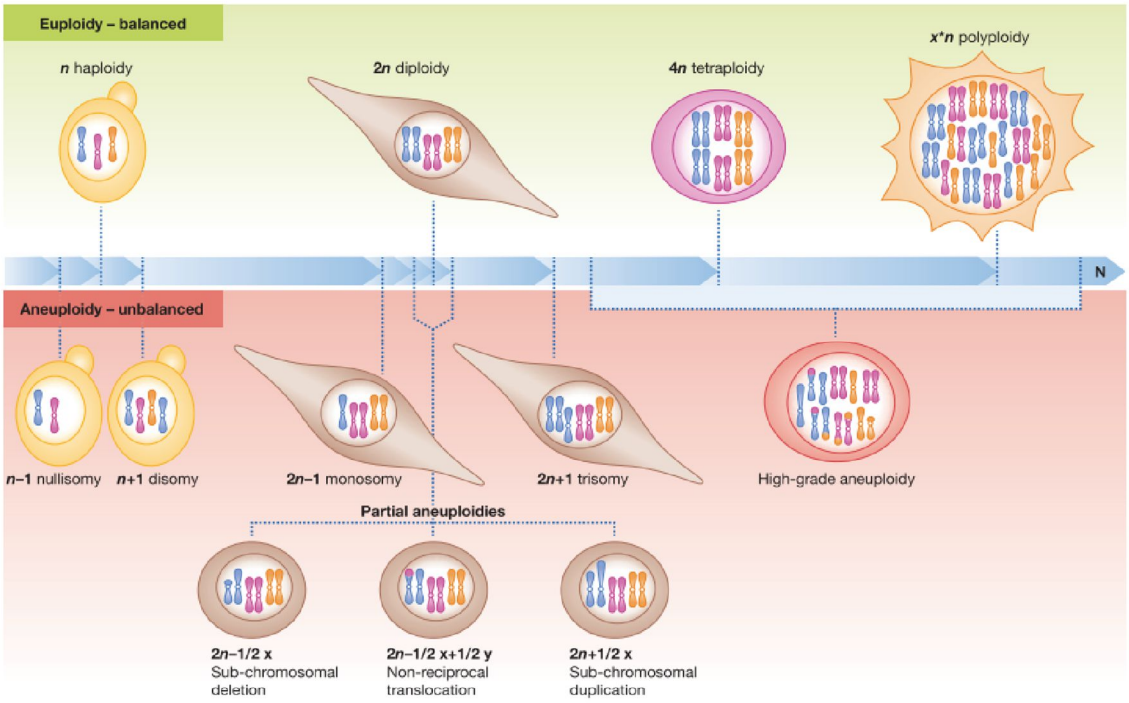

Figure 3.1
Chromosomal instability: polyploidy and aneuploidy
Schematic showing the difference between euploidy (a balanced karyotype) and aneuploidy (imbalanced karyotype). Polyploid cells contain an integer multiple of the haploid chromosomal complement (Pfau and Amon *et al*., 2012).

3.1.2 Results

3.1.2.1 Overview of the Caph2$^{nes/nes}$ developmental phenotype in T cells

Previous investigations into the *Caph2$^{nes/nes}$* mutation revealed that the mutant thymuses are considerably smaller than wildtype, with a hypocellular cortex and an increased proportion of $CD4^-$ $CD8^-$ DN stage cells relative to $CD4^+$ $CD8^+$ DP (Gosling *et al*., 2007). A 5-fold reduction in cell numbers at the DN4 stage and ~ 100-fold reduction at the DP stage was reported in mutant relative to wildtype. These results are consistent with a developmental block in T cell differentiation, specifically at the DN to DP transition (Figure 1.12). B cell differentiation was also analysed in the *Caph2$^{nes/nes}$* mice, but despite undergoing similar processes during development, only T cells were found to be affected by the mutation to *Caph2* (Gosling *et al*., 2007).

My results are broadly consistent with this previously published data: flow cytometry experiments reveal an increase in the proportion of mutant DN3 cells relative to wildtype (67.8% versus 35.9%) and approximately 2.5-fold reduction in the proportion of *Caph2$^{nes/nes}$* DN4 cells (Figures 3.2b and 3.2c). Additionally, a considerable reduction in the proportion of DP cells is apparent in mutant animals (Figures 3.2d and 3.2e). Finally, quantification of absolute cell numbers at various stages of T cell differentiation revealed a reduction in cell numbers in mutant animals, which peaks at approximately 85-fold at the DP 71^- resting stage (Figure 3.2f).Recently, PanCancer network analysis identified condensin subunit mutations in tumour genomes (Leiserson *et al*., 2015). This led other lab members to carry out aging studies on the condensin mutant mice to investigate the relationship between condensin deficiency and tumourigenesis, which revealed that the *Caph2$^{nes/nes}$* mice develop thymic lymphomas with high penetrance. Half of the mutant cohort had become moribund within 15 months (A. Wood, unpublished data, Figure 3.3a), with thymic lymphoma identified in all individuals. The thymic lymphomas originate from $CD4^+CD8^+$DP cells, i.e. the stage known to be vulnerable to the *Caph2$^{nes/nes}$* mutation (Wood, unpublished data, Figure 3.3b). I therefore set out to characterise the cellular events that lead to both the developmental block and the tumour phenotype in *Caph2$^{nes/nes}$* mutant mice.

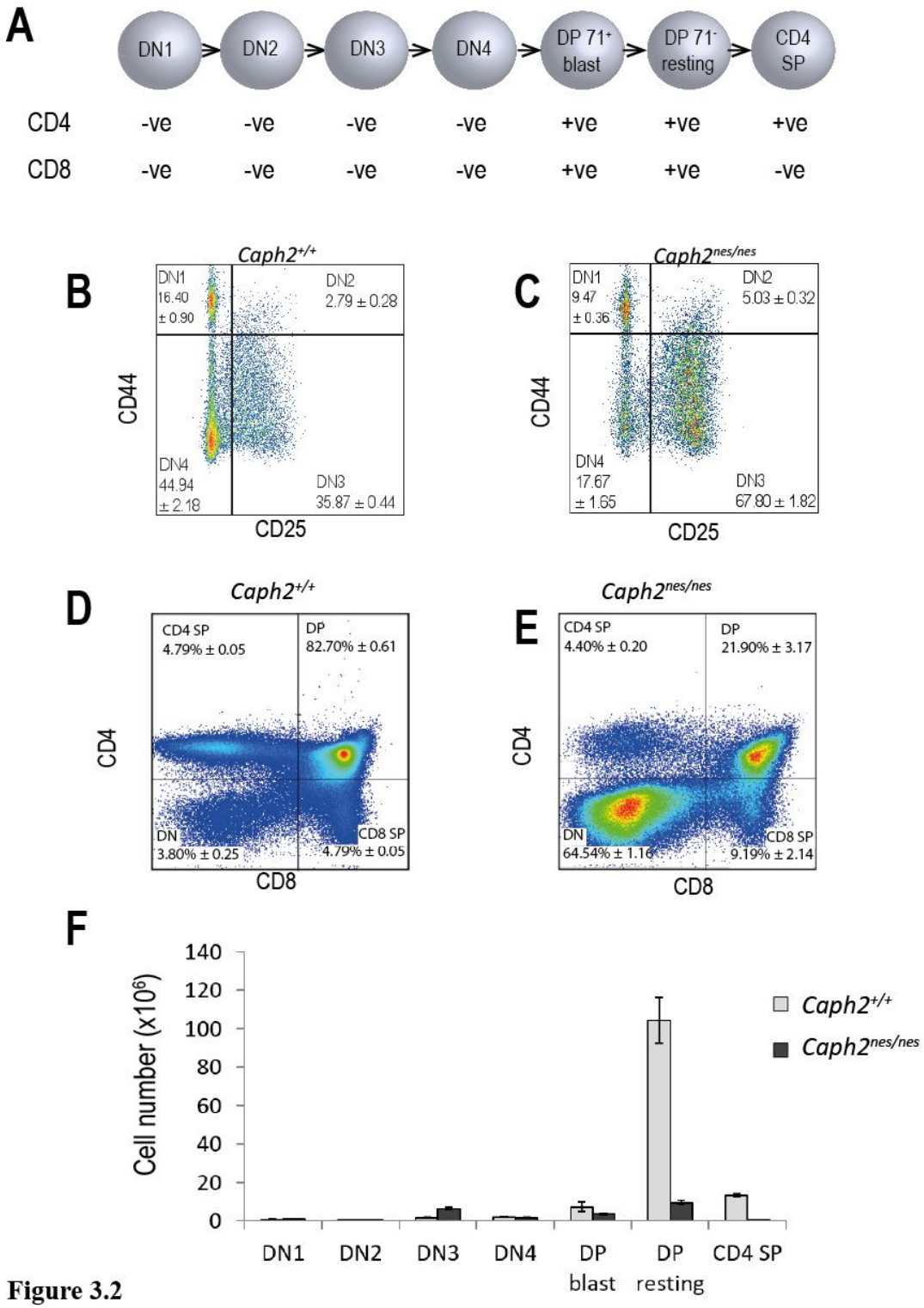

Figure 3.2

***Caph2*$^{nes/nes}$ mutation results in a block in T cell development**

A. Schematic showing stages of T cell development in relation to CD4 and Cd8 expression. **B.** Flow cytometry dot plot showing the distribution of wildtype subsets according to CD44 and CD25 expression. **C.** Distribution of *Caph2*$^{nes/nes}$ subsets (as for wildtype). **D.** Dot plot showing distribution of wildtype subsets according to CD44 and CD25 expression. **E.** Distribution of *Caph2*$^{nes/nes}$ subsets according to CD44 and CD25 expression. **F.** DNA content histogram showing the proportion of $CD4^+$ $CD8^+$ $CD71^+$ wildtype cells with 2N, 4N and >4N ploidy. **F.** Quantification of absolute cell numbers at different stages of wildtype (grey) and *Caph2*$^{nes/nes}$ (black) T cell development. Error bars represent the standard error of the mean and were calculated based on three biological replicates.

Cell percentages within the indicated subsets were calculated from three biological replicates. The mean value is presented, plus or minus the standard error of the mean.

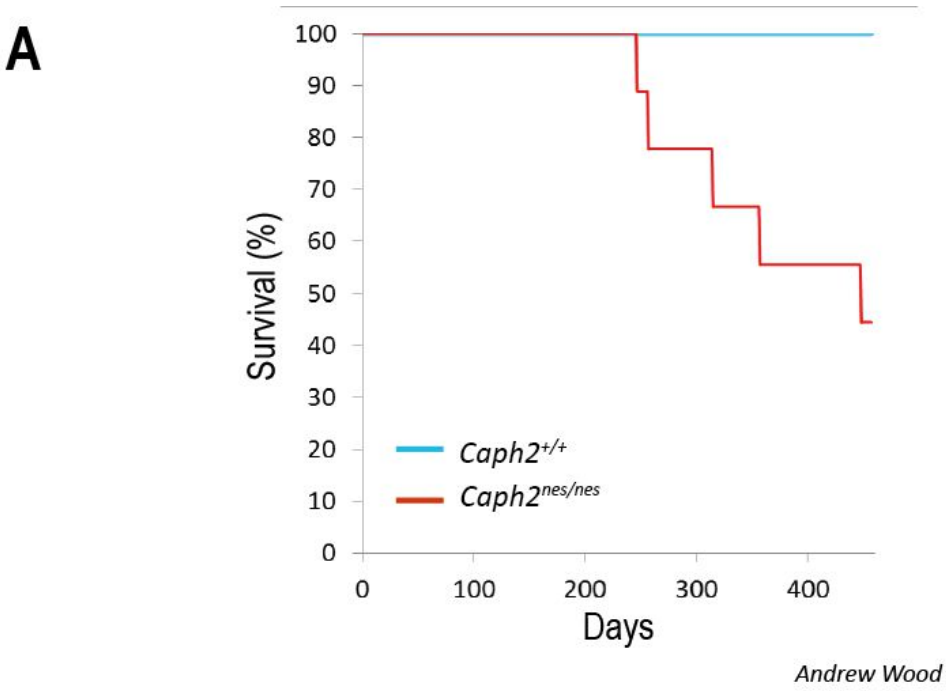

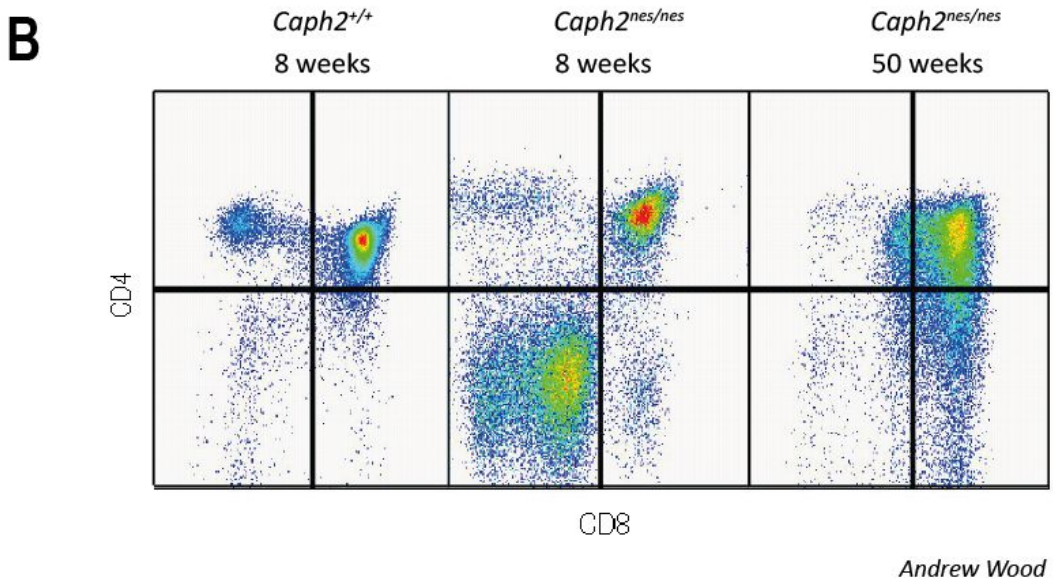

Figure 3.3
***Caph2*$^{nes/nes}$ mice develop thymic lymphomas**
A. Kaplan-Meier survival plot reveals that *Caph2*$^{nes/nes}$ mice experience a significant reduction in survival relative to wildtype over a 15 month period (p = 0.025). All surving *Caph2*$^{nes/nes}$ mice were found to have thymic lymphoma. **B.** Flow cytometry dot plot showing CD4 versus CD8 expression in one wildtype (left panel) and one mutant thymus (middle panel) aged 8 weeks pp, and a lymphoma from a *Caph2*$^{nes/nes}$ mouse at 50 weeks pp (Andrew Wood, unpublished data).

3.1.2.2 Investigating ploidy at the DP blast stage of T cell development using flow cytometry

To look for evidence of mitotic errors in *Caph2*$^{nes/nes}$ mice, I used flow cytometry to measure DNA content at the various stages of thymic T cell differentiation shown in Figure 3.2a. Cells were labelled with the DNA dye DAPI, in combination with fluorescently-conjugated antibodies to cell surface markers of T cell differentiation (Table 2.5). Interestingly, all later stages of *Caph2*$^{nes/nes}$ thymic T cell development show increases in the proportion of cells with 4N, or greater than 4N (hyperdiploid) DNA content. However, in this Chapter, I will focus on one specific developmental stage: CD4^{+} CD8^{+} double positive (DP) blast. This is the stage of development during which T cells proliferate rapidly following successful VDJ rearrangement of the TCR β-locus. This is also the stage at which the frequency of hyperdiploid cells is highest in the *Caph2*$^{nes/nes}$ mutant relative to *Caph2*$^{+/+}$, and from which lymphoma cells originate in aging *Caph2*$^{nes/nes}$ mice. A more detailed analysis of the dynamic changes in ploidy during differentiation is provided in Chapter 4.

Once dead cells and other debris had been excluded from the population using forward- and side-scatter properties (see Materials and Methods Section 2.2.7.2), the developmental stage of interest was selected using the gating strategies shown (Figure 3.4). Briefly, CD4 was plotted against CD8 and the population of cells positive for both cell-surface markers was selected. A histogram of CD71 - a cell surface marker for blasting DP cells (Brekelmans, van Soest, Leenen, & van Ewijk, 1994; Seitan *et al*., 2011) was plotted and the CD71 positive cells were selected. DNA-content profiles of these DP blast cells are shown (Figures 3.4e and 3.4f).

At this specific stage of development, there is an altered ploidy profile with a particular increase in the frequency of 4N and greater than 4N (hyperdiploid) DNA content in the *Caph2*$^{nes/nes}$ mutant. This may indicate that errors occur during mitosis at the DP blast stage of *Caph2*$^{nes/nes}$ development, resulting in increased levels of both tetraploid and hyperdiploid cells.

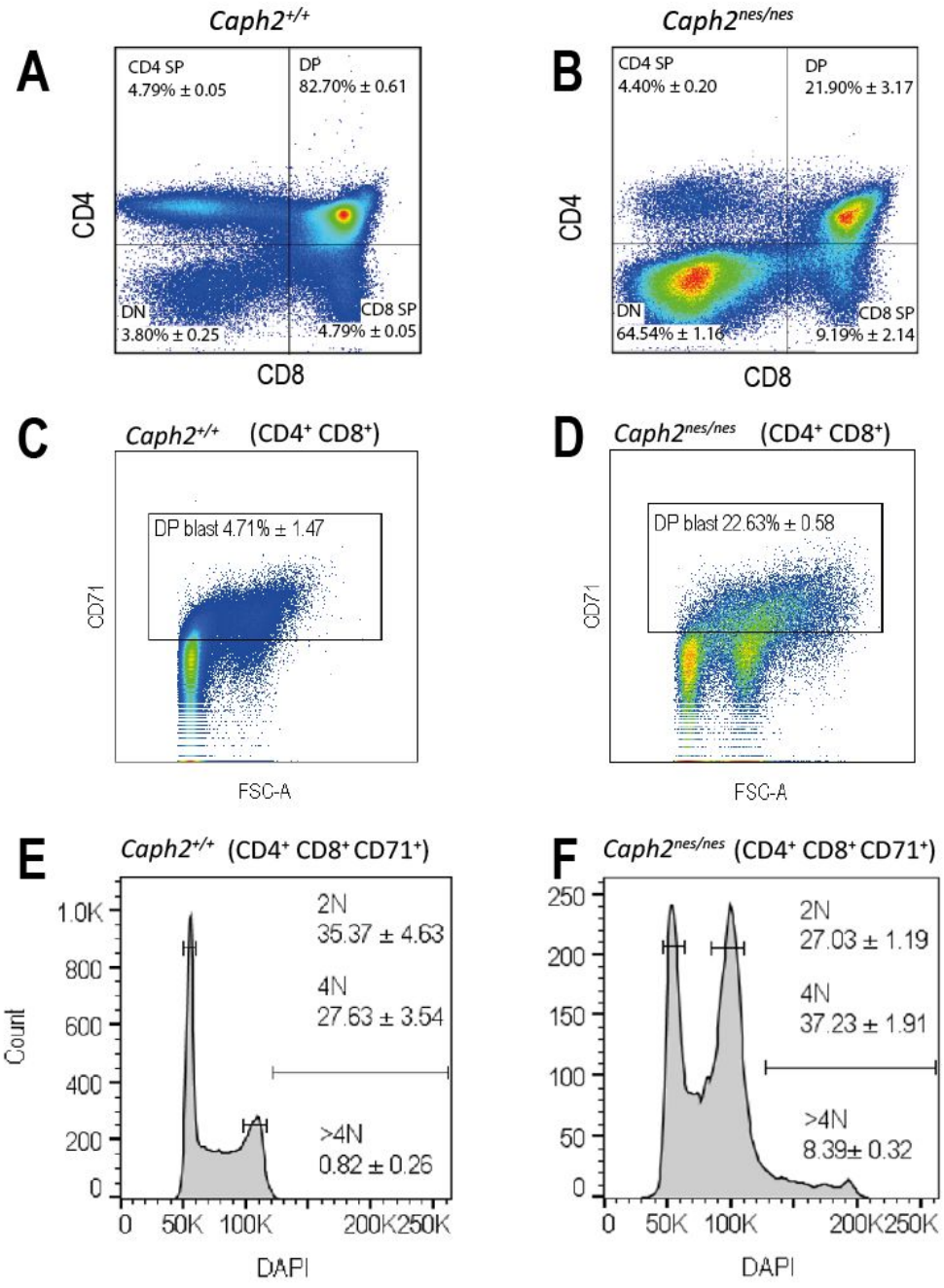

Figure 3.4

High frequency of hyperdiploid mutant cells versus wildtype at the DP blast stage of T cell development as determined by flow cytometry

A. Flow cytometry dot plot showing the distribution of wildtype subsets according to CD4 and CD8 expression. Cells are pre-gated based on FSC/SSC to eliminate aggregates **B.** Distribution of *Caph2*$^{nes/nes}$ subsets (as for wildtype). **C.** Dot plot showing cell size (FSC) and CD71 expression of CD4$^+$ CD8$^+$ wildtype cells. **D.** Dot plot showing cell size (FSC) and CD71 expression of CD4$^+$ CD8$^+$ *Caph2*$^{nes/nes}$ cells. **E.** DNA content histogram showing the proportion of CD4$^+$ CD8$^+$ CD71$^+$ wildtype cells with 2N, 4N and >4N ploidy. **F.** DNA content histogram showing the proportion of CD4$^+$ CD8$^+$ CD71$^+$ *Caph2*$^{nes/nes}$ cells with 2N, 4N and >4N ploidy.

Cell percentages within the indicated subsets were calculated from three biological replicates. The mean value is presented, plus or minus the standard error of the mean.

To confirm that the hyperdiploid cell populations are indeed individual cells rather than aggregates, a sample population was analysed using Image Stream: a technique that combines flow cytometry with imaging capabilities. Each cell is imaged as it passes through the laser beam, confirming whether the registered event is indeed a single cell, or aggregated cells. The results of this experiment provided visual confirmation that the vast majority of the hyperdiploid events detected by conventional flow cytometry are indeed single cells (Figure 3.5), thereby validating the use of the greater than 4N gate to identify individual cells with abnormal ploidy. This flow cytometry analysis was carried out by David Jameson of Newcastle University.

3.1.2.3 Investigating ploidy at the DP blast stage of T cell development using FISH

Even when subjected to stringent doublet exclusion, flow cytometry can be hampered by the inclusion of cell aggregates within a population. Given the potentially interesting implications of increased levels of aneuploidy in *Caph2*$^{nes/nes}$ T cell development, it was important to verify this finding using an independent method that would not be subject to the same limitations. To do this, I carried out 3D 3-colour Fluorescence in situ Hybridisation (FISH) on DP blast *Caph2*$^{+/+}$ and *Caph2*$^{nes/nes}$ cells.

FISH is a well-established cytogenetic technique that allows copy number enumeration of specific chromosomal sequences based on the number of hybridisation signals per nucleus. However, the technique is vulnerable to false-positive signals, which could be mistaken for elevated copy number. I therefore used pairs of fosmid probes that hybridise within 200kb of each other, and only counted foci at which both probe signals were clearly present in close proximity (Figure 3.6).

The CD4$^+$ CD8$^+$ DP population of cells was FACS-sorted (Materials and Methods: Cell sorting) using fluorescently conjugated antibodies to cell surface markers (Table 2.5) and seeded onto polyprep/polylysine slides (as described in Materials and Methods: Preparation of Slides for FISH). Pairs of fosmids were selected to target two different loci: the *CD8* locus - which is highly transcribed at this stage of thymic development, and *HoxA*, which is inactive (Table 2.3). Both loci are located on chromosome 6 which allowed me to assess the copy number of chromosome 6, using two independent loci.

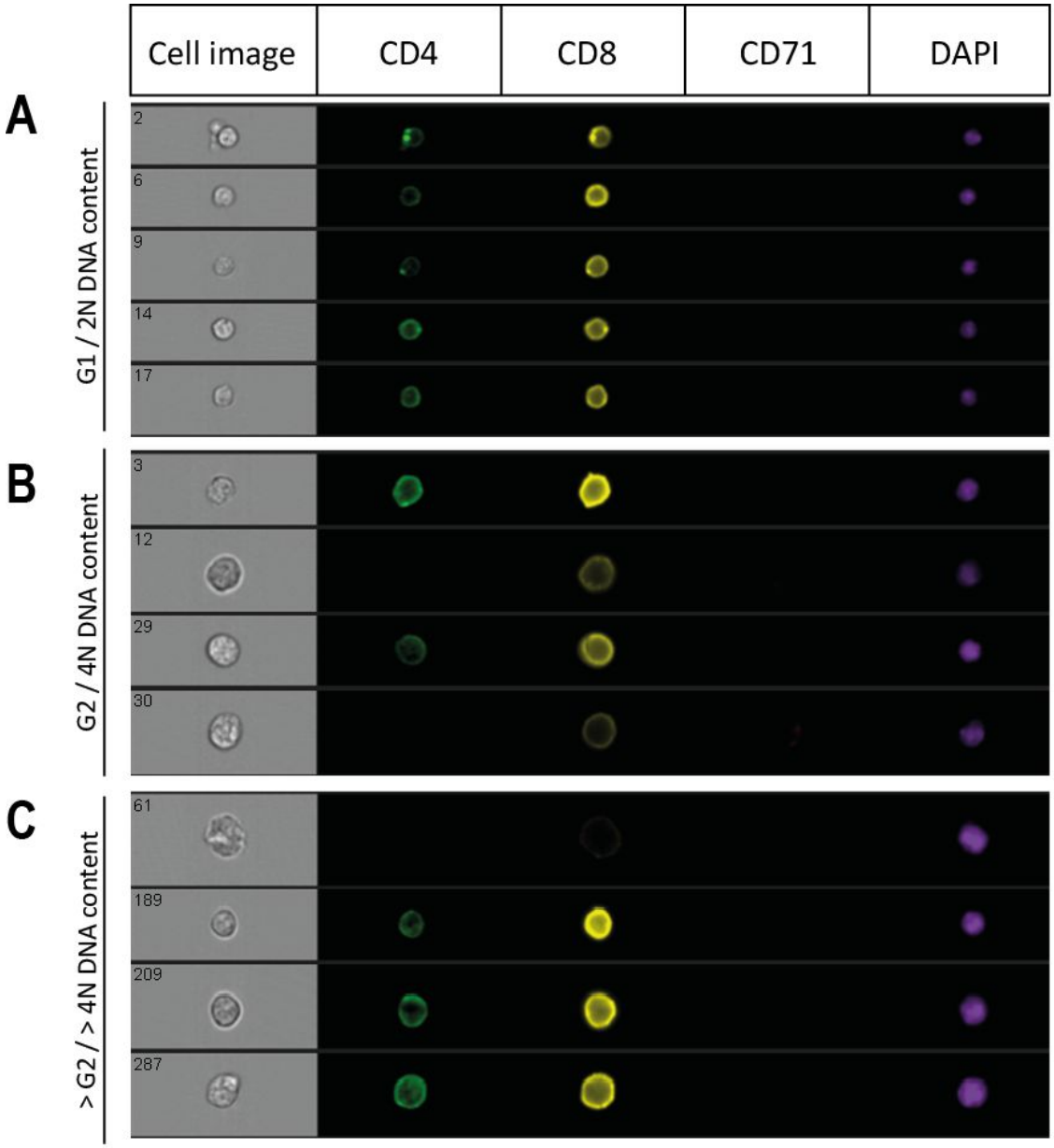

Figure 3.5
Confirmation that cells thought to contain abnormal ploidy are single cells, not cell doublets or aggregates
A. Cells with 2N DNA content as judged by DAPI / DNA content analysis are confirmed to be single cells when each event is imaged as it passes through the laser beam. **B.** Cells with 4N DNA content as judged by DAPI / DNA content analysis are confirmed to be single cells when each event is imaged as it passes through the laser beam. **C.** Hyperdiploid cells (>4N DNA content) as judged by DAPI / DNA content analysis are confirmed to be single cells when each event is imaged as it passes through the laser beam.

For each locus one probe was labelled with biotin-16-dUTP (biotin) and the other with digoxigenin-11-dUTP (DIG). Representative FISH images are shown for the CD8 locus (Figure 3.6a) and HoxA locus (Figure 3.6b).

The number of paired fosmid hybridisation signals were counted per nucleus, and the proportion of nuclei with one pair, two pairs, three, four and more than four pairs was calculated, and expressed as a percentage of the total number of nuclei imaged, and plotted as a histogram (Figure 3.6c). The results showed an increased frequency of *Caph2*$^{nes/nes}$ mutant DP blast cells with more than two copies of each locus. Although four copies was the next most frequent copy number after two (~22% in *Caph2*$^{nes/nes}$ versus ~4% in wildtype), three spots were also observed at frequencies that were elevated over wildtype (~8% versus ~1%). Differences in the number of fosmid pairs between wildtype and mutant were found to be significant at $p < 0.05$ using a Fisher test.

Very consistent results were obtained for both the *CD8* and *HoxA* loci, and the difference in the number of fosmid pairs was also found to be statistically significant for *HoxA* at $p < 0.05$. The similarity in the results for both loci implies that whole chromosome aneuploidy occurs in *Caph2*$^{nes/nes}$ DP blast T cells (at least of chromosome 6). These data support the finding of increased frequencies of hyperdiploid DP blast cells in *Caph2*$^{nes/nes}$ observed using flow cytometry.

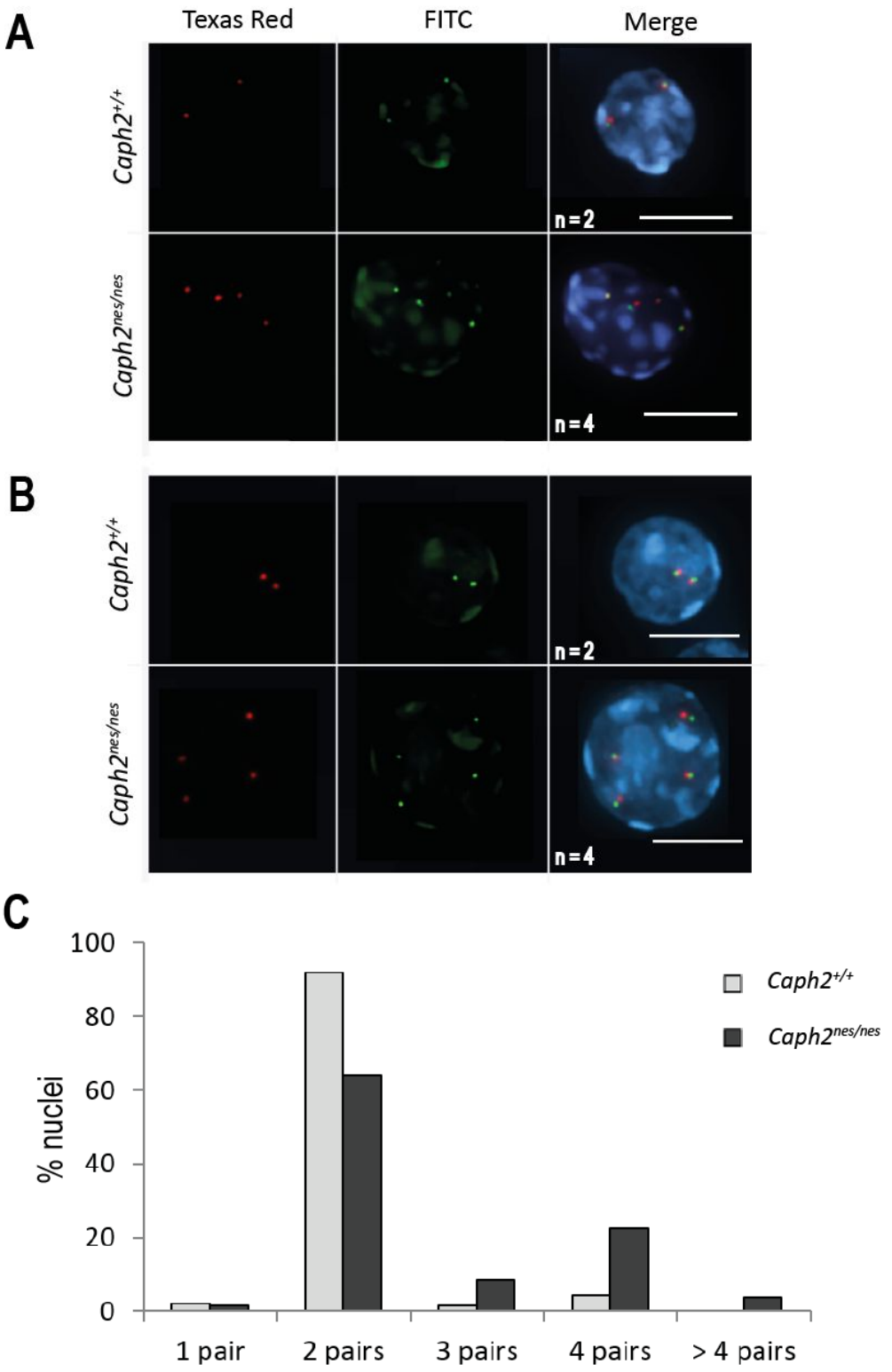

Figure 3.6

High frequency of hyperdiploid mutant cells versus wildtype at the DP blast stage of T cell development as determined by 3D FISH

A. Representative FISH images of wildtype and *Caph2*$^{nes/nes}$ cells with probes labelled to the CD8 locus (number of fosmid pairs are indicated on the figure). **B.** Representative FISH images of wildtype and *Caph2*$^{nes/nes}$ cells with probes labelled to the HoxA locus **C.** Histogram showing the percentage of wildtype and *Caph2*$^{nes/nes}$ cells with 1, 2, 3, 4 and greater than 4 pairs of spots with fosmid probes labelled to the CD8 locus. Data obtained from multiple experiments. A Fisher test was performed on the data, and differences in the number of fosmid pairs were found to be significant with a p value < 0.00001. Data represents 136 wildtype and 130 mutant nuclei. Consistent results were obtained with probes labelled to the HoxA locus.

3.1.2.4 Investigating ploidy during T cell development using an ex vivo T cell culture system

Finally, in order to confirm the elevated frequency of hyperdiploid mutant cells relative to wildtype using a third independent technique, I prepared metaphase spreads from T cells cultured briefly *ex vivo* using the OP9 DL1 *in vitro* T cell culture system (de Pooter and Zúñiga-Pflücker, 2007). T differentiation can be recapitulated *ex vivo* by culturing primary T cell precursors on a monolayer of OP9/DL1 cells: a stromal cell line that is induced to ectopically express the notch ligand Delta-like 1 (DL1). The use of an *ex vivo* culture system as a tool to study the abnormal ploidy phenotype in *Caph2*$^{nes/nes}$ was validated by DNA content analysis of CD4$^+$ CD8$^+$ DP T cells cultured on the OP9 DL1 monolayer, which revealed an increased proportion of hyperdiploid cells in mutant relative to wildtype (Figures 3.7a and 3.7b). However, the proportion of hyperdiploid mutant cells was lower than *in vivo* (Figures 3.4e and 3.4f).

To prepare metaphase spreads, I plated a monolayer of OP9 DL1 cells onto the wells

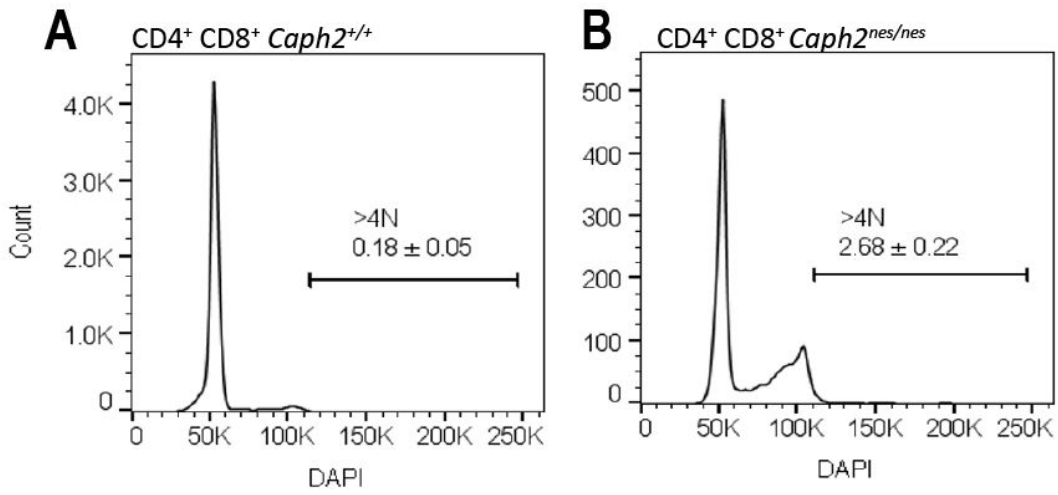

Figure 3.7
DNA content profiles of CD4$^+$ CD8$^+$ T cells cultured *ex vivo*
A. DNA content histogram showing the proportion of wildtype DP T cells with greater than 4N DNA content. **B.** DNA content histogram showing the proportion of *Caph2*$^{nes/nes}$ DP T cells with greater than 4N DNA content. There is an increase in the proportion of hyperdiploid mutant cells relative to wildtype, although this increase is less extreme than that observed *in vivo*.

Cell percentages within the indicated subsets were calculated from three biological replicates. The mean value is presented, plus or minus the standard error of the mean.

of a 6-well plate. MACS purified $CD4^-$ wildtype and *Caph2*$^{nes/nes}$ cells were added to separate wells onto the monolayer. T cells were cultured in the presence of IL-7 on the monolayer for four days (Materials and Methods: Section 2.2.9.5) resulting in a population of approximately 40%-50% $CD4^+$ $CD8^+$ wildtype DP cells and 15-20% mutant DP cells. The cells were treated with colcemid for two hours, before they were removed (Figure 3.8a), treated with hypotonic solution (0.5% sodium citrate, 0.25% potassium chloride in deionised water) and fixed with 3:1 methanol: acetic acid (Materials and Methods: Section 2.2.5).

After fixation, metaphase spreads were prepared by dropping the cell suspension onto slides. The sample was dehydrated before being rehydrated in PBS containing DAPI and the mitotic chromosomes imaged by confocal microscopy. Representative images are shown (Figure 3.8b). The number of centromeres in each of the spreads was counted and the proportion of hyperdiploid cells for both the *Caph2*$^{+/+}$ and *Caph2*$^{nes/nes}$ populations was determined, and plotted as a histogram (Figure 3.8c).

Optimisation of the conditions to provide fully spatially distinct chromosomes proved to be challenging for this cell type. I therefore chose to count the number of centromeres rather than the number of chromosomes, since the centromeres were easily discernible, whereas the chromosomes were not always easily distinguished from one another. This may be due to the amount of time spent in colcemid treatment, which is known to affect the morphology of chromosomes, but could also reflect intrinsic properties of the nuclear matrix and nuclear membrane in primary T cells that inhibit spreading.

To account for the potentially high margin of error using this approach, for example due to chromosomes lying on top of each other, or from individual chromosomes being spread beyond the field of view, I adopted a liberal definition of "~diploidy" for this analysis: 38 – 40 chromosomes. There are several reasons why diploid metaphase spreads may appear to have lost two centromeres: for example, if two centromeres lie on top of each other, it may be difficult to distinguish one from the other.

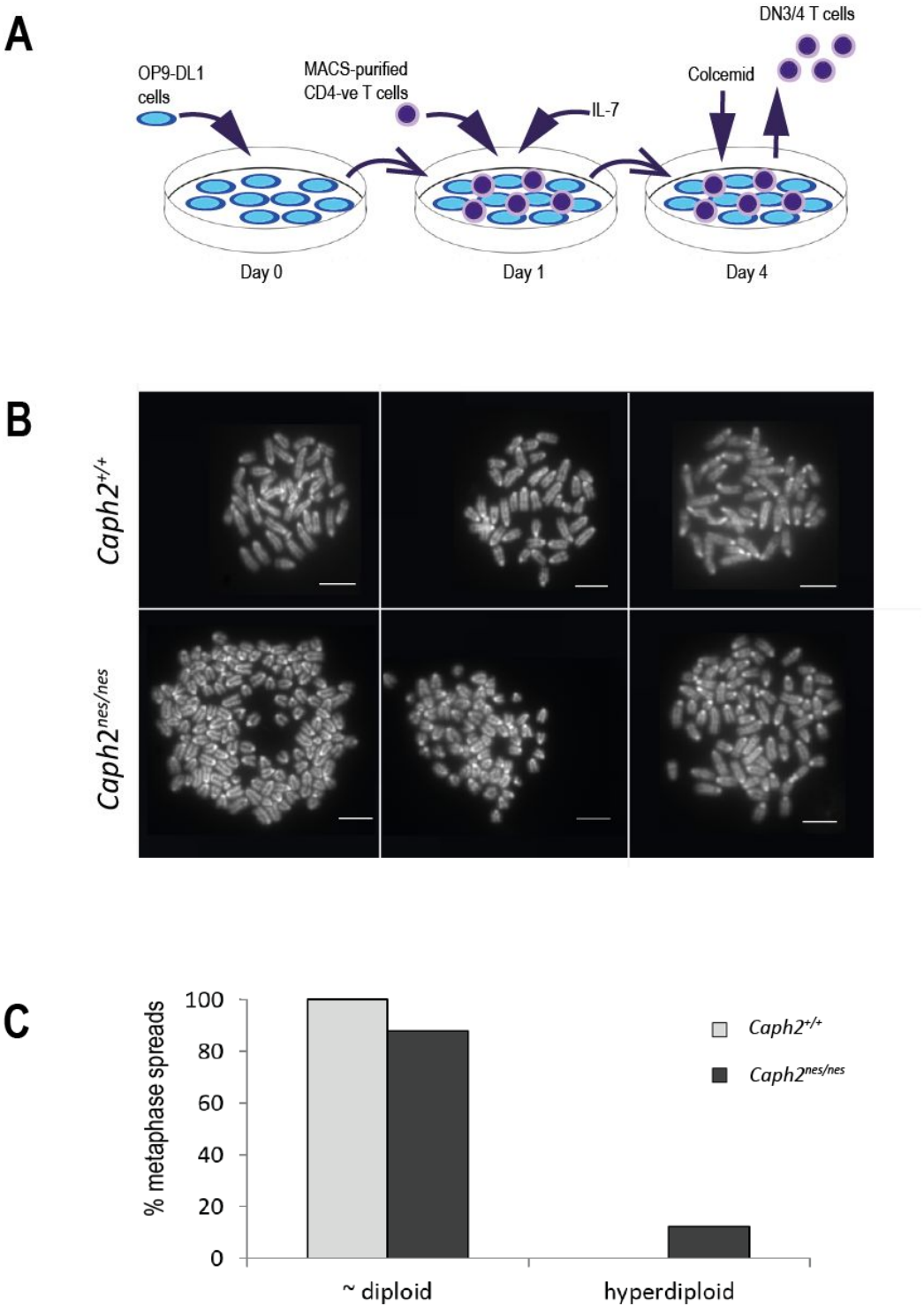

Figure 3.8
High frequency of hyperdiploid mutant cells versus wildtype determined using an ex-vivo T cell culture system
A. Schematic of ex-vivo T cell culture protocol. **B.** Representative images of wildtype and *Caph2*$^{nes/nes}$ T cell metaphase spreads. **C.** Histogram showing the percentage of wildtype and *Caph2*$^{nes/nes}$ metaphase spreads with ~diploid chromosome complement (38-40 chromosomes), or hyperdiploid complement. A total of 93 wildtype and 98 *Caph2*$^{nes/nes}$ speads were imaged and the number of chromosomes counted. A Fisher exact test was performed on the data and a significant increase in the percentage of mutant cells with a hyperdiploid chromosome complement was found in comparison to wildtype. (Fisher exact test statistic value is 0.000172).

Of the 93 wildtype spreads imaged, no hyperdiploidy was observed. In contrast, I observed 12 hyperdiploid mutant spreads within the 98 that were imaged. A Fisher exact test was performed on the data giving a statistic value of 0.000172. Therefore, the differences in the levels of hyperdiploidy between wildtype and mutant were found to be significant at $p < 0.05$. These data therefore show that the increased levels of hyperdiploidy in the *Caph2*$^{nes/nes}$ mutant, observed using two independent techniques, is also detected in primary cells following short-term culture.

The hyperdiploid mutant chromosomes were, in the majority of cases, intermediate between 2N and 4N, indicating that whole chromosome aneuploidy is present in the *Caph2*$^{nes/nes}$ mutant. However, flow cytometry revealed an increase in the proportion of cells with 4N as well as > 4N DNA content at the DP 71^{+} blast stage (Figures 3.4e and 3.4f). Therefore, as defined by Amon *et al*. (Pfau & Amon, 2012), the *Caph2*$^{nes/nes}$ mutant displays whole genome duplications in addition to whole chromosome aneuploidy.

3.1.2.5 BrdU chase assay to determine whether mutant 4N cells arise due to mitotic slip or G2 arrest

The population of 4N mutant cells may represent tetraploid cells that have undergone G1 arrest following unsuccessful mitosis, or diploid cells that have arrested after failing to enter mitosis. To distinguish between these two possibilities, I devised a BrdU "chase" assay that allowed S phase cells to be followed into mitosis over a time course. BrdU is a thymidine analogue, and is incorporated into genomic DNA during S phase DNA synthesis. For these experiments I cultured MACS purified CD4^{-} wildtype and *Caph2*$^{nes/nes}$ T cells on the OP9 DL1 system (Section 3.1.2.4). Once approximately 40%-50% of the wildtype and 15%-20% of mutant cells had progressed to the DP stage, the cells were simultaneously treated with the microtubule inhibitor nocodazole and the nucleotide analogue BrdU over a four hour time course (Materials and Methods: Section 2.2.9.5). The BrdU analogue was used to label S phase cells, while nocodazole arrests cells in prometaphase. The T cells were then removed from the monolayer and incubated with fluorescently conjugated anti- CD4 and CD8 antibodies as well as antibodies to BrdU and phosphorylated serine 10 on histone 3 (PH3S10: which labels cells from mitotic prophase). The cells that expressed both

CD4 and CD8 (the DP population) were analysed by flow cytometry.

PH3S10 was plotted against BrdU for each time point (Figure 3.9c), to determine the percentage of DP cells that had progressed to M phase from S phase (i.e. the proportion of $PH3S10^{+}$ $BrdU^{+}$ double-positive cells as a fraction of total cells positive for BrdU). Having progressed to M phase, the cells accumulate in prometaphase, due to the nocodazole treatment. The relevant time points in this experiment in relation to the cell cycle are indicated in Figure 3.9b. The rate of progression of the wildtype and mutant cells from S phase into M phase is shown as a line graph (Figure 3.9d).

The rate of progression from S to M phase is very similar between wildtype and mutant as judged by BrdU incorporation and PH3S10 (Figure 3.9d). This indicates that, at the relevant stage of T cell differentiation, the *Caph2*$^{nes/nes}$ cells are not impeded in their progression into mitosis i.e. there is an absence of a cell cycle block in G2. Therefore, it is likely that the increased frequency of 4N and > 4N cells is not a consequence of arrest at G2 stage. Finally, the data suggests that the tetraploid cells that arise in the *Caph2*$^{nes/nes}$ mutants are not a consequence of mitotic skip, since cells undergoing mitotic skip would not progress to, and accumulate in mitosis at all.

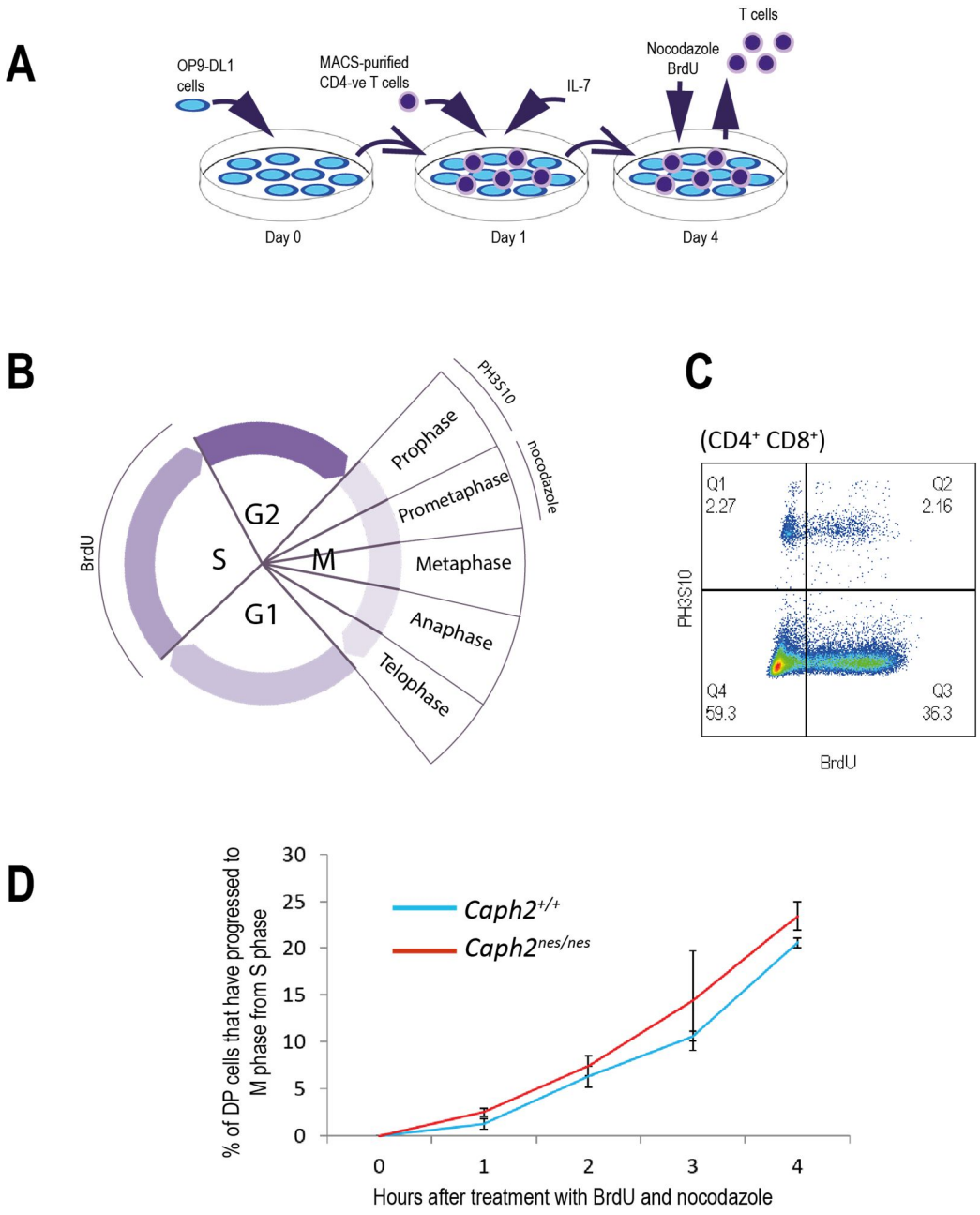

Figure 3.9

No difference in the rate of progression from S to M phase between wildtype and *Caph2*$^{nes/nes}$

A. Schematic of ex-vivo T cell culture protocol. **B.** Schematic of relevant timepoints. **C.** Representative image of flow cytometry dot plot 4 hour time point showing PH3S10 and BrdU expression of CD4$^+$ CD8$^+$ cells. The percentage of cells in each quadrant is indicated on the figure. The proportion of cells that progressed from S to M phase at each timepoint was calculated by dividing the PH3S10$^+$ BrdU$^+$ population (labelled Q2) by the proportion of BrdU$^+$ cells (quadrants Q2 and Q3). **D.** Line-graph showing the rate of progression of CD4$^+$ CD8$^+$ cells from S to M phase. The results show no major difference between wildtype and *Caph2*$^{nes/nes}$. This data indicates that the population of large arrested *Caph2*$^{nes/nes}$ cells with tetraploid DNA content does not arise due to G2 arrest.

Values have been set to zero at the zero hour time point.

Error bars represent the standard error of the mean and were calculated based on two technical replicates. The experiment was repeated with three biological and six technical replicates. No obvious differences were observed between *Caph2*$^{+/+}$ and *Caph2*$^{nes/nes}$ in any experiment.

3.1.2.6 Metaphase chromosome abnormalities in Caph2$^{nes/nes}$ mutant fetal liver erythroblasts (E12.5)

In the previous sections I confirmed the presence of increased levels of hyperdiploidy in the *Caph2$^{nes/nes}$* mutant at the DP blast stage of T cell development using two independent techniques. In addition, I found increased levels of aneuploid *Caph2$^{nes/nes}$* T cell metaphase spreads compared to wildtype. Therefore, I have confirmed using three independent techniques that there is an increase in the frequency of hyperdiploid *Caph2$^{nes/nes}$* T cells in comparison to wildtype.

To investigate possible causes of the abnormal ploidy, I next studied the consequences of the *Caph2$^{nes/nes}$* mutation on metaphase chromosome structure and explored the possibility that the increased frequency of hyperdiploid cells could be a consequence of aberrant mitosis. To do this, I imaged metaphase chromosomes directly, in order to look for any differences in structure resulting from *Caph2$^{nes/nes}$* mutation. I initially chose to use E14.5 fetal liver cells since this is a relatively synchronised population of cells, eliminating the need for MACS purification or flow cytometry sorting. DNA content quantification using flow cytometry confirmed that, like T cells, the *Caph2$^{nes/nes}$* erythroid cells also show an increase in the proportion of cells with hyperdiploid DNA content in comparison to wildtype. These experiments are described in Chapter 4 (Figure 4.6c). The erythroid cell lineage was therefore deemed a suitable choice to determine whether the increased proportion of cells with abnormal ploidy is reflected in an increased incidence of abnormal mitotic chromosome morphology.

Metaphase cells were treated with colcemid for 30 minutes, fixed with methanol-acetic acid (Materials and Methods: Section 2.2.5), DAPI-stained and imaged by confocal microscopy. Whereas wildtype chromosomes had long, thin chromosome arms with sister chromatids closely associated along their arms, in contrast many of the *Caph2$^{nes/nes}$* chromosomes appeared to be much more bloated or "puffier", indicating a disruption of chromosome architecture. In some instances, the *Caph2$^{nes/nes}$* chromatid arms appeared to be more splayed than in wildtype (Figures 3.10a and 3.10b). A higher mitotic index in mutant relative to wildtype might account for these differences, since the mitotic mutant cells would be exposed to colcemid for longer. However, the mitotic

index of the wildtype and mutant cells were estimated by eye, and substantially fewer mitotics were observed in the *Caph2*$^{nes/nes}$ spreads relative to wildtype.

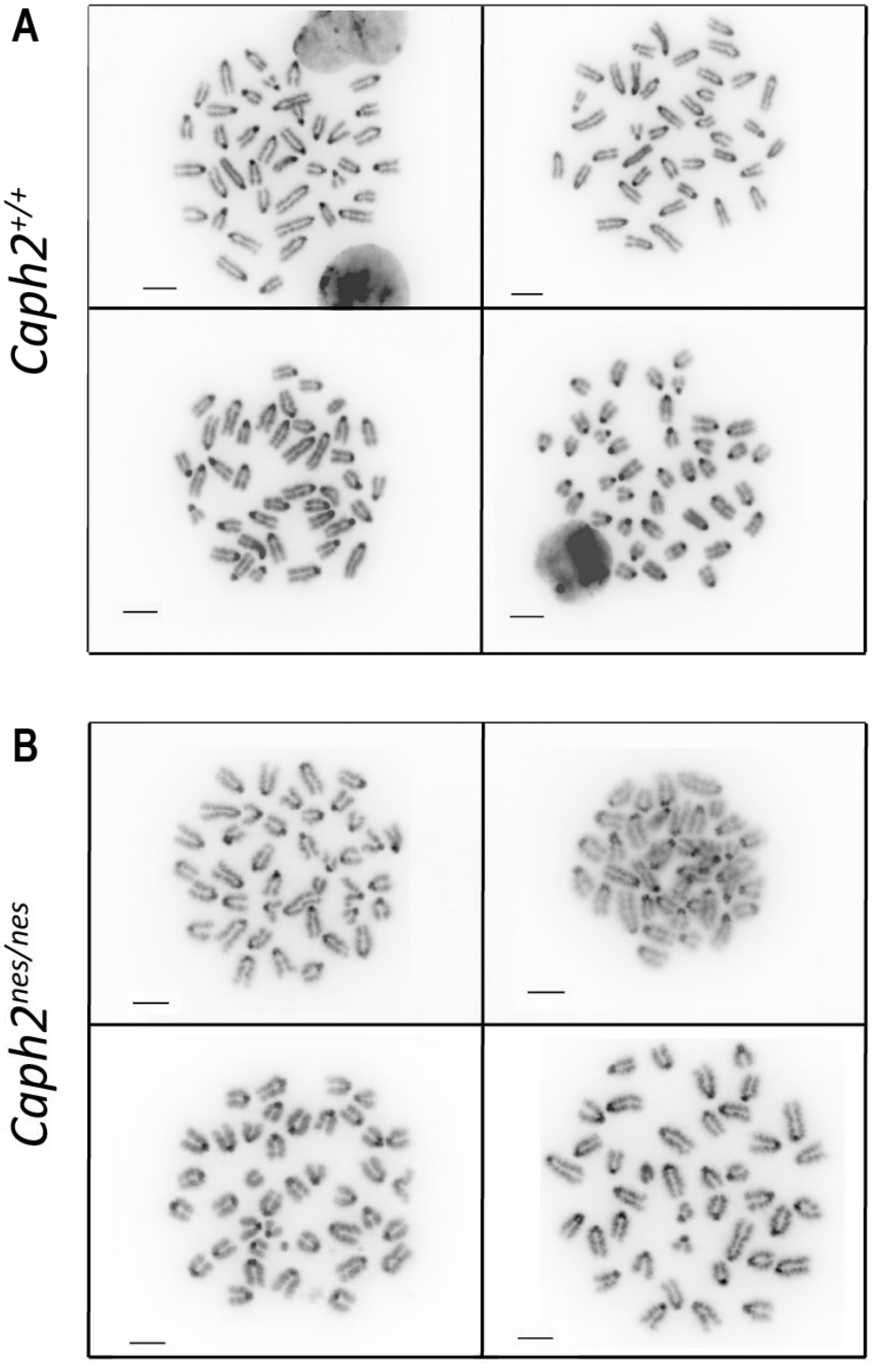

Figure 3.10
Metaphase chromosome abnormalities in *Caph2*$^{nes/nes}$ fetal liver erythroblasts imaged using a confocal microscope
A. Representative images of *Caph2*$^{+/+}$ 3:1 methanol:acetic acid fixed metaphase spreads. **B.** Representative images of *Caph2*$^{nes/nes}$ 3:1 methanol:acetic acid fixed metaphase spreads. Chromosmes appear more bloated compared to wildtype chromosomes. Several chromatid arms appear splayed.

In addition, the *Caph2*$^{nes/nes}$ chromosome arms appeared to have a "wavy" structure. This phenotype has previously been reported in condensin II-deficient cells (Ono *et al*., 2013). However, the low resolution of the confocal images made it difficult to draw any firm conclusions.

Traditional confocal microscopes are limited in the image resolution that can be obtained. As light passes through an aperture (for example, as the light passes through the objective aperture in a confocal microscope), the light is spread out due to diffraction. Therefore, a sharp point on the object being imaged will become blurred, in a process called the point spread function (PSF). The fine detail within this "spread" of light cannot be resolved. Therefore, the resolution of a conventional confocal microscope is diffraction limited.

In order to obtain higher resolution images of the metaphase chromosomes, I used Structured Illumination Microscopy (SIM). This process involves illuminating the sample with patterned light, causing the light diffracted by the fine detail in the sample and the grating pattern to interfere with one other. The resulting Moire fringe patterns are of much lower frequency than the original diffraction pattern produced by the sample. This allows more information to be collected from the sample that was previously outside the observable region: confocal imaging typically provides a resolution of approximately 200-210nm, whereas SIM allows a resolution of approximately 140nm.

The fetal liver erythroid cells were prepared as before (Section 3.1.2.4), but were dropped directly onto coverslips, rather than onto slides in order to reduce the distance between the sample and the light source, thereby minimising diffraction of light, and loss of information.

The SIM images revealed profound differences in the morphology of the metaphase chromatid arms (Figure 3.11). The wavy (zig-zag) shape of the chromatid arms was striking in the condensin mutant chromosomes, and this morphology was apparent in every *Caph2*$^{nes/nes}$ metaphase spread that was imaged (98 spreads in total). None of the 93 wildtype chromosome spreads that were observed revealed this morphology.

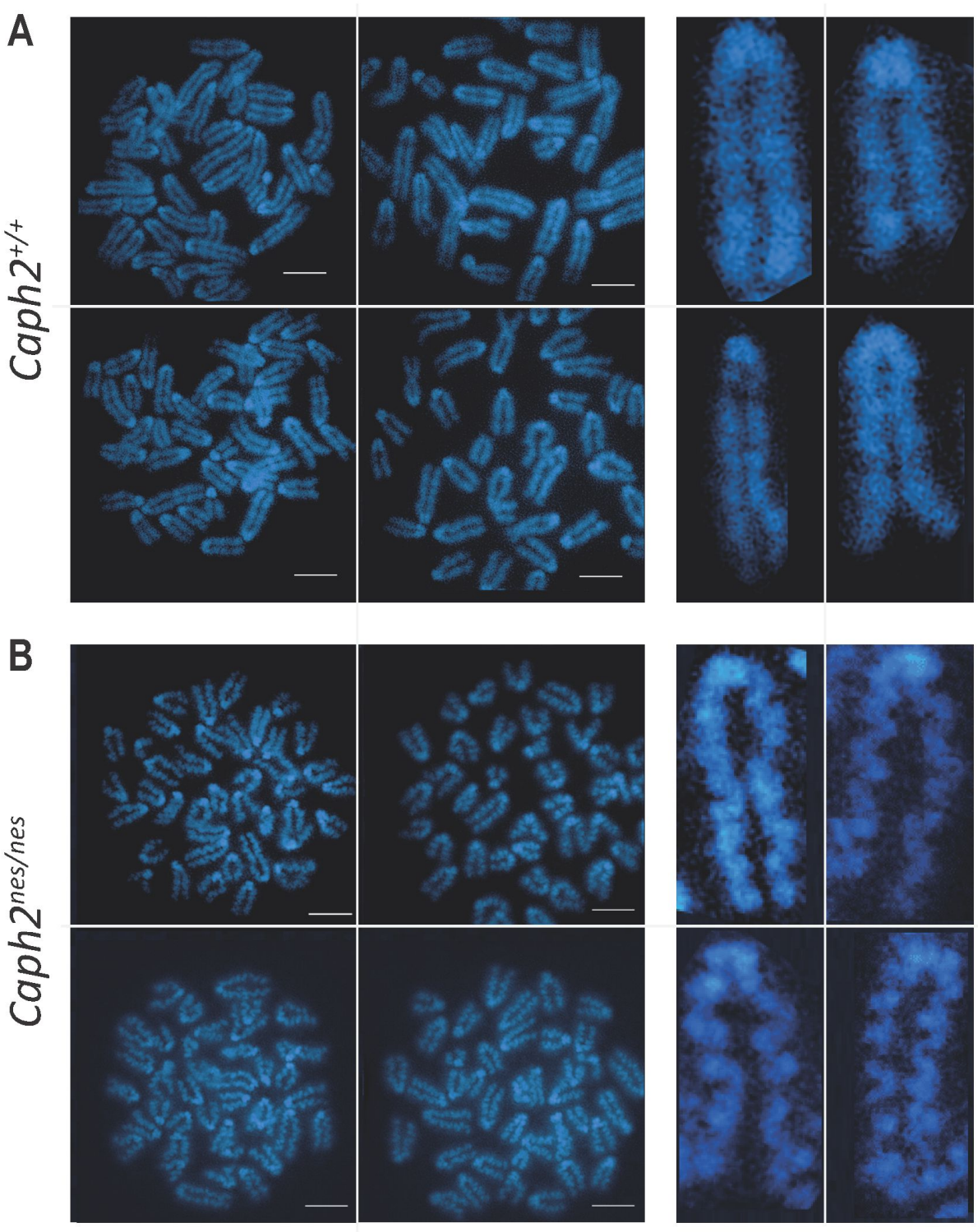

Figure 3.11
SIM images reveal profound differences in the morphology of *Caph2*$^{nes/nes}$ fetal liver erythroblast chromosomes compared with widtype
A. Representative images of *Caph2*$^{+/+}$ 3:1 methanol:acetic acid fixed metaphase spreads (left) and individual chromosomes (right). **B.** Representative images of *Caph2*$^{nes/nes}$ 3:1 methanol:acetic acid fixed metaphase spreads (left) and individual chromosomes (right). The zig-zag morphology of the mutant chromosome arms is evident when imaged using SIM.

3.1.2.7 Metaphase chromosome abnormalities in Caph2$^{nes/nes}$ mutant T cells

For the previous experiments fetal liver erythroblasts were used to make metaphase spreads. This was largely due to convenience, since there was no need to sort the cells to obtain a population of cells that were relatively homogeneous with respect to differentiation status. However, since the nessy phenotype appears to be most profound in thymic T cells, I next analysed the morphology of metaphase T cells.

Having cultured MACS purified CD4$^-$ T cells on OP9 DL1 monolayers for four days (as described above), the T cells were removed from the monolayer following two-hour colcemid treatment. The cells were prepared as before (Materials and Methods: Section 2.2.5). Differences in the metaphase chromosome morphologies were observed between wildtype and mutant spreads (Figure 3.12b). A higher proportion of the *Caph2$^{nes/nes}$* chromosomes appeared shorter and "puffier", with less well-defined structure compared to wildtype. In addition, a higher proportion of chromatid arms appeared "splayed" in mutant compared to wildtype T cells. Due to the "puffy" nature of the chromosomes, however, this was difficult to quantify (the chromosomes were not always easily distinguished from one another, as discussed in Section 3.1.2.4). A higher proportion of splayed chromosomes may indicate that the centromeres of the *Caph2$^{nes/nes}$* cells are less rigid than in wildtype (Rieder & Cole, 1999), although more work is needed to confirm this. Finally, several of the mutant chromosome spreads appeared to have a wavy (zig-zag) morphology, similar to that observed in the mutant fetal liver spreads (indicated by arrows), although a higher resolution, such as that provided by SIM would be required to attempt to quantify this. The puffy, zig-zag morphology was not observed in any of the wildtype spreads that were imaged.

The data presented thus far implies that T cells in *Caph2$^{nes/nes}$* mice experience abnormalities in mitotic chromosome structure, which leads to abnormal mitosis and increased levels of hyperdiploidy at specific stages of T cell development. This data called for a re-examination of previously published work on the *Caph2$^{nes/nes}$* mouse, which, based partly on the expectation that mutations affecting mitosis should impact all dividing cells, concluded that the observed phenotype is most likely caused by abnormal interphase processes (Gosling *et al*., 2007; Rawlings *et al*., 2011).

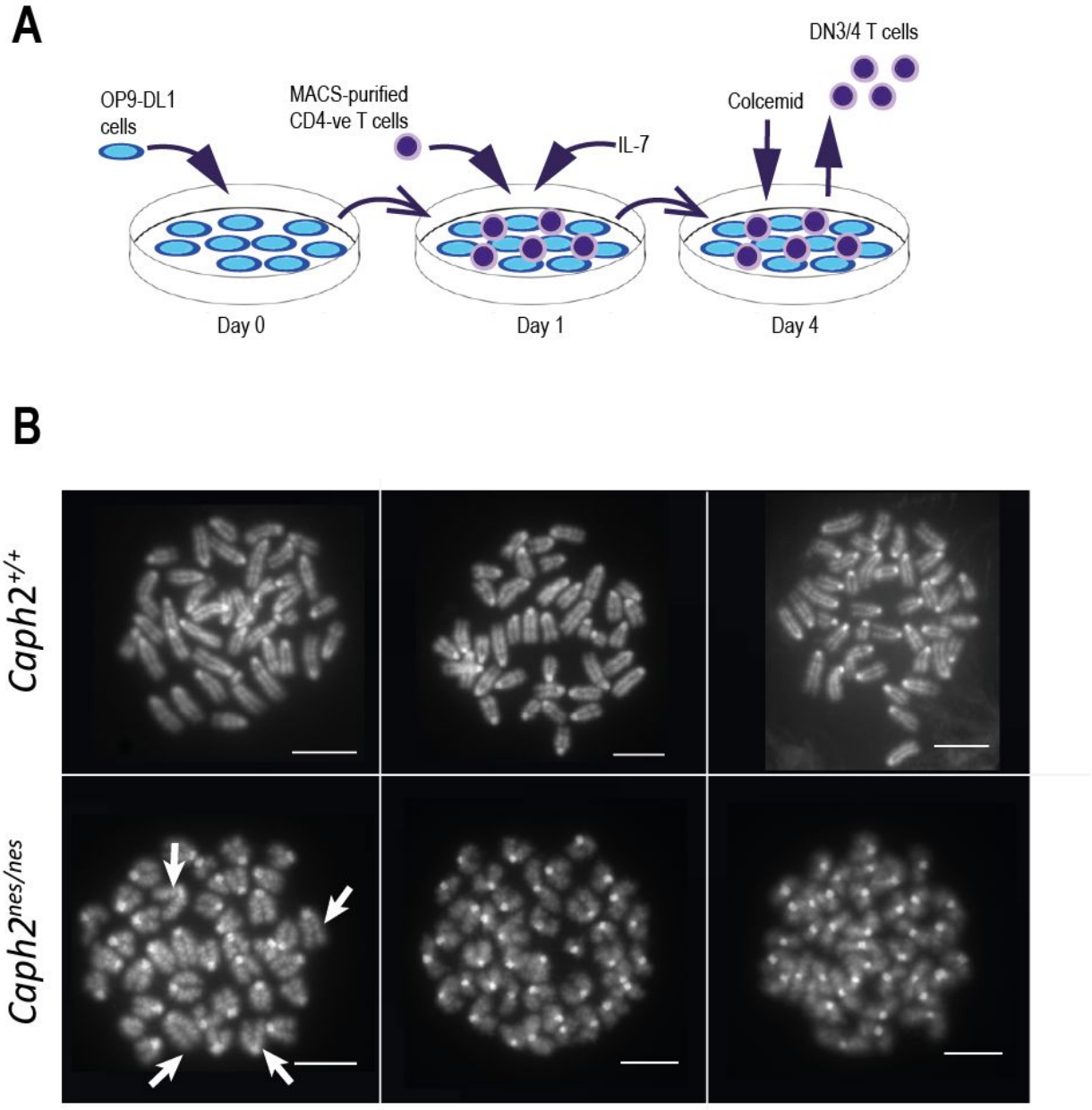

Figure 3.12
Metaphase chromosome abnormalities in *Caph2*$^{nes/nes}$ mutant T cells cultured ex vivo. **A.** Schematic of ex-vivo T cell culture protocol. **B.** Representative images of wildtype and *Caph2*$^{nes/nes}$ T cell 3:1 methanol:acetic acid metaphase spreads. *Caph2*$^{nes/nes}$ chromosomes appear shorter and more bloated in comparison to wildtype. In addition, the mutant chromosomes appear to be less spread out than wildtype. First and second wildtype images shown previously in Figure 3.8.

3.2 Analysis of interphase chromosome structure in Caph2$^{nes/nes}$ mutant cells

3.2.1 Introduction

Since condensin carries out an important role in all dividing cells, it is surprising that a mutation in one of its subunits causes a tissue-specific developmental phenotype. Given the well-documented epigenetic processes crucial for successful T cell development, and the role of condensins in regulating gene expression in several model organisms, previous studies into the *Caph2$^{nes/nes}$* mutation concluded that the T cell-specific phenotype is a result of abnormal interphase processes (Rawlings *et al*., 2011). I therefore decided to further investigate the possibility that the *Caph2$^{nes/nes}$* mutation could be affecting non-mitotic functions of condensin, such as its proposed role in organizing interphase chromosome structure (see Section 1.2.5).

3.2.1.1 Epigenetic processes during T cell differentiation

T cell differentiation is an extremely well-studied process, for which an increasing body of evidence implicates epigenetic processes. For example, certain regulatory, growth and transcription factors are necessary at multiple stages of T cell differentiation, but in each case this results in drastically different cell fates.

TCR-dependent signalling, for example, takes place during positive selection, and determines which cells will survive, and which will undergo apoptosis. In addition to this though, TCR signalling also helps to determine which cells will become CD4$^+$ single positive, and which will become CD8$^+$ single positive, depending on both the strength and duration of the signal (Alberola-Ila & Hernández-Hoyos, 2003; Bosselut, 2004; Singer, 2002). TCR-dependent signalling is also important during TCRγδ development, but again results in very different developmental pathways to cells that undergo TCR-dependent signalling in the TCRαβ lineage (Rothenberg & Taghon, 2005).

These differences in cell fate are caused by the expression of transcription factors such as Notch (Huang, Gallegos, Richards, Lehar, & Bevan, 2003; Schmitt, Ciofani, Petrie, & Zúñiga-Pflücker, 2004; Wolfer, Wilson, Nemir, MacDonald, & Radtke, 2002) and GATA-3 (Garćia-Ojeda *et al*., 2013; Hosoya *et al*., 2009), which are expressed at crucial stages of T cell development, such as β-selection and positive selection. It is clear, therefore, that epigenetic mechanisms such as transcription-factor-mediated regulation of cell fate decisions play an important role during T cell development.

Polycomb group proteins, a well-studied family of proteins known to induce epigenetic silencing of genes, have been shown to be vital for successful differentiation of haematopoietic lineages. Generally, knock-outs of the polycomb proteins is embryonic lethal – reflecting their importance – and so conditional knockouts have been used to study their functions. One such study found that knock-out of the polycomb gene Bmi-1 resulted in several defects in the haematopoietic lineages, including reduced cellularity of the thymus, bone marrow and spleen. A developmental block was observed at the $CD4^-$ $CD8^-$ DN stage of T cell development, and at an equivalent stage of B cell development resulting in reduced numbers of mature T and B cells (Van Der Lugt *et al*., 1994).

Mutations to other polycomb group genes have resulted in similar phenotypes: Mel-18 mutant mice reveal hypoplasia of both the spleen and thymus, with abnormalities resulting in developmental blocks at the $CD4^-$ $CD8^-$ DN stage of T cell development (Kimura *et al*., 2001) as well as at the pro-B cell stage of development (Tetsu *et al*., 1998). Reduced cellularity is also apparent in the spleen of Rae28 mutant mice, with a developmental block in B cell development (Ohta *et al*., 2002). Since polycomb mutant mice generally display developmental abnormalities after commitment to either the B or T cell lineages, it seems likely that the polycomb genes are involved in terminal gene silencing to maintain lineage decisions, rather than being involved in lineage decisions of cells (Raaphorst, Otte, & Meijer, 2001).

In addition to the role of transcription factors and polycomb group proteins in determining cell fate, further research has been carried out into the restructuring of chromatin during haematopoietic differentiation to facilitate gene silencing. This chromatin remodelling is thought to be transferred to daughter cells, thereby ensuring

that cell fate decisions are maintained across multiple rounds of cell division.

The $CD4^+$ $CD8^+$ DP stage of T cell development has been a useful model to study genes silencing, since cells that have successfully undergone VDJ recombination quickly downregulate the expression of genes that encode the recombination machinery. These genes are crucial for successful rearrangement and generation of diversity, and therefore a great deal of work has been carried out to better understand their roles. One of the genes associated with carrying out VDJ recombination, *Dntt*, has been studied in detail by Su *et al.* who investigated the process of silencing *Dntt* after successful VDJ recombination (Su, Sridharan, & Smale, 2005).

Using an *ex vivo* T cell differentiation system, Su *et al.* found that restriction enzyme accessibility to the promoter of *Dntt* was reduced following stimulation of the cells to differentiate. This was interpreted to represent a change in chromatin confirmation, which occurred as the *Dntt* locus was observed to relocate to pericentromeric heterochromatin. Deacetylation of H3-K9 occurred at the *Dntt* promoter, within the same time frame as the changes to chromatin confirmation. Following this, there is methylation of H3-K9 and demethylation of H3-K4: these events are all consistent with silencing of the *Dntt* locus.

In this chapter I describe the experiments undertaken to study chromatin compaction and decompaction of the mutant relative to wildtype cells. The extent of any compaction or decompaction was studied both on a large, whole-genome scale, as well as a more localised scale of 100Kb to 5Mb. Further experiments were carried out to investigate any other differences in interphase chromatin architecture between wildtype and mutant.

3.2.2 Results

3.2.2.1 Investigating interphase chromatin compaction using flow cytometry

Here, the term "compaction" is used to describe an increase in the amount of chromatin per unit volume. The term "condensation" is reserved to describe the restructuring of chromosomes into dense, individualised structures (e.g. before mitosis). As a first step to investigate interphase chromatin compaction in *Caph2*$^{nes/nes}$ T cells, I used flow cytometry to look for differences in cell size relative to wildtype. This was quantified using forward scatter: a measure of cell size. Given that the nucleus makes up a large majority of the cell volume in lymphocytes, forward scatter can be used as a reasonably accurate indicator of nuclear size (Jorgensen *et al*., 2007).

Before entry into the periphery, T cells become smaller and undergo quiescence. This has previously been interpreted as chromatin condensation, which was proposed to help prevent premature activation of naïve lymphocytes in the absence of T Cell Receptor stimulation (Rawlings *et al*., 2011). In that study, flow cytometry was used to show that *Caph2*$^{nes/nes}$ CD4^{+} CD8^{+} DP thymocytes are increased in size relative to wildtype. They used this data to infer abnormal interphase chromatin decompaction in *Caph2*$^{nes/nes}$ cells.

However, in light of the evidence described in Section 3.1.2 that was not previously reported, I decided to re-examine the evidence presented by Rawlings *et al*. I labelled wildtype and *Caph2*$^{nes/nes}$ thymocytes with fluorescently conjugated anti- CD4 and CD8, fixed the samples and stained with DAPI (as described in Materials and Methods: Section 2.2.9.1). The samples were analysed using a flow cytometer. Stringent doublet exclusion was carried out (Materials and Methods: Section 2.2.7.5) – this was particularly necessary here, since cell aggregates would display forward scatter profiles consistent with very large cells. In order to achieve a direct comparison with the Rawlings data set, I gated on the same population (the CD4^{+} CD8^{+} DP cells). The cells expressing CD4 and CD8 epitopes were selected (quadrant labelled DP Figures 3.13a and 3.13b) and their forward scatter profiles analysed (Figure 3.13c). My results confirm that CD4^{+} CD8^{+} DP *Caph2*$^{nes/nes}$ thymocytes display a higher

forward scatter (FSC) profile compared with *Caph2*$^{+/+}$ DP cells. Specifically, the *Caph2*$^{nes/nes}$ forward scatter profile reveals a bimodal distribution, with cells corresponding to the larger modal value much more abundant relative to *Caph2*$^{+/+}$. The lower forward scatter population is similar in size to the bulk of the wildtype population. This suggests that if interphase decompaction occurs in *Caph2*$^{nes/nes}$, it only affects a subset of cells.

However, large differences in ploidy exist between wildtype and *Caph2*$^{nes/nes}$ thymocytes (Figures 3.13d and 3.13e), which are very likely to affect the cell size distribution of the DP population independently of genome compaction. This was not considered by Rawlings *et al*. In order to control for differences in DNA content, I next gated specifically on CD4^{+} CD8^{+} DP cells with either 2N or 4N ploidy based on DAPI fluorescence (Figures 3.13d and 3.13e). The forward scatter profiles of the 2N and 4N populations were then compared between wildtype and *Caph2*$^{nes/nes}$.

For both populations (2N and 4N DNA content), there was no obvious difference in the mutant forward scatter profiles relative to wildtype (Figure 3.13f). This indicates that the differences in cell size observed by Rawlings *et al*. using forward scatter are a result of an increase in ploidy in the *Caph2*$^{nes/nes}$ mutant cells. The absence of cell size differences between wildtype and *Caph2*$^{nes/nes}$ populations that were matched for both differentiation status and ploidy suggest that global decompaction of interphase chromatin is either subtle or absent.

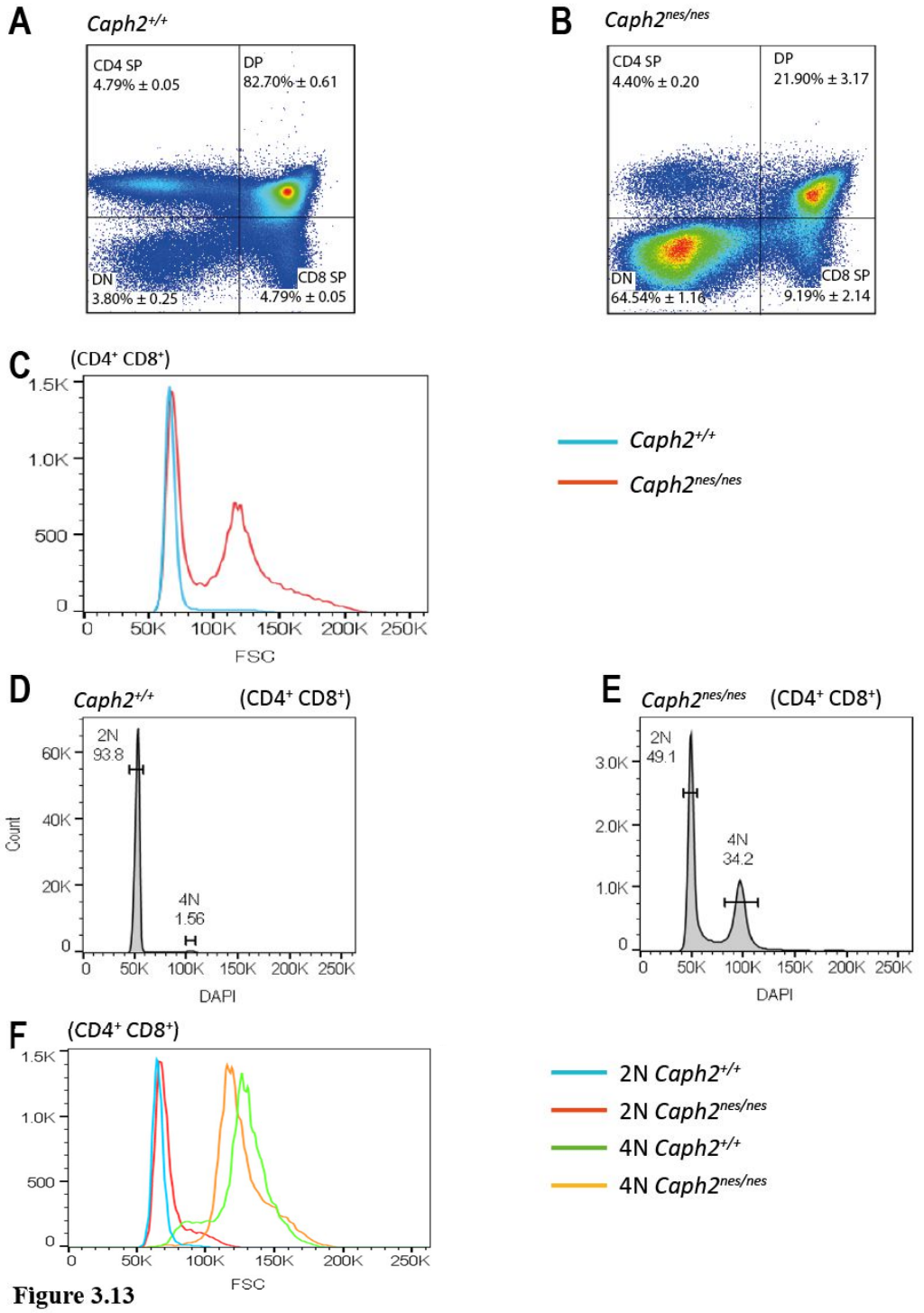

Figure 3.13

No difference in interphase global chromatin compaction as judged by flow cytometry

A. Flow cytometry dot plot showing the distribution of wildtype subsets according to CD4 and CD8 expression. **B.** Flow cytometry dot plot showing the distribution of *Caph2*$^{nes/nes}$ subsets according to CD4 and CD8 expression. Cell percentages within the indicated subsets were calculated from three biological replicates. The mean value is presented, plus or minus the standard error of the mean. **C.** Histogram showing cell size (FSC) for CD4$^+$ CD8$^+$ wildtype and *Caph2*$^{nes/nes}$ cells. *Caph2*$^{nes/nes}$ appear larger than wildtype. **D.** DNA content histogram of CD4$^+$ CD8$^+$ wildtype cells. Percentage of cells with 2N and 4N ploidy shown in figure. **E.** DNA content of CD4$^+$ CD8$^+$ *Caph2*$^{nes/nes}$ cells. There is a large proportion of cells with 4N DNA content. **F.** Histogram showing cell size (FSC) for CD4$^+$ CD8$^+$ wildtype and *Caph2*$^{nes/nes}$ cells with 2N or 4N DNA content.

3.2.2.2 Investigating interphase chromatin compaction using FISH

Although I was unable to find evidence for large scale decompaction of chromatin in *Caph2*$^{nes/nes}$ mutant cells, I next investigated the possibility that condensin deficient cells may undergo decompaction of interphase chromatin on a more localised scale.

FISH has been used extensively to study chromatin compaction across a specified genomic distance, in multiple cell types (Chambeyron, Da Silva, Lawson, & Bickmore, 2005; Gilbert *et al*., 2004; Morey, Da Silva, Perry, & Bickmore, 2007), and to study localized differences in chromosome compaction between wildtype and mutant cells (Eskeland *et al*., 2010; Tark-Dame, Jerabek, Manders, Heermann, & van Driel, 2014). I chose to carry out 3D rather than 2D FISH, since it is possible to prepare the flow cytometer-sorted T cells in such a way that their 3D structure is preserved (described in Materials and Methods: Section 2.2.4.7). Although less time is required to image, process and analyse 2D FISH, 3D FISH provides more information since the distances between probes in the z-direction are taken into account.

I first measured the distances between the hybridisation signals from two probes, situated approximately 100kb apart in the linear genome, in three-dimensional nuclear space. I selected two tissue-specific loci to analyse: one – *CD8* -that is activated during thymic development (Figure 3.14a), and one gene cluster that is inactive during this stage of development (*HoxA* – Figure 3.14c). By choosing fosmid probes that flank each of these two loci, I was able to study the impact of *Caph2* mutation on chromatin compaction across active and inactive loci.

The fosmid probes were chosen using the UCSC genome browser fosmid end pairs track (http://genome.ucsc.edu/), and details of these are given in Table 2.3. Labelling and detection of the selected fosmids was carried out as described in Materials and Methods (Section 2.2.4).

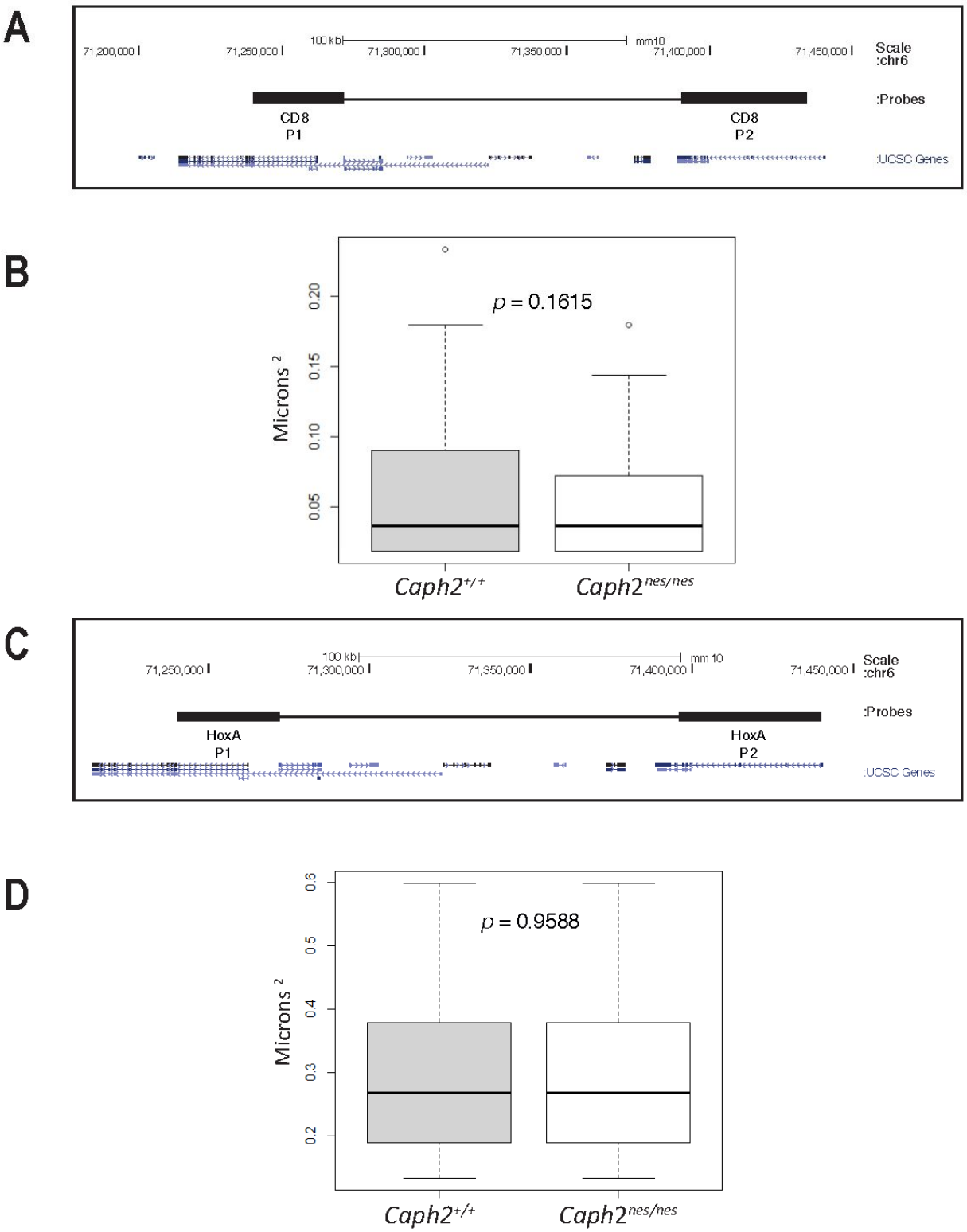

Figure 3.14

No significant difference in interphase chromatin compaction between probes to the CD8 or HoxA loci situated 100kb apart in the linear genome

A. Schematic of UCSC genome fosmid end pairs track illustrating the locations of the fosmid probes used to the CD8 locus. Fosmid pairs were situated 100kb apart in the linear genome. **B.** Boxplot showing distances between probes to the CD8 locus for both wild-type (in grey) and *Caph2*$^{nes/nes}$ (in white). n = 73 wildtype and 62 *Caph2*$^{nes/nes}$ nuclei. **C.** Schematic of UCSC genome fosmid end pairs track illustrating the locations of the fosmid probes used to the HoxA locus. Fosmid pairs were situated 100kb apart in the linear genome. **D.** Boxplot showing distances between probes to the HoxA locus for both wild-type (in grey) and *Caph2*$^{nes/nes}$ (in white). n = 212 wildtype and 205 *Caph2*$^{nes/nes}$ nuclei. Statistical significance assessed using Wilcox test.

The inter-probe distances, determined by the distance between the centroids of the red and green hybridisation signals, were calculated using an in-house script (Materials and Methods: Section 2.2.4.11). The units of the distances between fosmid probes were converted from pixels to microns and then squared (d^2), which has been shown to be proportional to genomic distance (Gilbert *et al*., 2004; van den Engh, Sachs, & Trask, 1992). This is due to the fact that interphase chromatin follows a random walk giant-loop mathematical model, where chromatin behaves like a flexible polymer (Sachs, van den Engh, Trask, Yokota, & Hearst, 1995). Distances squared were used to determine the level of chromatin compaction in all comparisons between wildtype and *Caph2*$^{nes/nes}$. Statistical significance and *p*-values were assessed using the Wilcox test, with a cut-off value of $p < 0.05$. This non-parametric test was used since it does not assume that the data follows a normal distribution. All data (distance between probes (d), distance squared (d^2), and significance levels (*p*-values)) are provided in Table 2.4.

When analysing 2D FISH, it is customary to normalise to the nuclear area (d^2/r^2). However, for 3D FISH the nuclear volume is very difficult to determine due to decreased resolution in the z-direction. In addition, there are substantial differences in cell size between wildtype and mutant (shown using forward scatter profiles – Figure 3.13c). Since the differences in cell size are not due to large-scale decompaction of chromatin, but instead due to an increase in ploidy at the $CD4^+$ $CD8^+$ DP stage of *Caph2*$^{nes/nes}$ development, normalising to nuclear volume would therefore skew the data, making the mutant loci appear more compact than they really are. Therefore, absolute d^2 values are presented here and throughout, without normalisation to nuclear volume.

3.2.2.2.1 Investigation into chromatin compaction at the 100kb scale

When FISH was performed on the rapidly cycling $CD4^+$ $CD8^+$ DP blast ($CD71^+$) T cells, i.e. the stage at which the *Caph2*$^{nes/nes}$ ploidy abnormalities are most severe, there were no significant differences in the mean distance squared between probe pair signals flanking either *CD8* or *HoxA* in wildtype compared to *Caph2*$^{nes/nes}$ (*p*-values are displayed on the boxplots (Figures 3.14b and 3.14d)). This data suggests that, at least at the two loci investigated, the condensin mutation does not cause a difference

in the compaction of interphase chromatin.

3.2.2.2.2 Further investigation of chromatin compaction across increasing genomic distances

In order to extend this analysis across progressively larger genomic distances, I next studied compaction using an additional fosmid probe, Igkv, situated 1Mb away from *CD8* (Figure 3.15a, details of the fosmid are given in Table 2.3). It has previously been shown that the random walk model is valid for probes separated by up to 1.5Mb in the linear genome, and so chromatin compaction between these loci can be correctly inferred using d^2 values (van den Engh *et al*., 1992).

3D FISH was carried out as before, on cells at the same stage of T cell development as used previously: DP 71^+ blast T cells and representative FISH images are shown in Figure 3.15b. The distance between fosmid probes in wildtype and mutant was determined, and the results are plotted as boxplots. No significant difference was found in the compaction of interphase chromatin between wildtype and mutant at loci situated 1Mb apart in the linear genome (Figure 3.15c).

Finally, I chose a probe situated 5Mb away from *CD8* (Figure 3.15a, Table 2.3). Since the Random-walk model breaks down at approximately 1.5Mb – 2Mb (van den Engh *et al*., 1992), the use of d^2 to determine chromatin compaction will be less accurate than in previous experiments. However, since it is the differences in compaction between wildtype and *Caph2*$^{nes/nes}$ mutant that are of interest, useful information may be obtained from the comparison of the two datasets (wildtype and mutant) despite the potential uncertainty in the calculation of absolute compaction.

For probes situated 5Mb apart in the linear genome it was not always possible to be sure which probe paired with which. Therefore, nuclei in which it was difficult or impossible to reliably match fosmid pairs were excluded from the analysis. The frequency of discarded nuclei was very similar in wildtype and mutant, and therefore did not bias the results. I again found no significant difference between wildtype and *Caph2*$^{nes/nes}$ in the compaction of interphase chromatin (Figure 3.15c).

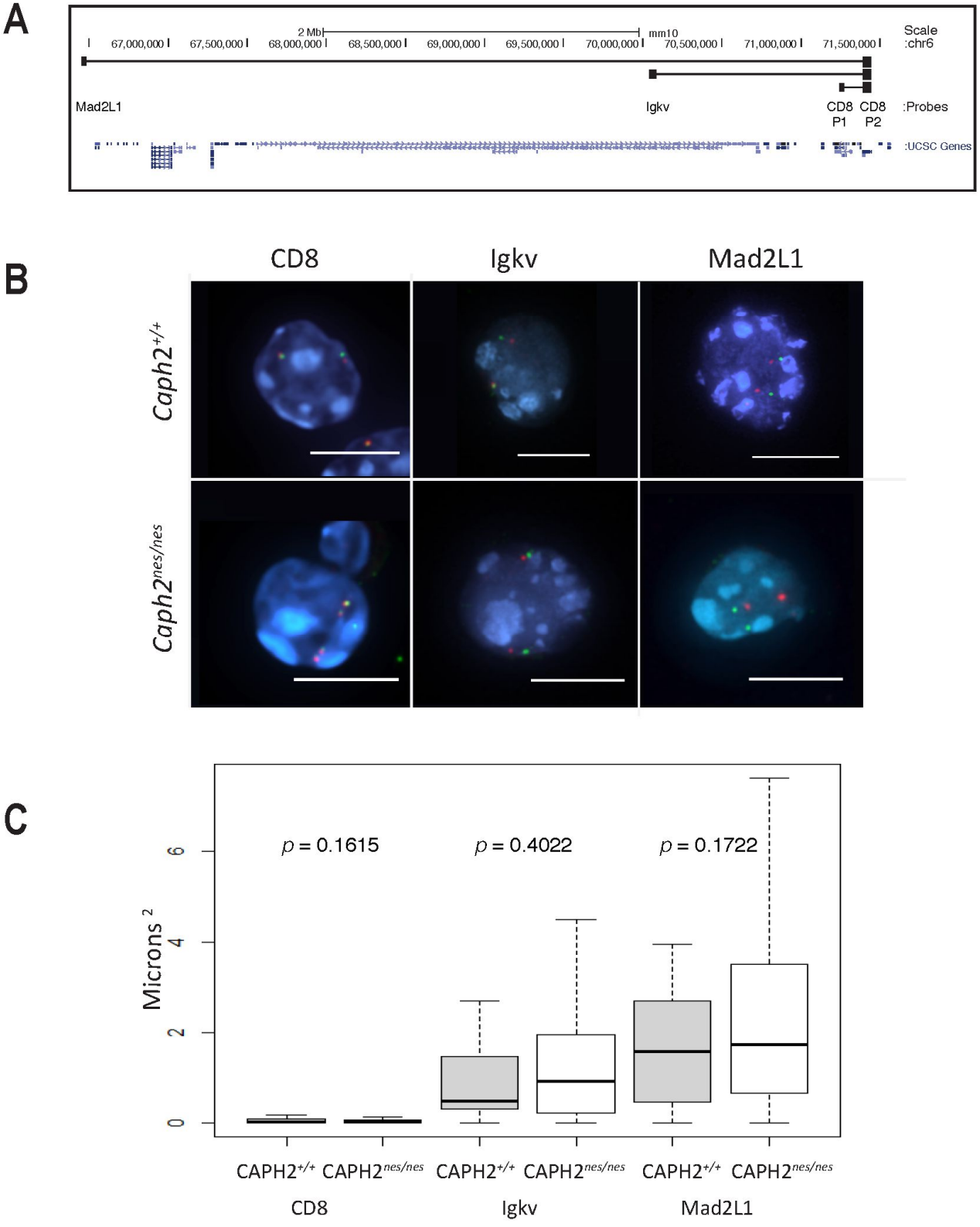

Figure 3.15

No significant difference in interphase chromatin compaction between probes situated 100kb, 1Mb or 5Mb apart in the linear genome

A. Schematic of UCSC genome fosmid end pairs track illustrating the locations of the fosmid probes used. Fosmid pairs were situated 100kb apart (CD8), 1Mb apart (Igkv) or 5Mb apart (Mad2L1) in the linear genome. **B.** Representative FISH images of wildtype and *Caph2*$^{nes/nes}$ nuclei. Inter-probe distances clearly increase from those labelled to the CD8 locus to probes labelled to Igkv and finally to the Mad2L1 locus. **C.** Boxplot showing distances between probes for both wildtype (in grey) and *Caph2*$^{nes/nes}$ (in white). n = 62 and 73 nuclei for wildtype and *Caph2*$^{nes/nes}$ respectively for CD8; n = 66 for both wildtype and *Caph2*$^{nes/nes}$ for Igkv and n = 57 and 65 for wildtype and *Caph2*$^{nes/nes}$ respectively for Mad2L1. Statistical significance assessed using Wilcox test.

Therefore, having measured inter-probe distances across sequentially larger distances at the CD8 locus, I was unable to find a significant difference in the compaction of interphase chromatin at any of the distances studied (Figure 3.15c).

3.2.2.2.3 Chromatin compaction measurements using a control cell type

Finally, in order to ensure that interphase chromatin compaction did not differ between wildtype and *Caph2*$^{nes/nes}$ in cell lines that were not obviously affected by the condensin mutation, I performed FISH on the closely related B cell lineage. As a direct comparison with DP blast T cells, Fraction C (rapidly proliferating) B cells were selected using flow cytometry with antibodies to B220, CD43, BP1 and CD24 (see Materials and Methods: Section 2.2.8). The cells were prepared and analysed as described previously. When 3D FISH was carried out on this cell type using fosmid probes to the CD8 locus, no significant difference in the distance between probe pairs between wildtype and the condensin mutant cells was observed (Figure 3.16).

For each FISH experiment, a minimum of 50 wildtype and 50 mutant nuclei were analysed. Prior experience using the FISH technique indicates that analysis of 50 nuclei provides sufficient power to detect differences in compaction. Despite this, the possibility that subtle decompaction takes place in the mutant nuclei cannot be ruled out. However, these differences are of insufficient magnitude to result in a statistically

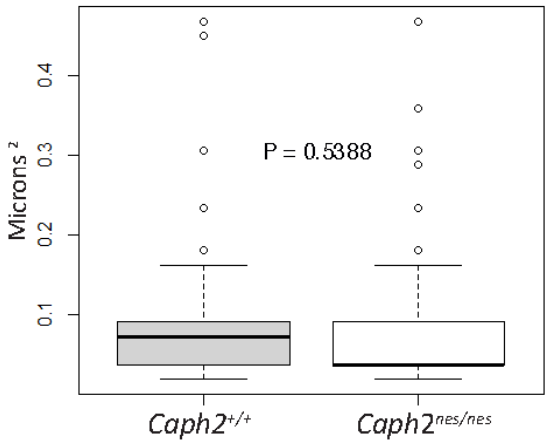

Figure 3.16
No difference in interphase chromatin compaction between probes to the CD8 locus situated 100kb apart in the linear genome in Fraction C B cells
Boxplot showing distances between probes to the CD8 locus for both wildtype (in grey) and *Caph2*$^{nes/nes}$ (in white) Fraction C (rapidly proliferating) B cells. A total of 117 wildtype and 93 *Caph2*$^{nes/nes}$ nuclei were analysed. Statistical significance assessed using Wilcox test.

significant difference.

3.2.2.3 Further analysis into interphase chromatin organisation of Caph2$^{nes/nes}$ cells at the DP 71+ blast stage of T cell development

Having found no evidence for chromatin decompaction in *Caph2$^{nes/nes}$* T cells at the active and silent loci studied, I went on to investigate whether other aspects of interphase chromosome structure might be affected by the condensin II deficiency.

3.2.2.3.1 Radial nuclear organisation

Radial organization of the interphase genome appears to be non-random, and is conserved in eukaryotes (Meister & Taddei, 2013). Actively transcribed regions are often located towards the centre of the nucleus, and in contrast, gene-poor and late replicating regions are often located towards the periphery. I was interested in determining whether the nuclear organization of $CD4^+$ CD^+ DP T cells changes in mutant relative to wildtype. The nuclear position of the CD8 locus and the HoxA locus was quantified using FISH images captured previously with fosmid probes located 100kb apart in the linear genome: Table 2.3. The nuclear area was divided into five concentric shells, each with equal area using a nuclear erosion script used previously by the lab (Rafique, Thomas, Sproul, & Bickmore, 2015; Therizols *et al*., 2014), Figure 3.17a, Materials and Methods: Section 2.2.4.11.

Nuclei were eroded in from the periphery (shell 1) to the centre (shell 5) and the proportion of signals within each shell counted and the percentage of CD8 and HoxA signals in each shell were plotted as histograms. A Mann-Whitney test was performed on the data and the difference between the localisation of signals in wildtype and mutant was not found to be significant at $p < 0.05$, for either *CD8* (Figure 3.17b) or *HoxA* (Figure 3.17c). This implies that no nuclear re-localisation of chromosome 6 occurs as a result of the condensin II mutation. A Kolmogorov-Smirnov test was performed on the data to test whether the wildtype and nessy datasets are drawn from the same distribution. The K-S test statistic was 0.2 for the *CD8* locus and 0.4 for the *HoxA* locus, with p-values of 1 and 0.873 respectively, indicating that the wildtype and mutant datasets originate from the same distribution. Therefore, it is unlikely that differences in the radial organization between wildtype and mutant would become

significant if more nuclei were analysed.

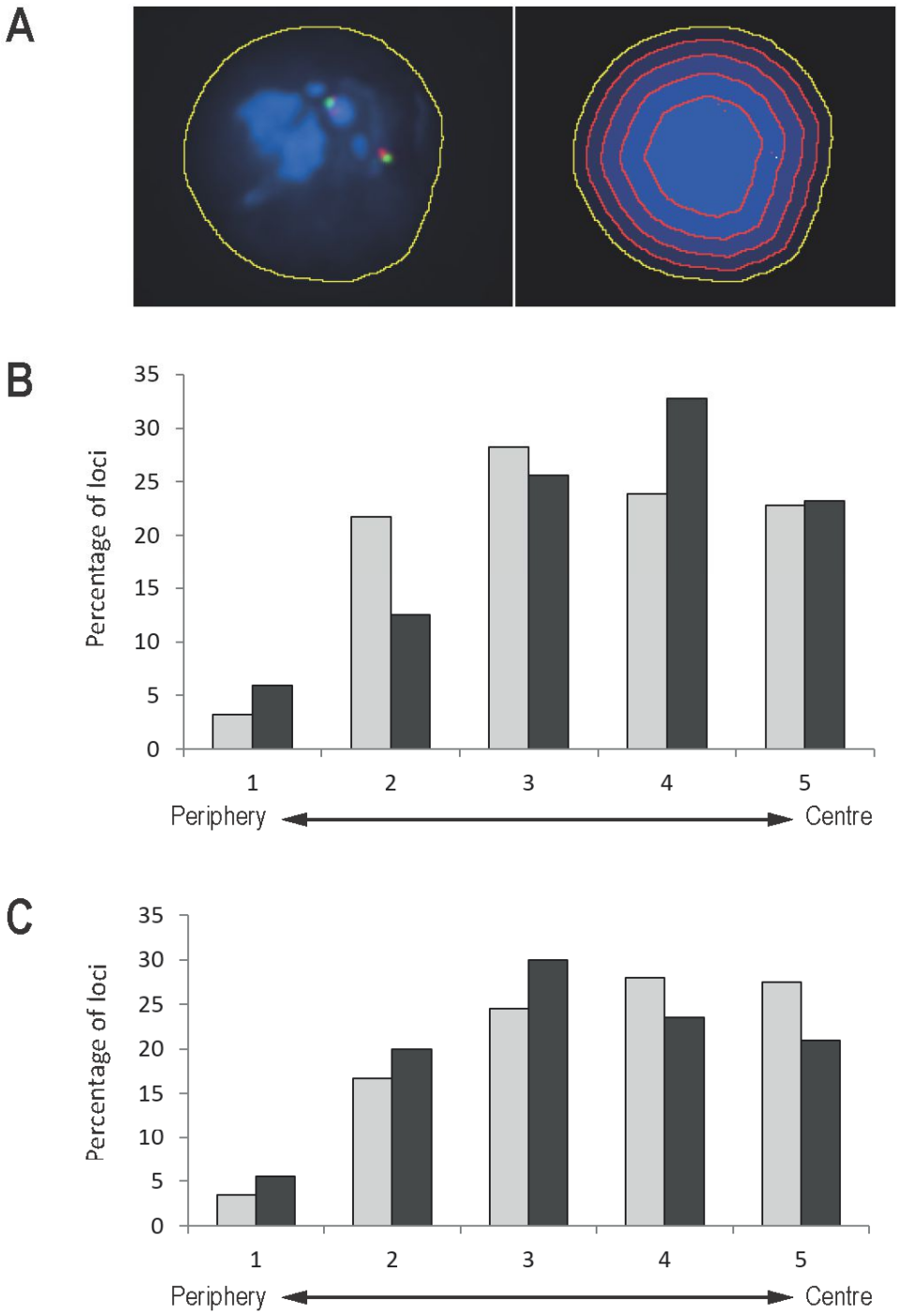

Figure 3.17
No significant difference in fosmid probe localisation as measured by nuclear erosion of FISH images
A. Example of a DAPI stained nucleus (blue channel). The DAPI are is delineated (left) and eroded into five consecutive shells of equal nuclear area, as calculated by the number of pixels in each shell (right). B. Histogram quantifies the nuclear distribution of CD8 fosmid probes (n = 184 wildtype and 168 *Caph2*$^{nes/nes}$). A Mann-Whitney test was performed giving a p-value is 0.92034 and therefore the result is not significant at $p < 0.05$. C. Histogram quantifies the nuclear distribution of HoxA fosmid probes (n = 184 wildtype and 168 *Caph2*$^{nes/nes}$). The p-value is 1.0000 and therefore the result is not significant at $p < 0.05$.

3.2.2.3.2 Chromocenter clustering

In addition to studying chromatin compaction and nuclear organisation to determine whether differences exist in the organisation of interphase chromatin, I was interested in the analysis of chromocenters. These structures are composed of blocks of pericentric heterochromatin with major satellite repeats from multiple different chromosomes, which associate together in sub-nuclear compartments during interphase. They can be detected by probes for centromeric regions (Mayer *et al*., 2005), or by regions of intense DNA staining (Nishide & Hirano, 2014).

The spatial organization of centromeres has been shown to change during differentiation of multiple cell types (Manuelidis, 1985; Solovei, Grandi, Knoth, Volk, & Cremer, 2004), including during T cell development (Kim *et al*., 2004), suggesting that the nuclear organization of centromeres may be important for proper gene expression. In addition, the distribution patterns of chromocenters during haematopoietic differentiation have been analysed in relation to gene expression. These studies found that chromocenter localisation is closely related to gene silencing (Brown *et al*., 1997, 2001). Analysis of chromocenters, therefore, is likely to provide further insight into any potential differences between wildtype and mutant T cells in the organisation of interphase chromatin.

A study into the different roles of condensin I and condensin II found that condensin II deficient mouse neuronal stem cells contain significantly decreased numbers of chromocenters, whereas no reduction was observed in condensin I conditional knock-outs (Nishide & Hirano, 2014). The researchers concluded that the reduction in chromocenter number is a consequence of hyperclustering, and that condensin II specifically (rather than condensin I) is involved in interphase nuclear organisation of the neuronal cells to prevent chromocenter hyperclustering.

Given this interesting discovery, I investigated whether nuclear architecture might be altered in the condensin II mutated T cells, resulting in a reduced number of chromocenters. I therefore counted the number of intense DAPI stained regions of DP 71^{+} blast *Caph2*$^{+/+}$ and *Caph2*$^{nes/nes}$ T cells using maximum intensity projections. Examples of the types of high intensity DAPI-stained regions counted are shown in

Figure 3.18a. The mutant cells showed a larger distribution of chromocenter numbers than wildtype, however the mean number of regions was very similar. A Wilcoxon rank test was performed on the data and no significant difference was found in the numbers of chromocenters present in DP 71^{+} blast stage nuclei ($p < 0.05$, Figure 3.18b). However, as shown previously (Section 3.1.2), there is a higher proportion of mutant cells with >4N DNA content versus wildtype, which might affect the chromocenter counts. Future work could include repeating this assay on cells matched for ploidy, as well as developmental stage.

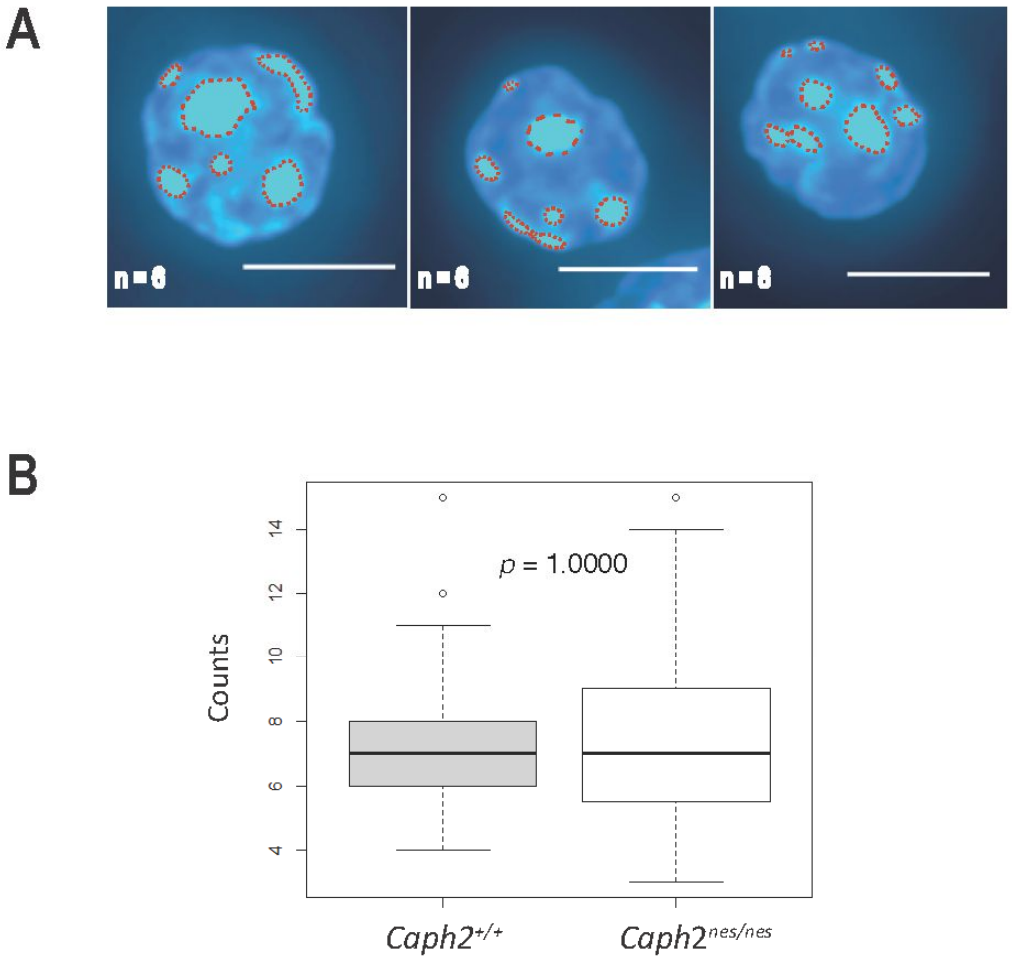

Figure 3.18
No significant difference in chromocenter numbers
A. Examples of high intensity DAPI stained regions are shown as very bright spots within the nuclei (outlined by a dashed red line). Number of chromocenters counted per image are indicated. **B.** Boxplot showing the number of chromocenters per nucleus (n = 72). A Wilcoxon rank test was performed on the data, giving a *p*-value of 1.0000 and therefore the result is not significant at $p < 0.05$.

3.3 Discussion

In this chapter, I have provided several pieces of evidence to suggest that the abnormalities observed in the *Caph2*$^{nes/nes}$ mice arise due to aberrant mitosis and not due to altered nuclear organisation of chromatin. Increased levels of hyperdiploidy were observed in the mutant cells using several independent techniques.

3.3.1 Evaluation of the strengths and limitations of the techniques used to assess ploidy

The purpose of utilising several independent techniques to assess ploidy is to ensure that the weaknesses of an individual approach will not result in inaccurate conclusions. Each of the techniques used to assess ploidy are subject to different limitations. In the following section I seek to critically assess the validity of different methods used.

3.3.1.1 Flow cytometry as a method to assess ploidy

There are several advantages of using flow cytometry: it is fast and provides quantitative information about whole populations on a cell-by-cell basis, i.e. each cell is analysed individually. A particular advantage of this technique for my work is the ability to simultaneously quantify DNA content and cell surface marker expression, allowing the accurate detection of changes in ploidy during cellular differentiation in a relatively quick and straightforward manner. However, even when employing stringent doublet exclusion techniques, flow cytometry is vulnerable to the inclusion of cell aggregates, where multiple cells are analysed as a single event. This results in an apparent increased proportion of hyperdiploid cells.

To eliminate the possibility that cell aggregates were being recorded as single events, the samples were re-analysed using Image Stream: a technique that combines flow cytometry with imaging capabilities. Using this technique, the vast majority of the hyperdiploid events detected by conventional flow cytometry were confirmed to be single cells (Figure 3.5).

A drawback of flow cytometry is the inability to distinguish diploid cells in S phase from arrested aneuploid cells, as both will contain DNA quantities that are intermediate between multiples of the haploid genome complement (Figure 3.19). By focusing on >4N cells, I have identified the frequency of a subpopulation of cells containing abnormal ploidy. However, this parameter would fail to detect many cells containing whole chromosome aneuploidies without whole genome duplication. Also, tetraploid cells arrested in G1 would be indistinguishable from diploid cells in G2. Therefore, the results obtained using flow cytometry may underestimate the overall proportion of cells with abnormal ploidy that arise due to aberrant mitosis.

Finally, in order for a cell to register within the > 4N gate, cells must be actively cycling, i.e. a cell with the correct chromosome complement must undergo aberrant cytokinesis resulting in a daughter cell that is hyperdiploid. This cell must then progress into S phase and duplicate its chromosome complement, in order to be identified as having greater than 4N DNA content. This may be particularly important in non-transformed cells such as the primary T cells analysed here, because aneuploidy often results in cell cycle exit (Davoli & de Lange, 2011).

3.3.1.2 Fluorescence in situ Hybridisation (FISH) as a method to assess ploidy

FISH enables direct visualization of DNA copy number using fluorescent probes, and each cell is analysed individually. Unlike flow cytometry, FISH does not require the cells to be actively cycling in order to be included in the hyperdiploid population. Importantly, unlike flow cytometry, it is possible to detect the copy number of individual loci using FISH, since these cells will contain one pair, rather than two pairs of locus-specific hybridisation signals. Hyperdiploid cells, in contrast, will contain greater than two pairs of spots.

However, the use of fosmid probes to only one locus per chromosome will not provide information about whether the abnormal copy number is due to gain or loss of a whole chromosome (polyploid), or the partial gain or loss of a chromosome (aneuploid). To take this into account, fosmid probes to two loci on chromosome 6 were used. The number of fosmid pairs observed was very consistent using both sets of fosmids,

indicating that whole-chromosome duplication occurs in the majority of instances.

Whole chromosome duplications and losses sometimes precede the acquisition of an

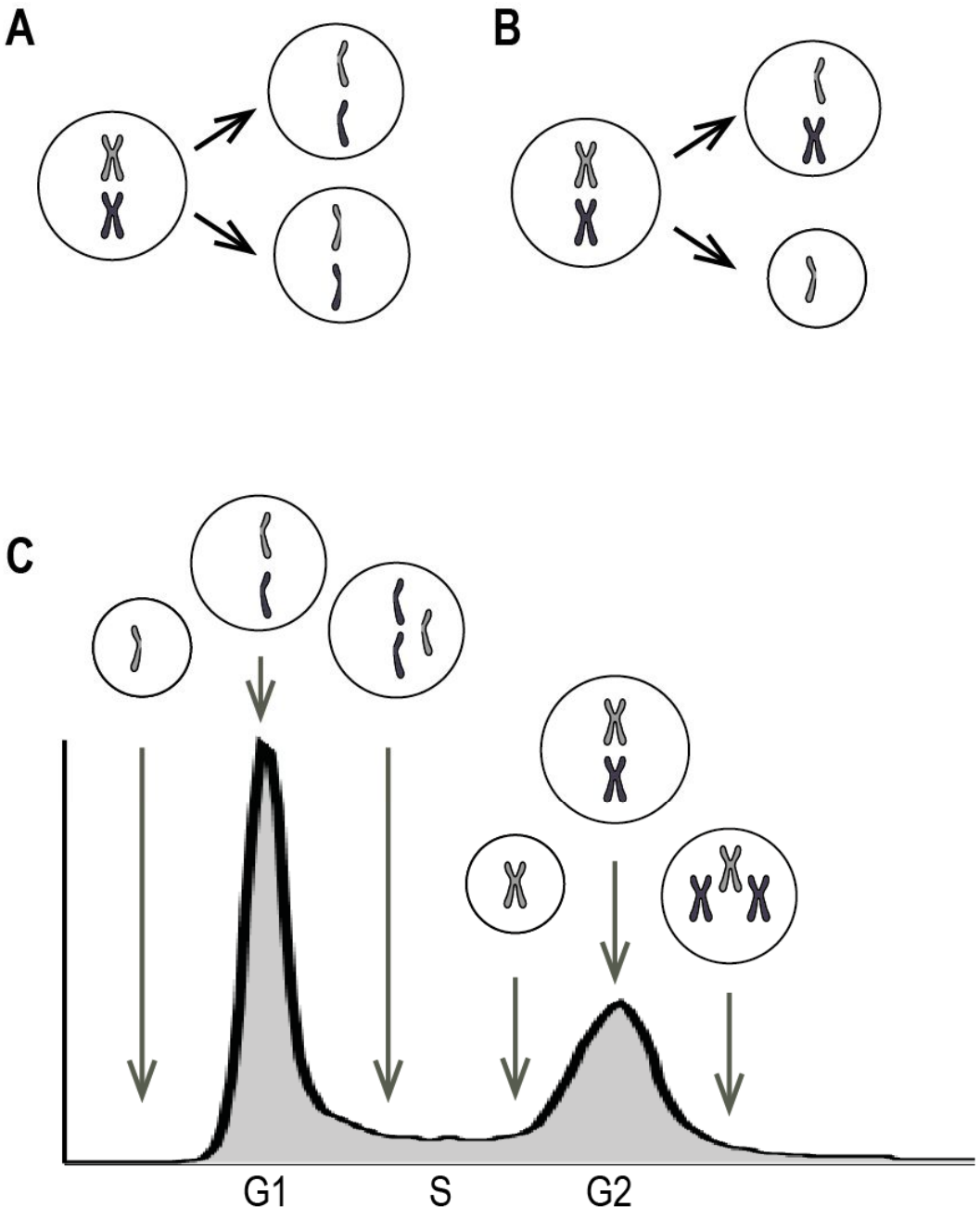

Figure 3.19
Inability to distinguish between diploid S phase cells, hyperdiploid G1 cells and hypodiploid G2 cells using flow cytometry
A. Successful mitosis results in equal separation of sister chromatids into daughter cells. **B.** Aberrant cytokinesis may result in an unequal distribution of sister chromatids between daughter cells. **C.** Representative flow cytometry DNA content plot. Diploid S phase cells, hyperdiploid G1 cells and hypodiploid G2 cells all contain DNA quantities that are intermediate between 2N and 4N, and threfore can not be distinguished from one another.

aneuploid karyotype, which is generally considered to be an early event in tumourigenesis (Pfau & Amon, 2012).

Like flow cytometry, however, FISH is vulnerable to artefacts including promiscuous probes hybridization , or failed hybridization, resulting in either gain or loss of fosmid signal and an overestimation or underestimation of copy number, respectively. Therefore, single cell copy number analysis would provide the most accurate indication of levels of aneuploidy. This technique involves the isolation of single cells from the tissue of interest, amplification of genomic DNA via PCR, and sequencing of the amplified DNA. The copy number is inferred by comparison with a control genome, which is known to contain no copy number aberrations (Knouse, Wu, Whittaker, & Amon, 2014).

3.3.1.3 Centromere counts of metaphase spreads as a method to assess ploidy

Although counting of chromosomes and/or centromeric sequences can give information relating to karyotype, this approach also probably underestimates the total fraction of cells with abnormal ploidy. In order to progress to and be blocked in M phase, cells must be actively cycling. Therefore unlike FISH, only the cycling cells will be included in the analysis. Just as for flow cytometry analysis, therefore, this method may also underestimate the proportion of hyperdiploid cells.

3.3.2 Summary of investigation into mitotic abnormalities

The increase in the proportion of hyperdiploid DP 71^{+} cells in nessy mutant mice may arise due to mitotic slip, where the cells enter mitosis but fail to divide successfully (Brito *et al.*, 2008) or alternatively may represent a population of diploid cells that have been arrested in G2. Experiments carried out on cultured primary T cells suggest that this arrested tetraploid population most likely arises due to mitotic slippage, rather than a G2 delay resulting in mitotic skip (Figure 3.9).

In addition, FISH analyses on tetraploid cells revealed a lack of SCC, consistent with removal of cohesin during mitosis and arguing against a mitotic skip mechanism

(Wood, unpublished data). Furthermore, abnormal anaphase figures were observed directly following washout of the proteasome inhibitor MG132. Anaphase bridges were the most frequent abnormality (Wood, unpublished data).

Abnormal metaphase morphology of both fetal liver erythrocytes and cultured primary T cells was observed. In the future, it would be interesting to attempt to quantify some of the metaphase abnormalities observed in the *Caph2*$^{nes/nes}$ cells. For example, the axial length of the mutant chromosomes relative to wildtype might be determined by measuring the length of the chromatids, with "puffier" chromosomes appearing to be shorter than wildtype. Future experiments might also include immunofluorescence for chromosomal axis proteins, including topoisomerase I and condensin.

Additionally, chromatid arms appeared more splayed in several mutant metaphase spreads in comparison to wildtype. Previous work carried out by Ribeiro *et al*. revealed that condensin depletion affects the stiffness of centromeric chromatin in DT40 cells (Ribeiro *et al*., 2009). This could allow more bending at the centromere resulting in increased distance between chromatid arms and could provide a possible explanation of the observed phenotype in *Caph2*$^{nes/nes}$ mutant spreads.

Quantification of the degree to which the chromatid arms are splayed could be determined using FISH with fosmid probes situated along the length of the chromatid arm. The distance between fosmid signals located on sister chromatids would be measured and compared between wildtype and mutant. If a significant difference is found between wildtype and *Caph2*$^{nes/nes}$, further work could be carried out to determine whether this is a consequence of reduced centromeric stiffness. These assays might resemble those carried out by Ribeiro *et al*., where a cell line bearing a conditional knock out of SMC2 was used with a lacO array inserted in the pericentromeric region of a micro-chromosome (Ribeiro *et al*., 2009).

Finally, it would be interesting to image T cell metaphase spreads using SIM and attempt to quantify the zig-zag morphology observed in both fetal liver erythrocytes and T cell chromosomes.

In summary, the results of this section indicate that DP cells reveal normal cell cycle kinetics (Section 3.1.2.5), but abnormal metaphase structure (Sections 3.1.2.6 and 3.1.2.7).

3.3.3 Summary of investigation into interphase abnormalities

Although it is very difficult to state categorically that interphase processes are completely normal in the *Caph2*$^{nes/nes}$ mutant T cells, I was unable to find any statistically significant difference in chromatin decompaction across any of the genomic distances that I analysed. In addition, no evidence for interphase chromosome abnormalities was observed, either in terms of a reduction in the average number of chromocenters per nucleus, or a repositioning of loci as determined by nuclear erosion scripts. Transcriptome comparisons, which were performed by other members of the Wood lab, also did not identify abnormal expression of known regulators of T cell differentiation such as Notch or TCR signalling (A. Wood, unpublished data). Instead, deregulated genes were mostly involved in stress response pathways known to respond to aneuploidy and DNA damage, including P53, interferon and proteostasis.

A previous study into the *Caph2*$^{nes/nes}$ mutation concluded that the phenotype most likely arises due to abnormal interphase processes (Rawlings *et al*., 2011). However, this assumption was based on forward scatter data from cells that had not been normalised for ploidy. In addition, Rawlings *et al.* provided evidence for chromatin decompaction in the *Caph2*$^{nes/nes}$ mutant using transmission electron microscopic images of wildtype and mutant cells. However, this data was not quantified, and is likely due to the different proportion of cycling ($CD71^+$) versus non-cycling ($CD71^-$) cells within the DP population in wildtype relative to *Caph2*$^{nes/nes}$ mutant. Analysis of the $CD4^+$ $CD8^+$ DP population reveals that approximately 5% of wildtype cells are at the DP 71^+ stage (Figure 3.13a), whereas more than four times as many *Caph2*$^{nes/nes}$ cells are DP 71^+ (Figure 3.13b). Large-scale changes in nuclear organisation occur as cells enter and exit the quiescent state, and so the higher proportion of cycling mutant cells may account for the observations described by Rawlings *et al*.

From the results of this chapter, I conclude that the *Caph2*$^{nes/nes}$ phenotype most likely arises due to abnormalities that occur during mitosis. However, given that the

requirements for mitosis are thought to be similar between differentiated cell types, it would be expected that many, if not all stages of haematopoietic differentiation would be affected by condensin deficiency, since all lineages undergo several rounds of division before becoming quiescent. Therefore, in the next chapter, I describe experiments designed to characterise cell cycle parameters across different haematopoietic lineages, in wildtype and *Caph2*$^{nes/nes}$ mice.

CHAPTER 4: CELL CYCLE REGULATION DURING HAEMATOPOIESIS IN WILDTYPE AND CHROMOSOMALLY UNSTABLE (CIN) CAPH2 MUTANT MICE

4.1 Introduction

Haematopoiesis is a well-characterised developmental process in which cells undergo multiple rounds of division and several stages of rapid proliferation. Haematopoietic precursors are self-renewing and give rise to all haematopoietic lineages. Certain stages of haematopoiesis are associated with particularly high levels of proliferation: for example $CD4^+$ $CD8^+$ DP blast stage T cells that have successfully undergone TCR beta rearrangement proliferate rapidly in response to signalling via the pre-T cell receptor (Miosge & Goodnow, 2005; Rothenberg, Moore, & Yui, 2008). B cells also undergo a burst in proliferation following successful VDJ recombination at Fraction C of development (R. Hardy *et al*., 1991; R. R. Hardy & Hayakawa, 2001). In the periphery, both T and B naïve cells undergo further rapid proliferation when presented with their cognate antigen, in an effort to destroy the invading pathogen (Tangye & Tarlinton, 2009; Yamane & Paul, 2012).

The data presented in the previous chapter suggests that the *Caph2*$^{nes/nes}$ mutation affects the well-established function of condensin II in the regulation of mitotic chromosome structure. Given that condensin II is likely to function in many, if not all dividing cells, this raised the question of whether additional stages of development are also affected in *Caph2*$^{nes/nes}$ mice.

In this chapter I describe experiments which set out to investigate the effect of the condensin II mutation on multiple stages of haematopoietic differentiation. I used BrdU incorporation studies to establish levels of proliferation in wildtype cells and flow cytometry to determine the levels of aneuploidy across multiple stages of development for both wildtype and mutant. I went on to study the consequences of the *Caph2*$^{nes/nes}$ mutation on cellularity across different haematopoietic lineages. Finally, I investigated possible reasons for the apparent T cell specific *Caph2*$^{nes/nes}$ phenotype.

4.2 Results

4.2.1 Cell cycle regulation during T cell differentiation

The *Caph2*$^{nes/nes}$ mutation results in a developmental block in T cells, at the CD4$^-$ CD8$^-$ DN to CD4$^+$ CD8$^+$ DP transition. As described in the previous chapter, an increase in the proportion of hyperdiploid *Caph2*$^{nes/nes}$ was observed relative to wildtype, specifically at the DP 71$^+$ blast stage of T cell development. Given the possibility that these abnormalities may arise due to abnormal chromosome segregation, I decided to study the possible cause of the aberrant mitosis at this stage of development. It could be that increased frequencies of proliferating cells at the DP 71$^+$ blast stage impose additional strain on the mitotic machinery. In order to test this hypothesis, I carried out a cell proliferation assay to determine levels of proliferation across individual stages of T cell development.

4.2.1.1 Investigation into extent of proliferation during T cell differentiation

Wildtype mice were intra-peritoneally (IP) injected with bromo-deoxyuridine (BrdU) and incorporation studies were undertaken two hours following treatment (Materials and Methods: Section 2.2.9.2). Frequencies of proliferating cells at individual stages of T cell development were determined using fluorescently conjugated antibodies to CD4, CD8 and CD71 (Table 2.5), in combination with anti-BrdU. Following cell fixation and permeabilisation, the cells were analysed on a flow cytometer. Exclusion of debris and cell aggregates was carried out (as described previously) and the gating strategies used to differentiate the individual stages of T cell development are shown in Figure 2.2. The same gating strategies were used for all T cell experiments.

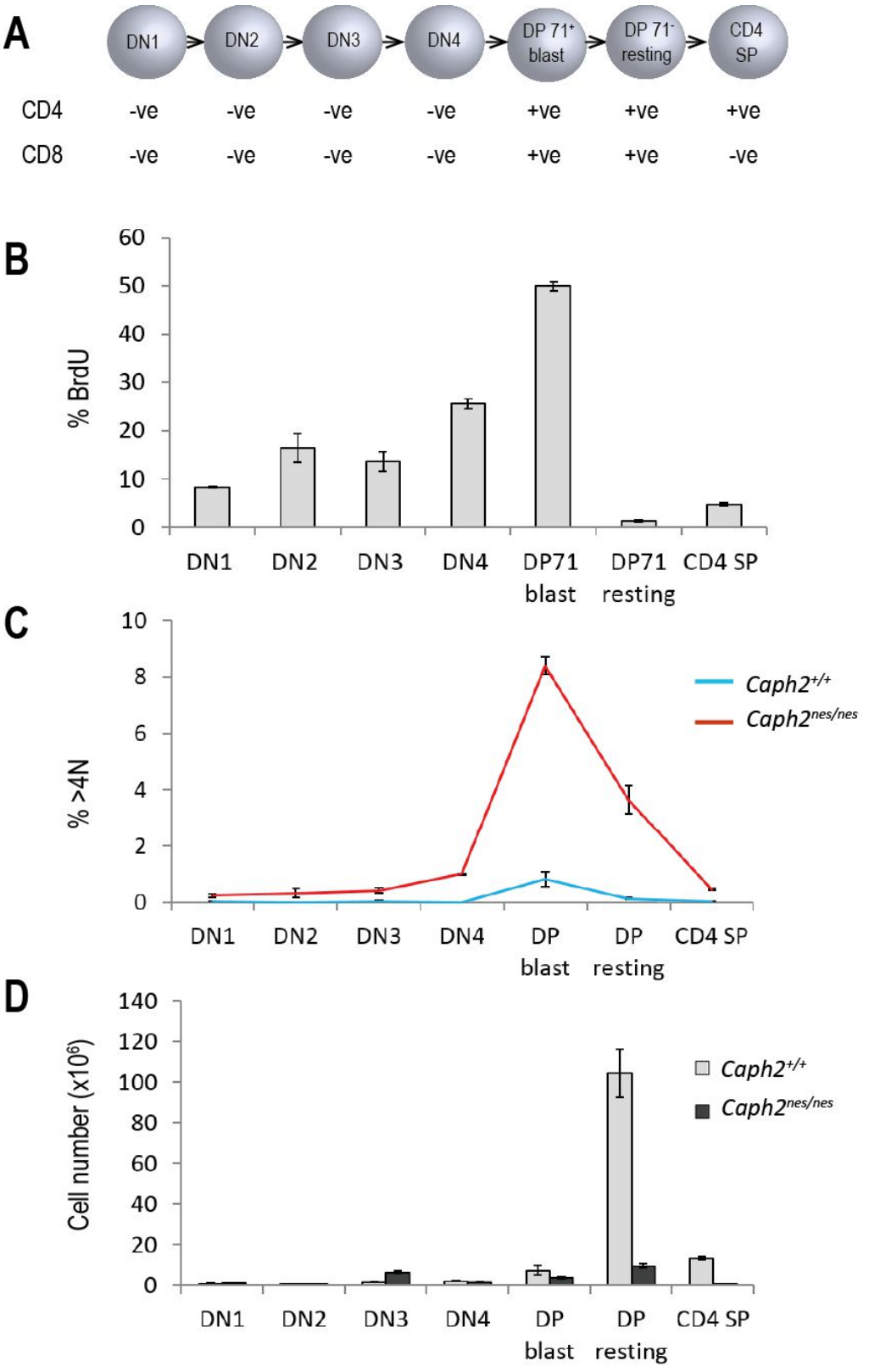

Figure 4.1
Analysis of cell cycle parameters during T cell development
A. Stages of T cell development in relation to CD4 and CD8 expression. **B.** Quantification of cell proliferation in T cells using BrdU assays. **C.** Proportion of cells with greater than 4N DNA content as judged by DAPI / DNA content analysis at different stages of wildtype (blue) and *Caph2*$^{nes/nes}$ (red) T cell development. **D.** Quantification of absolute cell numbers at different stages of wildtype (grey) and *Caph2*$^{nes/nes}$ (black) T cell development. Error bars represent the standard error of the mean and were calculated based on three biological replicates.

The proportion of cells positive for BrdU was calculated for each developmental stage (Figure 4.1b). The lowest proportion of S phase cells was found at the $DP71^-$ resting stage of development (as expected) with the DP $CD71^+$ blast cells undergoing the highest rates of proliferation. These data may suggest that the $DP71^+$ blast stage of development could be particularly predisposed to mitotic defects, due to more rapid proliferation at this stage compared to other stages of T cell development. Alternatively, it could be that the higher frequency of cycling cells provides a greater opportunity for abnormal mitosis to occur.

4.2.1.2 Consequences of the Caph2$^{nes/nes}$ mutation on hyperdiploidy during T cell differentiation

Cells that undergo aberrant mitosis produce daughter cells with a hyperdiploid or hypodiploid chromosome complement. Once hyperdiploid cells have progressed through S phase, they can be distinguished from the population with the correct complement using flow cytometry. Therefore, this proportion of hyperdiploid cells at each stage of differentiation is an indicator of the frequency of aberrant mitoses. In order to determine the stage of T cell differentiation at which the *Caph2$^{nes/nes}$* mutation caused abnormal mitosis, I investigated the dynamic changes in ploidy during wildtype and mutant T cell development using flow cytometry. The individual stages of differentiation were determined using fluorescently-conjugated antibodies to CD4, CD8 and CD71 (Table 2.5) and the DNA dye DAPI was used to assess ploidy. Cell debris and doublets were excluded from the analysis as described previously.

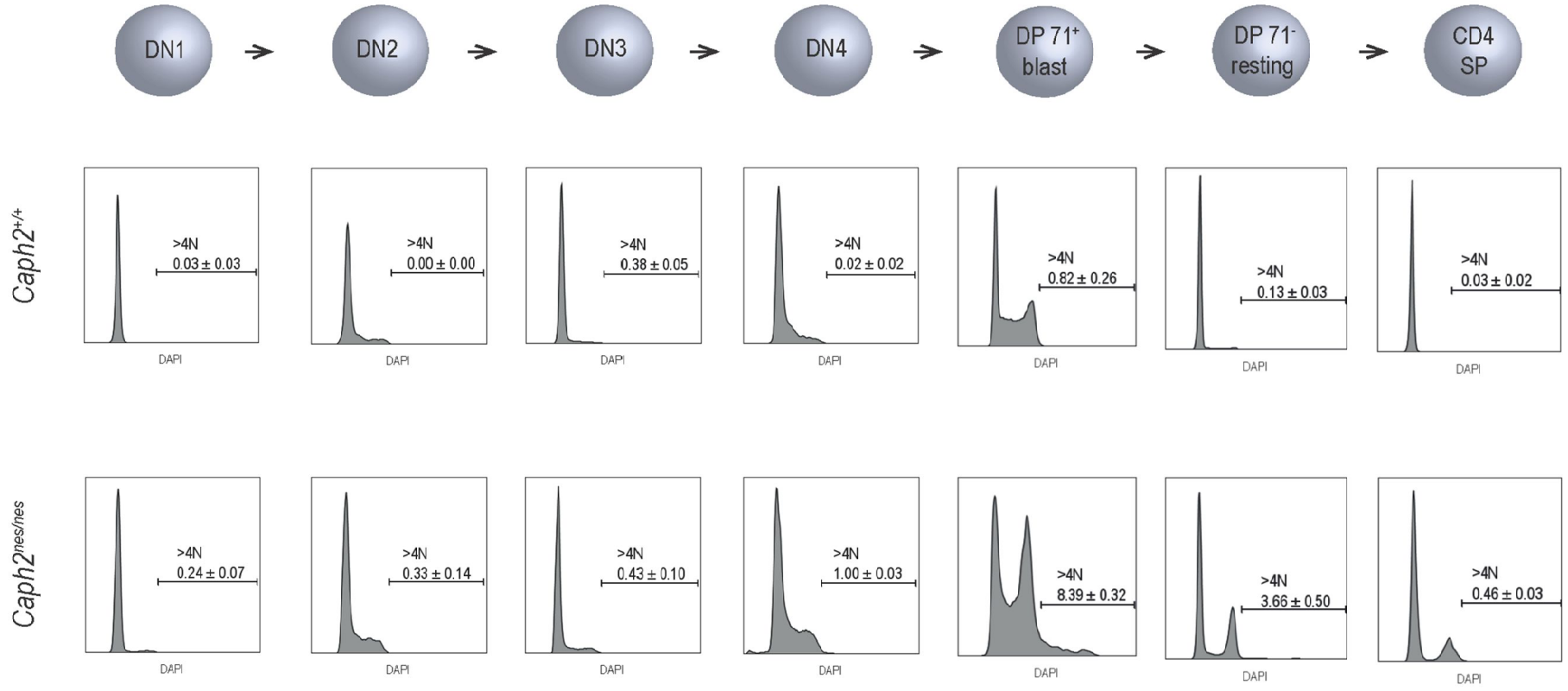

Figure 4.2

Representative flow cytometry DNA content histograms showing the proportion of hyperdiploid cells at each of the stages of T cell differentiation for both wildtype and *Caph2*$^{nes/nes}$. Cell percentages within the indicated subsets were calculated from three biological replicates. The mean value is presented, plus or minus the standard error of the mean.

In order to compare frequencies of hyperdiploid cells between experiments, gating strategies were kept consistent: the hyperdiploid gate was set to the point at which the gradient of the histogram changes most dramatically, following the 4N peak. DNA content histograms for each of the stages of differentiation are shown in Figure 4.2. The hyperdiploid gate is illustrated for each stage. Slightly elevated frequencies of hyperdiploid mutant cells relative to wildtype were observed at most stages of thymic T cell differentiation. However, there was a large increase in the frequency of cells with > 4N DNA content at the DP 71^+ blast stage in mutant versus wildtype (8% vs < 1%, respectively). The highest frequencies of hyperdiploid cells, for both wildtype and mutant, occurred at the stage associated with the highest levels of BrdU incorporation, which may indicate that the elevated frequency of hyperdiploid mutant cells is a consequence of more rapid proliferation at this stage (Figure 4.1c).

4.2.1.3 Consequences of the Caph2$^{nes/nes}$ mutation on absolute cell numbers during T cell differentiation

Having discovered that the DP blast stage of *Caph2*$^{nes/nes}$ development contains an elevated frequency of hyperdiploid cells, I investigated whether this affects absolute cell numbers. I used the automated cell counter Moxi Z (Orflo cat#MXZ001) to accurately determine the number of cells per wildtype and *Caph2*$^{nes/nes}$ thymus. The cells were incubated with cell surface antibodies which allowed individual stages to be distinguished from one another (as before: Table 2.5). Exclusion of cell debris and doublets was carried out as described previously, and absolute cell numbers were calculated from the proportion of cells at each stage (given as percentages) multiplied by the initial number of cells, calculated using the cell counter.

Cell numbers were found to be relatively consistent between wildtype and *Caph2*$^{nes/nes}$ mutant at the early stages of development. However, the most dramatic difference in cell number between wildtype and mutant occurs at the DP 71^- resting stage. At this stage there is an approximate 10-fold reduction in *Caph2*$^{nes/nes}$ mutant cell numbers relative to wildtype (upwards of $1x10^8$ wildtype cells per thymus compared with roughly $1x10^7$ mutant cells). This reduction in mutant cell numbers occurs immediately after the DP 71^+ blast stage, where the highest rates of proliferation and also the highest levels of mutant hyperdiploid cells were observed (Figure 4.1d).

4.2.1.4 Investigation into the proportion of cells with 4N DNA content during T cell differentiation in wildtype and mutant

Having established that the *Caph2*$^{nes/nes}$ cells exhibit increased levels of abnormal ploidy at a specific stage of T cell development, I investigated whether there is a similar increase in the proportion of cells with 4N DNA content in the mutant relative to wildtype. An increase in the proportion of mutant cells with 4N DNA content relative to wildtype may indicate an increased incidence of failed mitosis due to mitotic slip, or an increased incidence of failed entry into mitosis due to G2 arrest/mitotic skip, as discussed in Chapter 3: Section 3.1.2.5. In contrast, aneuploid cells (cells that do not contain an integer multiple of the haploid complement) cannot arise solely due to mitotic slip or skip, but instead must remain cycling before loss or gain of chromosomes in a subsequent tetraploid mitosis. The stages of differentiation were determined as described previously, and the DNA dye DAPI was used to assess ploidy, as before. The results of this experiment are displayed as a histogram (Figure 4.3a).

Interestingly, the DP 71^{-} resting population of mutant cells contained a high frequency of cells with 4N DNA content relative to wildtype (approximately 1% in wild-type vs 32% of mutant cells) (Figures 4.3b and 4.3c). The CD71 transferrin receptor is a marker of T cell proliferation (Brekelmans *et al*., 1994; Seitan *et al*., 2011) and so this result indicates that mutant cells frequently exit the cell cycle with an inappropriate DNA content.

In order to investigate this 4N population further, the CD71 marker was plotted against forward scatter, and a population of CD71^{-} (non-cycling) mutant cells was identified (Figures 4.4a and 4.4b). These cells are abnormally large (as judged by their forward scatter profiles). Approximately 37% of the mutant DP population fall within this CD71^{-}FSC^{hi} gate, compared to just 4% of the wildtype population. The DNA content profiles of these populations were analysed, and the majority (74%) of mutant cells were found to have 4N, rather than 2N DNA content compared with only 27% of wildtype cells (Figures 4.4c and 4.4d).

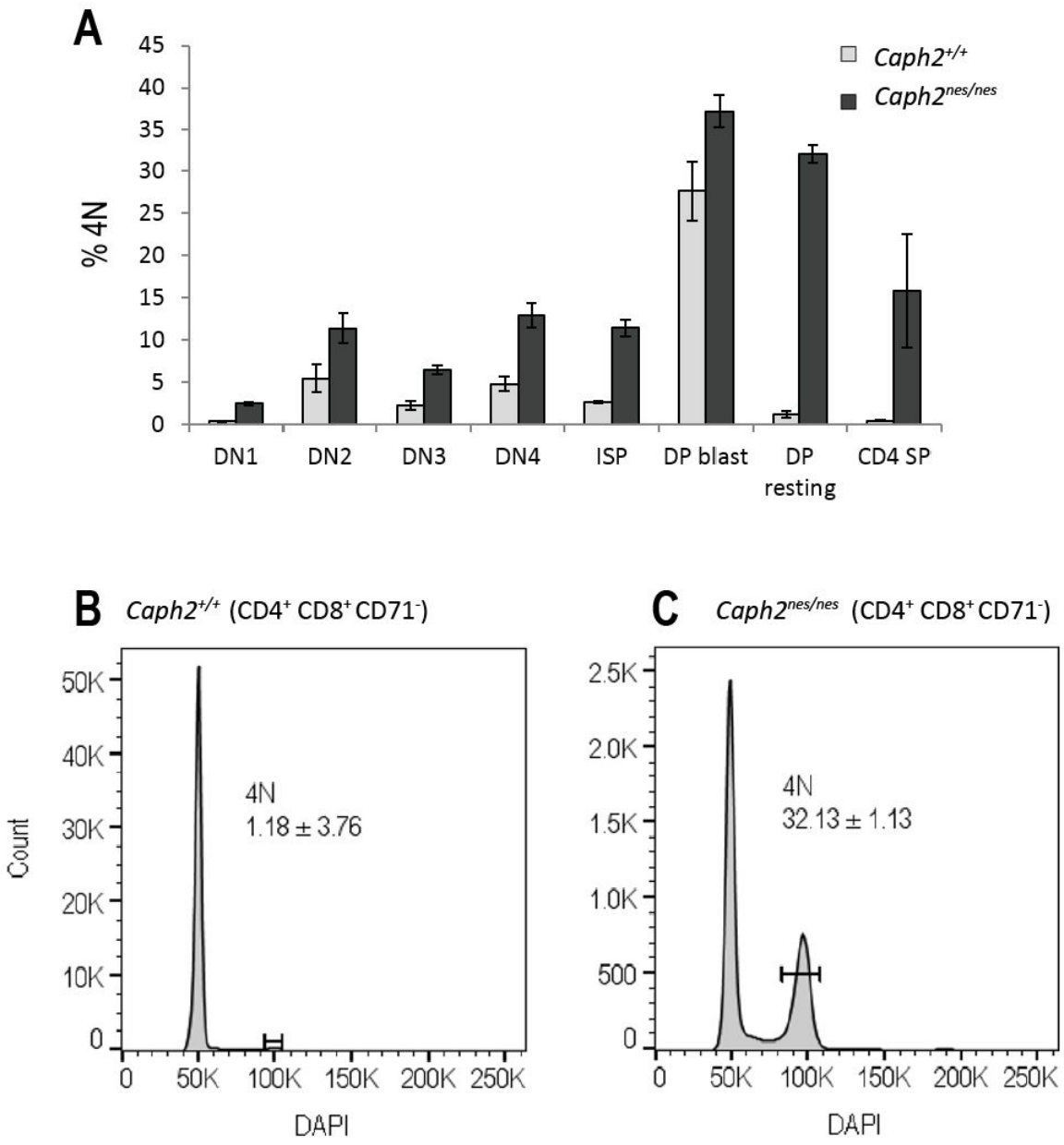

Figure 4.3
Determination of the proportion of tetraploid cells during T cell development
A. Histogram showing the proportion of cells with 4N DNA content as judged by DAPI staining at different stages of wildtype (grey) and *Caph2*$^{nes/nes}$ (black) T cell development. Error bars represent the standard error of the mean and were calculated based on three biological replicates. **B.** DNA content histogram of wildtype DP CD71^{-} cells. **C.** DNA content histogram of *Caph2*$^{nes/nes}$ DP CD71^{-} cells, revealing that most cells are tetraploid. Cell percentages within the indicated subsets were calculated from three biological replicates. The mean value is presented, plus or minus the standard error of the mean.

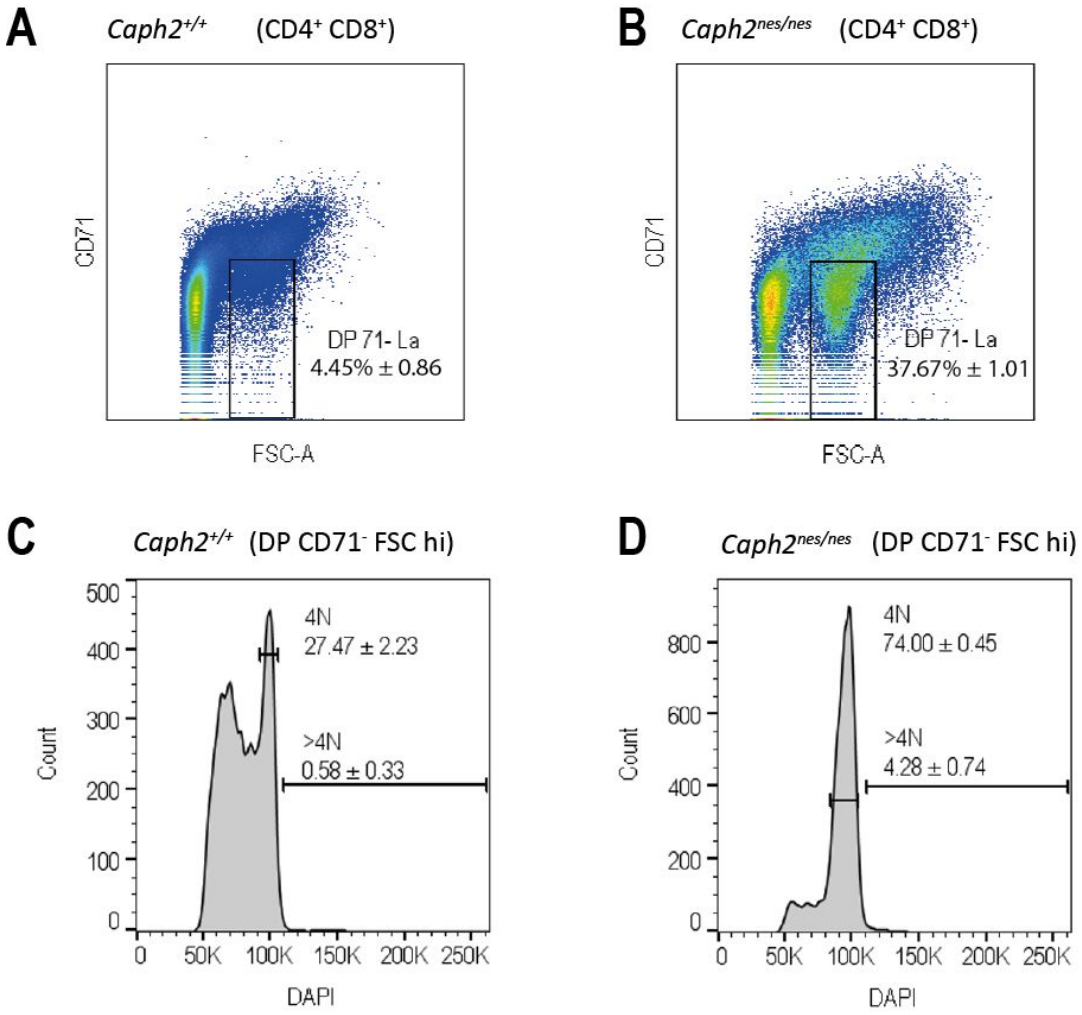

Figure 4.4
Analysis of the population of cells with 4N DNA content at the DP71- resting stage
A. Flow cytometry dot plot showing cell size (FSC) and CD71 expression of $CD4^+$ $CD8^+$ wildtype cells. The $CD71^-$ FSC^{hi} (large) population is indicated by the black gate. **B.** Flow cytometry dot plot showing cell size (FSC) and CD71 expression of $CD4^+$ $CD8^+$ *Caph2*$^{nes/nes}$ cells. There is a substantial increase in the proportion of $CD71^-$ FSC^{hi} cells, in comparison to wildtype. **C.** DNA content histogram of wildtype DP $CD71^-$ FSC^{hi} cells. **D.** DNA content histogram of *Caph2*$^{nes/nes}$ DP $CD71^-$ FSC^{hi} cells, revealing that most cells are tetraploid. Cell percentages within the indicated subsets were calculated from three biological replicates. The mean value is presented, plus or minus the standard error of the mean.

Further analysis of the DP cells revealed a population of $BrdU^-$ FSC^{hi} cells in mutants (Figure 4.5b) that are largely absent from wildtype (Figure 4.5a). This result is consistent with the existence of a non-cycling population of large mutant cells, observed using CD71 versus forward scatter.

The population of large non-cycling mutant cells may represent tetraploid cells that have undergone G1 arrest following unsuccessful mitosis, or diploid cells that are arrested after failing to enter mitosis. Previous experiments (Chapter 3: Section 3.1.2.5) revealed no difference in the rate of progression from S to M phase between wildtype and mutant $CD4^+$ $CD8^+$ DP cells, indicating that the 4N population arises due to mitotic slip, rather than G2 arrest or mitotic slip.

Analysis of T cell ploidy data (both 4N, Section 4.2.1.4 and >4N, Section 4.2.1.2) indicates that once mutant cells have undergone abnormal cytokinesis (likely due to mitotic slip), the cells may exit the cell cycle with 4N DNA content, as revealed by the high frequency of tetraploid $CD71^-$ resting cells. Alternatively, the cells may continue to cycle and re-synthesize their DNA during S phase, as indicated by the high frequency of $CD71^+$ blast cells with hyperdiploid (greater than 4N) DNA content.

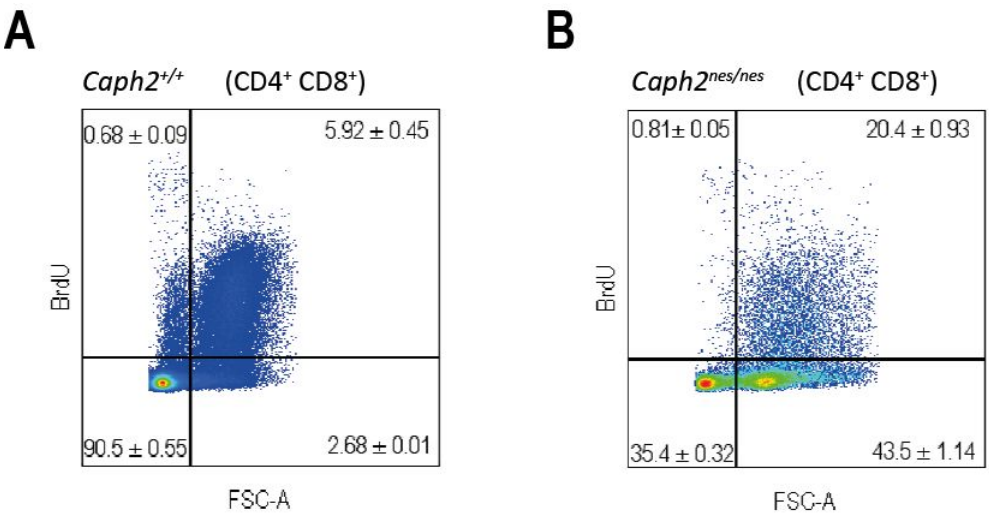

Figure 4.5
Population of abnormally large quiescent ($BrdU^-$ FSC^{hi}) DP cells largely absent from wildtype
A. Flow cytometry dot plot showing cell size (FSC) and BrdU incorporation in $CD4^+$ $CD8^+$ wildtype cells. The percentage of cells in each quadrant is indicated, and represents three biological replicates. Less than 3% of wildtype cells are abnormally large and quiescent ($BrdU^-$ FSC^{hi}). **B.** Flow cytometry dot plot showing cell size (FSC) and CD71 expression of $CD4^+$ $CD8^+$ *Caph2*$^{nes/nes}$ cells. The percentage of cells in each quadrant is indicated, and represents three biological replicates. Approximately 43% of *Caph2*$^{nes/nes}$ cells are abnormally large and quiescent ($BrdU^-$ FSC^{hi}).

4.2.2 Cell cycle regulation during Erythrocyte differentiation

Having investigated the rates of BrdU incorporation, the relative frequencies of hyperdiploidy in wildtype and mutant and the consequences on cell number across multiple stages of T cell development, I next extended this analysis to additional haematopoietic cell lineages. Since T cells form part of the lymphoid branch of haematopoiesis, I next analysed a cell type belonging to the myeloid lineage: the erythrocytes. Analysis was carried out on cells undergoing bone marrow erythropoiesis. Erythrocyte differentiation (like T and B lymphopoiesis) involves extensive proliferation, and therefore cell cycle abnormalities might be expected in *Caph2*$^{nes/nes}$.

4.2.2.1 Investigation into extent of proliferation during erythrocyte differentiation

BrdU incorporation studies were carried out as described previously. Individual stages of erythrocyte development were determined using fluorescently conjugated antibodies to Ter119 and CD71 (Table 2.5). Following cell fixation and permeabilisation, the cells were incubated with a fluorescently conjugated antibody to BrdU (Table 2.5) and analysed by flow cytometer, as before. The proportion of BrdU positive cells was calculated for each developmental stage. Gating strategies used to determine the individual stages of erythrocyte development are shown in Figure 2.3a, and these gates were used for all erythrocyte experiments.

For erythrocytes, the developmental stage associated with the highest levels of BrdU incorporation (and therefore the highest proportion of S phase cells) was found to be Stage 3 (Figure 4.6b), which is identified based on high expression of both CD71 and Ter119 (Figure 4.6a). In fact, the proportion of cells positive for BrdU is higher during Stage 3 of erythrocyte development than at the DP 71$^+$ blast stage of T cell development (Figure 4.1b), which may indicate that the Stage 3 erythrocytes undergo more extensive proliferation than DP 71$^+$ T cells.

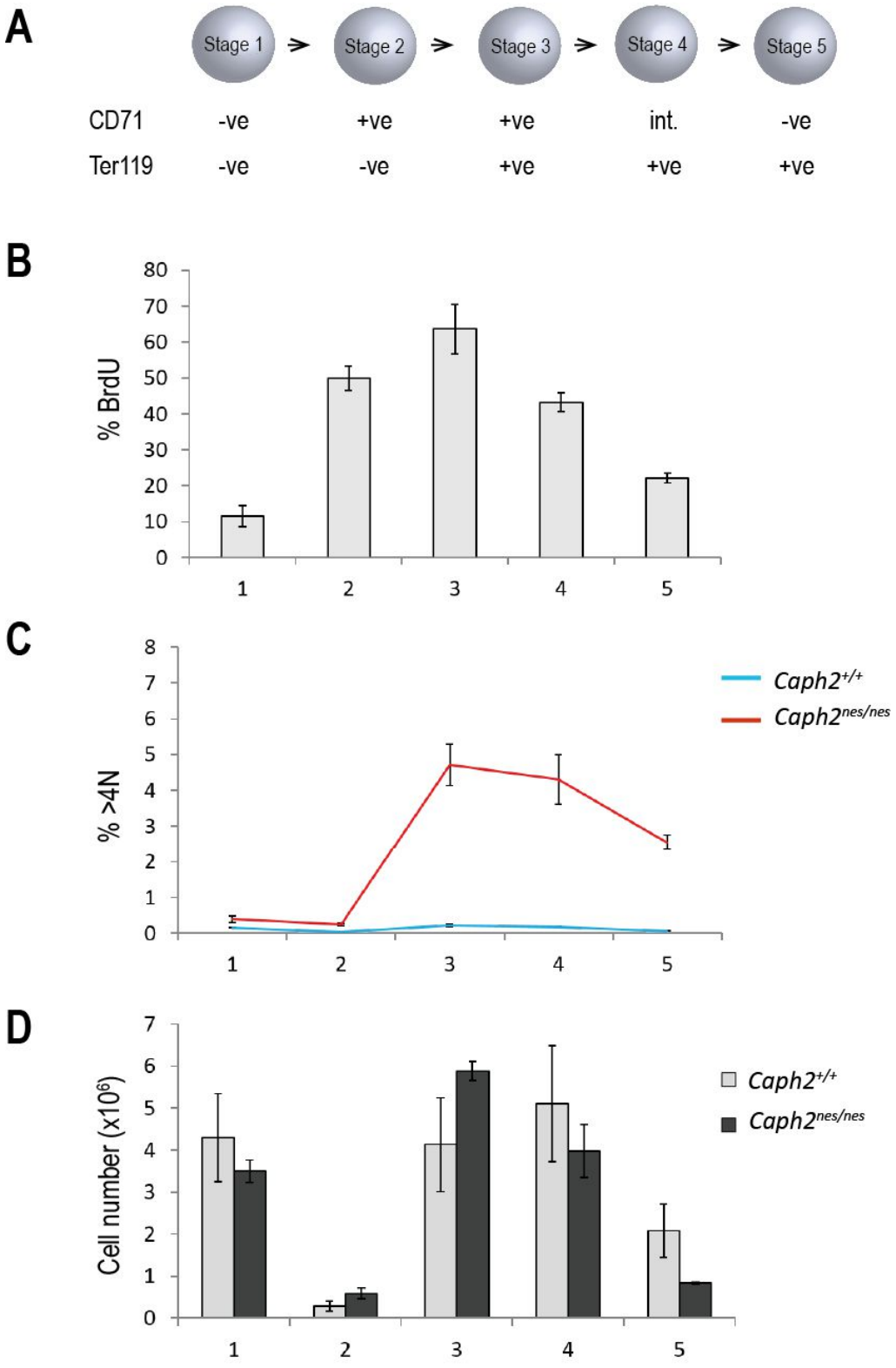

Figure 4.6
Analysis of cell cycle parameters during Erythrocyte development
A. Stages of erythrocyte development in relation to CD71 and Ter119 expression. **B.** Quantification of cell proliferation in erythrocytes using BrdU assays. **C.** Proportion of cells with greater than 4N DNA content as judged by DAPI / DNA content analysis at different stages of wildtype (blue) and *Caph2*$^{nes/nes}$ (red) erythrocyte development. **D.** Quantification of absolute cell numbers at different stages of wildtype (grey) and *Caph2*$^{nes/nes}$ (black) erythrocyte development.
Error bars represent the standard error of the mean and were calculated based on three biological replicates.

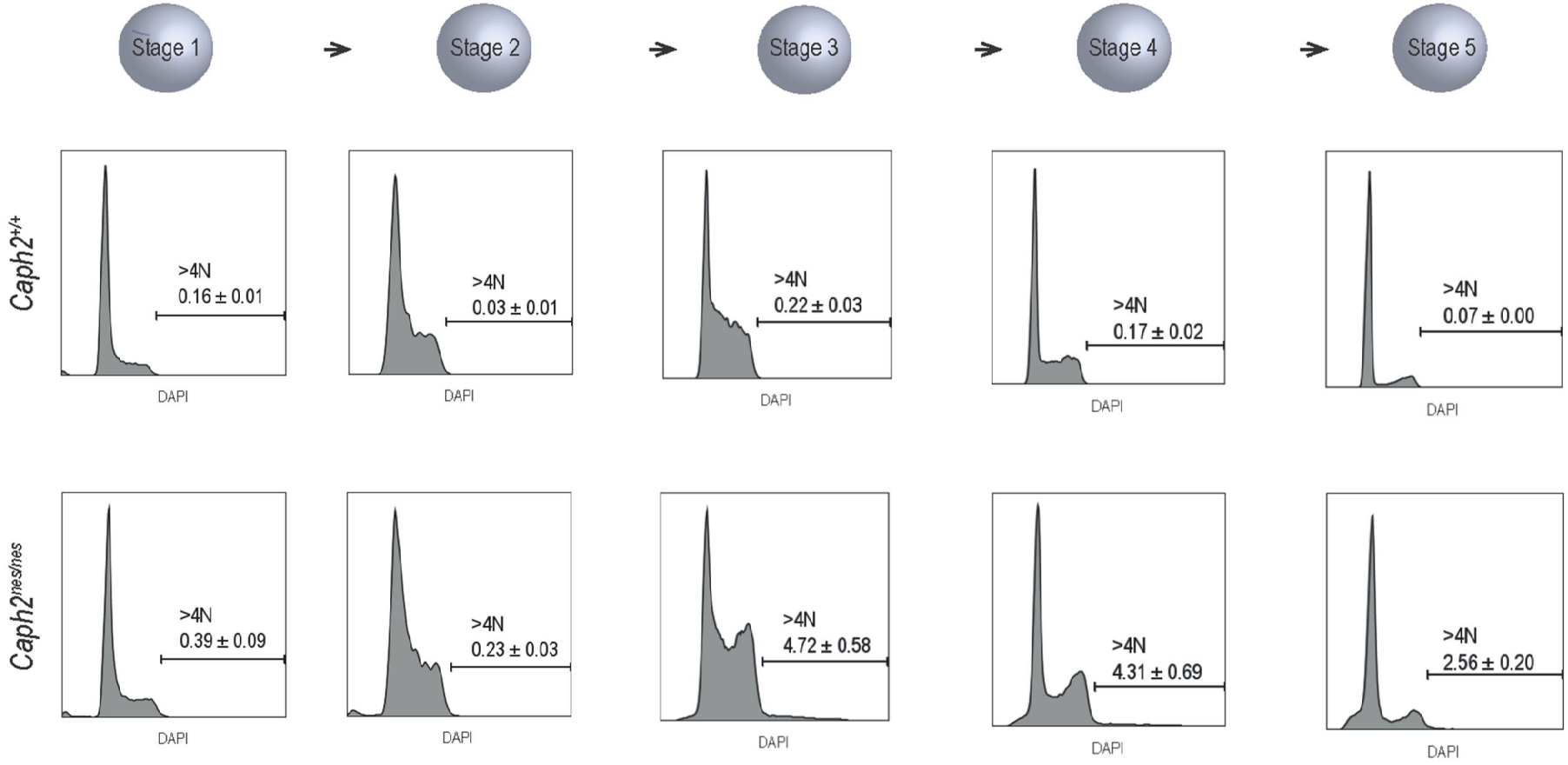

Figure 4.7

Representative flow cytometry DNA content histograms showing the proportion of hyperdiploid cells at each of the stages of erythroid differentiation for both wildtype and *Caph2*$^{nes/nes}$. Cell percentages within the indicated subsets were calculated from three biological replicates. The mean value is presented, plus or minus the standard error of the mean.

4.2.2.2 Consequences of the Caph2$^{nes/nes}$ mutation on hyperdiploidy and cell number during erythrocyte differentiation

I next investigated the dynamic changes in ploidy during wildtype and mutant erythrocyte development using flow cytometry, in the same way as described for T cells. The individual stages of differentiation were determined using fluorescently-conjugated antibodies to Ter119 and CD71 (Table 2.5) and the DNA dye DAPI was used to assess ploidy. DNA content histograms for each of the stages of differentiation are shown in Figure 4.7. The hyperdiploid gate is illustrated for each stage.

As observed in the T cells, a spike in the frequency of hyperdiploid *Caph2*$^{nes/nes}$ erythroid cells occurred at the stage (Stage 3) associated with the highest rates of BrdU incorporation. However, the frequency of hyperdiploid erythroid cells was lower than for T cells: the frequency of hyperdiploid mutant erythroid cells peaked at approximately 5% compared to 8% observed at the DP 71^{+} blast stage of T cells. The frequency of hyperdiploid wildtype cells did not vary greatly between stages of development: in fact, the levels remained fairly consistently below 1% throughout all tested stages of erythropoiesis (Figure 4.6c). From the data presented above, it is clear that the rapid increase in the proportion of hyperdiploid *Caph2*$^{nes/nes}$ T cells coincides with dramatic reductions in cell numbers. Since a similar peak in the frequency of hyperdiploid mutant cells is observed at a comparable stage of erythrocyte development, I was interested in investigating the consequences of the high levels of hyperdiploidy on mutant erythroid cell numbers relative to wildtype numbers.

Experiments to determine cell number at each of the stages of erythrocyte development were carried out in the same way as described for T cells (see above). Accurate determination of the number of cells per tibia and femur was achieved using an automated cell counter. Cell surface antibodies to Ter119 and CD71 (Table 2.5) were used to determine the stage of development. Surprisingly, although a similar peak in the levels of hyperdiploid mutant cells was observed in both the T cell and erythroid lineages, no corresponding large-scale reduction in *Caph2*$^{nes/nes}$ cells was observed relative to wildtype at any stage of development (Figure 4.6d).

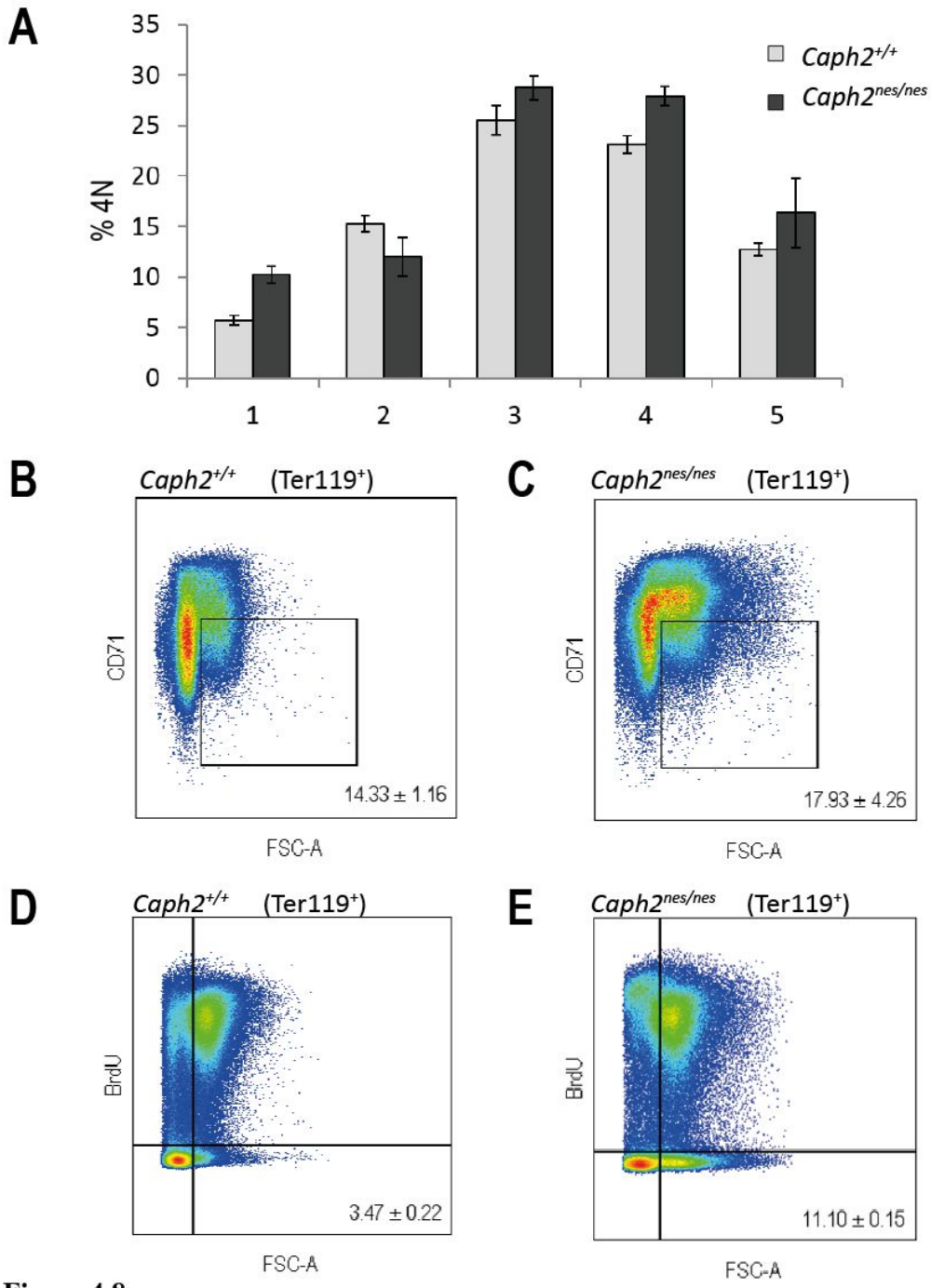

Figure 4.8

Determination of the proportion of tetraploid cells during erythroid development

A. Histogram showing the proportion of cells with 4N DNA content as judged by DAPI staining at different stages of wildtype (grey) and *Caph2*$^{nes/nes}$ (black) T cell development. Error bars represent the standard error of the mean and were calculated based on three biological replicates. **B.** Flow cytometry dot plot showing cell size (FSC) and CD71 expression of Ter119^{+} wildtype cells. The CD71^{-} FSC^{hi} (large) population is indicated by the black gate. **C.** Flow cytometry dot plot showing cell size (FSC) and CD71 expression of Ter119^{+} *Caph2*$^{nes/nes}$ cells. Unlike for T cells, there is no substantial increase in the proportion of CD71^{-} FSC^{hi} cells relative to wildtype. **D.** Dot plot showing cell size (FSC) and BrdU incorporation in Ter119^{+} wildtype cells. Approximately 3% of cells are large and quiescent (BrdU^{-} FSC^{hi}). **E.** Dot plot showing cells size (FSC) and BrdU incorporation in Ter119^{+} *Caph2*$^{nes/nes}$ cells. Approximately 11% of cells are large and quiescent (BrdU^{-} FSC^{hi}).

Cell percentages within the indicated subsets were calculated from three biological replicates. The mean value is presented, plus or minus the standard error of the mean.

4.2.2.3 Investigation into the proportion of cells with 4N DNA content during erythroid differentiation in wildtype and mutant mice

Having discovered a population of large arrested mutant T cells that were predominantly tetraploid (Figure 4.4d), I next wanted to establish whether a similar population exists within the erythroid lineage. The percentage of 4N wildtype and mutant cells for each of the stages of differentiation (determined in the same way as described for T cells) was plotted as a histogram (Figure 4.8a). Unlike the T cells, no stage of erythroid development revealed a considerably higher proportion of 4N mutant cells relative to wildtype.

In order to further compare the data with that obtained from the T cells, CD71 was plotted against forward scatter. In contrast to the T cells, where an almost ten-fold increase in the proportion of abnormally large $CD71^-$ cells was observed in mutant compared to wildtype (Figures 4.4a and 4.4b), no sizeable difference was found between mutant and wildtype erythroid cells. Approximately 14% of wildtype cells were labelled as $CD71^-$ FSC^{hi}, compared to approximately 18% of mutant cells (Figures 4.8b and 4.8c).

Further analysis revealed a < four-fold increase in the proportion of mutant cells that are BrdU negative and FSC-hi (Figures 4.8d and 4.8e). This increase is much smaller than for T cells, where a > 15-fold increase was observed (Figure 4.5). This implies that tetraploid erythroid cells are far less likely to undergo cell cycle arrest in comparison to tetraploid T cells.

From this data, it is evident that both stages of haematopoietic development analysed thus far are affected by the condensin II deficiency, resulting in increased frequencies of cells with abnormal ploidy. However, the consequences of the increased frequency of hyperdiploid cells in mutant relative to wildtype vary between the two cell types. The reason for this difference may be that the erythrocytes are better able to cope with the abnormal ploidy and so do not undergo such dramatic cell number reductions. One could speculate that since erythroid cells enucleate upon terminal differentiation (Keerthivasan, Wickrema, & Crispino, 2011), the potential for negative consequences arising from chromosomal instability (CIN) and abnormal ploidy is less severe. In

contrast, T cells must maintain the capacity for massive clonal expansion during an adaptive immune response, and may therefore require more stringent safeguards to protect against malignant transformation.

4.2.3 Cell cycle regulation during B cell differentiation

Having investigated cell cycle dynamics in two haematopoietic lineages, I next extended my analysis to B cells. The B cells, like the T cells, are members of the lymphoid lineage. Both cell types undergo VDJ recombination at antigen receptor loci, and massive clonal expansion when presented with cognate antigen, and so analysis of the consequences of condensin deficiency between these two cell types may provide valuable insight into the effect of CIN and condensin II deficiency on cell viability.

B cell progression in the condensin II mutant mouse was analysed in detail by Gosling *et al*. but no difference was found in the percentage of B cells in *Caph2*$^{nes/nes}$ compared to wildtype at any of the stages analysed (Gosling *et al*., 2007). Given that B cells and T cells undergo very similar processes during development, such as recombination followed by rapid proliferative bursts, it is surprising that the mutation in condensin II seems to result in such a T cell specific phenotype. Therefore, I decided to further investigate cell cycle dynamics during B cell development in wildtype and mutant cells.

4.2.3.1 Cell proliferation during B cell differentiation

BrdU incorporation studies were undertaken as described previously. The cells were incubated with fluorescently conjugated antibody to BrdU, as well as to the cell surface markers B220, CD24 and CD43 (Table 2.5). Stages of B cell differentiation were identified based on the Hardy B cell classification scheme (R. Hardy *et al*., 1991). Due to insufficient flow cytometer channels, antibodies to BP-1 or IGM were not included. Consequently, Fractions B and C are presented as a single stage, as are Fractions D and E. The cells were fixed and analysed using flow cytometry (A. Wood, unpublished data). The gating strategies used to determine B cell stages in each experiment are indicated in Figure 2.3b.

Rearrangement of the IgH locus occurs in Fraction B and C of B cell development (R. R. Hardy & Hayakawa, 2001). Cells that successfully undergo VDJ rearrangement then undergo a stage of rapid proliferation. This is supported by the BrdU incorporation data, which shows that the stage associated with the highest levels of BrdU incorporation occurs during Fraction B/C (Figure 4.9b – A. Wood, unpublished data).

4.2.3.2 Consequences of the Caph2$^{nes/nes}$ mutation on hyperdiploidy during B cell development

Having established that the most extensive proliferation during B cell development occurs within Fraction B/C, as judged by BrdU incorporation, I next investigated the dynamic changes in ploidy during wildtype and mutant B cell development using flow cytometry. This was achieved in the same way as described for T cells and erythrocytes. DNA content histograms for each of the stages of differentiation are shown in Figure 4.10. The hyperdiploid gate is illustrated for each stage.

Intriguingly, unlike in either the T cell or erythroid lineages, no significant increase in the frequency of hyperdiploid mutant cells relative to wildtype was observed at any stage of B cell development. A small increase in hyperdiploidy (~ 1% of cells) was observed at Fraction B/C, however this was true for both wildtype and mutant (Figure 4.9c).

B cells reveal similar frequencies of proliferating cells compared to T cells, as judged by BrdU incorporation: approximately 47% of cells are BrdU$^+$ during Fraction B/C of B cell development (Figure 4.9b) compared with 50% of DP 71$^+$ blast T cells (Figure 4.1b). Therefore, the spike in the frequency of hyperdiploid mutant T cells cannot be solely due to increased frequencies of proliferating cells at the DP 71$^+$ blast stage.

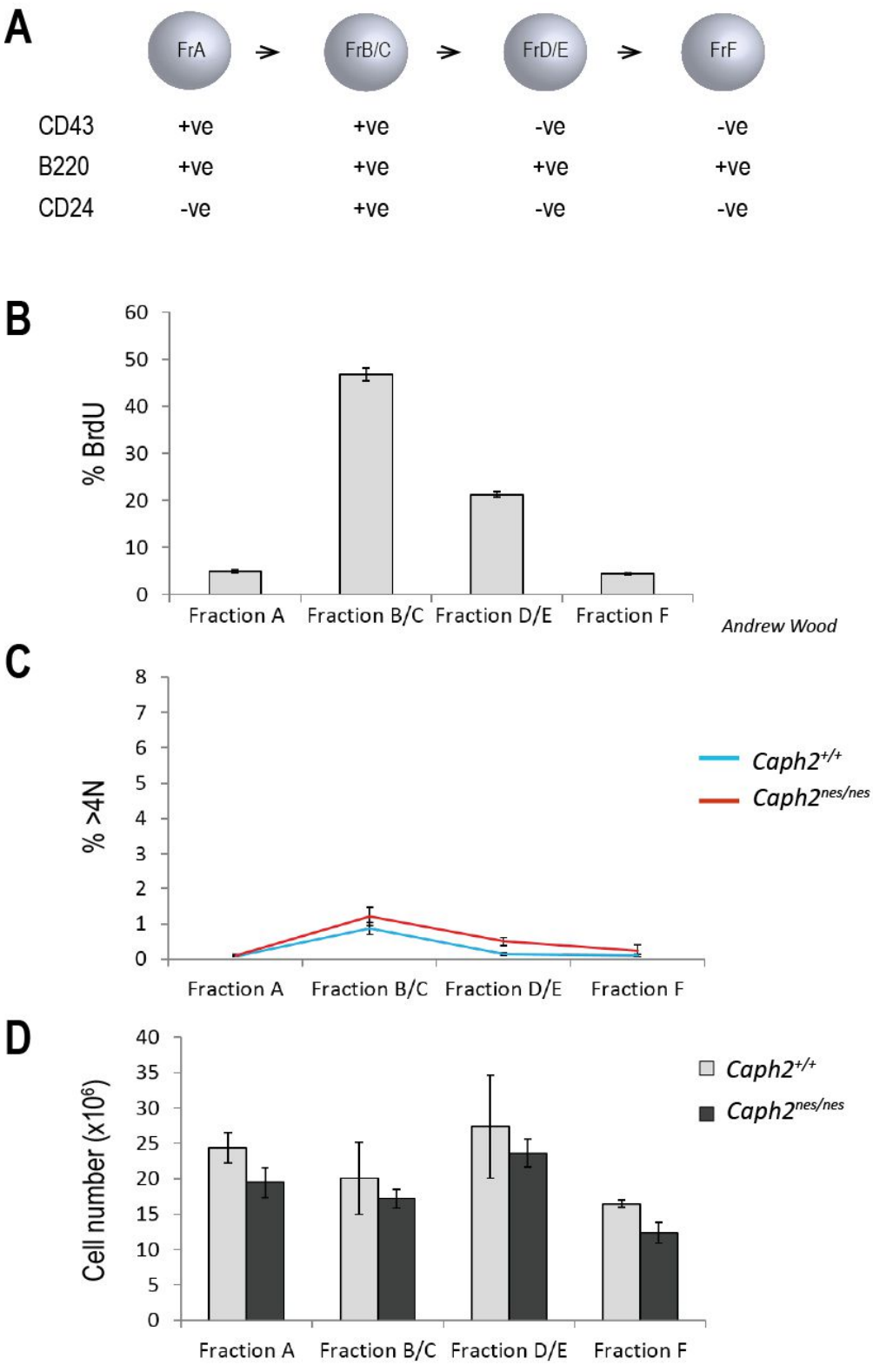

Figure 4.9
Analysis of cell cycle parameters during B cell development
A. Stages of B cell development in relation to CD43 and B220 expression. **B.** Quantification of cell proliferation in erythrocytes using BrdU assays. **C.** Proportion of cells with greater than 4N DNA content as judged by DAPI / DNA content analysis at different stages of wildtype (blue) and *Caph2*$^{nes/nes}$ (red) erythrocyte development. **D.** Quantification of absolute cell numbers at different stages of wildtype (grey) and *Caph2*$^{nes/nes}$ (black) erythrocyte development.
Error bars represent the standard error of the mean and were calculated based on three biological replicates.

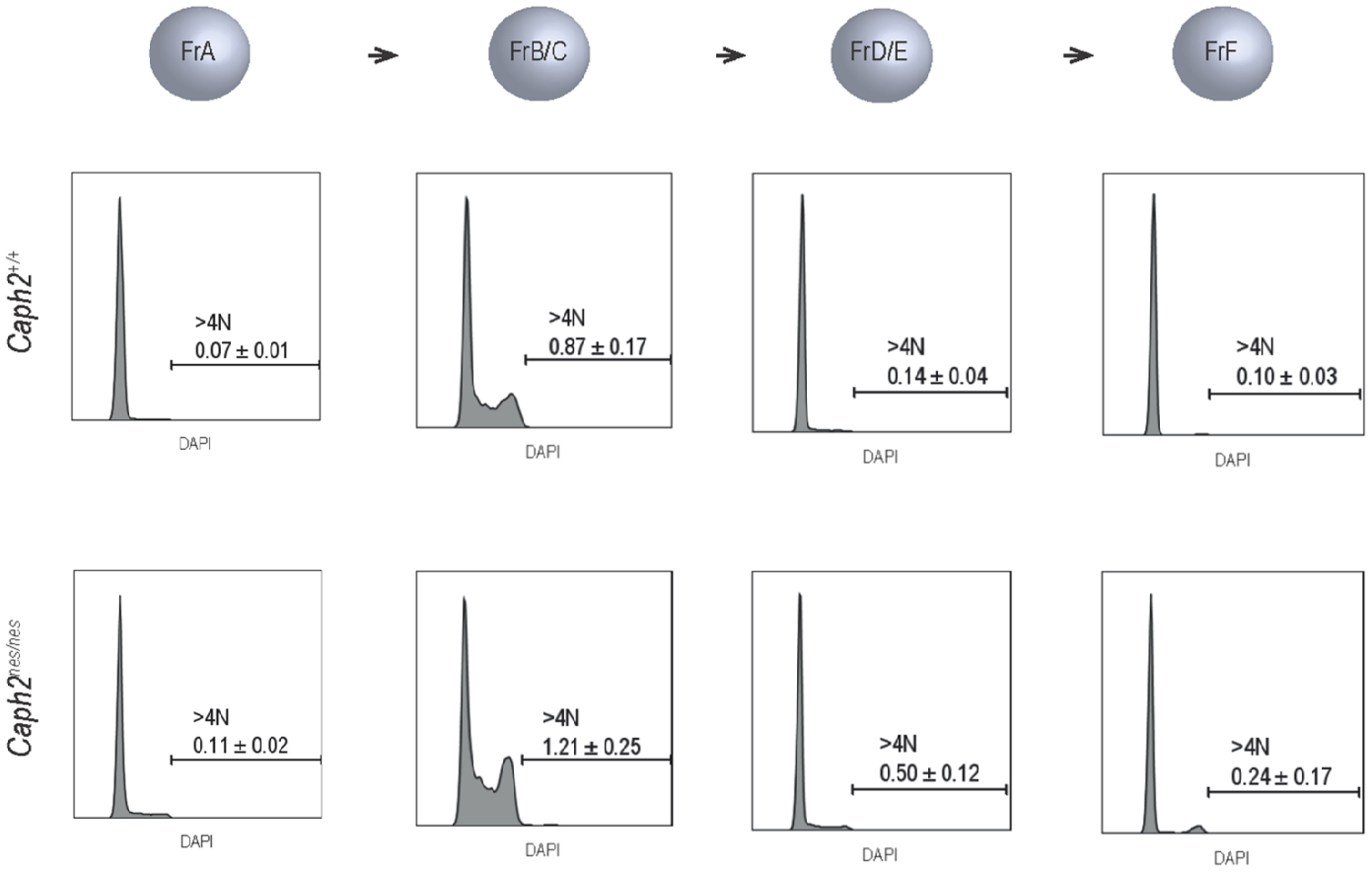

Figure 4.10

Representative flow cytometry DNA content histograms showing the proportion of hyperdiploid cells at each of the stages of B cell differentiation for both wildtype and *Caph2*$^{nes/nes}$. Cell percentages within the indicated subsets were calculated from three biological replicates. The mean value is presented, plus or minus the standard error of the mean.

4.2.3.3 Consequences of the Caph2$^{nes/nes}$ mutation on absolute cell numbers during B cell differentiation

Finally, I studied whether B cell numbers were affected by the condensin II mutation. An automated cell counter was used to accurately determine the number of cells per tibia and femur. The cells were then incubated with cell surface antibodies, analysed on the flow cytometer and absolute cell numbers calculated, as before.

No sizeable reductions in cell numbers were observed in mutant relative to wildtype at any stage of B cell development analysed. Since B cells do not undergo large-scale changes in ploidy as a result of the condensin II mutation (unlike T or erythroid cells), it is unsurprising that B cell numbers are unaffected in the mutant (Figure 4.9d).

4.2.4 Cell cycle regulation at the haematopoietic precursor stage of development

Analysis of the three haematopoietic lineages studied thus far reveals that each cell type is affected differently by mitotic stress and CIN: the *Caph2$^{nes/nes}$* mutation results in different outcomes, in terms of levels of aneuploidy and a reduction in cell numbers, in each cell type. Each of the haematopoietic cell lineages analysed so far have contained cells engaged in the process of differentiation and lineage commitment. For the next stage of my analysis, I investigated the consequences of the condensin II mutation on abnormal ploidy or cell number in earlier haematopoietic precursors.

In adult mice, the haematopoietic stem cells are located in the bone marrow, where they undergo self-renewal (which replenishes the stem cell population) and differentiate into multipotent progenitor cells (Giebel & Bruns, 2008; Marciniak-Czochra, Stiehl, Ho, Jäger, & Wagner, 2009). The balance between self-renewal and differentiation must be carefully regulated, since sufficient cells must always be available to replenish peripheral blood cells of all lineages, but extensive and uncontrolled self-renewal may lead to tumourigenesis. Several mechanisms to maintain the appropriate balance between renewal and differentiation have been suggested, including asymmetric cell division (Roegiers & Jan, 2004; Yu, Kuo, & Jan, 2006), in which only one daughter cell inherits the necessary proteins to maintain self-

renewal. Additionally, stem cells located within certain regions (termed stem cell niches) may be provided with an external stimulus which allows the cell to remain as stem cells. Cells that are not located in these "niches" are not exposed to these signals, and therefore differentiate (Giebel & Bruns, 2008; Lin, 2002).

True stem cells are capable of replicating indefinitely, whereas there is a limit to the amount of divisions the precursor cells are capable of (Seaberg & Van Der Kooy, 2003). The stages of haematopoietic differentiation that I analysed were: the $Lin^{-}Sca\text{-}1^{+}c\text{-}kit^{+}$ (LSK) population, the common myeloid progenitor (CMP) and the common lymphoid progenitor (CLP). The LSK population contains the true haematopoietic stem cells and other early derivatives (Spangrude *et al*., 1989). The common lymphoid progenitor produces cells that can differentiate into T and B cells, while the common myeloid progenitor is a precursor of erythrocytes and other myeloid cell types (Iwasaki & Akashi, 2007).

4.2.4.1 Consequences of the Caph2$^{nes/nes}$ mutation on DNA content and absolute cell number of haematopoietic precursor cells

Ploidy was determined using the fluorescent DNA stain propidium iodide (PI) (Materials and Methods: Section 2.2.9.1). The cells were analysed by flow cytometry, and doublets were excluded using both forward-scatter width versus area, and forward scatter area versus height. Exclusion of dead cells, debris, doublets and lineage committed cells was carried out as before. Finally, c-kit was plotted against Sca-1 to differentiate between the LSK, CMP and CLK populations (Figure 2.4).

An increase in the proportion of hyperdiploid mutant cells was observed relative to wildtype in both the LSK and CMP populations. However, the increase was small: approximately 0.1% of mutant LSK cells were hyperdiploid compared to 0.06% of wildtype, and 0.2% of mutant CMP cells compared with 0.1% of wildtype. None of the progenitor populations analysed revealed levels of hyperdiploidy above 0.3%, which is 28-fold lower than DP blast cells in the T cell lineage (Figure 4.11a). The DNA content histograms for the progenitor cells, as well as the T, B and erythroid cells are displayed together in Figure 4.12, for ease of comparison.

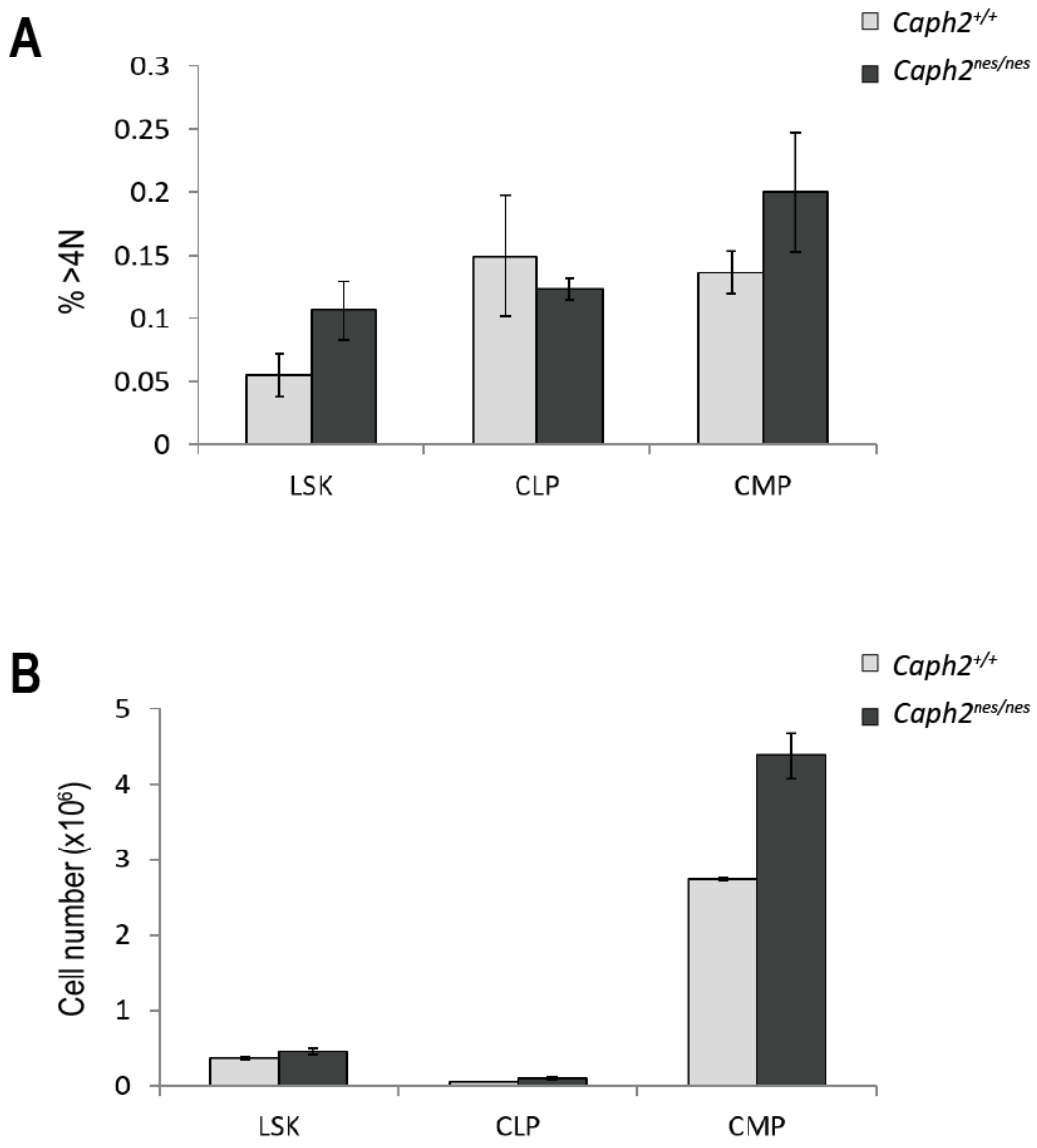

Figure 4.11
Hematopoietic precursors do not reveal increased levels of hyperdiploid or reductions in cell number as a consequence of the *Caph2*$^{nes/nes}$ mutation
A. Histogram showing the percentage of hematopoietic pecursor cells with greater than 4N DNA content. The results show no obvious increase in the proportion of hyperdiploid cells in *Caph2*$^{nes/nes}$ (in black) relative to wildtype (in grey). None of the stages analysed revealed levels of hyperdiploidy above 0.3%. Data represents three biological replicates. **B.** Quantification of absolute cell numbers at each of the precursor stages. The *Caph2*$^{nes/nes}$ mutation does not result in a cell number reduction at any of the stages analysed. Data represents three biological replicates.

Error bars represent the standard error of the mean and were calculated based on three biological replicates.

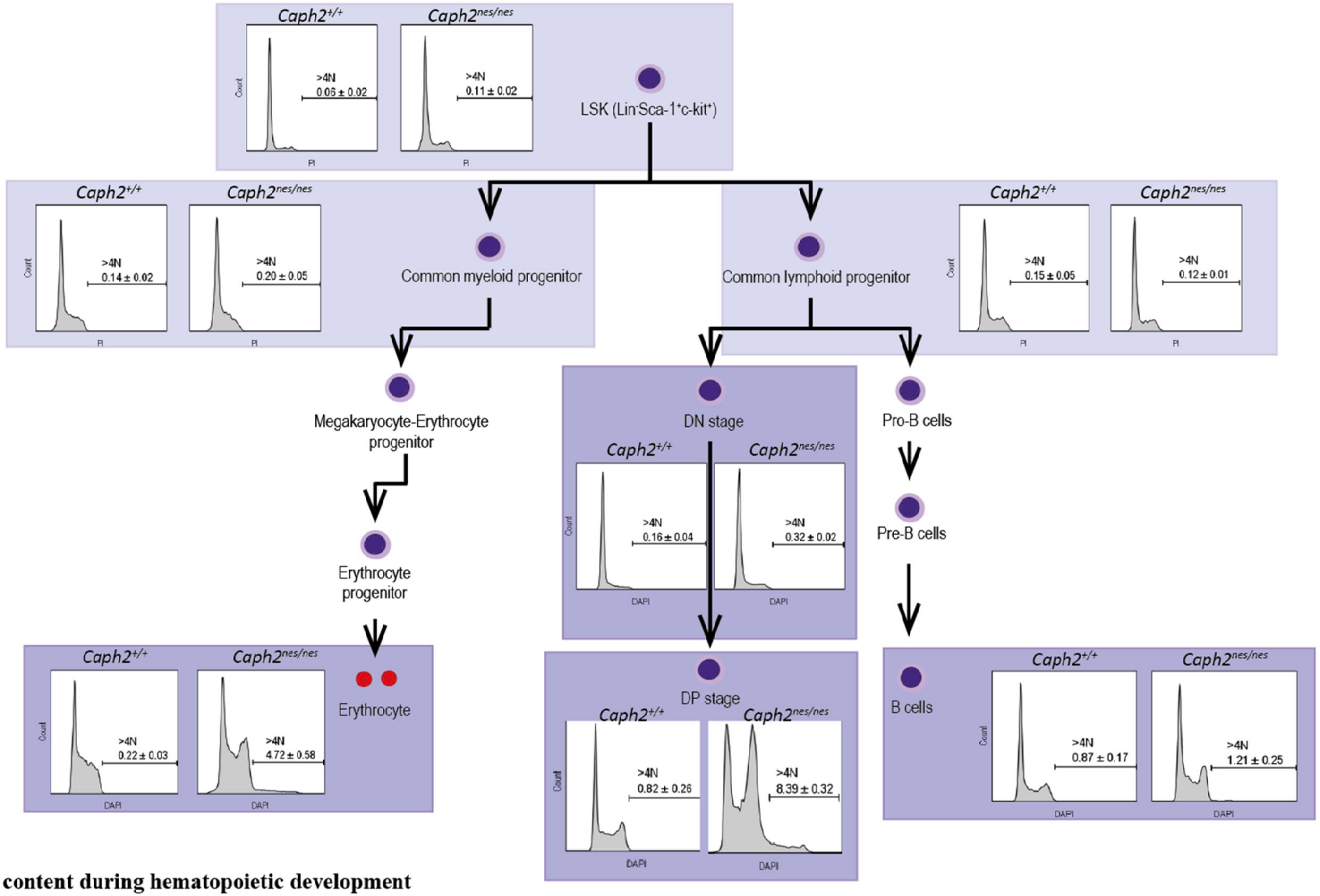

Figure 4.12
Analysis of DNA content during hematopoietic development
DNA content histograms for various stages of hematopoietic differentition. Percentages of cells with >4N DN content were calculated from three biological replicates. The mean value is presented, plus or minus the standard error of the mean.

In addition to studying the DNA content of the haematopoietic precursors, I investigated whether progenitor cell numbers were affected by the condensin II mutation. Given that the *Caph2*$^{nes/nes}$ progenitor cells did not reveal increased levels of hyperdiploidy, it is unsurprising that the mutant precursor cells, like the B cells, do not undergo reductions in cell numbers. In fact, a slight increase in the number of mutant progenitor cells is observed relative to wildtype (Figure 4.11b). The difference in cell numbers, however, is relatively small.

Interestingly, the largest difference occurs at the common myeloid progenitor (CMP) stage where there are approximately 2.5 million wildtype cells in comparison to approximately 4.5 million mutant cells. Having shown that the *Caph2*$^{nes/nes}$ erythroid cells show increased levels of hyperdiploidy (Figure 4.6c), but no reduction in cell number (Figure 4.6d), the increased numbers of mutant cells at the progenitor stage might suggest the existence of an autoregulatory feedback loop, to replenish cell numbers that are impacted by abnormal chromosome segregation later during differentiation at the erythroblast stage. In contrast, the difference between the number of wildtype and mutant lymphoid progenitor cells is considerably smaller (~0.4 million versus ~0.5 million for wildtype and mutant, respectively) which may suggest the absence of effective autoregulatory feedback, resulting in cell number reductions following chromosome segregation failure in the T cell lineage (Figure 4.1d).

4.2.5 Consequences of Caph2$^{nes/nes}$ *on DNA content of Mouse Embryonic Fibroblasts (MEFs)*

The primary cell type most commonly used to characterise cellular defects in mouse models of chromosomal instability are MEFs (Liu *et al*., 2009; Vitre & Cleveland, 2012; Wijshake *et al*., 2012). Therefore, in order to complete my investigation into the consequence of the *Caph2*$^{nes/nes}$ mutation on ploidy in different cell types, cultured MEFs were obtained from both wildtype and mutant mice. The cells were DAPI stained, and their DNA content profiles analysed by flow cytometry. Representative DNA content profiles for both *Caph2*$^{+/+}$ and *Caph2*$^{nes/nes}$ are shown in Figures 4.13a and 4.13b. The percentage of cells with >4N DNA content was calculated and the results plotted as a histogram (Figure 4.13c). A small increase in the proportion of hyperdiploid cells was observed in mutant versus wildtype (approximately 5% mutant versus 4% wildtype). However, this difference was not substantial.

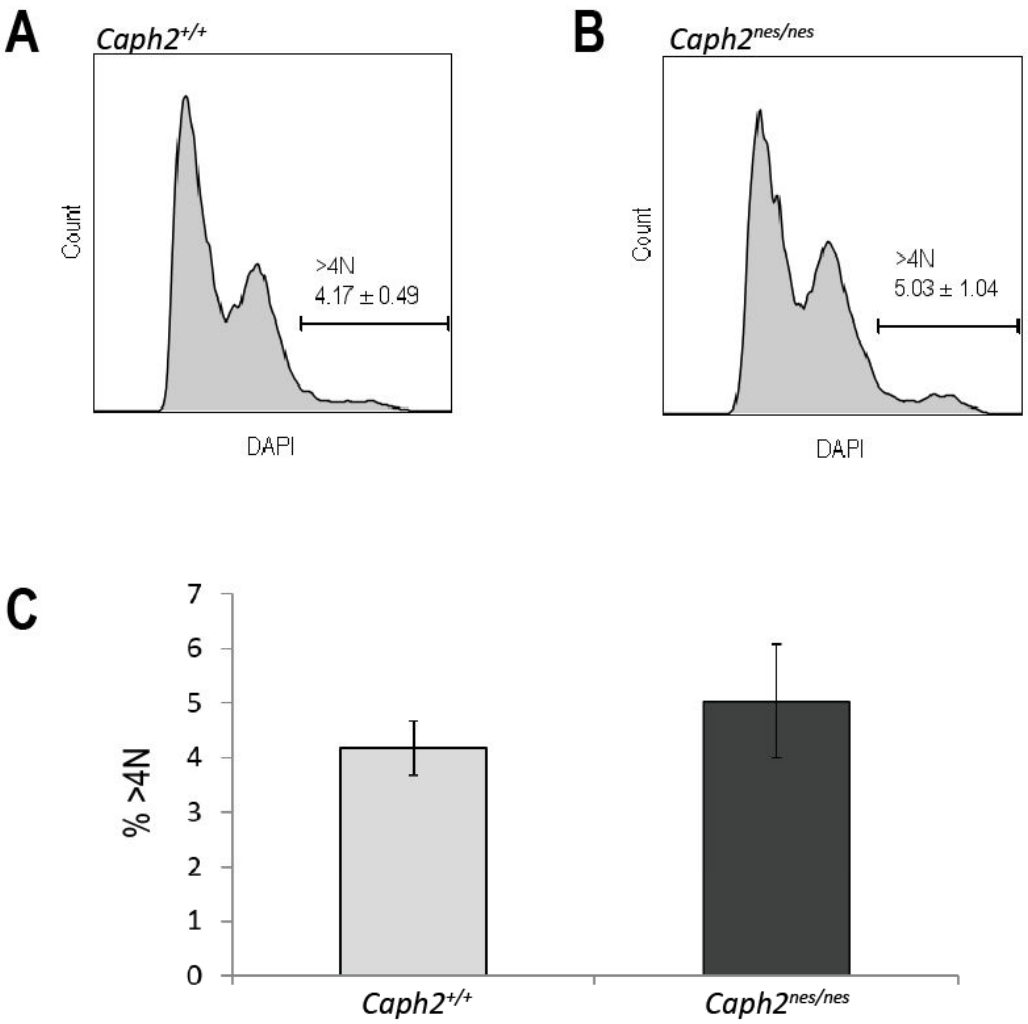

Figure 4.13
MEFs do not reveal increased levels of hyperdiploid or reductions in cell number as a consequence of the *Caph2*$^{nes/nes}$ mutation
A. DNA content histogram showing the proportion of wildtype MEFs with greater than 4N DNA content. Approximately 4% of wildtype MEFs are hyperdiploid. **B.** DNA content histogram showing the proportion of *Caph2*$^{nes/nes}$ MEFs with greater than 4N DNA content. Approximately 5% of *Caph2*$^{nes/nes}$ MEFs are hyperdiploid. **C.** Histogram showing the percentage of MEFs with greater than 4N DNA content. The results show no obvious increase in the proportion of hyperdiploid cells in *Caph2*$^{nes/nes}$ (in black) relative to wildtype (in grey). Data represents three biological replicates. Error bars represent the standard error of the mean and were calculated based on three biological replicates.

Cell percentages within the indicated subsets were calculated from three biological replicates. The mean value is presented, plus or minus the standard error of the mean.

4.2.6 A preliminary investigation into the cause of the differential susceptibility to the Caph2$^{nes/nes}$ mutation

Investigations into the consequences of the *Caph2*$^{nes/nes}$ mutation have revealed that different haematopoietic lineages are affected differently by the mutation to condensin II. The haematopoietic precursors are not affected in terms of abnormal ploidy or reduction in cell numbers, and this is also true for B cells and MEFs. The erythroid cells reveal abnormal ploidy, but no reduction in cell numbers. In contrast, the T cells display profound defects as a result of the mutation: a high proportion of cells reveal abnormal DNA content at a specific stage of development, which coincides with a drastic reduction in cell numbers. The next stage of my analysis focusses on investigating the reason why different stages of haematopoietic differentiation exhibit differential susceptibility to condensin II mutation.

The essential role of eukaryotic condensins in preparing chromosomes for segregation must take place between genome duplication during S phase, and chromosome segregation during anaphase. Alleviation of increasing mechanical stress during replication is thought to occur by fork rotations, resulting in the introduction of sister-chromatid catenations into circular chromosomes (Champoux & Been, 1980). These catenations must be resolved before chromosome segregation can proceed. Due to the difficulty in maintaining and visualizing catenations in linear chromosomes, it is not known whether fork rotations resulting in sister catenations also occur in higher eukaryotes. However, given the evidence for the introduction of precatenations into circular chromosomes during replication, it seems likely that similar processes may give rise to sister catenations in linear chromosomes.

Thus, although the phenotype of condensin deficient cells is most striking during and following mitosis, it is possible that the cell type differences in susceptibility to condensin mutation originate from differences during S phase. For example, S phase conditions which result in higher frequencies of catenations may impose a greater requirement for condensin activity.

Based on the results of the study carried out by Gruber *et al*. (discussed in Section 1.2.6.1), I investigated the possibility that the *Caph2*$^{nes/nes}$ phenotype arises due to

different rates of progression between cell types through various stages of the cell cycle. Faster progression through S phase into M phase might result in increased pressure on cell cycle machinery to resolve catenations between sister chromatids and quickly condense chromosomes into discrete structures, in preparation for cell division. Cells undergoing rapid progression from S to M phase may therefore be more vulnerable to condensin deficiency in comparison to cells that undergo a slower rate of progression. The possibility that condensin is required to a greater extent at the DP stage of T cell development is supported by transcriptome data assembled from more than 150 different immune cell subsets, which reveals that transcripts of the subunits of the condensin complexes are most highly expressed in DP $CD71^+$ T cells (Figure 4.14).

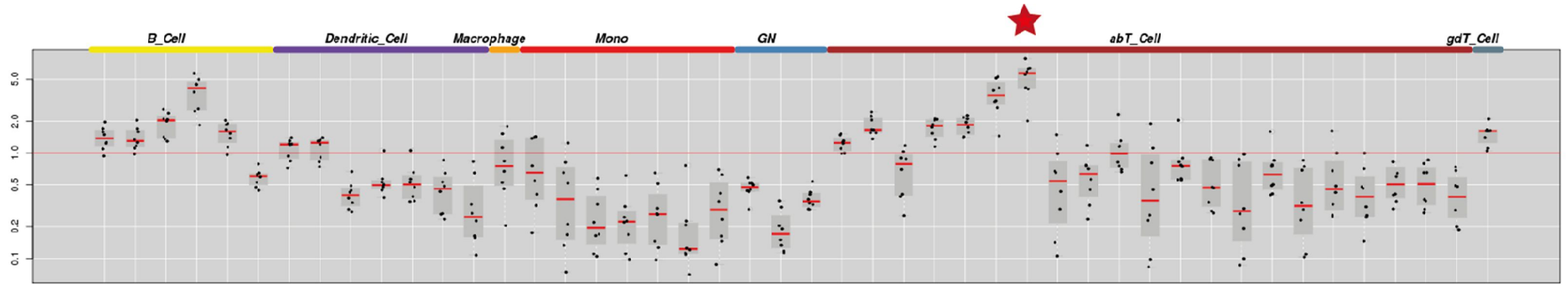

Figure 4.14

Transcriptome data assembled from more than 150 different immune cell subsets reveals that condensin subunit transcripts are most highly expressed at the DP 71+ stage of T cell development

W plot showing means-normalized expression value of the condensin subunit genes (SMC2/4, nCAPH/H2, nCAPG/G2, nCAPD2/D3) in each of the cell subsets. The cell subset associated with the highest transcript expression of condensin genes are the DP 71^{+} blast T cells (indicated by a red star). Data was assembled by the Immgen consortium: *Heng TS, et al, Immunological Genome Project Consortium, Nat Immunol. 2008 10 : 1091.*

4.2.6.1 Measurement of the rate of progression of Caph2$^{+/+}$ and Caph2$^{nes/nes}$ T cells from S phase to M phase

In order to investigate the rate of progression from S phase to M phase at the DN and DP stages of T cell development, I used the BrdU chase assay outlined above in Figure 3.9. MACS-purified CD4$^-$ wildtype and mutant T cells were added to the OP9 DL1 monolayer. The cells were cultured as described previously, until judged to be proliferating rapidly with approximately 40%-50% CD4$^+$ CD8$^+$ DP and 30% CD4$^-$ CD8$^-$ DN wildtype cells, and 15-20% DP 60%-70% DN mutant. I then treated the cells with nocodazole and BrdU over a four-hour time course, as described previously, before staining with CD4 and CD8 antibodies to determine differentiation state, and BrdU and pH3S10 to determine cell cycle progression. The rate of progression of the wildtype and mutant cells from S phase into M phase is shown as a line graph for CD4$^-$ CD8$^-$ DN and CD4$^+$ CD8$^+$ DP cells (Figure 4.15d), Results for DP cells shown previously in Figure 3.9, Section 3.1.2.5.

As discussed previously, no difference in the rate of progression from S to M phase was observed between wildtype and mutant at the DP stage and additionally, no difference was observed at the DN stage. Interestingly, however, the data shows that the rate at which BrdU$^+$ cells accumulate in a nocodazole block increases upon differentiation from the CD4$^-$ CD8$^-$ DN stage of development to the DP stage. This change in the rate of progression is apparent in both wildtype and mutant cells. In total, four biological replicates and eight technical replicates were performed and the general trend of the data was very consistently replicated.

In contrast, the CD4$^-$ CD8$^-$ DN stage of development does not reveal such rapid rates of progression from S to M phase. As shown previously, the DN cells do not display dramatic abnormalities (such as high levels of hyperdiploidy or large-scale reductions in cell numbers) as a consequence of the *Caph2$^{nes/nes}$* mutation *in vivo* (Figures 4.1c and 4.2). Mutant DN T cells cultured *ex vivo* also do not display dramatic increases in levels of hyperdiploidy in comparison to wildtype (0.55% ± 0.2 DN wildtype cells are hyperdiploid versus 0.78% ± 0.1 DN mutant. Figures are based on three biological replicates).

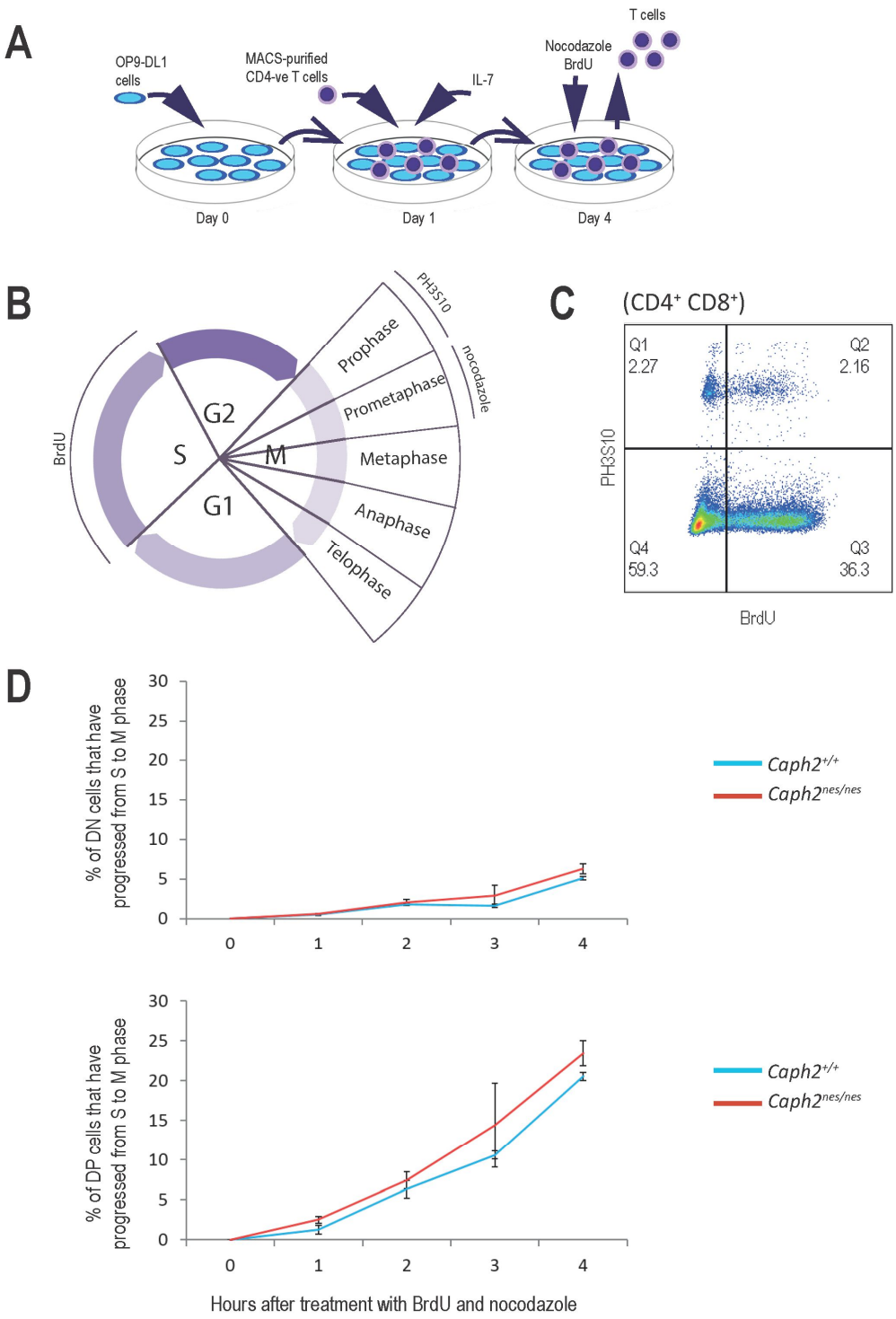

Figure 4.15

CD4⁺ CD8⁺ DP cells progress more rapidly from S to M phase in comparison to CD4⁻ CD8⁻ DN cells

A. Schematic of ex-vivo T cell culture protocol. **B.** Schematic of relevant time points. **C.** Representative image of flow cytometry dot plot showing PH3S10 and BrdU expression of CD4⁺ CD8⁺ cells. **D.** Line-graph showing the rate of progression of CD4⁻ CD8⁻ DN cells (top) and CD4⁺ CD8⁺ DP (bottom) from S to M phase. The rate of progression of CD4⁺ CD8⁺ cells is more rapid in comparison to CD4⁻ CD8⁻ cells. Values have been set to zero at the zero hour time point.

Error bars represent standard error of the mean, calculated based on two technical replicates. The experiment was repeated with three biological and six technical replicates. The general trend of the data was very consistent between replicates.

This result may provide a potential explanation for why the DP blast T cells are specifically affected by the condensin II deficiency. If the speed at which cells progress from S to M phase is particularly fast at this stage of differentiation compared to others, this could influence the workload for condensins. For example, rapid replication fork progression could lead to more catenations that require removal, and/or a reduced window of time for the removal to take place.

If the accelerated rate of progression from S phase to M phase observed as DN thymocytes differentiate to the DP stage is linked to the vulnerability of DP cells to *Caph2* mutation, the rate at which $BrdU^+$ cells accumulate in nocodazole block should be more rapid than in other cell types that are able to maintain ploidy in $Caph2^{nes/nes}$ mice. I therefore proceeded to analyse the rates of progression of cell types that were not obviously affected by the $Caph2^{nes/nes}$ mutation.

4.2.6.2 Measuring the rate of progression of $Caph2^{+/+}$ B cells and MEFs from S to M phase

The rate of progression of IGM^- (Fractions A, B, C and D) and IGM^+ (Fractions E and F) B cells from S phase to M phase was determined in a similar way as described for T cells. I MACS purified IGM^- $B220^+$ wildtype B cells and added the cells to an OP9 monolayer. The OP9 cell line supports the differentiation of B cells in the presence of IL-7. The cells were cultured in the presence of IL-7 and Flt-3 for four days until they were judged to be proliferating rapidly. I then treated the cells with nocodazole and BrdU over a four-hour time course, as described for the T cells.

The B cells were removed from the monolayer, treated with fluorescently conjugated antibodies to IGM, BrdU and PH3S10, and analysed by flow cytometry. The data was analysed in the same way as for T cells. The results indicate that both B cell populations (IGM^- and IGM^+) progress from S to M phase at a slower rate in comparison to DP T cells, but more rapidly than T cells at the DN stage (Figure 4.16).

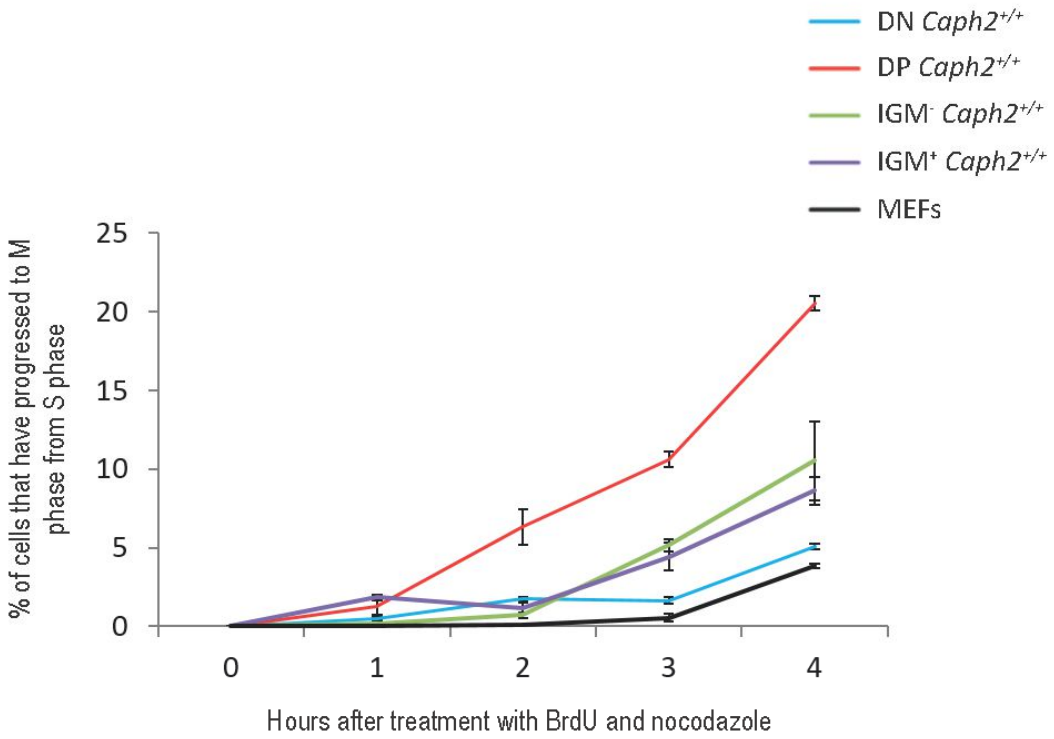

Figure 4.16
$CD4^+$ $CD8^+$ DP T cells progress more rapidly from S to M phase in comparison to DN T cells, IGM^- and IGM^+ B cells and MEFs
Line-graph showing the rate of progression of various cell types from S to M phase. The data indicates that the $CD4^+$ $CD8^+$ DP population is the outlier of all the cell types analysed, since these cells progress from S to M phase considerably more rapidly than any other cell type analysed.
Values have been artificially set to zero at the zero hour time point.
Error bars represent the standard error of the mean and were calculated based on two technical replicates. The experiment was repeated with four biological and eight technical replicates for T cells, three biological and six technical replicates for B cells, and two biological and 4 technical replicates for MEFs. The general trend of the data was very consistent between replicates.

In order to confirm that the difference in the rates of progression between cell types was not due to differences in the reagents used, T cell cultures were prepared simultaneously with B cell cultures, treated with the same media and reagents, and processed as before (Section 4.2.6.1). The results of this experiment were consistent with data obtained from previous T cell experiments, indicating that the reagents used did not impact the rate of progression of the cells from S to M phase.

To determine the relative rates of progression from S to M phase between cell types the data is normalised to the proportion of cells in S phase at each time point. This is to ensure that differing frequencies of proliferating cells do not affect the results: for example, a higher proportion of S phase cells in one lineage compared to another would result in an increased proportion of cells progressing from S to M phase if the data were not normalised.

The proportion of $BrdU^+$ cells were calculated for all cell type at each of the time points measured (Figure 4.17). In fact, DP T cells do not reveal higher frequencies of proliferating cells compared to many of the other cell lineages, as judged by BrdU incorporation. The results indicate that the extent of proliferation is highest in the IGM^- B cells, i.e. the IGM^- B cells are comprised of the highest proportion of S phase cells. This confirms that the rapid progression of DP T cells from S to M phase is not a consequence of an increased proportion of DP T cells in S phase, but more likely reflects a genuine increase in the speed at which DP T cells progress through S phase and G2 and into mitosis. This indicates that BrdU incorporation alone is a poor indicator of the rate of progression through the cell cycle: only the DP 71^+ cells show high levels of BrdU incorporation (Figure 4.1b), however the DP 71^+ cells make up a very small proportion of the total DP stage (Figure 4.1d). The majority of DP cells do not reveal high levels of S phase cells.

Having established that DP T cells progress more quickly from S to M phase relative to DN T cells and IGM^- and IGM^+ B cells, I next investigated the rate of progression of MEFs. Data described previously revealed that the *Caph2*$^{nes/nes}$ MEFs do not exhibit drastically higher levels of aneuploidy in comparison to wildtype MEFs (Figures 4.13a and 4.13b). Therefore, a slower rate of progression into M phase from S phase in comparison to DP T cells would provide further evidence that, of all the cell types

analysed, the DP T cells are unique both in the proportion of cells with abnormal ploidy, and in their rate of progression through certain stages of the cell cycle.

Wildtype CD1 MEFs were cultured until judged to be proliferating rapidly. The cells were then treated with BrdU and nocodazole in the same way as described for T and B cells. The MEFs were trypsinized to dissociate, neutralised with media, before being fixed and incubated with fluorescently conjugated antibodies to BrdU and PH3S10, as described for T and B cells. The cells were analysed on the flow cytometer.

The results revealed that very few cells progressed to S phase from M phase: by the four hour time point approximately 4% of MEFs had reached M phase from S phase (Figure 4.16). This result indicates that the MEFs progress very slowly from S to M phase in comparison to the $CD4^+$ $CD8^+$ DP T cells. The experiment was repeated for two biological replicates, each with two technical replicates, and the general trend of the data was very consistent between replicates.

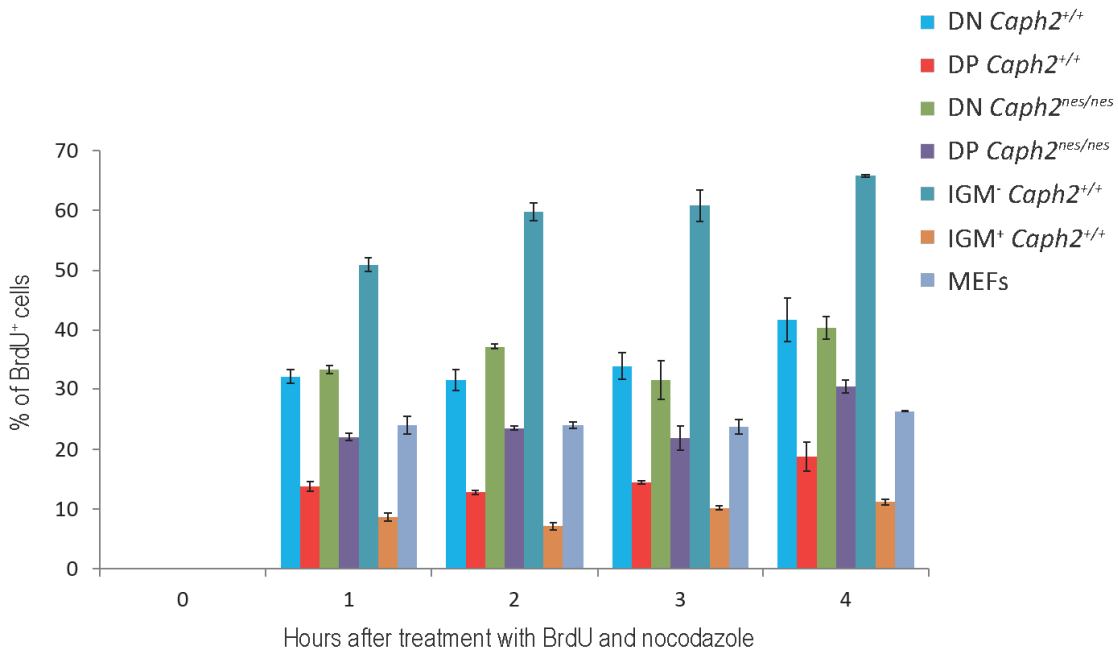

Figure 4.17
***Ex-vivo* IGM$^-$ B cells reveal the highest frequency of proliferating cells of all cell types analysed, as judged by BrdU incorporation**
Histogram showing the percentage of $BrdU^+$ cells for each of the cell types analysed. Values have been artificially set to zero at the zero hour time point.
Error bars represent the standard error of the mean and were calculated based on two technical replicates. The experiment was repeated with four biological and eight technical replicates for T cells, and two biological and four technical replicates for B cells. The general trend of the data was very consistent between replicates.

4.3 Discussion

The results described in this Chapter reveal that the consequences of the *Caph2*$^{nes/nes}$ mutation vary between cell types. The *Caph2*$^{nes/nes}$ T cells show increased levels of hyperdiploidy at the DP blast stage of differentiation, as well as an increase in the proportion of tetraploid arrested cells at the DP resting stage. Experiments carried out on cultured primary T cells described in Chapter 3 suggest that this arrested tetraploid population most likely arises due to mitotic slippage, rather than a G2 delay resulting in mitotic skip (Figure 3.9).

Erythroid cells from nessy mice do not undergo drastic reductions in cell number (Figure 4.6d) despite an increase in the levels of hyperdiploid mutant cells (Figure 4.6c). In addition, in contrast to the T cells, there is no increase in the fraction of large, BrdU^{-}, mutant erythroid cells (Figure 4.8). These data indicates that although erythroid cells also undergo abnormal chromosome segregation, unlike in T cells, this does not result in reduced cell numbers or obvious cell cycle arrest. Analysis of the myeloid progenitor population reveals higher numbers of mutant cells relative to wildtype (Figure 4.11b). This may suggest the existence of an autoregulatory feedback loop during erythroid development, which could explain the apparent lack of mutant cell number reductions in the erythroid lineage at later stages. There is other evidence to suggest that erythroid cells are subject to signalling networks that act to maintain homeostasis. For example, erythropoietin is produced in response to hypoxia, thereby stimulating increased erythropoiesis. In addition, computer modelling has identified a negative autoregulatory network motif, mediated by the death receptor FAS, and its ligand. This mechanism is activated when Ter119^{+} erythroid cell numbers reach a sufficient number, and acts to reduce proliferation at the preceding Ter119^{-}CD71^{+} stage, thereby maintaining homeostasis (Socolovsky *et al*., 2007). Interestingly, no substantial increase in the number of mutant lymphoid progenitor cells was observed relative to wildtype (Figure 4.11b).

As discussed previously, the consequences of abnormal ploidy may be less deleterious in erythroid cells relative to lymphocytes, since they undergo enucleation during development. It will be of interest to characterise the stress response signalling pathways that are activated in different primary haematopoietic cells containing

abnormal ploidy following mitotic errors. In other work carried out in the Wood lab, it has been shown that mutation of P53 partially rescues the block in T cell differentiation in *Caph2*$^{nes/nes}$ mice, and also drastically accelerates the T cell lymphoma phenotype, while having no detectable effect in the erythroid lineage. It is notable that P53 mutant mice, which are wildtype for *Caph2,* also develop T cell lymphomas originating from the DP blast stage, more rapidly than any other tumour type (Donehower, Harvey, & Slagle, 1992; Jacks *et al*., 1994). These tumours are highly aneuploid, providing independent evidence that the DP blast stage is vulnerable to cell cycle-related stress.

Finally, no difference in the levels of hyperdiploid cells was observed between wildtype and mutant for either the B cells or the cultured MEFs. Therefore, it is possible that the widespread use of MEFs to characterise cellular phenotypes in mouse models of CIN may miss important information if other cell types are not also analysed. As well as revealing no increase in the levels of hyperdiploidy, *Caph2*$^{nes/nes}$ B cells also exhibited no reduction in cell numbers. This result is particularly surprising, given the similarly high frequency of proliferating cells at specific stages of B cell and T cell differentiation (as judged by BrdU incorporation: Figures 4.1b and 4.9b). Therefore, the reason for the T cell specific phenotype cannot simply be that more stress is put on the replication machinery in T cells due to an increased frequency of cycling cells.

Transcriptome data from more than 150 different types of immune cell stages described previously (Section 4.2.6) implies that the cellular requirements for condensin complexes are particularly acute at this stage of haematopoietic development, resulting in more extreme consequences for the DP 71^{+} blast cells when CAP-H2 is depleted. This led me to investigate the possibility that certain cell types, such as DP T cells, undergo rapid rates of progression at specific cell cycle stages, in comparison to other cell types.

BrdU experiments described in this Chapter were used to assess the extent of proliferation at various stages of differentiation. However, these experiments provide a momentary "snapshot" of the proportion of cells in S phase at any given time, rather than information about the rate of progression of cells through different stages of the

cell cycle. In fact, time course experiments on cultured primary cells revealed that DP T cells undergo more rapid progression from S to M phase in comparison to B cells, DN stage T cells and MEFs. That is, the DP T cells undergo faster progression from S to M phase in comparison with cells that do not show altered ploidy profiles as a consequence of the *Caph2*$^{nes/nes}$ mutation (Figure 4.16).

Proteinaceous links and DNA intertwines are formed between sister chromatids during DNA replication (Michaelis, Ciosk, & Nasmyth, 1997; Sundin & Varshavsky, 1980) and must be resolved before cell division in order for correct chromosomes segregation to take place. Work carried out by Liang *et al*. suggests that some inter-chromatid links persist until late prophase, when removal of these links results in a conformational change in chromosome structure (Liang *et al*., 2015). However, most topological links between strands are removed during replication by topoisomerase II, as shown in *S. cerevisiae* (Charbin *et al*., 2014) and *Xenopus* (Lucas, Germe, Chevrier-Miller, & Hyrien, 2001).

Increased rates of progression from S to M phase could result in faster replication fork progression, increased frequencies of fork collisions and an increased pressure on the replication machinery to quickly relax the accumulation of positive supercoils and sister chromatid catenations that arise due to the progression of the replication fork. Faster progression may therefore result in an increased incidence of sister chromatid catenations. In addition to this, the time taken to resolve the catenations is reduced due to faster progression into mitosis. Together, this might result in the persistence of a higher frequency of unresolved catenations between sister chromatids, at the point of entry into M phase.

Therefore, the cell cycle stage at which T cells progress most rapidly in comparison to other cell types occurs between replication and cell division, when condensins are required to resolve sister catenations and restructure chromosomes (Jonathan Baxter & Aragón, 2012). This data may therefore begin to explain why the DP T cells, specifically, suffer severe consequences in cell division as a consequence of condensin II deficiency. However, this data does not indicate whether the increased rate of progression is due to a shorter S phase, or more rapid progression through G2. More rapid S phase progression may indicate that the abnormal cell division likely arises

due to increased formation of sister-chromatid catenations. In contrast, more rapid G2 would favour the hypothesis that abnormal chromosome segregation arises due to insufficient time to resolve catenations.

To distinguish between these two possibilities, experiments could be carried out to infer whether DP cells progress more rapidly than other cell types from G2 to M. This would be determined by calculating the percentage of $BrdU^-$ $PH3S10^+$ cells at one-hour time points up to, and including, 4 hours. This represents the proportion of cells that have progressed to M phase from G2. Because S phase is thought to take at least 4 hours in post-embryonic mammalian cells (Cooper & Hausman, 2007), $BrdU^-$ $PH3S10^+$ cells must have been in G2, or early M phase at the start of the experiment. The data would then be normalised to the percentage of G2/M cells at time point zero, to control for different frequencies of cells that start in G2 at time point zero between cell types. The proportion of G2 cells would be calculated by labelling the cells with relevant cell surface antibodies as well as antibodies to PH3S10 and finally, the cells would be DAPI-stained. Slower DP T cell progression from G2 to M in comparison to other cell types would indicate that these cells progress more rapidly through S phase, rather than through G2 to M.

Perhaps a more direct method of assessing rate of progression through S phase would be to carry out a double labelling experiment – injecting a mouse first with a thymidine analogue (e.g. BrdU) followed by a second analogue (e.g. EdU) ninety minutes later. The mouse would be culled after a further thirty minutes. A single cell suspension of the T and B cells would be obtained, and labelled with cell surface antibodies to determine the stage of development, as well as antibodies to each of the thymidine analogues. Assuming that the proportion of cells leaving S phase remains constant (and equally, the proportion entering S phase is constant), then the total length of the cell cycle can be calculated by dividing the time period between the first and second injections by the fraction of cells leaving S phase (which can be determined by the proportion of cells that are $BrdU^+$ and EdU^-). Secondly, assuming that the proportion of cells in S phase is constant at any given time, then the length of S phase can be calculated by multiplying the total length of the cell cycle by the fraction of cells in S phase (i.e. cells that are $BrdU^+$ EdU^+). These concepts are illustrated in Figure 4.18.

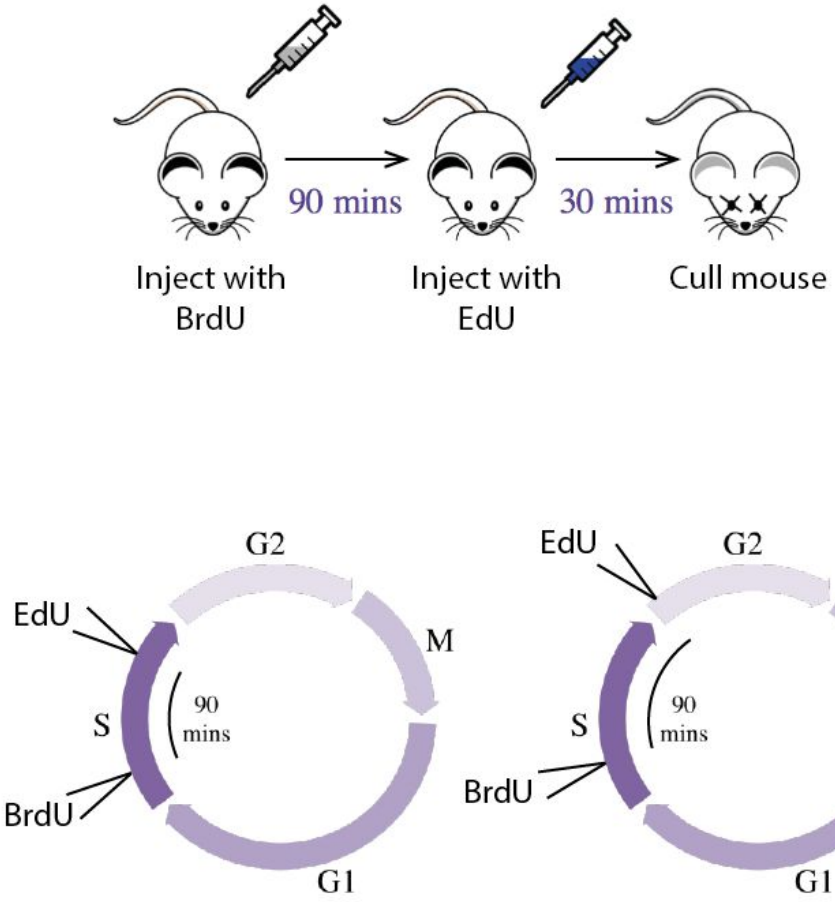

Figure 4.18
Schematic illustrating double labelling experiment to determine length of S phase
A mouse is injected with a thymidine analogue (BrdU) followed by a second analogue after 90 minutes. Cells are treated with fluorescently conjugated antibodies to the two analogues, and cells that have been in S phase for the full 90 minutes are positive for both BrdU and EdU. $BrdU^+$ EdU^- cells have exited S phase within the time frame (similarly, $BrdU^-$ EdU^+ have entered S phase within the same time frame).

Work carried out by Rudner *et al.* in *B. subtilis*, revealed that inactivation of the SMC condensin subunit results in an inability to separate origins of replication during mitosis. In addition, topoisomerase IV inactivation (known to be involved in sister chromatid decatenations) results in an inability to separate sister chromatid arms. Surprisingly, however, topoisomerase IV inactivation had no effect on the separation of origins of replication (Wang *et al*., 2014). This may suggest that, in bacteria at least, the inability of chromatids to separate their origins of replication is not caused by persistent DNA intertwining. Alternatively, fast replication may result in the production of large swathes of DNA in close proximity to its sister DNA. This could increase the likelihood of stable bridges forming between sisters by nucleoid-associated proteins. The role of the condensin II complex may be to rapidly condense newly synthesised DNA away from its sister DNA, thereby limiting the potential for the formation of linkages between the sisters (Gruber *et al*., 2014). This mechanism might not be relevant in higher eukaryotes, where replication and condensation do not occur concomitantly, however, some work on HeLa cells indicates that condensin mediated chromosome individualisation may begin as early as S phase (Ono *et al*., 2013). If this is the case, it is possible that individualisation of sister chromatids during S phase could inhibit the formation of inter-chromatid linkages by contracting sister chromatids away from one another.

However, investigations into the process of decatenation of circular chromosomes in budding yeast found that depletion of condensin subunits did not result in an increase in the accumulation of catenanes, but instead resulted in slower resolution, with approximately 15% of catenations persisting through mitosis into G1 (Charbin *et al*., 2014). This may reflect differences between prokaryotes and eukaryotes since it conflicts with the hypothesis that condensin is involved in the prevention of link formation between sister chromatids, rather than their resolution in *B. subtilis*. Importantly, however, these experiments indicate that condensin promotes catenane removal in eukaryotes, rather than inhibiting the introduction of linkages.

Given that the majority of sister chromatid catenations are resolved quickly by topoisomerase II (Charbin *et al*., 2014; Lucas *et al*., 2001; Wang, 2002), the discovery that a subset of the catenanes persist late into the cell cycle and can only be resolved in the presence of condensin led to the hypothesis that DNA replication may result in

two different types of catenations. Easily resolved catenations are separated quickly by topoisomerase II alone, whereas more complex topological linkages between sister chromosomes require condensin activity (Charbin *et al*., 2014). If this is the case, it could be that certain properties of the DNA sequence at the origin of replication in *B. subtilis* results in complex, or "knotty" sister catenations during replication, which cannot be fully resolved in the absence of condensin. Interestingly, SMC is recruited to parS sequences that cluster near the origin of replication (Minnen, Attaiech, Thon, Gruber, & Veening, 2011; N. L. Sullivan, Marquis, & Rudner, 2009), which may indicate that condensin is particularly necessary at the origin, perhaps to resolve topologically complex catenations.

Similarly, fast S phase progression could result in a higher incidence of this type of catenations, which would explain the increased requirement of condensin at the DP stage of T cell development, when S phase progression is most rapid. This hypothesis, however, is very difficult to test, given the lack of tools available to detect catenations on linear chromosomes.

Reduced replication fork velocity rescues the condensin deficient phenotype in *B. subtilis* (Gruber *et al*., 2014), implying that some aspect of fast fork progression results in an increased necessity for condensin activity in *B. subtilis*. Further work must be carried out to investigate whether the observed rapid rate of progression from S to M phase in T cells results in an increased replication fork velocity relative to other lineages. Alternatively, it could be that the $CD4^+$ $CD8^+$ DP T cells licence more origins of replication during S phase. More replication forks covering the same distance would not need to travel as quickly, resulting in fewer opportunities for the formation of sister chromatid bridges. Experiments designed to artificially reduce the rate of replication fork progression (such as treatment with hydroxurea, HU) would indicate whether slower replication fork progression at the DP stage of T cell development would result in fewer *Caph2*$^{nes/nes}$ cells with abnormal DNA content. Additionally, replication fork velocity and number of fired origins could be determined using DNA combing (Herrick & Bensimon, 1999; Michalet *et al*., 1997). This involves pulse-labelling cells with two different thymidine analogues sequentially (e.g. IdU followed by CIdU), which would be incorporated into newly replicated DNA. The long DNA strands are stretched out onto a glass slide after cell lysis and each of the thymidine analogues

detected with fluorescently conjugated antibodies. DNA replication tracts are identified by the presence of adjacent thymidine signals under fluorescence microscopy. The number of fired origins is inferred from the proportion of IdU signals (i.e. the newly synthesised DNA adjacent to the origin). The rate of progression of the fork would be calculated by dividing the length of the first signal (IdU) by the period of time between pulses (IdU treatment followed by CIdU). The concepts of fibre spreading are illustrated schematically in Figure 4.19 (Merrick, Jackson, & Diffley, 2004).

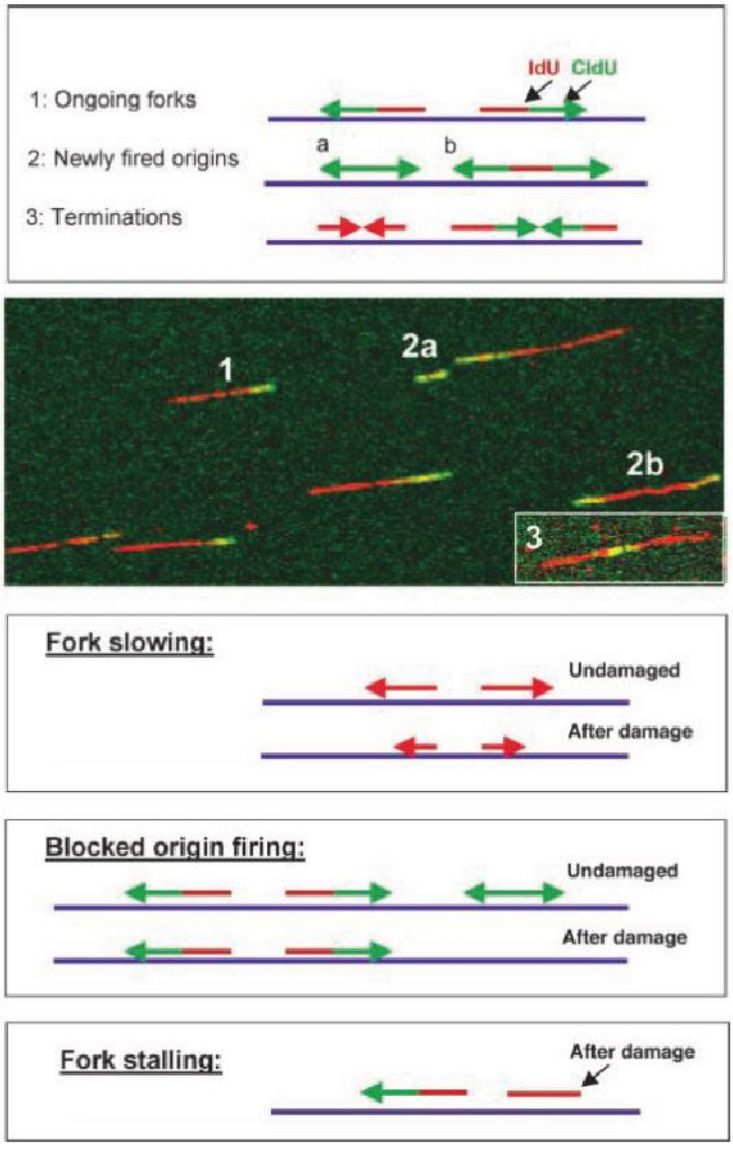

Merrick et al., 2004

Figure 4.19
Visualization of replication fork kinetics using DNA fibre spreading

Double labelling by e.g. IdU and CldU to determine replication fork velocity and number of fired origins (Merrick *et al.*, 2004).

CHAPTER 5: PRELIMINARY INVESTIGATION INTO THE BIOCHEMICAL PROPERTIES OF THE CONDENSIN COMPLEXES

5.1 Introduction

The condensins belong to a family of SMC proteins, which also includes cohesin and SMC5/6. Eukaryotes possess condensin I and condensin II, which share the same heterodimer of SMC proteins, a kleisin subunit, and different accessory subunits (Nasmyth & Haering, 2005). The structure and function of condensin I is well conserved from yeast to humans, although some organisms lack condensin II. Prokaryotes also possess condensin-like complexes, which are involved in the organisation of chromosome structure.

The dramatic process of restructuring interphase chromatin into mitotic chromosome structures is a poorly understood process, due to the difficulty in removing chromosomes whilst maintaining the structure and interactions that are present *in vivo*. Topoisomerase II could be removed from the chromatin by washing with weak salt solutions, whereas the remaining two proteins could not (Hirano & Mitchison, 1993). Immunodepletion of SMC4 was shown to prevent chromosome condensation and the formation of mitotic chromosomes, confirming its importance in mitotic chromosome assembly (Hirano & Mitchison, 1994).

Affinity purification experiments using an antibody to SMC4 confirmed the presence of additional proteins that associate with the SMC2 and SMC4 proteins. These proteins are now known to be the condensin I non-SMC proteins CAP-G, CAP-D2 and CAP-H (also known as kleisin gamma). The affinity-purified sample was run on a sucrose gradient and assayed via immunoblot with antibodies to SMC2, SMC4 and the associated subunits. The researchers found that the SMC proteins and non-SMC subunits form a complex with a sedimentation coefficient of 13S, whereas the SMC proteins, without additional subunits, form a complex that sediments at 8S (Hirano, Kobayashi, & Hirano, 1997). Further experiments have confirmed that the condensin II complex (SMC2, SMC4, CAP-G2, CAP-D3 and kleisin beta/CAP-H2) approximately co-sediments with condensin I at 13S (Figure 5.1a) (Ono *et al*., 2003).

Cohesin and condensin are both known to form tripartite ring-like structures: the SMC proteins form anti-parallel coiled coils (Melby, Ciampaglio, Briscoe, & Erickson, 1998), connected to each other by a dimerization domain which forms a V-structure (Figure 1.5). The carboxy and amino termini of the kleisin protein bridge the opposing SMC head domains, which closes the ring. Cross-linking experiments have shown that the N-terminal of the kleisin protein in cohesin (Scc1/Rad21) binds to the coiled coil of SMC3, while the C-terminal of the kleisin interacts with SMC1 head domain (Gligoris *et al*., 2014). It has been suggested that this ring structure allows the cohesin complex to entrap sister DNA strands (Gligoris *et al*., 2014; Gruber *et al*., 2003) by the formation of both intra- and inter-chromosomal topological links. Given the structural similarity between condensin and cohesin, condensin could act to restructure chromatin in a similar way: by topologically encircling the DNA strand and introducing intra-chromosomal links by binding to another segment within the same strand, (as shown in Figure 5.1b, left), or by encircling both segments (Figure 5.1b, right) (Cuylen *et al*., 2011). Alternatively, condensin may compact chromatin by introducing right-handed supercoils, as discussed previously (Chapter 1 Section 1.2.4, Chapter 4 Section 4.3).

In this chapter, I set out to further characterise the biochemical properties of the condensin complexes in order to better understand their roles in reorganising chromatin structure and promoting accurate cell division. Specifically, I was interested in comparing the biochemical features of condensins between the primary haematopoietic cell types analysed in Chapter 4, in order to determine whether condensin complexes have any unique properties in T cells, compared to other haematopoietic lineages.

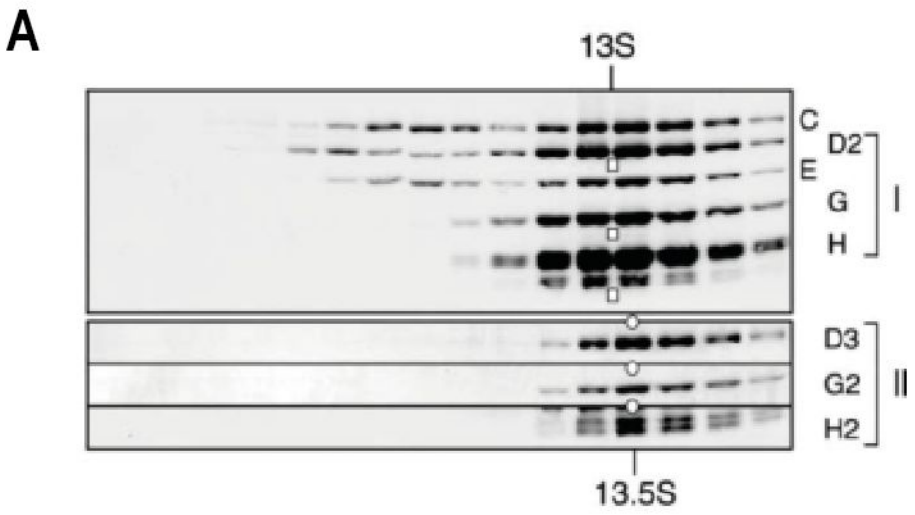

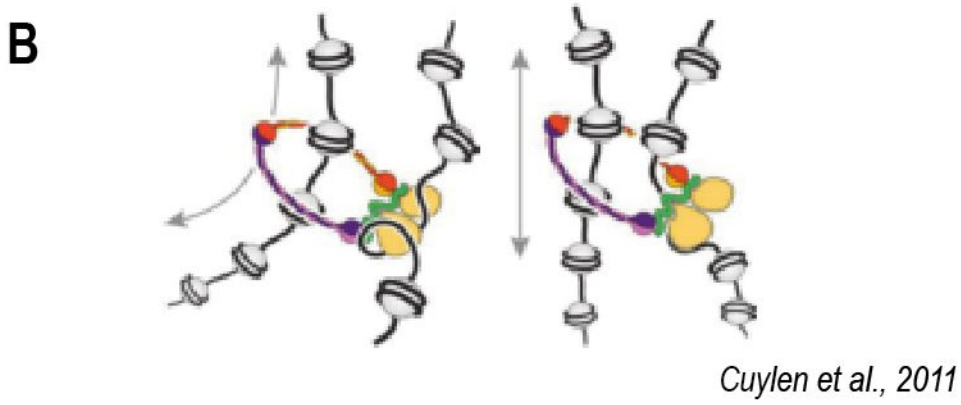

Figure 5.1
Analysis of the biochemical properties of condensin
A. HeLa cell nuclear extract was run on a 5%-20% sucrose gradient and centrifuged for 15 hours at 36,000 rpm. Fractions were analyzed by immunoblotting (Ono *et al.*, 2003). **B.** Schematic representation of two proposed models of chromatin condensation by condensin. Two segments of a DNA strand may by linked by condensin encircling one segment and binding to the other (left), or condensin may encircle both segments (right) (Cuylen *et al.* 2011).

5.2 Results

5.2.1 Expression of Caph2 mRNA

First, I measured *Caph2* mRNA abundance in three hematopoietic lineages (T, B and erythroid) by quantitative PCR on cDNA generated from MACS-purified $B220^+$ B cells, $Ter119^+$ erythroid cells and $CD4^+$ T cells, as described in Materials and Methods: Section 2.2.2.5. Actin primers were used as a reference to determine ΔCt values and transcript levels were normalized to $CD4^+$ T cell expression. The results indicate that the relative abundance of the *Caph2* mRNA is reasonably consistent between cell types (there is a less than 1.6-fold difference between cell types), with slightly increased expression in the erythroid cells, although more replicates would be required to determine whether this difference is significant (Figure 5.2).

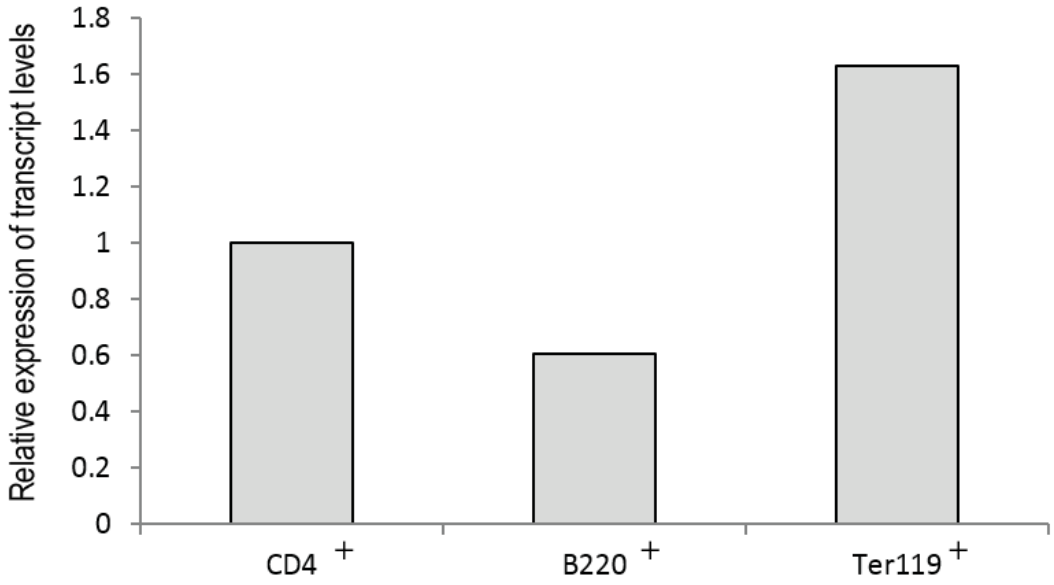

Figure 5.2
Analysis of the relative abundance of *Caph2* transcript by qPCR shows only small differences between cell types
Histogram showing the relative abundance of *Caph2* in MACS-purified $CD4^+$, $B220^+$ and $Ter119^+$ cells. Quantitative PCR was performed on cDNA generated from each of these cell types. Actin primers were used to determine ΔCt values. Transcript levels were normalized to $CD4^+$ T cell expression. More biological replicates are necessary to calculate error bars.

5.2.2 Caph2 mRNA splice variants between cell types

Six possible isoforms of CAP-H2 have been reported, arising due to three methods of alternative splicing in the mouse *Caph2* gene: a long or a short 3'-UTR, a NAGNAG variation at the 5' end of exon 16, and alternative exon 1 isoforms. Three splice variants of the first exon of the condensin II subunit *Caph2* were identified using expressed sequence tag (EST) data: a long form of exon 1 (the exon is not truncated), an intermediate form (the last 17 base pairs are lost) and a short form (lacking the last 93 base pairs). These exon 1 variants were potentially of relevance to the $Caph2^{nes/nes}$ phenotype, because the single nucleotide substitution causes distinct missense mutations in the long and intermediate isoforms, but lies within an intron of the short isoform.

The *Caph2* reading frame is conserved in both the long and short isoforms, but a truncated protein would result from the intermediate isoform if the same start codon is used. Alternatively, the intermediate isoform could give rise to a protein with a different amino acid sequence from exon 1, but identical to exon 2 onwards if an alternative downstream start codon was used (Figure 5.3a).

Since EST data represents transcribed mRNA, it seemed likely that these splice variants were real, and produced transcripts. This was confirmed by RT-PCR on RNA from different mouse tissues. Given the developmental defect evident in $Caph2^{nes/nes}$ thymocytes, the researchers (Theodoratos, Wilson, Gosling, & Fahrer, 2012) investigated the possibility that the exon 1 splice variants may be differentially expressed across different stages of T cell differentiation (DN, DP, CD4 SP and CD8 SP). Although differences were observed in the expression levels between cell types, the pattern of expression of each isoform remained consistent.

To test whether each of these transcripts can give rise to Caph2 protein, cDNA from each splice variant was cloned into a GFP fusion protein vector. Each splice variant produced GFP fusion protein, demonstrating that all three variants can produce stable protein (Theodoratos et al., 2012).

Previous studies into the $Caph2^{nes/nes}$ mutation revealed that the introduction of

wildtype *Caph2* expressing the long isoform of exon 1, was sufficient to rescue the *Caph2*$^{nes/nes}$ phenotype (Gosling *et al*., 2007). Moreover, the portion of Caph2 ORF that is unique to the long isoform is highly conserved between species, which is not the case for the intermediate isoform. This may suggest that the long isoform is predominant in T cells. This is supported by the EST data, which shows that the most abundant transcript is the long form.

Since the *Caph2*$^{nes/nes}$ mutation (a single nucleotide change within exon 1) is absent from the short isoform (Figure 5.3a) and does not result in the same amino acid change in the intermediate isoform (due to the alternative start codon), I investigated the possibility that different isoforms are preferentially expressed in different cell types. If, for example, the short or the intermediate isoforms are preferentially expressed in cell types that are apparently unaffected by the *Caph2*$^{nes/nes}$ mutation, such as B cells, then this would suggest a possible explanation for the apparent T cell specificity.

I carried out non-quantitative PCR experiments to directly compare the relative abundance of the long, intermediate and short isoforms between cDNA generated from MACS-purified B220^{+} B cells, Ter119^{+} Erythroid cells and CD4^{+} T cells, as well as mouse ES cells (Materials and Methods: Section 2.2.2.5). Information about the primers used is provided in Table 2.2. Comparisons were made by densitometry analysis using Quantity One 4.6.9 software (Bio Rad Ltd). The results revealed no substantial difference in the relative expression of the long isoform compared to the intermediate isoform between cell types (Figures 5.3b and 5.3c). The short isoform was not detected in any of the cell types. This result is consistent with the EST data described by Theodoratos *et al*, which estimates from the number of ESTs representing each splice variant that the short isoform is the least abundant (Theodoratos *et al*., 2012).

The data presented here suggests that the cause of the apparent resistance of certain cell types (such as B cells) to the *Caph2*$^{nes/nes}$ mutation is not a consequence of differential expression of splice isoforms of *Caph2*.

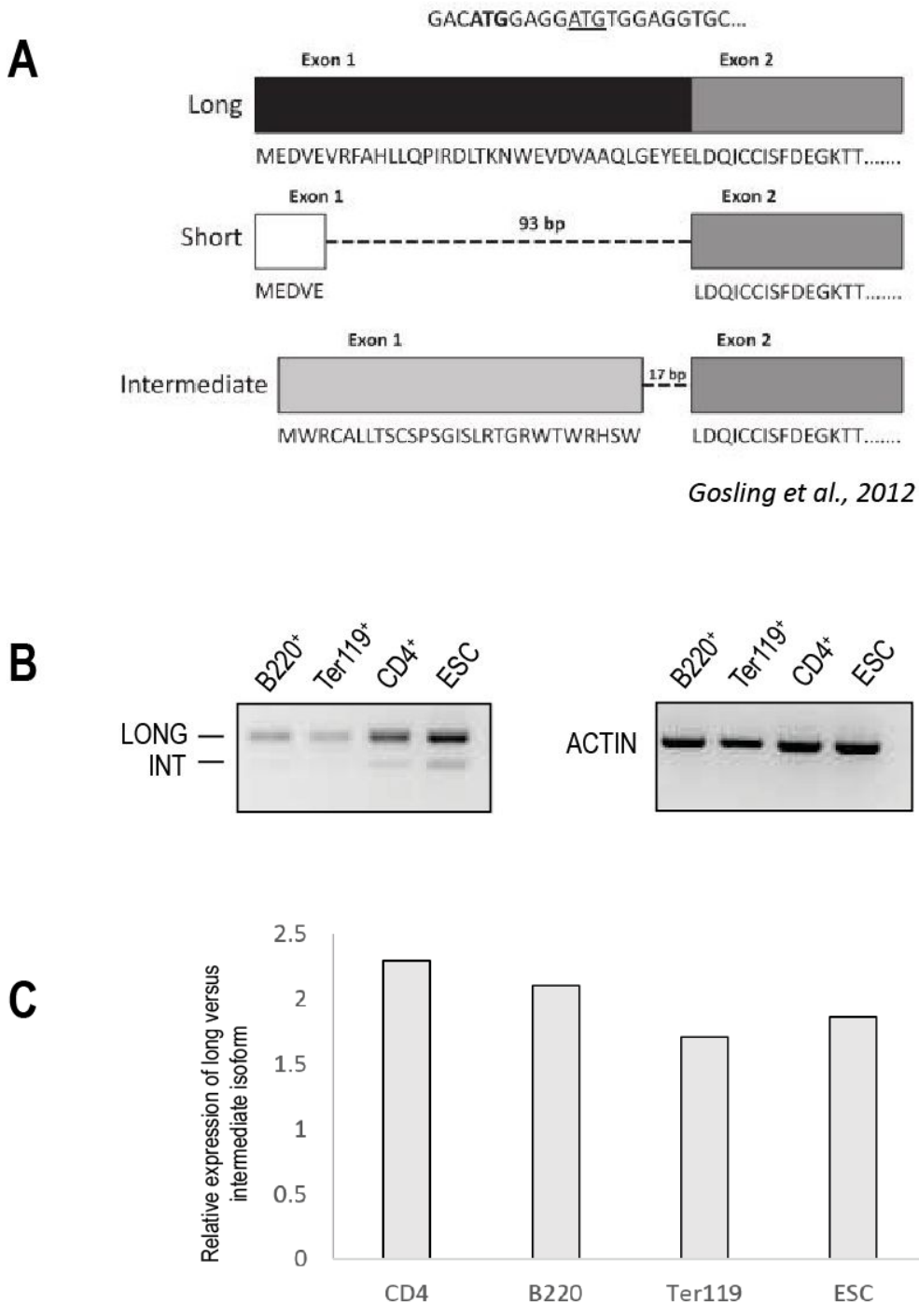

Figure 5.3
No difference in the relative expression of *Caph2* splice variants between cell types
A. Schematic representation of the three splice variants of *Caph2* and amino acid sequence encoded by exon 1 (Gosling et al., 2012). **B.** Non-quantitative PCR on MACS-purified B (B220), erythroid (Ter119) and T (CD4) cells. Actin primers were used as a loading control. Samples were run on a 2% agarose gel. **C.** Histogram showing the expression of the long isoform relative to the intermediate isoform in MACS-purified $CD4^+$, $B220^+$ and $Ter119^+$ cells, as well as mouse ES cells. Non quantitative PCR was performed on cDNA generated from each of these cell types. Data represents two biological replicates.

5.2.3 Expression of condensin subunits at the protein level

The relative abundance of condensin subunit proteins was analysed across three haematopoietic lineages. Cells obtained from the thymus and bone marrow were MACS-purified to obtain populations of $B220^+$ B cells, $Ter119^+$ Erythroid cells and $CD4^+$ T cells. The concentration of total protein in each sample was evaluated using the Bradford protein assay (Materials and Methods: Section 2.2.3.2). A total of 20µg of protein per sample was assayed via Western blot, and antibodies specific to SMC4, CAP-H2 and CAP-H (Table 2.5) were used to determine the relative levels of protein across the different cell types (Figure 5.4).

The relative abundance of SMC4 appeared to be fairly consistent across the three different cell types. However, although CAP-H2 and CAP-H were detected in $CD4^+$ T cells, they were not detected in either the $B220^+$ B cell or the $Ter119^+$ erythroid populations. It seems unlikely that the kleisin subunits are completely absent from the B- or erythroid cells, but rather that the protein levels of these condensin subunits are much lower in those cell populations in comparison to T cells.

These results appear to reveal stoichiometric imbalances in the expression of condensin subunits between cell types. SMC4 appears to be uniformly expressed, whereas the levels of the condensin subunits vary. Given that it was possible to detect the *Caph2* transcript in all three cell types analysed with an apparent increase in erythroid cells (Figure 5.2), difference in transcript abundance between cell types is not sufficient to explain the differences in the levels of CAP-H2 protein that are detected. Although it is difficult to compare the techniques of western blot and PCR, it could be that some post-transcriptional modification occurs in these cell types. This possibility is discussed in greater detail in Section 5.3. An alternative explanation could be that each of the cell types analysed are comprised of different frequencies of cells that are proliferating rapidly – condensin "accessory" subunits might be expected to be most abundant in proliferating cells (discussed in more detail in Section 5.3).

One further possible explanation of this apparent imbalance is that the non-SMC

condensin subunits form a non-canonical complex with proteins other than the SMC2 SMC4 heterodimer, specifically in T cells.

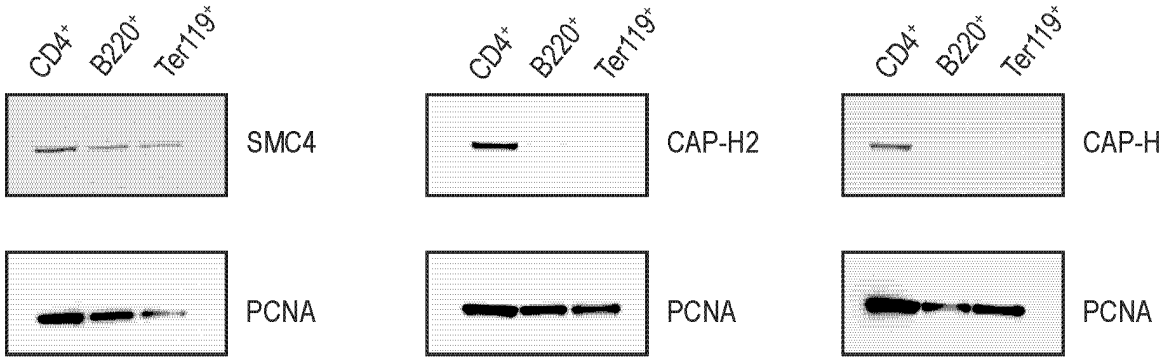

Figure 5.4
Analysis of the relative abundance of condensin subunit proteins reveals stoichiometric imbalances
Whole cell lysis followed by western blot showing levels of SMC4, CAP-H, CAP-H2 and PCNA (loading control) in MACS-purified $CD4^+$, $B220^+$ and $Ter119^+$ cells. Samples were run on a 4-12% Bis/Tris gel.

5.2.4 Sedimentation profiles of condensin subunits

Sucrose gradient experiments using HeLa cell extracts suggest that the condensin subunits (CAP-D2, CAP-D3, CAP-G, CAP-G2, CAP-H and CAP-H2) do not exist on their own, without forming a complex with the SMC2 SMC4 heterodimer proteins; i.e. the subunits are not present in any of the light fractions where SMC2 or SMC4 are absent (T Hirano *et al*., 1997; Keiji Kimura & Hirano, 1997; Ono *et al*., 2003). If this is also found to be the case in T cells, it would suggest that the increase in the levels of subunits relative to SMC4 in T cells (Figure 5.4) may be due to the CAP-H and CAP-H2 proteins forming stable complexes with other proteins, rather than there being an increase in the presence of kleisins as individual proteins. To test this hypothesis, I performed sucrose gradient experiments on whole thymus extracts to determine whether the CAP-H and CAP-H2 subunits could be detected in any fractions where SMC4 was absent.

A single cell suspension was made from a wildtype thymus, which is comprised primarily of $CD4^+$ $CD8^+$ $CD71^-$ thymocytes (approximately 80% of the wildtype thymus is comprised of $CD4^+$ $CD8^+$ DP thymocytes, of which 85-90% are $CD71^-$/non cycling). The cells were lysed and the lysate was added to a linear gradient of 5% - 20% sucrose. The samples were centrifuged overnight to separate proteins based on the molecular weight of the macromolecular complexes in which they reside (Materials and Methods: Section 2.2.6). The fractions were manually removed, and assayed via Western blot.

SMC4 is detected in almost every fraction, from approximately Fraction 6, onwards (Figure 5.5). The intensity of the signal is strongest from approximately Fraction 10 to Fraction 16. SMC4 has previously been shown to sediment in this way in HeLa cell extracts: it is absent from the very lightest fractions but is present in all remaining fractions, although the intensity of the signal diminishes following the 13S peak, Figure 5.1a (Ono *et al*., 2003).

CAP-H co-sediments with SMC4 (fractions 10 to 14) and is not present in any of the other fractions where SMC4 is absent (Figure 5.5, top). This is in agreement with the previously published data showing the fractionation patterns of CAP-H in HeLa cells

(Kimura & Hirano, 1997; Ono *et al*., 2003). These data suggest that CAP-H does not form a complex of different molecular weight to the complex it forms with SMC4.

CAP-H2 also co-sediments with SMC4 (Figure 5.5, bottom). However, unlike CAP-H, CAP-H2 is detected in the heaviest molecular weight fractions. In fact, the intensity of the CAP-H2 signal remains strong, even after the intensity of the SMC4 signal diminishes. Unfortunately, no information is provided about the number of fractions taken by Hirano *et al.* in their sucrose density sedimentation experiments with antibodies specific to condensin II subunits, Figure 5.1a (Ono *et al*., 2003). Therefore, no direct comparison can be made between the two experiments to determine whether the sedimentation profile seen in T cells is atypical. Experiments are ongoing to obtain sedimentation profiles for CAP-H2 in other primary cell types.

Although the sucrose gradient experiments described above do not provide conclusive proof that CAP-H2 forms a complex with a protein other than SMC4, it leaves open the possibility that this may be the case. Further experiments, including mass spectrometry following immunoprecipitation for *Caph2*, must be carried out to further investigate this result. If, indeed, it is the case that CAP-H2 forms a novel complex with non-SMC proteins specifically in T cells, it may be this second complex that is affected by the *Caph2*$^{nes/nes}$ mutation. For example, if the region of *Caph2* containing the I15 residue was more important for interactions with non-canonical condensin subunits than for canonical subunits, then the non-canonical interaction would be more severely affected. This would provide an explanation for the observed T cell specificity. However, the fact that the cellular phenotype in *Caph2*$^{nes/nes}$ T cells is consistent with perturbation to the canonical condensin II complex argues against this possibility, or at least suggests that any additional complex possesses related cellular functions.

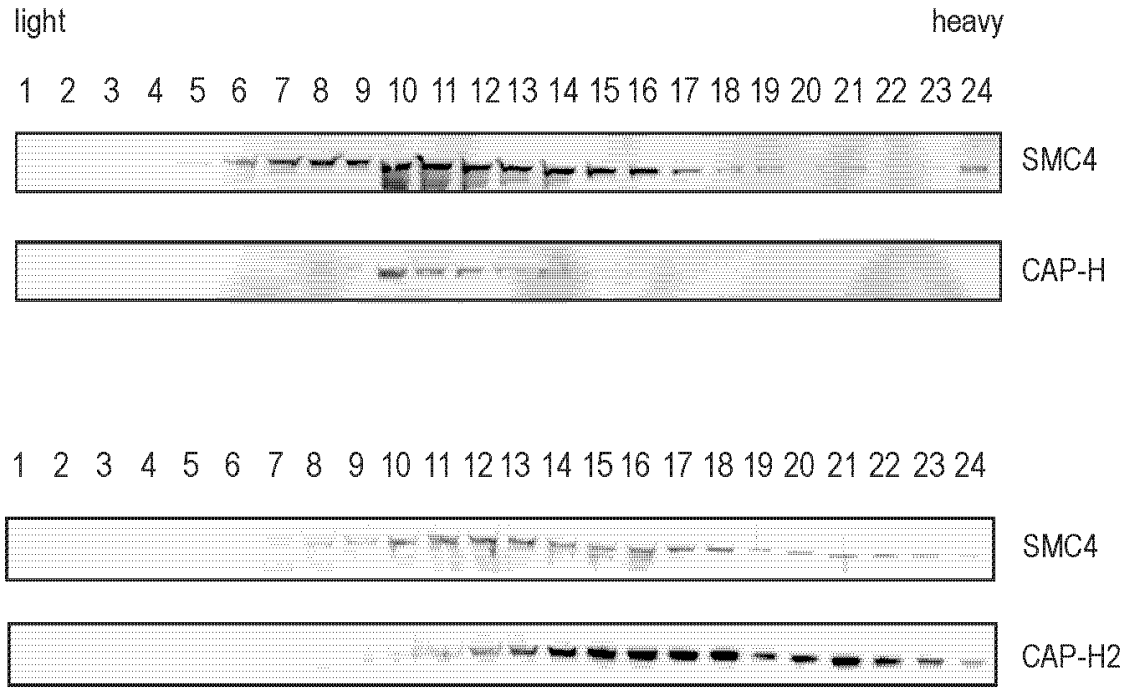

Figure 5.5
Sedimentation profiles of condensin subunits suggest CAP-H2 may form a non-canonical complex with non-SMC proteins
A single cell suspension was obtained from a wildtype thymus. The cells were lysed and loaded onto a 5 - 10% sucrose gradient. The gradients were centrifuged at 36,000 rpm for 15 hours. 24 samples were taken manually and run on a 4-12% Bis/Tris gel. Western blot shows sedimentation profiles of SMC4, CAP-H, CAP-H2. SMC4 is present from fractions 6 onwards, with the strongest intensity signal in Fractions 10-16. CAP-H is present in Fractions 10-14. In contrast, CAP-H2 is present from approximately Fraction 10-24, with the intensity of the signals remaining strong throughout.

5.3 Discussion

From the results described in this Chapter, several experimental avenues present themselves. There appear to be stoichiometric imbalances in the expression of condensin subunits as shown by western blot (Figure 5.4). Further analysis into the expression of condensin I subunits revealed further imbalances at the sub-cellular level (Taylor, unpublished data). CAP-H, a subunit of condensin I (which has been shown to gain access to the chromosomes only after breakdown of the nuclear membrane during prometaphase (Hirano, 2012; Ono *et al*., 2003) was detected in the nucleus of T cells and mES cells, specifically. In contrast, SMC4 was uniformly detected in the cytoplasm and nucleus across all cell types tested. Taken together, this data may suggest that condensin subunits form different complexes in different tissues.

The sedimentation profile of CAP-H2 does not exclude the possibility that it forms a complex with non-SMC proteins. The next step in this analysis is to perform immunoprecipitation (IP) experiments followed by mass spectrometry to determine whether CAP-H2 associates with proteins other than those in the canonical condensin II complex.

Further work must be carried out to determine whether the CAP-H2 sedimentation pattern is unique to T cells, by performing sucrose gradient experiments on bone marrow, HeLa cell and MEF extracts. If this non-canonical complex is found to be specific to T cells, then this could potentially explain the *Caph2*$^{nes/nes}$ cell type specific phenotype: i.e. if the CAP-H2 mutation specifically disrupts the function of the non-canonical complex. However, this seems unlikely since the results from the previous chapters suggest that the *Caph2*$^{nes/nes}$ mutation affects the well-known function of condensin in mitosis.

From the sedimentation pattern of CAP-H, it is unlikely that this subunit forms a complex with any proteins other than SMC2 and SMC4, since CAP-H co-sediments with SMC4, and is only detected in a small number of fractions. It could be that neither CAP-H nor CAP-H2 form complexes with proteins other than the SMC heterodimer. If this is the case, then the increase in the levels of CAP-H and CAP-H2 detected in T

cells compared to other cell lineages must have another explanation.

A survey of transcriptome data (Immgen) reveals that the expression of condensin I and condensin II subunit transcripts is highest at the DP CD71$^+$ blast stage of T cell development, in comparison with over 150 other immune cell subsets (Figure 4.14). The increase in the expression levels of *Caph* and *Caph2* (and other condensin subunits) at the DP 71$^+$ blast stage is evident when the data is viewed as a heatmap (Figure 5.6). This supports the hypothesis that condensin is required to a greater extent at the DP 71$^+$ blast stage of development, perhaps due to more rapid progression through S phase resulting in an increase in the number of catenations introduced between sister DNA strands (as discussed in Chapter 4, Section 4.3), although further work must be carried out to determine whether the increase in the abundance of condensin subunits at the DP71$^+$ stage is also true at the protein level. Interestingly, the Fraction C stage of B cell development also exhibits high levels of condensin subunit transcripts, although to a lesser extent than DP 71$^+$ blast T cells (Figures 4.14 and 5.6).

However, the increased levels of CAP-H and CAP-H2 proteins in CD4$^+$ thymocytes versus other cell types cannot simply be due to an increased requirement for condensins at the DP stage of T cell development, since if this were the case, higher levels of SMC4 would be detected in T cells in addition to the increase in expression of CAP-H and CAP-H2 (Figure 5.4). It is known that the levels of the cohesin kleisin Scc1 vary throughout the cell cycle (Uhlmann & Nasmyth, 1998) and a study into the structure of cohesin found that the kleisin subunit Scc1 is rate limiting for the formation of the cohesin complex (Mishra *et al*., 2010). Given the structural similarity of condensin and cohesin, it may be that CAP-H2 is the limiting factor in condensin II formation. Indeed, some evidence exists for CAP-H2 acting as the rate limiting subunit for holocomplex formation in Drosophila (Hartl, Smith, *et al*., 2008). Additionally, CAP-D2 is rate limiting to condensin I formation in Xenopus oocytes (Watrin, Cubizolles, Osborne, Le Guellec, & Legagneux, 2003).

The hypothesis that CAP-H2 is rate limiting to mammalian condensin II holocomplex formation is supported by transcriptome data, which shows that despite exhibiting the highest expression levels of condensin subunit transcripts at the DP 71$^+$ blast stage,

Caph2 transcripts are the least expressed of all the condensin subunits (Figure 5.6). If CAP-H2 is indeed the limiting factor, then stages of development that undergo very rapid progression from S to M phase (such as at the DP stage of T cell development), may require higher levels of CAP-H2, so that condensin II holocomplex formation can take place more readily.

The expression data reveals that *Caph* and *Caph2* transcript levels in Fraction C B cells are slightly lower, but in the same range as DP 71^+ blast T cells (Figure 5.6). This agrees with experiments described in this Chapter, which reveal similar transcript levels of *Caph2* in $B220^+$ B cells and $CD4^+$ T cells as determined by qPCR. The expression of *Caph2* in erythroid cells is slightly higher compared to the other two cell types, although more replicates are required to determine whether the difference is significant (Figure 5.2). In contrast, CAP-H and CAP-H2 protein levels are not detected in B cells or erythroid cells (Figure 5.4). This may imply that the kleisin subunits of both condensin complexes are regulated at the level of translation.

Using ribosome profiling, Stumpf *et al*. provided evidence for the widespread translational control of hundreds of mRNAs during the cell cycle (Stumpf, Moreno, Olshen, Taylor, & Ruggero, 2013). Ribosome profiling (Ribo-seq) uses deep sequencing of mRNA fragments in a process that is similar to RNA-seq. Unlike RNA-seq, however, this technique sequences only the ribosome-protected mRNA fragments. This provides information about the location of transcription start sites, as well as the rate of progression of the ribosome. In their study, Stumpf *et al*. reported cell cycle-dependent regulation of mRNAs involved in wide-ranging processes including metabolism, nuclear transport and DNA repair. Interestingly, ribosome occupancy of condensin and cohesin subunits is high during S and G2, and diminishes during mitosis. This result therefore confirms that cell cycle-dependent control of condensin does take place at the translational level (Stumpf *et al*., 2013).

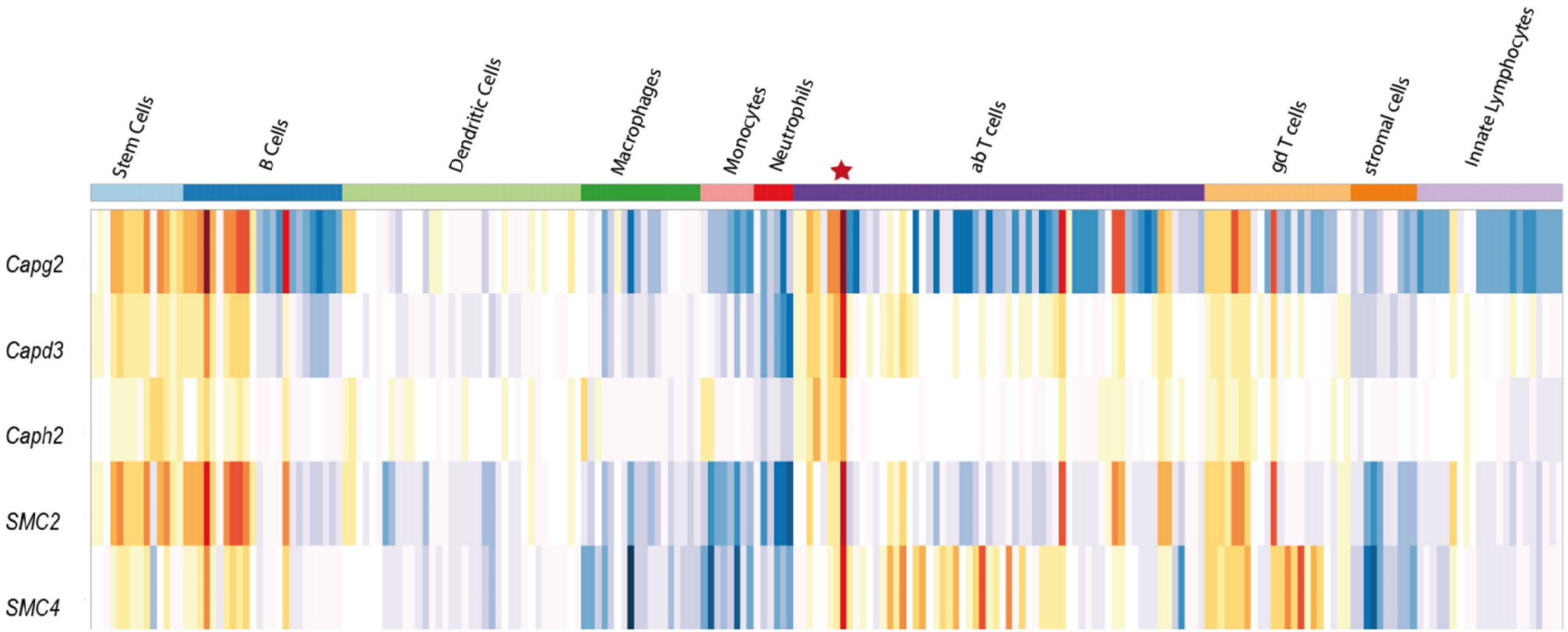

Figure 5.6

Transcriptome data reveals that condensin subunit transcripts are most highly expressed at the DP 71^{+} stage of T cell development

Hierarchically-clustered heatmap showing means-normalized expression value of the condensin subunit genes (SMC2/4, nCAPH/H2, nCAPG/G2, nCAPD2/D3) in each of the cell subsets. The cell subset associated with the highest transcript expression of condensin genes are the DP 71^{+} blast T cells (indicated by the red star). Data was assembled by the Immgen consortium: *Heng TS, et al, Immunological Genome Project Consortium, Nat Immunol. 2008 10 : 1091.*

Upstream open reading frames (u-ORFs) have been shown to regulate the expression of genes at the downstream ORF by triggering mRNA decay or by regulating translation (Barbosa, Peixeiro, & Romão, 2013; Morris & Geballe, 2000). A highly conserved u-ORF has been located in the CAP-H2 mRNA (Theodoratos *et al*., 2012). In humans, it was predicted that CAP-H2 translation initiates from two start codons, resulting in the production of two different sized proteins. Both proteins were depleted by shRNA against CAP-H2 transcripts. By knocking out the uORF start codon, Yokoyami *et al*. proceeded to show that translational regulation from the two start codons was regulated by the u-ORF. It was hypothesised that the u-ORF may be involved in the regulation of expression of the two translational variants in a cell-cycle dependant manner (Yokoyama, Zhu, Zhang, & Noma, 2015).

However, the second AUG start site is absent in mice, and so only one of the translational variants exists. Despite this, the u-ORF itself is conserved in mice, which raises the question: what is its purpose? One hypothesis could be that the u-ORF is involved in cell cycle regulation of CAP-H2 expression. Additionally, it could be that the u-ORF is involved in the cell-type dependent repression of CAP-H2 translation, resulting in a reduction of CAP-H2 protein in B cells and erythroid cells, relative to T cells. Further work must be carried out to test these hypotheses. This might include ribosome profiling to determine whether the uORF sequence exhibits a higher ribosome occupancy in some cell types in comparison to others. In addition, it would be interesting to knock out the uORF in a mouse, and analyse whether CP-H2 transcription is upregulated in some cell times rather than others.

CHAPTER 6: DISCUSSION

The requirement for condensin in efficient chromosome segregation is a general property of almost all characterised organisms, as indicated by the presence of anaphase bridges, which are common in condensin depleted cells (Vagnarelli *et al*., 2006). However, it has been suggested that the cellular requirements for condensin activity differ between species, as well as between cell types (Hirano, 2012). The first studies of condensin were performed in *Xenopus* oocyte extract, where condensin I appears to be essential for the condensation of sperm chromatin (Hirano & Mitchison, 1994). However, in subsequent studies using cellular systems such as chicken DT40 cells (Vagnarelli *et al*., 2006) or *C. elegans* (Hagstrom *et al*., 2002), chromosome condensation can still occur when condensin function is perturbed. In mice, condensin I and II were both shown to be essential for neuronal stem cell divisions (Hirano, 2012), while condensin II but not condensin I is essential for murine meiosis I and the first embryonic mitosis (Houlard *et al*., 2015).

Arguably the most striking example of tissue-specific condensin function in the literature is the mouse model *Caph2*$^{nes/nes}$ (Gosling *et al*., 2007), which, as discussed, reveals cellular abnormalities primarily in the T cell lineage. Before the work presented in this thesis, it was not known whether the T cell developmental block occurred due to abnormal mitosis, or one of the other cellular functions that have been attributed to condensins.

I have described experiments carried out during my PhD, which provide strong evidence to suggest that these cellular abnormalities arise due to errors in segregation. I went on to investigate the possibility that the T cell specific abnormalities arise due to abnormal interphase processes within the T cell lineage, but I did not find any strong evidence for this. While it is possible that condensin II is involved in epigenetic processes during interphase in T cells specifically (Rawlings *et al*., 2011), my analysis does not support the hypothesis that it is this function of condensin II that is perturbed in *Caph2*$^{nes/nes}$.

I proceeded to study the different stages of hematopoietic differentiation in a

systematic manner, and, based on ploidy profiling, was able to pinpoint the precise stage of differentiation that was most vulnerable to condensin II deficiency: the DP blast T cells. This discovery led me to investigate what property of this particular developmental stage could cause increased vulnerability to condensin II deficiency.

6.1 Evidence to suggest that the Caph2$^{nes/nes}$ phenotype arises due to errors in mitosis

The T cell phenotypes arising from *Caph2*$^{nes/nes}$ mutation I have described in this thesis include abnormal chromosome structure and increased ploidy in the T cell lineage, which are likely to be the cause and consequence of abnormal mitosis, respectively. Further characterisation of these defects was carried out using T cells cultured on OP9/DL1 monolayers. In unsynchronised cultures, *Caph2*$^{nes/nes}$ cells showed a significant decrease in the fraction of anaphase cells in which sister chromatids were resolved, suggesting that mitosis is specifically impaired during this stage (Wood, unpublished data). To enrich for anaphase cells, T cell cultures were treated with the proteasome inhibitor MG132 to arrest cells in metaphase, before being released into anaphase by wash out of MG132. Analysis of mitotic figures following MG132 washout revealed an elevated incidence of anaphase bridges and occasionally other defects associated with aberrant mitosis, including lagging chromosomes, multipolar spindles and micronuclei (Wood, unpublished data). Together, these data provide strong evidence that the developmental block during T cell differentiation in *Caph2*$^{nes/nes}$ mice arises from defects in the well-known role of condensin II in restructuring chromosomes between DNA replication and chromosome segregation.

However, the question of cell-type specificity remains: why would condensin II deficiency impact the DP T cells so drastically in comparison with other lineages? As discussed in Section 3.2, condensins have been implicated in interphase processes, and specifically gene regulation (Bauer *et al*., 2012; Haeusler *et al*., 2008; Kruesi *et al*., 2013), but the evidence for cell cycle independent functions of condensin in mammals is relatively sparse (Li *et al*., 2015). Unlike regulators of mitotic chromosome structure, regulators of gene expression are well known to impact individual cell types differently. One possible explanation for the *Caph2*$^{nes/nes}$ cell-type specificity is that the phenotype arises due to a separation of function mutation in the kleisin β subunit, which would affect its hypothesised role in T cell-specific gene regulation, rather than its established role in mitosis (Gosling *et al*., 2007). A similar separation of function mutation was described for the cohesin/condensin kleisin subunit ScpA in *Bacillus subtilis* (Dervyn *et al*., 2004). Mutations were isolated in ScpA which only subtly affected the ability of the complex to condense or segregate chromosomes, but strongly affected epigenetic processes including DNA damage repair and transcriptional control.

In addition to its role in chromosome cohesion, cohesin is known to function in the regulation of gene expression (Dorsett, 2007; Gause, Schaaf, & Dorsett, 2008; Rollins, Korom, Aulner, Martens, & Dorsett, 2004). Heterozygous mutations in cohesin subunits (SMC1 and SMC3) and regulatory proteins (NIPBL) have been identified in patients with Cornelia de Lange–like Syndrome (CdLS) (Gil-Rodríguez *et al*., 2015). This was initially surprising since sister chromatid cohesion is a fundamental process which, like chromosome condensation and decatenation, is important in all dividing cells. However, it's now believed that the developmental abnormalities arise due to the secondary role of cohesin in the regulation of gene expression during development (Liu *et al*., 2009; Revenkova *et al*., 2009).

One of the symptoms associated with Cornelia de Lange syndrome is microcephaly (reduction in head size). Interestingly, condensin II has been shown to interact directly with MCPH1: one of the causative genes responsible for this condition (Wood, Liang, Li, & Chen, 2008). In addition, combined MCPH1 and NCAPG2 (condensin II

subunit) deletions were discovered in a patient with severe microcephaly (Perche *et al*., 2013). Given that condensins have been implicated in interphase processes in invertebrates, it is tempting to speculate that condensin II may also play a role in mammalian gene regulation, like the structurally similar complex cohesin.

However, *Caph2*$^{nes/nes}$ mice have no overt dysmorphology similar to CdLS and I was unable to find any significant difference in interphase chromatin compaction between wildtype and *Caph2*$^{nes/nes}$ using 3D FISH (Figure 3.15) or any differences in compaction in ploidy-matched cells using flow cytometry (Figure 3.13). Further investigation revealed no obvious interphase abnormalities in *Caph2*$^{nes/nes}$ mutant T cells (Figures 3.17 and 3.18). Transcriptome studies in DP T cell subsets from wildtype and *Caph2nes/nes* animals uncovered relatively subtle differences in transcript levels (Wood, unpublished). Gene ontology analysis revealed that the most significantly deregulated genes were part of signalling pathways that are known to respond to aneuploidy, such as P53 and protein homeostasis (Sheltzer, Torres, Dunham, & Amon, 2012; Thompson & Compton, 2010; Wood, unpublished data). Together the data implies that the I15N mutation in *Caph2*$^{nes/nes}$ does not primarily impact the proposed role of condensin II in interphase processes.

Although I was unable to find any statistically significant differences in interphase chromatin compaction between wildtype and mutant, that is not to say that chromatin is not at all decompacted in *Caph2*$^{nes/nes}$. Perhaps the differences are subtle, and require analysis of an increased number of nuclei to become apparent. Additionally, condensin may be involved in restructuring of TAD boundaries, as has been shown for the dosage compensation complex (DCC) in *C. elegans* (Crane *et al*., 2015). The related complex cohesin is also thought to introduce TAD-like structures into fission yeast chromosomes (Mizuguchi *et al*., 2014). Investigations into whether condensin acts in this way in mammals would involve Hi-C analysis of the *Caph2*$^{nes/nes}$ genome.

The work described here does not rule out the possibility that condensins carry out interphase functions in vertebrates independently of their role in cell division, rather that the single nucleotide change within condensin II in *Caph2*$^{nes/nes}$ animals mutates the protein to such a degree that mitotic processes are affected, but results in a change in confirmation or structure that is below the threshold required to affect interphase

functions.

6.3 Cell type-specific vulnerability and response to condensin II deficiency

My work provides evidence that different cell types reveal differential susceptibility to condensin II deficiency. The consequences of the deficiency differ in two important ways. Firstly, some stages of differentiation ($CD4^+$ $CD8^+$ DP T cells and Stage 3 erythroid cells) exhibit high levels of hyperdiploidy, whereas the B cells and fibroblasts do not. Secondly, of the two cell types that display abnormal ploidy, only T cell numbers are decimated, which occurs at least in part due to cell cycle arrest (Figure 4.5). In contrast, the erythroid cells do not appear undergo cell cycle arrest (Figure 4.8). The possibility that cell fate decisions following abnormal mitosis are cell type-specific is supported by several studies (Foijer *et al*., 2013; Gascoigne & Taylor, 2008; Wertz *et al*., 2011). It has been suggested that the cause of the variability in cell fates is due to two competing networks: one that promotes cell death, and the other preventing mitotic exit (Gascoigne & Taylor, 2008). Cell fate is determined by which of the networks passes its critical threshold first. If cyclin B1 levels fall low enough, the cell will undergo mitotic slip, exit mitosis and perhaps continue through the cell cycle. Conversely, if the critical threshold for cell death occurs first, the cell will undergo apoptosis. However, this study does not provide a model for cell fate after mitotic exit.

I found a substantial population of T cells arrested in a tetraploid state (Figure 4.4), but no equivalent population in the erythroid lineage (Figure 4.8), implying these two cell lineages are prone to undergo different cell fates following failed cytokinesis. It could be that the erythroid cells are likely to downregulate the retinoblastoma protein (pRb) more quickly, and upregulate the S phase promoting E2F transcription factors before sufficient signals have accumulated to activate P53 and cell cycle arrest. For T cells, however, the opposite may be true, with downregulation of pRb occurring much more slowly.

Work carried out by other members of the Wood lab supports the observation that T cells and erythroid cells respond differently to abnormal cytokinesis. Prolonged exposure to nocodazole revealed that primary T cells cultured *ex vivo* are removed

from the cell cycle, shown using DAPI DNA content analysis and flow cytometry. Analysis of primary erythroid cell cultured *ex vivo* in the presence of nocodazole, however, revealed a high proportion of cells with greater than 4N DNA content and an accumulation of 8N cells. This indicates that, unlike the T cells, a proportion of the erythroid cells do not drop out of the cell cycle in the absence of spindles but re-synthesize their DNA and continue on to a second mitosis (Taylor, unpublished data).

Since my results indicate that cell cycle arrest is activated in a substantial fraction of *Caph2*$^{nes/nes}$ DP T cells but not erythroid cells, despite both cell types revealing increased frequencies of cells with abnormal DNA content, (Figures 4.1c and 4.6c) this raises the question of what signalling pathways operate downstream from mitotic failure to induce cell cycle arrest in thymic T cells, but not erythroid cells. Failure to arrest tetraploid cells often results in the acquisition of an aneuploid karyotype. However, tetraploid cells are usually prevented from becoming aneuploid by undergoing cell cycle arrest. Using transformed cell lines, this cell cycle arrest has been shown to be dependent on P53 (Andreassen, Lohez, Lacroix, & Margolis, 2001; Takeshi Fujiwara *et al*., 2005).

6.3.1 The CD4$^+$ CD8$^+$ DP stage of T cell development is vulnerable to transformation in P53$^{-/-}$ mice

In an aging cohort of nine *Caph2$^{nes/nes}$* individuals, all nine animals developed T cell lymphoma within the 15 month study. Five of nine animals became moribund within the study period (Wood, unpublished data). Lymphoma cells were typically CD4$^+$ CD8$^+$, indicating that they originated from the stage of thymic T cell differentiation during which I have shown tetraploidy arises in young animals.

Interestingly, the DP stage of T cell development, which I have shown to be uniquely vulnerable to condensin II deficiency, is known to be vulnerable to transformation in *P53$^{-/-}$* mice. Mice inheriting null mutations in *P53* develop thymic lymphomas originating from CD4$^+$CD8$^+$ cells more rapidly than any other type of tumour (Donehower *et al*., 1992; Jacks *et al*., 1994). Like the *Caph2$^{nes/nes}$* phenotype (Gosling *et al*., 2007), the vulnerability of *P53$^{-/-}$* animals to thymic lymphoma is independent of VDJ recombination (Liao *et al*., 1998). This suggests that the DP stage of thymic T cell differentiation is unusually susceptible to malignant transformation, and that the tumour suppressive properties of P53 are of particular importance at this stage of development.

Work has therefore been carried out to test the involvement of P53-dependent pathways in the *Caph2$^{nes/nes}$* phenotypes during development and aging. To achieve this, *Caph2$^{nes/nes}$* mice were crossed with P53 null mice, generating double homozygous mutants. Kaplan Meier survival analysis of these mice revealed a marked reduction in survival of the *Caph2$^{nes/nes}$ P53$^{-/-}$* double mutants in comparison to *P53$^{-/-}$* single mutants: the median survival of the double homozygotes was 76 days, in comparison to a median of 144 days for *P53$^{-/-}$* mutants. Individual tumours were found to be comprised of either CD4$^+$CD8$^+$ or CD4$^-$CD8$^+$ cells (A. Wood, unpublished data).

Further investigation was carried out into the role of P53 specifically at the DP stage of T cell development before lymphoma establishment, which partial rescue of the *Caph2$^{nes/nes}$*-dependent block in both proliferation and differentiation during T cell development in *Caph2$^{nes/nes}$ P53$^{-/-}$* mice aged 7 days *post partum* (pp) (Wood, unpublished data). Gene expression analysis revealed that known P53 targets

important for cell cycle arrest (CDKN1A) and apoptosis (NOXA, FASL) were upregulated in *Caph2*$^{nes/nes}$ T cells in a P53-dependent manner, which potentially accounts for the proliferative block. By 6 weeks pp, the thymus had been taken over by $CD4^+$ $CD8^+$ or $CD4^-$ $CD8^+$ lymphoma cells (Wood, unpublished data). These data indicate that inactivation of the P53 pathway can drastically accelerate lymphomagenesis in *Caph2*$^{nes/nes}$ mice. In addition, *Caph2*$^{nes/nes}$ *P53*$^{+/-}$ became moribund within a decreased time frame in comparison with *P53*$^{+/-}$ cohorts (147 vs 471 days) (Baker *et al*., 2009), and tumours consistently undergo loss of heterozygosity to lose the single wildtype allele of P53. Somatic loss of wildtype P53 alleles is thus selected for in *Caph2*$^{nes/nes}$ tumours.

6.3.2 The $CD4^+$ $CD8^+$ DP stage of T cell development progresses more rapidly from S to M phase in comparison to other cell types

It is striking that a mutation that causes CIN and also one that protects against the negative effects of CIN manifest at the same point in differentiation, despite the mutations being present in every cell. Why should T cells at the $CD4^+$ $CD8^+$ stage show extreme vulnerability to reduced condensin II function and loss of P53? It is clear that the cell cycle role of condensin is relevant specifically between duplication (when catenations arise due to fork progression) and segregation. Therefore, as discussed previously, the stages that might be most vulnerable to condensin deficiency are S phase and M phase.

Preliminary experiments (Chapter 4 Section 4.2.6) indicate that the increased requirement for condensin and the activation of the P53 checkpoint to maintain cell cycle arrest at the DP stage of T cell development may be due to more rapid progression from S to M phase at this specific stage of development. Replication fork velocity is known to change during development (Estefanía *et al*., 2012) and as a consequence of disease (Di Micco *et al*., 2006). As discussed previously, rapid progression through S phase could result in an increased incidence of replication fork collisions, resulting in more DNA catenations (Sundin & Varshavsky, 1980). Alternatively, catenations may persist into and beyond anaphase due to insufficient time for decatenation to occur. These two alternatives are not necessarily mutually exclusive.

The hypothesis that the persistent catenation arise due to increased synthesis rather than reduced resolution is supported by experiments in yeast which indicate that although topoisomerase begins to resolve sister catenations as early as S phase, condensin's role in positively supercoiling DNA to facilitate decatenation occurs between prophase and anaphase, specifically. Experiments carried out by Baxter *et al.* in which circular yeast plasmids treated with either nocodazole (a microtubule inhibitor, which blocks cells in prometaphase) or Cdc20 inhibitors (which prevent anaphase onset), revealed that the condensin-dependent transition from premitotic negatively supercoiled catenanes to positively supercoiled mitotic catenanes occurs in the absence of the anaphase promoting complex subunit Cdc20 (i.e. before anaphase), but not in the absence of microtubules. In addition, it was discovered that the transition from negative to positive supercoils does not take place in the absence of centromeres: i.e. spindles must be engaged with kinetochores (Baxter *et al.*, 2011), implying that condensin's role in decatenation is specific to metaphase. However, the extent to which the mechanism of condensin-dependent decatenation observed on circular plasmids can be extrapolated to the linear chromosomes of yeast, or indeed the much larger chromosomes of vertebrates, is not clear.

As discussed above, work carried out by Ono *et al.* provides evidence to suggest that condensin is involved in the individualisation of sister chromatids of HeLa cells during S phase (Ono *et al.*, 2013). If this is also the case in other cell types, then the increased frequency of persistent catenations in condensin mutants are just as likely to be a result of an inability to resolve the catenations due to limited time between S and M phase. The persistent mutations observed in *Caph2*$^{nes/nes}$ DP T cells may, in fact, arise due to a combination of these two possibilities. As discussed previously, (Section 4.3), analysis of the rate of progression from G2 to M phase would provide the opportunity to infer which of these alternatives is more likely: if the DP T cells progress more slowly from G2 to M phase in comparison to DN T cells, B cells or MEFs, then it would imply that S phase progression is quicker. A more direct experiment (although perhaps more challenging) would be to calculate the length of S phase in each of these cell types using a double labelling technique (discussed previously – Section 4.3). Finally, relative replication fork velocities could be analysed using DNA combing on these different cell types.

I have discussed the possibility that DNA replication may introduce two different types of catenations: ones that are easily resolved by topoisomerase II, and more complex catenations that require condensin activity during early metaphase (Charbin *et al*., 2014). It has been shown that in budding yeast, condensin is particularly important at the rDNA locus (Freeman, Aragon-Alcaide, & Strunnikov, 2000). This locus is very highly transcribed by RNA PolI, and is therefore vulnerable to collisions between DNA and RNA polymerases (Takeuchi, Horiuchi, & Kobayashi, 2003). Interestingly, despite condensin localization being dynamic throughout the cell cycle, it becomes enriched at the rDNA locus during anaphase (D'Amours, Stegmeier, & Amon, 2004). It is possible, therefore, that increased fork collisions results in an increase in topologically complex catenations, which condensin is required to resolve.

Rapid S phase progression in higher eukaryotes may also introduce more of these topologically complex linkages. This raises the question: why do certain types of catenations persist into mitosis, and are only removed after kinetochore attachment in the presence of condensin (again, assuming that this is also true for higher eukaryotes) (Charbin *et al*., 2014). If these catenations are indeed more topologically complex and difficult to resolve (as discussed in Section 4.3), then it would make more sense to remove them as early as possible. Eukaryotic condensin II is nuclear throughout the cell cycle (Tatsuya Hirano, 2012; Ono *et al*., 2004), so would have the opportunity to begin to resolve catenations in collaboration with topoisomerase II as early as S phase.

Could it be that these particular type of catenations are maintained in order to stabilize the cohesin-mediated linkages between sister chromatids? The hypothesis that sister chromatid catenations may act in concert with cohesion machinery to ensure close physical proximity of sister DNA strands has been suggested previously (Hirano, 2000) and work carried out by Vagnarelli *et al*. indicates that catenations are able to maintain sister chromatid cohesion if topoisomerase is inhibited (Vagnarelli *et al*., 2004). Additionally, Bickmore and Oghene revealed the presence of apparent catenations between sisters in alpha satellite DNA (Bickmore & Oghene, 1996). However, it is not known whether sister catenations act to maintain cohesion *in vivo*, when topoisomerases are uninhibited.

An alternative explanation could be that condensin-mediated decatenation, through the process of positively supercoiling DNA, is related to a series of tightly regulated compaction and expansion events throughout different stages of mitosis. Progression from mid to late prophase has been linked to a reorganization of chromatin structure, which includes an increase in chromosome width, sister individualization, topoisomerase axes splitting and reorganization of chromatin into a radial confirmation around a central topoisomerase axis. These conformational changes are consistent with removal of constraining topological linkages resulting in expansion of chromatin, and reorganization into a lower energy state. The removal of these constraints at late prophase was shown to be topoisomerase II dependent (Liang *et al*., 2015). Topoisomerase II mediated decatenation during late prophase may represent the removal of the final linkages of the kind that are easily resolved, and do not require condensin. Following expansion during late prophase, Liang *et al.* demonstrated that rapid compaction of chromosomes occurs during metaphase (Liang *et al*., 2015). It is tempting to hypothesise that this compaction occurs due to condensin-mediated decatenation of sister chromatids, which locks in structural changes that were introduced as a consequence of chromosome expansion occurring in late prophase (Liang *et al*., 2015). However, firm conclusions cannot be drawn, since the experiments which indicate that condensin is involved in decatenation during metaphase were carried out in circular yeast chromosomes (Baxter *et al*., 2011), whereas the mitotic expansion and compaction cycles were investigated using mammalian cells (Liang *et al*., 2015). Therefore, theories developed to explain observations in one experimental system might not necessarily apply to other organisms.

6.4 Concluding remarks

In agreement with previous studies (Ono *et al*., 2003, 2013; Vagnarelli *et al*., 2004), I have shown that condensin II deficiency results in abnormal chromosome structure, with metaphase chromosomes revealing a wavy morphology. This supports the hypothesis that condensin II contributes to chromosome structural integrity.

The experiments described in Section 4.2.6 indicating that the rate of progression from S to M phase varies between cell types, with faster progression resulting in an

increased dependency on condensin activity, provide an exciting explanation for the cell type specific phenotype observed in the *Caph2*$^{nes/nes}$ mouse. However, at present this data is correlative, and more work is required: initially to characterise which stage from S to M phase is accelerated, and secondly to rescue the phenotype. In the future, I would like to confirm that manipulation of S phase kinetics impacts the condensin-deficient phenotype, as has been shown using drugs such as hydroxyurea (HU) in bacteria (Gruber *et al*., 2014).

In addition, it would be interesting to characterise the rate of progression from S to M phase of erythroid cells: since the Stage 3 erythroid cells also reveal high levels of hyperdiploidy (albeit to a lesser extent than DP blast T cells) it could be that erythroid cells also progress more rapidly than B cells or fibroblasts. These experiments address the first level of complexity of the condensin deficient phenotype; i.e. that some cell types (T and erythroid) display increased hyperdiploidy, whereas others (B cells and fibroblasts) do not. The second level of complexity relates to the difference between those cells that undergo a higher frequency of cytokinesis failure (discussed above). As a consequence of increased levels of hyperdiploidy, T cells appear to undergo cell cycle arrest and cell number reduction, whereas erythroid cells do not. In order to better understand this process, single cell transcriptome profiling could be carried out, with comparisons made between tetraploid arrested versus tetraploid cycling T and erythroid cells. This may help to elucidate the different checkpoint activity operating in each of these cell types.

BIBLIOGRAPHY

Abe, S., Nagasaka, K., Hirayama, Y., Kozuka-Hata, H., Oyama, M., Aoyagi, Y., … Hirota, T. (2011). The initial phase of chromosome condensation requires Cdk1-mediated phosphorylation of the CAP-D3 subunit of condensin II. *Genes and Development*, *25*(8), 863–874. http://doi.org/10.1101/gad.2016411

Abrieu, A., Fisher, D., Simon, M. N., Dorée, M., & Picard, A. (1997). MAPK inactivation is required for the G2 to M-phase transition of the first mitotic cell cycle. *EMBO Journal*, *16*(21), 6407–6413. http://doi.org/10.1093/emboj/16.21.6407

Adams, D. E., Shekhtman, E. M., Zechiedrich, E. L., Schmid, M. B., & Cozzarelli, N. R. (1992). The role of topoisomerase IV in partitioning bacterial replicons and the structure of catenated intermediates in DNA replication. *Cell*, *71*(2), 277–288. http://doi.org/10.1016/0092-8674(92)90356-H

Adolph, K. W., Cheng, S. M., & Laemmli, U. K. (1977). Role of Nonhistone Proteins Chromosome Structure in Metaphase. *Cell*, *12*(November), 805–816.

Alberola-Ila, J., & Hernández-Hoyos, G. (2003). The Ras/MAPK cascade and the control of positive selection. *Immunological Reviews*, *191*, 79–96. http://doi.org/10.1034/j.1600-065X.2003.00012.x

Alexander, V. S., Hogan, E., & Koshland, D. (1995). SMC2 , a Saccharomyces cerevisiae gene essential for chromosome segregation and condensation , defines a subgroup within the SMC family. *Genes and Development*, *9*, 587–599.

Anderson, G., & Takahama, Y. (2012). Thymic epithelial cells: Working class heroes for T cell development and repertoire selection. *Trends in Immunology*, *33*(6), 256–263. http://doi.org/10.1016/j.it.2012.03.005

Andreassen, P. R., Lohez, O. D., Lacroix, B., & Margolis, R. L. (2001). Tetraploid State Induces p53-dependent Arrest of Nontransformed Mammalian Cells in G1. *Molecular Biology of the Cell*, *12*(May), 1315–1328.

Andrews, A. J., & Luger, K. (2011). Nucleosome structure(s) and stability: variations on a theme. *Annual Review of Biophysics*, *40*, 99–117. http://doi.org/10.1146/annurev-biophys-042910-155329

Baker, D. J., Jeganathan, K. B., Cameron, J. D., Thompson, M., Juneja, S., Kopecka, A., … van Deursen, J. M. (2004). BubR1 insufficiency causes early onset of aging-associated phenotypes and infertility in mice. *Nature Genetics*, *36*(7), 744–

9. http://doi.org/10.1038/ng1382

Baker, D. J., Jin, F., Jeganathan, K. B., & van Deursen, J. M. (2009). Whole chromosome instability caused by Bub1 insufficiency drives tumorigenesis through tumor suppressor gene loss of heterozygosity. *Cancer Cell*, *16*(6), 475–86. http://doi.org/10.1016/j.ccr.2009.10.023

Bakhrebah, M., Zhang, T., Mann, J. R., Kalitsis, P., & Hudson, D. F. (2015). Disruption of a conserved CAP-D3 threonine alters condensin loading on mitotic chromosomes leading to chromosome hyper-condensation. *The Journal of Biological Chemistry*, 1–23. http://doi.org/10.1074/jbc.M114.627109

Barbosa, C., Peixeiro, I., & Romão, L. (2013). Gene Expression Regulation by Upstream Open Reading Frames and Human Disease. *PLoS Genetics*, *9*(8), 1–12. http://doi.org/10.1371/journal.pgen.1003529

Bauer, C. R., Hartl, T. A., & Bosco, G. (2012). Condensin II promotes the formation of chromosome territories by inducing axial compaction of polyploid interphase chromosomes. *PLoS Genetics*, *8*(8), e1002873. http://doi.org/10.1371/journal.pgen.1002873

Baxter, J., & Aragón, L. (2012). A model for chromosome condensation based on the interplay between condensin and topoisomerase II. *Trends in Genetics : TIG*, *28*(3), 110–7. http://doi.org/10.1016/j.tig.2011.11.004

Baxter, J., & Diffley, J. F. X. (2008). Topoisomerase II Inactivation Prevents the Completion of DNA Replication in Budding Yeast. *Molecular Cell*, *30*(6), 790–802. http://doi.org/10.1016/j.molcel.2008.04.019

Baxter, J., Sen, N., Martínez, V. L., De Carandini, M. E. M., Schvartzman, J. B., Diffley, J. F. X., & Aragón, L. (2011). Positive supercoiling of mitotic DNA drives decatenation by topoisomerase II in eukaryotes. *Science (New York, N.Y.)*, *331*(6022), 1328–32. http://doi.org/10.1126/science.1201538

Bermúdez, I., García-Martínez, J., Pérez-Ortín, J. E., & Roca, J. (2010). A method for genome-wide analysis of DNA helical tension by means of psoralen-DNA photobinding. *Nucleic Acids Research*, *38*(19). http://doi.org/10.1093/nar/gkq687

Bhalla, N., Biggins, S., & Murray, A. W. (2002). Mutation of YCS4 , a Budding Yeast Condensin Subunit , Affects Mitotic and Nonmitotic Chromosome Behavior. *Molecular Biology of the Cell*, *13*(February), 632–645.

http://doi.org/10.1091/mbc.01

Bhat, M. A., Philp, A. V., Glover, D. M., & Bellen, H. J. (1996). Chromatid Segregation at Anaphase Requires the barren Product , a Novel Chromosome-Associated Protein That Interacts with Topoisomerase II. *Cell*, *87*, 1103–1114.

Bhattacharyya, A., Murchie, A. I., von Kitzing, E., Diekmann, S., Kemper, B., & Lilley, D. M. (1991). Model for the interaction of DNA junctions and resolving enzymes. *Journal of Molecular Biology*, *221*(4), 1191–1207. http://doi.org/10.1016/0022-2836(91)90928-Y

Bickmore, W. A., & Oghene, K. (1996). Visualizing the Spatial Relationships between Defined DNA Sequences and the Axial Region of Extracted Metaphase Chromosomes. *Cell*, *84*(1), 95–104. http://doi.org/10.1016/S0092-8674(00)80996-4

Bönisch, C., & Hake, S. B. (2012). Histone H2A variants in nucleosomes and chromatin: More or less stable? *Nucleic Acids Research*, *40*(21), 10719–10741. http://doi.org/10.1093/nar/gks865

Boos, D., Sanchez-Pulido, L., Rappas, M., Pearl, L. H., Oliver, A. W., Ponting, C. P., & Diffley, J. F. X. (2011). Regulation of DNA replication through Sld3-Dpb11 interaction is conserved from yeast to humans. *Current Biology*, *21*(13), 1152–1157. http://doi.org/10.1016/j.cub.2011.05.057

Bosselut, R. (2004). CD4/CD8-lineage differentiation in the thymus: from nuclear effectors to membrane signals. *Nat Rev Immunol*, *4*(7), 529–540. Retrieved from http://dx.doi.org/10.1038/nri1392

Brekelmans, P., van Soest, P., Leenen, P. J., & van Ewijk, W. (1994). Inhibition of proliferation and differentiation during early T cell development by anti-transferrin receptor antibody. *European Journal of Immunology*, *24*(11), 2896–902. http://doi.org/10.1002/eji.1830241147

Brito, D. a, Yang, Z., & Rieder, C. L. (2008). Microtubules do not promote mitotic slippage when the spindle assembly checkpoint cannot be satisfied. *The Journal of Cell Biology*, *182*(4), 623–9. http://doi.org/10.1083/jcb.200805072

Brown, K. E., Amoils, S., Horn, J. M., Buckle, V. J., Higgs, D. R., Merkenschlager, M., & Fisher, A. G. (2001). Expression of [alpha]- and [beta]-globin genes occurs within different nuclear domains in haemopoietic cells. *Nat Cell Biol*, *3*(6), 602–606. Retrieved from http://dx.doi.org/10.1038/35078577

Brown, K. E., Guest, S. S., Smale, S. T., Hahm, K., Merkenschlager, M., & Fisher, A. G. (1997). Association of transcriptionally silent genes with Ikaros complexes at centromeric heterochromatin. *Cell*, *91*(6), 845–854. http://doi.org/10.1016/S0092-8674(00)80472-9

Bürmann, F., Shin, H.-C., Basquin, J., Soh, Y.-M., Giménez-Oya, V., Kim, Y.-G., … Gruber, S. (2013). An asymmetric SMC-kleisin bridge in prokaryotic condensin. *Nature Structural & Molecular Biology*, *20*(3), 371–9. http://doi.org/10.1038/nsmb.2488

Calladine, C., Drew, H., Luisi, B., & Travers, A. (1994). *Understanding DNA: The molecule and how it works* (Third). Biochemical Education.

Chambeyron, S., Da Silva, N. R., Lawson, K. a, & Bickmore, W. a. (2005). Nuclear re-organisation of the Hoxb complex during mouse embryonic development. *Development (Cambridge, England)*, *132*(9), 2215–2223. http://doi.org/10.1242/dev.01813

Champoux, J., & Been, M. (1980). Mechanistic Studies of DNA Replication and Genetic Recombination. *New York: Academic*, 809–815.

Champoux, J. J. (2001). DNA TOPOISOMERASES : Structure , Function , and Mechanism. *Annual Review of Biochemistry*, *70*, 369–413.

Charbin, A., Bouchoux, C., & Uhlmann, F. (2014). Condensin aids sister chromatid decatenation by topoisomerase II. *Nucleic Acids Research*, *42*(1), 340–8. http://doi.org/10.1093/nar/gkt882

Chuang, P. T., Albertson, D. G., & Meyer, B. J. (1994). DPY-27: A chromosome condensation protein homolog that regulates C. elegans dosage compensation through association with the X chromosome. *Cell*, *79*(3), 459–474. http://doi.org/10.1016/0092-8674(94)90255-0

Cobbe, N., & Heck, M. M. (2000). Review: SMCs in the world of chromosome biology- from prokaryotes to higher eukaryotes. *J Struct Biol*, *129*(2-3), 123–143. http://doi.org/10.1006/jsbi.2000.4255

Cockerill, P. N., & Garrard, W. T. (1986). Chromosomal loop anchorage of the kappa immunoglobulin gene occurs next to the enhancer in a region containing topoisomerase II sites. *Cell*, *44*(2), 273–282. http://doi.org/10.1016/0092-8674(86)90761-0

Coelho, P. a, Queiroz-Machado, J., & Sunkel, C. E. (2003). Condensin-dependent

localisation of topoisomerase II to an axial chromosomal structure is required for sister chromatid resolution during mitosis. *Journal of Cell Science*, *116*(Pt 23), 4763–4776. http://doi.org/10.1242/jcs.00799

Cook, P. R. (1994). RNA polymerase: structural determinant of the chromatin loop and the chromosome. *BioEssays : News and Reviews in Molecular, Cellular and Developmental Biology*, *16*(6), 425–430. http://doi.org/10.1002/bies.950160611

Cooper, G. M., & Hausman, R. E. (2007). *The Cell: A Molecular Approach 2nd Edition*. *Sinauer Associates*.

Coschi, C. H., Martens, A. L., Ritchie, K., Francis, S. M., Chakrabarti, S., Berube, N. G., & Dick, F. A. (2010). Mitotic chromosome condensation mediated by the retinoblastoma protein is tumor-suppressive. *Genes and Development*, *24*, 1351–1363. http://doi.org/10.1101/gad.1917610.suggests

Coster, G., Frigola, J., Beuron, F., Morris, E. P., & Diffley, J. F. X. (2014). Origin Licensing Requires ATP Binding and Hydrolysis by the MCM Replicative Helicase. *Molecular Cell*, *55*(5), 666–677. http://doi.org/10.1016/j.molcel.2014.06.034

Crane, E., Bian, Q., McCord, R. P., Lajoie, B. R., Wheeler, B. S., Ralston, E. J., … Meyer, B. J. (2015). Condensin-driven remodelling of X chromosome topology during dosage compensation. *Nature*. http://doi.org/10.1038/nature14450

Crasta, K., Ganem, N. J., Dagher, R., Lantermann, A. B., Ivanova, E. V, Pan, Y., … Pellman, D. (2012). DNA breaks and chromosome pulverization from errors in mitosis. *Nature*, *482*(7383), 53–8. http://doi.org/10.1038/nature10802

Csankovszki, G., Collette, K., Spahl, K., Carey, J., Snyder, M., Petty, E., … Hagstrom, K. (2009). Three distinct condensin complexes control C. elegans chromosome dynamics. *Current Biology : CB*, *19*(1), 9–19. http://doi.org/10.1016/j.cub.2008.12.006

Cuylen, S., Metz, J., & Haering, C. H. (2011). Condensin structures chromosomal DNA through topological links. *Nature Structural & Molecular Biology*, *18*(8), 894–901. http://doi.org/10.1038/nsmb.2087

D'Amours, D., Stegmeier, F., & Amon, A. (2004). Cdc14 and condensin control the dissolution of cohesin-independent chromosome linkages at repeated DNA. *Cell*, *117*(4), 455–469. http://doi.org/10.1016/S0092-8674(04)00413-1

Davoli, T., & de Lange, T. (2011). The causes and consequences of polyploidy in

normal development and cancer. *Annual Review of Cell and Developmental Biology*, *27*, 585–610. http://doi.org/10.1146/annurev-cellbio-092910-154234

Dervyn, E., Noirot-Gros, M. F., Mervelet, P., McGovern, S., Ehrlich, S. D., Polard, P., & Noirot, P. (2004). The bacterial condensin/cohesin-like protein complex acts in DNA repair and regulation of gene expression. *Molecular Microbiology*, *51*(6), 1629–1640. http://doi.org/10.1111/j.1365-2958.2003.03951.x

Dewar, J. M., Budzowska, M., & Walter, J. C. (2015). The mechanism of DNA replication termination in vertebrates. *Nature*. http://doi.org/10.1038/nature14887

Di Cerbo, V., Mohn, F., Ryan, D. P., Montellier, E., Kacem, S., Tropberger, P., … Schneider, R. (2014). Acetylation of histone H3 at lysine 64 regulates nucleosome dynamics and facilitates transcription. *eLife*, *2014*(3). http://doi.org/10.7554/eLife.01632

Di Micco, R., Fumagalli, M., Cicalese, A., Piccinin, S., Gasparini, P., Luise, C., … d'Adda di Fagagna, F. (2006). Oncogene-induced senescence is a DNA damage response triggered by DNA hyper-replication. *Nature*, *444*(7119), 638–642. http://doi.org/10.1038/nature05327

Dikovskaya, D., Cole, J., Mason, S., Nixon, C., Karim, S., McGarry, L., … Adams, P. (2015). Mitotic Stress Is an Integral Part of the Oncogene-Induced Senescence Program that Promotes Multinucleation and Cell Cycle Arrest. *Cell Rep*, *12*(9), 1483–96.

DiNardo, S., Voelkel, K., & Sternglanz, R. (1984). DNA topoisomerase II mutant of Saccharomyces cerevisiae: topoisomerase II is required for segregation of daughter molecules at the termination of DNA replication. *Proceedings of the National Academy of Sciences of the United States of America*, *81*(9), 2616–2620. http://doi.org/10.1073/pnas.81.9.2616

Dixon, J. R., Selvaraj, S., Yue, F., Kim, A., Li, Y., Shen, Y., … Ren, B. (2012). Topological domains in mammalian genomes identified by analysis of chromatin interactions. *Nature*, *485*(7398), 376–80. http://doi.org/10.1038/nature11082

Donehower, L., Harvey, M., & Slagle, B. (1992). Mice deficient for p53 are developmentally normal but susceptible to spontaneous tumours. *Nature*. Retrieved from http://www.tmd.ac.jp/med/phy2/Rindokupapers/p53KOmice.pdf

Dorsett, D. (2007). Roles of the sister chromatid cohesion apparatus in gene

expression, development, and human syndromes Dale. *NIH Public Access*, *116*(1), 1–13. http://doi.org/10.1016/j.biotechadv.2011.08.021.Secreted

Dreier, M. R., Bekier, M. E., & Taylor, W. R. (2011). Regulation of sororin by Cdk1-mediated phosphorylation. *Journal of Cell Science*, *124*(Pt 17), 2976–2987. http://doi.org/10.1242/jcs.085431

Earnshaw, W. C., & Heck, M. . (1985). Localization of topoisomerase II in mitotic chromosomes. *The Journal of Cell Biology*, *100*(5), 1716–1725. http://doi.org/10.1083/jcb.100.5.1716

Eskeland, R., Leeb, M., Grimes, G. R., Kress, C., Boyle, S., Sproul, D., … Bickmore, W. a. (2010). Ring1B compacts chromatin structure and represses gene expression independent of histone ubiquitination. *Molecular Cell*, *38*(3), 452–64. http://doi.org/10.1016/j.molcel.2010.02.032

Estefanía, M. M., Ganier, O., Hernández, P., Schvartzman, J. B., Mechali, M., & Krimer, D. B. (2012). DNA Replication Fading As Proliferating Cells Advance in Their Commitment to Terminal Differentiation. *Scientific Reports*, *2*, 1–8. http://doi.org/10.1038/srep00279

Fan, J. Y., Gordon, F., Luger, K., Hansen, J. C., & Tremethick, D. J. (2002). The essential histone variant H2A.Z regulates the equilibrium between different chromatin conformational states. *Nature Structural Biology*, *9*(3), 172–6. http://doi.org/10.1038/nsb767

Fazzio, T. G., & Panning, B. (2010). Condensin complexes regulate mitotic progression and interphase chromatin structure in embryonic stem cells. *The Journal of Cell Biology*, *188*(4), 491–503. http://doi.org/10.1083/jcb.200908026

Foijer, F., DiTommaso, T., Donati, G., Hautaviita, K., Xie, S. Z., Heath, E., … Bradley, A. (2013). Spindle checkpoint deficiency is tolerated by murine epidermal cells but not hair follicle stem cells. *Proceedings of the National Academy of Sciences of the United States of America*, *110*(8), 2928–33. http://doi.org/10.1073/pnas.1217388110

Forbes, S. a., Beare, D., Gunasekaran, P., Leung, K., Bindal, N., Boutselakis, H., … Campbell, P. J. (2014). COSMIC: exploring the world's knowledge of somatic mutations in human cancer. *Nucleic Acids Research*, *43*(D1), D805–D811. http://doi.org/10.1093/nar/gku1075

Freeman, L., Aragon-Alcaide, L., & Strunnikov, A. (2000). The condensin complex

governs chromosome condensation and mitotic transmission of rDNA. *Journal of Cell Biology*, *149*(4), 811–824. http://doi.org/10.1083/jcb.149.4.811

Fujiwara, T., Bandi, M., Nitta, M., Ivanova, E. V, Bronson, R. T., & Pellman, D. (2005). Cytokinesis failure generating tetraploids promotes tumorigenesis in p53-null cells. *Nature*, *437*(7061), 1043–7. http://doi.org/10.1038/nature04217

Fujiwara, T., Tanaka, K., Kuroiwa, T., & Hirano, T. (2013). Spatiotemporal dynamics of condensins I and II: evolutionary insights from the primitive red alga Cyanidioschyzon merolae. *Molecular Biology of the Cell*, *24*(16), 2515–27. http://doi.org/10.1091/mbc.E13-04-0208

Fussner, E., Strauss, M., Djuric, U., Li, R., Ahmed, K., Hart, M., … Bazett-Jones, D. P. (2012). Open and closed domains in the mouse genome are configured as 10-nm chromatin fibres. *EMBO Reports*, *13*(11), 992–6. http://doi.org/10.1038/embor.2012.139

Ganem, N. J., & Pellman, D. (2012). Linking abnormal mitosis to the acquisition of DNA damage. *The Journal of Cell Biology*, *199*(6), 871–81. http://doi.org/10.1083/jcb.201210040

Ganem, N. J., Storchova, Z., & Pellman, D. (2007). Tetraploidy, aneuploidy and cancer. *Current Opinion in Genetics and Development*. http://doi.org/10.1016/j.gde.2007.02.011

Garćia-Ojeda, M. E., Wolterink, R. G. J. K., Lemâitre, F., Le Goff, O. R., Hasan, M., Hendriks, R. W., … Di Santo, J. P. (2013). GATA-3 promotes T-cell specification by repressing B-cell potential in pro-T cells in mice. *Blood*, *121*(10), 1749–1759. http://doi.org/10.1182/blood-2012-06-440065

Gascoigne, K. E., & Taylor, S. S. (2008). Cancer cells display profound intra- and interline variation following prolonged exposure to antimitotic drugs. *Cancer Cell*, *14*(2), 111–22. http://doi.org/10.1016/j.ccr.2008.07.002

Gasser, S., Amati, B., Cardenas, M., & Hofmann, J. (1989). Studies on scaffold attachment sites and their relation to genome function. *Int Rev Cytol*, *119*, 57–96.

Gasser, S. M., & Laemmli, U. K. (1986). The organization of chromatin loops: characterization of a scaffold attachment site. *EMBO*, *5*(3), 511–518.

Gause, M., Schaaf, C. a., & Dorsett, D. (2008). Cohesin and CTCF: Cooperating to control chromosome conformation? *BioEssays*, *30*(8), 715–718. http://doi.org/10.1002/bies.20787

Ge, X. Q., & Blow, J. J. (2010). Chk1 inhibits replication factory activation but allows dormant origin firing in existing factories. *Journal of Cell Biology*, *191*, 1285–1297. http://doi.org/10.1083/jcb.201007074

Gerlich, D., Hirota, T., Koch, B., Peters, J. M., & Ellenberg, J. (2006). Condensin I stabilizes chromosomes mechanically through a dynamic interaction in live cells. *Current Biology*, *16*(4), 333–344. http://doi.org/10.1016/j.cub.2005.12.040

Giebel, B., & Bruns, I. (2008). Self-renewal versus differentiation in hematopoietic stem and progenitor cells: a focus on asymmetric cell divisions. *Current Stem Cell Research & Therapy*, *3*(1), 9–16. http://doi.org/10.2174/157488808783489444

Giger, K. M., & Kalfa, T. A. (2015). Review Article Phylogenetic and Ontogenetic View of Erythroblastic Islands.

Gilbert, N., & Allan, J. (2001). Distinctive higher-order chromatin structure at mammalian centromeres. *Proceedings of the National Academy of Sciences of the United States of America*, *98*(21), 11949–11954. http://doi.org/10.1073/pnas.211322798

Gilbert, N., & Allan, J. (2013). Supercoiling in DNA and chromatin. *Current Opinion in Genetics and Development*, *25*(1), 15–21.

Gilbert, N., Boyle, S., Fiegler, H., Woodfine, K., Carter, N. P., & Bickmore, W. a. (2004). Chromatin architecture of the human genome: Gene-rich domains are enriched in open chromatin fibers. *Cell*, *118*(5), 555–566. http://doi.org/10.1016/j.cell.2004.08.011

Gil-Rodríguez, M. C., Deardorff, M. a., Ansari, M., Tan, C. a., Parenti, I., Baquero-Montoya, C., … Pié, J. (2015). De Novo Heterozygous Mutations in SMC3 Cause a Range of Cornelia de Lange Syndrome-Overlapping Phenotypes. *Human Mutation*, *36*(4), 454–462. http://doi.org/10.1002/humu.22761

Gligoris, T. G., Scheinost, J. C., Bürmann, F., Petela, N., Chan, K., Uluocak, P., … Löwe, J. (2014). Closing the cohesin ring: Structure and function of its Smc3-kleisin interface. *SCIENCE*, *346*(6212), 963–968.

Gosling, K. M., Makaroff, L. E., Theodoratos, A., Kim, Y.-H., Whittle, B., Rui, L., … Fahrer, A. M. (2007). A mutation in a chromosome condensin II subunit, kleisin beta, specifically disrupts T cell development. *Proceedings of the National Academy of Sciences of the United States of America*, *104*(30), 12445–50.

http://doi.org/10.1073/pnas.0704870104

Green, L. C., Kalitsis, P., Chang, T. M., Cipetic, M., Kim, J. H., Marshall, O., … Hudson, D. F. (2012). Contrasting roles of condensin I and condensin II in mitotic chromosome formation. *Journal of Cell Science*, *125*(Pt 6), 1591–604. http://doi.org/10.1242/jcs.097790

Greulich, K. O., Wachtel, E. J., Ausio, J., Seger, D., & Eisenberg, H. (1987). Transition of chromatin from the "10 nm" lower order structure, to the "30 nm" higher order structure as followed by small angle X-ray scattering. *Journal of Molecular Biology*, *193*(4), 709–721. Retrieved from http://www.ncbi.nlm.nih.gov/pubmed/3612790

Gruber, S., Haering, C. H., & Nasmyth, K. (2003). Chromosomal Cohesin Forms a Ring. *Cell*, *112*, 765–777.

Gruber, S., Veening, J. W., Bach, J., Blettinger, M., Bramkamp, M., & Errington, J. (2014). Interlinked sister chromosomes arise in the absence of condensin during fast replication in B. subtilis. *Current Biology*, *24*(3), 293–298. http://doi.org/10.1016/j.cub.2013.12.049

Guo, M., Davis, D., & Birchler, J. a. (1996). Dosage effects on gene expression in a maize ploidy series. *Genetics*, *142*(4), 1349–1355. http://doi.org/10.1016/0168-9525(96)81463-6

Haeusler, R. A., Pratt-hyatt, M., Good, P. D., Gipson, T. A., & Engelke, D. R. (2008). Clustering of yeast tRNA genes is mediated by specific association of condensin with tRNA gene transcription complexes. *Genes & Development*, *22*, 2204–2214. http://doi.org/10.1101/gad.1675908.Garrard

Hagstrom, K. A., Holmes, V. F., Cozzarelli, N. R., & Meyer, B. J. (2002). C . elegans condensin promotes mitotic chromosome architecture , centromere organization , and sister chromatid segregation during mitosis and meiosis. *Genes & Development*, *16*, 729–742. http://doi.org/10.1101/gad.968302.and

Ham, M. F., Takakuwa, T., Rahadiani, N., Tresnasari, K., Nakajima, H., & Aozasa, K. (2007). Condensin mutations and abnormal chromosomal structures in pyothorax-associated lymphoma. *Cancer Science*, *98*(7), 1041–7. http://doi.org/10.1111/j.1349-7006.2007.00500.x

Hara, K., Zheng, G., Qu, Q., Liu, H., Ouyang, Z., Chen, Z., … Yu, H. (2014). Structure of cohesin subcomplex pinpoints direct shugoshin-Wapl antagonism in

centromeric cohesion. *Nature Structural & Molecular Biology*, *21*(10), 864–870. http://doi.org/10.1038/nsmb.2880

Hardwick, K. G., Johnston, R. C., Smith, D. L., & Murray, A. W. (2000). MAD3 encodes a novel component of the spindle checkpoint which interacts with Bub3p, Cdc20p, and Mad2p. *Journal of Cell Biology*, *148*(5), 871–882. http://doi.org/10.1083/jcb.148.5.871

Hardy, C. D., Crisona, N. J., Stone, M. D., & Cozzarelli, N. R. (2004). Disentangling DNA during replication: a tale of two strands. *Philosophical Transactions of the Royal Society of London. Series B, Biological Sciences*, *359*(1441), 39–47. http://doi.org/10.1098/rstb.2003.1363

Hardy, R., Carmack, C., Shinton, S., Kemp, J., & Hayakawa, K. (1991). Resolution and Characterization of Pro-B and Pre-Pro-B Cell Stages in Normal Mouse Bone Marrow. *Journal of Experimental Medicine*, *173*, 1213 –1225.

Hardy, R. R., & Hayakawa, K. (2001). B cell development pathways, 595–621.

Hartl, T. a, Sweeney, S. J., Knepler, P. J., & Bosco, G. (2008). Condensin II resolves chromosomal associations to enable anaphase I segregation in Drosophila male meiosis. *PLoS Genetics*, *4*(10), e1000228. http://doi.org/10.1371/journal.pgen.1000228

Hartl, T., Smith, H., & Bosco, G. (2008). Chromosome alignment and Transvection are antagonized by Condensin II. *Science*, *322*(November), 1384–1387.

Hauf, S., Roitinger, E., Koch, B., Dittrich, C. M., Mechtler, K., & Peters, J. M. (2005). Dissociation of cohesin from chromosome arms and loss of arm cohesion during early mitosis depends on phosphorylation of SA2. *PLoS Biology*, *3*(3), 0419–0432. http://doi.org/10.1371/journal.pbio.0030069

Hauf, S., Waizenegger, I. C., & Peters, J. M. (2001). Cohesin cleavage by separase required for anaphase and cytokinesis in human cells. *Science (New York, N.Y.)*, *293*(5533), 1320–1323. http://doi.org/10.1126/science.1061376

Heale, J. T., Ball, A. R., Schmiesing, J. a., Kim, J. S., Kong, X., Zhou, S., … Yokomori, K. (2006). Condensin I interacts with the PARP-1-XRCC1 complex and functions in DNA single-strand break repair. *Molecular Cell*, *21*(6), 837–848. http://doi.org/10.1016/j.molcel.2006.01.036

Herrick, J., & Bensimon, a. (1999). Single molecule analysis of DNA replication. *Biochimie*, *81*(8-9), 859–71. http://doi.org/10.1016/S0300-9084(99)00210-2

Hirano, T. (2000). CHROMOSOME COHESION , CONDENSATION , AND SEPARATION. *Annual Review of Biochemistry*, *69*, 115 – 144.

Hirano, T. (2005). Condensins: organizing and segregating the genome. *Current Biology : CB*, *15*(7), R265–75. http://doi.org/10.1016/j.cub.2005.03.037

Hirano, T. (2012). Condensins: universal organizers of chromosomes with diverse functions. *Genes & Development*, *26*(15), 1659–78. http://doi.org/10.1101/gad.194746.112

Hirano, T., Kobayashi, R., & Hirano, M. (1997). Condensins, chromosome condensation protein complexes containing XCAP-C, XCAP-E and a Xenopus homolog of the Drosophila Barren protein. *Cell*, *89*(4), 511–21. Retrieved from http://www.ncbi.nlm.nih.gov/pubmed/9160743

Hirano, T., & Mitchison, T. J. (1993). Topoisomerase II does not play a scaffolding role in the organization of mitotic chromosomes assembled in Xenopus egg extracts. *The Journal of Cell Biology*, *120*(3), 601–12. Retrieved from http://www.pubmedcentral.nih.gov/articlerender.fcgi?artid=2119547&tool=pmcentrez&rendertype=abstract

Hirano, T., & Mitchison, T. J. (1994). A heterodimeric coiled-coil protein required for mitotic chromosome condensation in vitro. *Cell*, *79*(3), 449–58. Retrieved from http://www.ncbi.nlm.nih.gov/pubmed/7954811

Ho, I.-C., Tai, T.-S., & Pai, S.-Y. (2009). GATA3 and the T-cell lineage: essential functions before and after T-helper-2-cell differentiation. *Nature Reviews. Immunology*, *9*(2), 125–135. http://doi.org/10.1038/nri2476

Holland, A. J., & Cleveland, D. W. (2009). Boveri revisited: chromosomal instability, aneuploidy and tumorigenesis. *Nature Reviews. Molecular Cell Biology*, *10*(7), 478–87. http://doi.org/10.1038/nrm2718

Holm, C., Goto, T., Wang, J. C., & Botstein, D. (1985). DNA topoisomerase II is required at the time of mitosis in yeast. *Cell*, *41*(2), 553–563. http://doi.org/10.1016/S0092-8674(85)80028-3

Hosoya, T., Kuroha, T., Moriguchi, T., Cummings, D., Maillard, I., Lim, K.-C., & Engel, J. D. (2009). GATA-3 is required for early T lineage progenitor development. *The Journal of Experimental Medicine*, *206*(13), 2987–3000. http://doi.org/10.1084/jem.20090934

Houlard, M., Godwin, J., Metson, J., Lee, J., Hirano, T., & Nasmyth, K. (2015).

Condensin confers the longitudinal rigidity of chromosomes. *Nature Cell Biology*, *17*(6). http://doi.org/10.1038/ncb3167

Huang, E. Y., Gallegos, A. M., Richards, S. M., Lehar, S. M., & Bevan, M. J. (2003). Surface expression of Notch1 on thymocytes: correlation with the double-negative to double-positive transition. *Journal of Immunology (Baltimore, Md. : 1950)*, *171*(5), 2296–2304. http://doi.org/10.4049/jimmunol.171.5.2296

Hudson, D. F., Vagnarelli, P., Gassmann, R., & Earnshaw, W. C. (2003). Condensin is required for nonhistone protein assembly and structural integrity of vertebrate mitotic chromosomes. *Developmental Cell*, *5*(2), 323–36. Retrieved from http://www.ncbi.nlm.nih.gov/pubmed/12919682

Hudson, D., Ohta, S., Freisinger, T., MacIsaac, F., Sennels, L., Alves, F., … Earnshaw, W. C. (2008). Molecular and Genetic Analysis of Condensin Function in Vertebrate Cells. *Molecular Biology of the Cell*, *19*, 3070–3079. http://doi.org/10.1091/mbc.E08

Hwang, L. H. (1998). Budding Yeast Cdc20: A Target of the Spindle Checkpoint. *Science*, *279*(5353), 1041–1044. http://doi.org/10.1126/science.279.5353.1041

Ikuta, K., & Weissman, I. L. (1992). Evidence that hematopoietic stem cells express mouse c-kit but do not depend on steel factor for their generation. *Proceedings of the National Academy of Sciences of the United States of America*, *89*(4), 1502–1506. http://doi.org/10.1073/pnas.89.4.1502

Iwasaki, H., & Akashi, K. (2007). Hematopoietic developmental pathways: on cellular basis. *Oncogene*, *26*(47), 6687–6696. http://doi.org/10.1038/sj.onc.1210754

Jacks, T., Remington, L., Williams, B. O., Schmitt, E. M., Halachmi, S., Bronson, R. T., & Weinberg, R. a. (1994). Tumor spectrum analysis in p53-mutant mice. *Current Biology : CB*, *4*(1), 1–7. Retrieved from http://www.ncbi.nlm.nih.gov/pubmed/7922305

Jackson, D. a, Dickinson, P., & Cook, P. R. (1990). The size of chromatin loops in HeLa cells. *The EMBO Journal*, *9*(2), 567–571.

Je, E. M., Yoo, N. J., & Lee, S. H. (2014). Mutational and expressional analysis of SMC2 gene in gastric and colorectal cancers with microsatellite instability. *APMIS : Acta Pathologica, Microbiologica, et Immunologica Scandinavica*, *122*(6), 499–504. http://doi.org/10.1111/apm.12193

Jeganathan, K., Malureanu, L., Baker, D. J., Abraham, S. C., & van Deursen, J. M.

(2007). Bub1 mediates cell death in response to chromosome missegregation and acts to suppress spontaneous tumorigenesis. *The Journal of Cell Biology*, *179*(2), 255–67. http://doi.org/10.1083/jcb.200706015

Ji, P., Murata-Hori, M., & Lodish, H. F. (2011). Formation of mammalian erythrocytes: chromatin condensation and enucleation. *Trends in Cell Biology*, *21*(7), 409–15. http://doi.org/10.1016/j.tcb.2011.04.003

Johmura, Y., Shimada, M., Misaki, T., Naiki-Ito, A., Miyoshi, H., Motoyama, N., … Nakanishi, M. (2014). Necessary and sufficient role for a mitosis skip in senescence induction. *Molecular Cell*, *55*(1), 73–84. http://doi.org/10.1016/j.molcel.2014.05.003

Jorgensen, P., Edgington, N. P., Schneider, B. L., Rupes, I., Tyers, M., & Futcher, B. (2007). The size of the nucleus increases as yeast cells grow. *Molecular Biology of the Cell*, *18*(9), 3523–3532. http://doi.org/10.1091/mbc.E06-10-0973

Kagami, Y., Nihira, K., Wada, S., Ono, M., Honda, M., & Yoshida, K. (2014). Mps1 phosphorylation of condensin II controls chromosome condensation at the onset of mitosis. *The Journal of Cell Biology*, *205*(6), 781–90. http://doi.org/10.1083/jcb.201308172

Kas, E., & Chasin, L. A. (n.d.). No Title. *J. Mol. Biol.*, *1987*, 677–692.

Keerthivasan, G., Wickrema, A., & Crispino, J. D. (2011). Erythroblast Enucleation. *Stem Cells International*, *2011*, 1–9. http://doi.org/10.4061/2011/139851

Khodursky, A. B., Zechiedrich, E. L., & Cozzarelli, N. R. (1995). Topoisomerase IV is a target of quinolones in Escherichia coli. *Proceedings of the National Academy of Sciences*, *92*(December), 11801–11805.

Kim, S. H. (1998). Fission Yeast Slp1: An Effector of the Mad2-Dependent Spindle Checkpoint. *Science*, *279*(5353), 1045–1047. http://doi.org/10.1126/science.279.5353.1045

Kim, S. H., McQueen, P. G., Lichtman, M. K., Shevach, E. M., Parada, L. a., & Misteli, T. (2004). Spatial genome organization during T-cell differentiation. *Cytogenetic and Genome Research*, *105*(2-4), 292–301. http://doi.org/10.1159/000078201

Kimura, K., Hirano, M., Kobayashi, R., & Hirano, T. (1998). Phosphorylation and activation of 13S condensin by Cdc2 in vitro. *Science (New York, N.Y.)*, *282*(5388), 487–490. http://doi.org/10.1126/science.282.5388.487

Kimura, K., & Hirano, T. (1997). ATP-Dependent Positive Supercoiling of DNA by 13S Condensin : A Biochemical Implication, *90*, 625–634.

Kimura, K., Rybenkov, V. V, Crisona, N. J., Hirano, T., & Cozzarelli, N. R. (1999). 13S Condensin Actively Reconfigures DNA by Introducing Global Positive Writhe : Implications for Chromosome Condensation. *Cell*, *98*, 239–248.

Kimura, M., Koseki, Y., Yamashita, M., Watanabe, N., Shimizu, C., Katsumoto, T., … Nakayama, T. (2001). Regulation of Th2 cell differentiation by mel-18, a mammalian Polycomb group gene. *Immunity*, *15*(2), 275–287. http://doi.org/10.1016/S1074-7613(01)00182-0

Kitajima, T. S., Sakuno, T., Ishiguro, K., Iemura, S., Natsume, T., Kawashima, S. a, & Watanabe, Y. (2006). Shugoshin collaborates with protein phosphatase 2A to protect cohesin. *Nature*, *441*(7089), 46–52. http://doi.org/10.1038/nature04663

Knouse, K. a., Wu, J., Whittaker, C. a., & Amon, A. (2014). Single cell sequencing reveals low levels of aneuploidy across mammalian tissues. *Proceedings of the National Academy of Sciences*, *111*(37), 13409–13414. http://doi.org/10.1073/pnas.1415287111

Koch, U., & Radtke, F. (2011). Mechanisms of T cell development and transformation. *Annual Review of Cell and Developmental Biology*, *27*, 539–62. http://doi.org/10.1146/annurev-cellbio-092910-154008

Kornberg, R. (1974). Chromatin Structure : A Repeating Unit of Histones and DNA Chromatin structure is based on a repeating unit of eight. *Science*, *184*, 868–871.

Koury, S. T., Koury, M. J., & Bondurant, M. C. (1989). Cytoskeletal distribution and function during the maturation and enucleation of mammalian erythroblasts. *Journal of Cell Biology*, *109*(6 I), 3005–3013. http://doi.org/10.1083/jcb.109.6.3005

Kouzine, F., Levens, D., & Baranello, L. (2014). DNA topology and transcription. *Nucleus (Austin, Tex.)*, *5*(3). http://doi.org/10.4161/nucl.28909

Kouzine, F., Liu, J., Sanford, S., Chung, H.-J., & Levens, D. (2004). The dynamic response of upstream DNA to transcription-generated torsional stress. *Nature Structural & Molecular Biology*, *11*(11), 1092–1100. http://doi.org/10.1038/nsmb848

Kruesi, W. S., Core, L. J., Waters, C. T., Lis, J. T., & Meyer, B. J. (2013). Condensin controls recruitment of RNA polymerase II to achieve nematode X-chromosome

dosage compensation. *eLife*, *2*(Pol II), e00808. http://doi.org/10.7554/eLife.00808

Kulukian, A., Seok Han, J., & Cleveland, D. W. (2009). Unattached Kinetochores Catalyze Production of an Anaphase Inhibitor that Requires a Mad2 Template to Prime Cdc20 for BubR1 Binding. *Developmental Cell*, *16*(1), 105–117. http://doi.org/10.1016/j.devcel.2008.11.005.Unattached

Kumagai, A., Shevchenko, A., Shevchenko, A., & Dunphy, W. G. (2010). Treslin Collaborates with TopBP1 in Triggering the Initiation of DNA Replication. *Cell*, *140*(3), 349–359. http://doi.org/10.1016/j.cell.2009.12.049

Kumagai, A., Shevchenko, A., Shevchenko, A., & Dunphy, W. G. (2011). Direct regulation of Treslin by cyclin-dependent kinase is essential for the onset of DNA replication. *Journal of Cell Biology*, *193*(6), 995–1007. http://doi.org/10.1083/jcb.201102003

Kyewski, B., & Klein, L. (2006). A central role for central tolerance. *Annual Review of Immunology*, *24*, 571–606. http://doi.org/10.1146/annurev.immunol.23.021704.115601

Laemmli, U. K., Cheng, S. M., Adolph, K. W., Paulson, J. R., Brown, J. A., & Baumbach, W. R. (1978). Metaphase Chromosome Structure: The Role of Nonhistone Proteins. *Cold Spring Harbor Symposia on Quantitative Biology*, *42*, 351 – 360.

Lammens, A., Schele, A., & Hopfner, K. P. (2004). Structural biochemistry of ATP-driven dimerization and DNA-stimulated activation of SMC ATPases. Curr. Biol. 14, 1778–1782. 103. *Current Biology*, *14*, 1778–1782. http://doi.org/10.1016/j

Leiserson, M. D. M., Vandin, F., Wu, H.-T., Dobson, J. R., Eldridge, J. V, Niu, B., … Raphael, B. J. (2015). PanCancer Network Analysis Identifies Combinations of Rare Somatic Mutations across Pathways and Protein Complexes. *Nature Genetics*, *47*(2). http://doi.org/10.1038/ng.3168

Lettice, L. A. (2003). A long-range Shh enhancer regulates expression in the developing limb and fin and is associated with preaxial polydactyly. *Human Molecular Genetics*, *12*(14), 1725–1735. http://doi.org/10.1093/hmg/ddg180

Li, M., Fang, X., Wei, Z., York, J. P., & Zhang, P. (2009). Loss of spindle assembly checkpoint-mediated inhibition of Cdc20 promotes tumorigenesis in mice. *The Journal of Cell Biology*, *185*(6), 983–94. http://doi.org/10.1083/jcb.200904020

Li, W., Hu, Y., Oh, S., Ma, Q., Merkurjev, D., Song, X., … Rosenfeld, M. G. (2015). Condensin I and II Complexes License Full Estrogen Receptor α-Dependent Enhancer Activation. *Molecular Cell*, 1–15. http://doi.org/10.1016/j.molcel.2015.06.002

Li, Y., Stewart, N. K., Berger, A. J., Vos, S., Schoeffler, A. J., Berger, J. M., … Oakley, M. G. (2010). Escherichia coli condensin MukB stimulates topoisomerase IV activity by a direct physical interaction. *Proceedings of the National Academy of Sciences of the United States of America*, *107*(44), 18832–18837. http://doi.org/10.1073/pnas.1008678107

Liang, Z., Zickler, D., Prentiss, M., Chang, F. S., Witz, G., Maeshima, K., & Kleckner, N. (2015). Chromosomes Progress to Metaphase in Multiple Discrete Steps via Global Compaction/Expansion Cycles. *Cell*, *161*(5), 1124–1137. http://doi.org/10.1016/j.cell.2015.04.030

Liao, M., Zhang, X., Hill, R., Gao, J., Qumsiyeh, B., Nichols, W., … Dyke, T. V. A. N. (1998). No Requirement for V (D) J Recombination in p53-Deficient Thymic Lymphoma. *Molecular and Cellular Biology*, *18*(6), 3495 – 3501.

Lieberman-aiden, E., Berkum, N. L. Van, Williams, L., Ragoczy, T., Telling, A., Amit, I., … Leonid, A. (2010). Comprehensive mapping of long range interactions reveals folding principles of the human genome, *326*(5950), 289–293. http://doi.org/10.1126/science.1181369.Comprehensive

Lin, H. (2002). The stem-cell niche theory: lessons from flies. *Nature Reviews. Genetics*, *3*(12), 931–940. http://doi.org/10.1038/nrg952

Liu, H., Rankin, S., & Yu, H. (2013). Phosphorylation-enabled binding of SGO1-PP2A to cohesin protects sororin and centromeric cohesion during mitosis. *Nature Cell Biology*, *15*(1), 40–9. http://doi.org/10.1038/ncb2637

Liu, J., & Krantz, I. (2010). Cornelia de Lange syndrome, cohesin and beyond. *Clinical Genetics*, *76*(4), 303–314. http://doi.org/10.1111/j.1399-0004.2009.01271.x.Cornelia

Liu, J., Zhang, Z., Bando, M., Itoh, T., Deardorff, M. a, Clark, D., … Krantz, I. D. (2009). Transcriptional dysregulation in NIPBL and cohesin mutant human cells. *PLoS Biology*, *7*(5), e1000119. http://doi.org/10.1371/journal.pbio.1000119

Liu, L. F., & Wang, J. C. (1987). Supercoiling of the DNA template during transcription. *Proceedings of the National Academy of Sciences of the United*

States of America, *84*(20), 7024–7027. http://doi.org/10.1073/pnas.84.20.7024

Liu, Y., Malureanu, L., Jeganathan, K. B., Tran, D. D., Linduist, L. D., van Deursen, J. M., & Bram, R. J. (2009). CAML loss causes anaphase failure and chromosome missegregation. *Cell Cycle*, *8*(6), 940–949. http://doi.org/10.1111/j.1600-6143.2008.02497.x.Plasma

Longworth, M. S., Herr, A., Ji, J.-Y., & Dyson, N. J. (2008). RBF1 promotes chromatin condensation through a conserved interaction with the Condensin II protein dCAP-D3. *Genes & Development*, *22*(8), 1011–24. http://doi.org/10.1101/gad.1631508

Lucas, I., Germe, T., Chevrier-Miller, M., & Hyrien, O. (2001). Topoisomerase II can unlink replicating DNA by precatenane removal. *EMBO Journal*, *20*(22), 6509–6519. http://doi.org/10.1093/emboj/20.22.6509

Manning, A. L., Longworth, M. S., & Dyson, N. J. (2010). Loss of pRB causes centromere dysfunction and chromosomal instability. *Genes & Development*, *24*(13), 1364–76. http://doi.org/10.1101/gad.1917310

Manuelidis, L. (1985). Indications of centromere movement during interphase and differentiation. *Annals of the New York Academy of Sciences*, *450*, 205–221.

Marciniak-Czochra, A., Stiehl, T., Ho, A. D., Jäger, W., & Wagner, W. (2009). Modeling of asymmetric cell division in hematopoietic stem cells--regulation of self-renewal is essential for efficient repopulation. *Stem Cells and Development*, *18*(3), 377–385. http://doi.org/10.1089/scd.2008.0143

Martínez-Robles, M. L., Witz, G., Hernández, P., Schvartzman, J. B., Stasiak, A., & Krimer, D. B. (2009). Interplay of DNA supercoiling and catenation during the segregation of sister duplexes. *Nucleic Acids Research*, *37*(15), 5126–5137. http://doi.org/10.1093/nar/gkp530

Matsuno, K., Kumano, M., Kubota, Y., Hashimoto, Y., & Takisawa, H. (2006). The N-terminal noncatalytic region of Xenopus RecQ4 is required for chromatin binding of DNA polymerase alpha in the initiation of DNA replication. *Molecular and Cellular Biology*, *26*(13), 4843–4852. http://doi.org/10.1128/MCB.02267-05

Mayer, R., Brero, A., von Hase, J., Schroeder, T., Cremer, T., & Dietzel, S. (2005). Common themes and cell type specific variations of higher order chromatin arrangements in the mouse. *BMC Cell Biology*, *6*, 44. http://doi.org/10.1186/1471-2121-6-44

Mazouzi, A., Velimezi, G., & Loizou, J. I. (2014). DNA replication stress: Causes, resolution and disease. *Experimental Cell Research*, *329*, 85–93. http://doi.org/10.1016/j.yexcr.2014.09.030

Meister, P., & Taddei, A. (2013). Building silent compartments at the nuclear periphery: A recurrent theme. *Current Opinion in Genetics and Development*, *23*(2), 96–103. http://doi.org/10.1016/j.gde.2012.12.001

Mejlvang, J., Feng, Y., Alabert, C., Neelsen, K. J., Jasencakova, Z., Zhao, X., … Groth, A. (2014). New histone supply regulates replication fork speed and PCNA unloading. *Journal of Cell Biology*, *204*(1), 29–43. http://doi.org/10.1083/jcb.201305017

Melby, T. E., Ciampaglio, C. N., Briscoe, G., & Erickson, H. P. (1998). The symmetrical structure of structural maintenance of chromosomes (SMC) and MukB proteins: Long, antiparallel coiled coils, folded at a flexible hinge. *Journal of Cell Biology*, *142*(6), 1595–1604. http://doi.org/10.1083/jcb.142.6.1595

Merrick, C. J., Jackson, D., & Diffley, J. F. X. (2004). Visualization of altered replication dynamics after DNA damage in human cells. *The Journal of Biological Chemistry*, *279*(19), 20067–20075. http://doi.org/10.1074/jbc.M400022200

Michaelis, C., Ciosk, R., & Nasmyth, K. (1997). Cohesins: Chromosomal proteins that prevent premature separation of sister chromatids. *Cell*, *91*(1), 35–45. http://doi.org/10.1016/S0092-8674(01)80007-6

Michalet, X., Ekong, R., Fougerousse, F., Rousseaux, S., Schurra, C., Hornigold, N., … Bensimon, a. (1997). Dynamic molecular combing: stretching the whole human genome for high-resolution studies. *Science (New York, N.Y.)*, *277*(5331), 1518–1523. http://doi.org/10.1126/science.277.5331.1518

Micklem, H. S., & Loutit, J. F. (1966). Tissue Grafting and Radiation. *New York Academy of Sciences Press, New York*.

Minnen, A., Attaiech, L., Thon, M., Gruber, S., & Veening, J. W. (2011). SMC is recruited to oriC by ParB and promotes chromosome segregation in Streptococcus pneumoniae. *Molecular Microbiology*, *81*(3), 676–688. http://doi.org/10.1111/j.1365-2958.2011.07722.x

Miosge, L. A., & Goodnow, C. C. (2005). Genes, pathways and checkpoints in lymphocyte development and homeostasis. *Immunology and Cell Biology*.

http://doi.org/10.1111/j.1440-1711.2005.01353.x

Mirkin, E. V, & Mirkin, S. M. (2005). Mechanisms of transcription-replication collisions in bacteria. *Molecular and Cellular Biology*, *25*(3), 888–895. http://doi.org/10.1128/MCB.25.3.888-895.2005

Mirkovitch, J., Spierer, P., & Laemmli, U. K. (1986). Genes and loops in 320,000 base-pairs of the Drosophila melanogaster chromosome. *Journal of Molecular Biology*, *190*(2), 255–258. http://doi.org/10.1016/0022-2836(86)90296-2

Mishra, A., Hu, B., Kurze, A., Beckouët, F., Farcas, A. M., Dixon, S. E., … Nasmyth, K. (2010). Both Interaction Surfaces within Cohesin's Hinge Domain Are Essential for Its Stable Chromosomal Association. *Current Biology*, *20*(4), 279–289. http://doi.org/10.1016/j.cub.2009.12.059

Mizuguchi, T., Fudenberg, G., Mehta, S., Belton, J.-M., Taneja, N., Folco, H. D., … Grewal, S. I. S. (2014). Cohesin-dependent globules and heterochromatin shape 3D genome architecture in S. pombe. *Nature*, *516*(7531), 432–435. Retrieved from http://dx.doi.org/10.1038/nature13833

Mombaerts, P., Iacomini, J., Johnson, R. S., Herrup, K., Tonegawa, S., & Papaioannou, V. E. (1992). RAG-1-deficient mice have no mature B and T lymphocytes. *Cell*, *68*(5), 869–877. http://doi.org/10.1016/0092-8674(92)90030-G

Morey, C., Da Silva, N. R., Perry, P., & Bickmore, W. A. (2007). Nuclear reorganisation and chromatin decondensation are conserved, but distinct, mechanisms linked to Hox gene activation. *Development (Cambridge, England)*, *134*(5), 909–919. http://doi.org/10.1242/dev.02779

Morris, D. R., & Geballe, a P. (2000). Upstream open reading frames as regulators of mRNA translation. *Molecular and Cellular Biology*, *20*(23), 8635–8642. http://doi.org/10.1128/MCB.20.23.8635-8642.2000

Müller, I., Boyle, S., Singer, R. H., Bickmore, W. a., & Chubb, J. R. (2010). Stable morphology, but dynamic internal reorganisation, of interphase human chromosomes in living cells. *PLoS ONE*, *5*(7). http://doi.org/10.1371/journal.pone.0011560

Nasmyth, K., & Haering, C. H. (2005). The structure and function of SMC and kleisin complexes. *Annual Review of Biochemistry*, *74*, 595–648. http://doi.org/10.1146/annurev.biochem.74.082803.133219

Naughton, C., Avlonitis, N., Corless, S., Prendergast, J. G., Mati, I. K., Eijk, P. P., … Gilbert, N. (2013). Transcription forms and remodels supercoiling domains unfolding large-scale chromatin structures. *Nature Structural & Molecular Biology*, *20*(3), 387–95. http://doi.org/10.1038/nsmb.2509

Naumova, N., Imakaev, M., Fudenberg, G., Zhan, Y., Lajoie, B. R., Mirny, L. a, & Dekker, J. (2013). Organization of the mitotic chromosome. *Science (New York, N.Y.)*, *342*(6161), 948–53. http://doi.org/10.1126/science.1236083

Neganova, I., & Lako, M. (2008). G1 to S phase cell cycle transition in somatic and embryonic stem cells. *Journal of Anatomy*, *213*(1), 30–44. http://doi.org/10.1111/j.1469-7580.2008.00931.x

Nishide, K., & Hirano, T. (2014). Overlapping and Non-overlapping Functions of Condensins I and II in Neural Stem Cell Divisions. *PLoS Genetics*, *10*(12), e1004847. http://doi.org/10.1371/journal.pgen.1004847

Nishino, Y., Eltsov, M., Joti, Y., Ito, K., Takata, H., Takahashi, Y., … Maeshima, K. (2012). Human mitotic chromosomes consist predominantly of irregularly folded nucleosome fibres without a 30-nm chromatin structure. *The EMBO Journal*, *31*(7), 1644–53. http://doi.org/10.1038/emboj.2012.35

Ohta, H., Sawada, A., Kim, J. Y., Tokimasa, S., Nishiguchi, S., Humphries, R. K., … Takihara, Y. (2002). Polycomb group gene rae28 is required for sustaining activity of hematopoietic stem cells. *The Journal of Experimental Medicine*, *195*(6), 759–770. http://doi.org/10.1084/jem.20011911

Ohta, S., Bukowski-Wills, J. C., Sanchez-Pulido, L., Alves, F. D. L., Wood, L., Chen, Z. a., … Rappsilber, J. (2010). The Protein Composition of Mitotic Chromosomes Determined Using Multiclassifier Combinatorial Proteomics. *Cell*, *142*(5), 810–821. http://doi.org/10.1016/j.cell.2010.07.047

Okada, T. a, & Comings, D. E. (1980). A search for protein cores in chromosomes: is the scaffold an artifact? *American Journal of Human Genetics*, *32*(6), 814–832.

Oliveira, R. a, Hamilton, R. S., Pauli, A., Davis, I., & Nasmyth, K. (2010). Cohesin cleavage and Cdk inhibition trigger formation of daughter nuclei. *Nature Cell Biology*, *12*(2), 185–192. http://doi.org/10.1038/ncb2018

Oliveira, R. A., & Nasmyth, K. (2010). Getting through anaphase: splitting the sisters and beyond. *Biochemical Society Transactions*, *38*(6), 1639–1644. http://doi.org/10.1042/BST0381639

Olsen, J. V, Vermeulen, M., Santamaria, A., Kumar, C., Miller, M. L., Jensen, L. J., … Mann, M. (2010). Quantitative phosphoproteomics reveals widespread full phosphorylation site occupancy during mitosis. *Science Signaling*, *3*(104), ra3. http://doi.org/10.1126/scisignal.2000475

Ong, C.-T., & Corces, V. (2011). Enhancer function: new insights into the regulation of tissue- specific gene expression. *Nat Rev Genet*, *12*(4), 283–293. http://doi.org/10.1038/nrg2957.Enhancer

Ono, T., Fang, Y., Spector, D. L., & Hirano, T. (2004). Spatial and temporal regulation of Condensins I and II in mitotic chromosome assembly in human cells. *Molecular Biology of the Cell*, *15*(7), 3296–308. http://doi.org/10.1091/mbc.E04-03-0242

Ono, T., Losada, A., Hirano, M., Myers, M. P., Neuwald, A. F., & Hirano, T. (2003). Differential contributions of condensin I and condensin II to mitotic chromosome architecture in vertebrate cells. *Cell*, *115*(1), 109–21. Retrieved from http://www.ncbi.nlm.nih.gov/pubmed/14532007

Ono, T., Yamashita, D., & Hirano, T. (2013). Condensin II initiates sister chromatid resolution during S phase. *Journal of Cell Biology*, *200*(4), 429–441. http://doi.org/10.1083/jcb.201208008

Papp, B., Pál, C., & Hurst, L. D. (2003). Dosage sensitivity and the evolution of gene families in yeast. *Nature*, *424*(6945), 194–197. http://doi.org/10.1038/nature01771

Perche, O., Menuet, A., Marcos, M., Liu, L., Pâris, A., Utami, K. H., … Briault, S. (2013). Combined deletion of two Condensin II system genes (NCAPG2 and MCPH1) in a case of severe microcephaly and mental deficiency. *European Journal of Medical Genetics*, *56*(11), 635–641. http://doi.org/10.1016/j.ejmg.2013.07.007

Peric-Hupkes, D., Meuleman, W., Pagie, L., Bruggeman, S. W. M., Solovei, I., Brugman, W., … van Steensel, B. (2010). Molecular maps of the reorganization of genome-nuclear lamina interactions during differentiation. *Molecular Cell*, *38*(4), 603–13. http://doi.org/10.1016/j.molcel.2010.03.016

Perry, J. a, & Kornbluth, S. (2007). Cdc25 and Wee1: analogous opposites? *Cell Division*, *2*, 12. http://doi.org/10.1186/1747-1028-2-12

Peter, B. J., Ullsperger, C., Hiasa, H., Marians, K. J., & Cozzarelli, N. R. (1998). The

structure of supercoiled intermediates in DNA replication. *Cell*, *94*(6), 819–827. http://doi.org/10.1016/S0092-8674(00)81740-7

Pezzulo, A. a, Tang, X. X., Hoegger, M. J., Alaiwa, M. H. A., Ramachandran, S., Moninger, T. O., … College, L. a C. (2013). Transcription dependent dynamic supercoiling is a short-range genomic force. *Nat Struct Biol*, *487*(7405), 109–113. http://doi.org/10.1038/nature11130.Reduced

Pfau, S. J., & Amon, A. (2012). Chromosomal instability and aneuploidy in cancer: from yeast to man. *EMBO Reports*, *13*(6), 515–27. http://doi.org/10.1038/embor.2012.65

Piazza, I., Rutkowska, A., Ori, A., Walczak, M., Metz, J., Pelechano, V., … Haering, C. H. (2014). Association of condensin with chromosomes depends on DNA binding by its HEAT-repeat subunits. *Nature Structural & Molecular Biology*, *21*(6), 560–568. http://doi.org/10.1038/nsmb.2831

Postow, L., Crisona, N. J., Peter, B. J., Hardy, C. D., & Cozzarelli, N. R. (2001). Topological challenges to DNA replication : Conformations at the fork. *PNAS*, *98*(15), 8219–8226.

Qian, J., Beullens, M., Lesage, B., & Bollen, M. (2013). Aurora B defines its own chromosomal targeting by opposing the recruitment of the phosphatase scaffold Repo-Man. *Current Biology*, *23*(12), 1136–1143. http://doi.org/10.1016/j.cub.2013.05.017

Raaphorst, F. M., Otte, A. P., & Meijer, C. J. L. M. (2001). Polycomb-group genes as regulators of mammalian lymphopoiesis. *Trends in Immunology*, *22*(12), 682–690. http://doi.org/10.1016/S1471-4906(01)02082-8

Rafique, S., Thomas, J. S., Sproul, D., & Bickmore, W. a. (2015). Estrogen-induced chromatin decondensation and nuclear re-organization linked to regional epigenetic regulation in breast cancer. *Genome Biology*, *16*(1), 145. http://doi.org/10.1186/s13059-015-0719-9

Rao, C. V, Yang, Y.-M., Swamy, M. V, Liu, T., Fang, Y., Mahmood, R., … Dai, W. (2005). Colonic tumorigenesis in BubR1+/-ApcMin/+ compound mutant mice is linked to premature separation of sister chromatids and enhanced genomic instability. *Proceedings of the National Academy of Sciences of the United States of America*, *102*(12), 4365–70. http://doi.org/10.1073/pnas.0407822102

Rawlings, J. S., Gatzka, M., Thomas, P. G., & Ihle, J. N. (2011). Chromatin

condensation via the condensin II complex is required for peripheral T-cell quiescence. *The EMBO Journal*, *30*(2), 263–76. http://doi.org/10.1038/emboj.2010.314

Razin, S., Hancock, R., Iarovaia, O., Westergaad, O., Gromova, I., & Georgiev, G. (1993). Structural–functional organization of chromosomal domains. 58, 25–35. *Cold Spring Harbor Symp. Quant. Biol.*, *58*, 25–35.

Reichman-Fried, M., Hardy, R. R., & Bosma, M. J. (1990). Development of B-lineage cells in the bone marrow of scid/scid mice following the introduction of functionally rearranged immunoglobulin transgenes. *Proceedings of the National Academy of Sciences of the United States of America*, *87*(7), 2730–2734. http://doi.org/10.1073/pnas.87.7.2730

Remeseiro, S., Cuadrado, A., Carretero, M., Martínez, P., Drosopoulos, W. C., Cañamero, M., … Losada, A. (2012). Cohesin-SA1 deficiency drives aneuploidy and tumourigenesis in mice due to impaired replication of telomeres. *The EMBO Journal*, *31*(9), 2076–89. http://doi.org/10.1038/emboj.2012.11

Repasky, E. A., & Eckert, B. S. (1981). A reevaluation of the process of enucleation in mammalian erythroid cells. *Progress in Clinical and Biological Research*, *55*, 679–692.

Revenkova, E., Focarelli, M. L., Susani, L., Paulis, M., Bassi, M. T., Mannini, L., … Musio, A. (2009). Cornelia de Lange syndrome mutations in SMC1A or SMC3 affect binding to DNA. *Human Molecular Genetics*, *18*(3), 418–427. http://doi.org/10.1093/hmg/ddn369

Ribeiro, S. A., Gatlin, J. C., Dong, Y., Joglekar, A., Cameron, L., Hudson, D. F., … Vagnarelli, P. (2009). Condensin Regulates the Stiffness of Vertebrate Centromeres. *Molecular Biology of the Cell*, *20*, 2371–2380. http://doi.org/10.1091/mbc.E08

Rieder, C. L., & Cole, R. (1999). Chromatid cohesion during mitosis: lessons from meiosis. *Journal of Cell Science*, *112 (Pt 1*, 2607–2613.

Roegiers, F., & Jan, Y. N. (2004). Asymmetric cell division. *Current Opinion in Cell Biology*, *16*(2), 195–205. http://doi.org/10.1016/j.ceb.2004.02.010

Rollins, R. a, Korom, M., Aulner, N., Martens, A., & Dorsett, D. (2004). Drosophila nipped-B protein supports sister chromatid cohesion and opposes the stromalin/Scc3 cohesion factor to facilitate long-range activation of the cut gene.

Molecular and Cellular Biology, *24*(8), 3100–3111. http://doi.org/10.1128/MCB.24.8.3100-3111.2004

Rothenberg, E. V, Moore, J. E., & Yui, M. A. (2008). Launching the T-cell-lineage developmental programme. *Nature Reviews. Immunology*, *8*(1), 9–21. http://doi.org/10.1038/nri2232

Rothenberg, E. V, & Taghon, T. (2005). Molecular genetics of T cell development. *Annual Review of Immunology*, *23*, 601–649. http://doi.org/10.1146/annurev.immunol.23.021704.115737

Sachs, R. K., van den Engh, G., Trask, B., Yokota, H., & Hearst, J. E. (1995). A random-walk/giant-loop model for interphase chromosomes. *Proceedings of the National Academy of Sciences of the United States of America*, *92*(7), 2710–2714. http://doi.org/10.1073/pnas.92.7.2710

Saitoh, N., Goldberg, I. G., Wood, E. R., & Earnshaw, W. C. (1994). ScII: An abundant chromosome scaffold protein is a member of a family of putative ATPases with an unusual predicted tertiary structure. *Journal of Cell Biology*, *127*(2), 303–318. http://doi.org/10.1083/jcb.127.2.303

Saitoh, Y., & Laemmli, U. K. (1994). Metaphase chromosome structure: Bands arise from a differential folding path of the highly AT-rich scaffold. *Cell*, *76*(4), 609–622. http://doi.org/10.1016/0092-8674(94)90502-9

Sansam, C. G., Goins, D., Siefert, J. C., Clowdus, E. a, & Sansam, C. L. (2015). Cyclin-dependent kinase regulates the length of S phase through TICRR / TRESLIN phosphorylation. *Genes & Development*, *29*, 555–566. http://doi.org/10.1101/gad.246827.114.GENES

Sansam, C. L., Cruz, N. M., Danielian, P. S., Amsterdam, A., Lau, M. L., Hopkins, N., & Lees, J. a. (2010). A vertebrate gene, ticrr, is an essential checkpoint and replication regulator. *Genes and Development*, *24*(2), 183–194. http://doi.org/10.1101/gad.1860310

Schleiffer, A., Kaitna, S., Maurer-Stroh, S., Glotzer, M., Nasmyth, K., & Eisenhaber, F. (2003). Kleisins: A superfamily of bacterial and eukaryotic SMC protein partners. *Molecular Cell*, *11*(3), 571–575. http://doi.org/10.1016/S1097-2765(03)00108-4

Schmiesing, J. a, Gregson, H. C., Zhou, S., & Yokomori, K. (2000). A human condensin complex containing hCAP-C-hCAP-E and CNAP1, a homolog of

Xenopus XCAP-D2, colocalizes with phosphorylated histone H3 during the early stage of mitotic chromosome condensation. *Molecular and Cellular Biology*, *20*(18), 6996–7006. http://doi.org/10.1128/MCB.20.18.6996-7006.2000

Schmitt, T. M., Ciofani, M., Petrie, H. T., & Zúñiga-Pflücker, J. C. (2004). Maintenance of T cell specification and differentiation requires recurrent notch receptor-ligand interactions. *The Journal of Experimental Medicine*, *200*(4), 469–479. http://doi.org/10.1084/jem.20040394

Seaberg, R. M., & Van Der Kooy, D. (2003). Stem and progenitor cells: The premature desertion of rigorous definitions. *Trends in Neurosciences*, *26*(3), 125–131. http://doi.org/10.1016/S0166-2236(03)00031-6

Seitan, V. C., Hao, B., Tachibana-Konwalski, K., Lavagnolli, T., Mira-Bontenbal, H., Brown, K. E., … Merkenschlager, M. (2011). A role for cohesin in T-cell-receptor rearrangement and thymocyte differentiation. *Nature*, *476*(7361), 467–71. http://doi.org/10.1038/nature10312

Sheltzer, J. M., Torres, E. M., Dunham, M. J., & Amon, A. (2012). Transcriptional consequences of aneuploidy. *PNAS*, *109*(31), 12644–12649. http://doi.org/10.1073/pnas.1209227109/-/DCSupplemental.www.pnas.org/cgi/doi/10.1073/pnas.1209227109

Sheu, Y.-J., Kinney, J. B., Lengronne, A., Pasero, P., & Stillman, B. (2014). Domain within the helicase subunit Mcm4 integrates multiple kinase signals to control DNA replication initiation and fork progression. *Proceedings of the National Academy of Sciences of the United States of America*, *111*(18), E1899–908. http://doi.org/10.1073/pnas.1404063111

Shinkai, Y., Rathbun, G., Lam, K. P., Oltz, E. M., Stewart, V., Mendelsohn, M., … Stall, a M. (1992). RAG-2-deficient mice lack mature lymphocytes owing to inability to initiate V(D)J rearrangement. *Cell*, *68*(5), 855–867. http://doi.org/10.1016/0092-8674(92)90029-C

Shintomi, K., & Hirano, T. (2011). The relative ratio of condensin I to II determines chromosome shapes. *Genes and Development*, *25*, 1464–1469. http://doi.org/10.1101/gad.2060311.1464

Shintomi, K., Takahashi, T. S., & Hirano, T. (2015). Reconstitution of mitotic chromatids with a minimum set of purified factors. *Nature Cell Biology*, *17*(8). http://doi.org/10.1038/ncb3187

Sicinska, E., Aifantis, I., Le Cam, L., Swat, W., Borowski, C., Yu, Q., … Sicinski, P. (2003). Requirement for cyclin D3 in lymphocyte development and T cell leukemias. *Cancer Cell*, *4*(6), 451–461. http://doi.org/10.1016/S1535-6108(03)00301-5

Singer, A. (2002). New perspectives on a developmental dilemma: The kinetic signaling model and the importance of signal duration for the CD4/CD8 lineage decision. *Current Opinion in Immunology*, *14*(2), 207–215. http://doi.org/10.1016/S0952-7915(02)00323-0

Skourti-Stathaki, K., & Proudfoot, N. J. (2014). A double-edged sword: R loops as threats to genome integrity and powerful regulators of gene expression. *Genes and Development*, *28*(13), 1384–1396. http://doi.org/10.1101/gad.242990.114

Skutelsky, E., & Danon, D. (1970). Comparative study of nuclear expulsion from the late erythroblast and cytokinesis. *Cell Research*, *60*(3), 427–436.

Socolovsky, M., Murrell, M., Liu, Y., Pop, R., Porpiglia, E., & Levchenko, A. (2007). Negative autoregulation by FAS mediates robust fetal erythropoiesis. *PLoS Biology*, *5*(10), e252. http://doi.org/10.1371/journal.pbio.0050252

Solovei, I., Grandi, N., Knoth, R., Volk, B., & Cremer, T. (2004). Positional changes of pericentromeric heterochromatin and nucleoli in postmitotic Purkinje cells during murine cerebellum development. *Cytogenetic and Genome Research*, *105*(2-4), 302–310. http://doi.org/10.1159/000078202

Spangrude, G. J., Heimfeld, S., & Weissman, I. L. (1989). Purification and Characterization of Mouse Hematopoietic Stem Cells. *Science*, *241*, 58–62.

Steffensen, S., Coelho, P. a., Cobbe, N., Vass, S., Costa, M., Hassan, B., … Sunkel, C. E. (2001). A role for Drosophila SMC4 in the resolution of sister chromatids in mitosis. *Current Biology*, *11*(5), 295–307. http://doi.org/10.1016/S0960-9822(01)00096-3

Strachan, T. (2005). Cornelia de Lange Syndrome and the link between chromosomal function, DNA repair and developmental gene regulation. *Current Opinion in Genetics and Development*, *15*(3 SPEC. ISS.), 258–264. http://doi.org/10.1016/j.gde.2005.04.005

Strukov, Y. G., Sural, T. H., Kuroda, M. I., & Sedat, J. W. (2011). Evidence of activity-specific, radial organization of mitotic chromosomes in Drosophila. *PLoS Biology*, *9*(1). http://doi.org/10.1371/journal.pbio.1000574

Strunnikov, a. V., Hogan, E., & Koshland, D. (1995). SMC2, a Saccharomyces cerevisiae gene essential for chromosome segregation and condensation, defines a subgroup within the SMC family. *Genes and Development*, *9*(5), 587–599. http://doi.org/10.1101/gad.9.5.587

Stumpf, C., Moreno, M., Olshen, A., Taylor, B., & Ruggero, D. (2013). The translational landscape of the mammalian cell cycle. *Molecular Cell*, *52*(4), 574–582. http://doi.org/10.1016/j.molcel.2013.09.018

Su, R. C., Sridharan, R., & Smale, S. T. (2005). Assembly of silent chromatin during thymocyte development. *Seminars in Immunology*, *17*(2 SPEC. ISS.), 129–140. http://doi.org/10.1016/j.smim.2005.01.003

Sudakin, V., Chan, G. K., & Yen, T. J. (2001). Checkpoint inhibition of the APC/C in HeLa cells is mediated by a complex of BUBR1, BUB3, CDC20, and MAD2. *The Journal of Cell Biology*, *154*(5), 925–36. http://doi.org/10.1083/jcb.200102093

Sullivan, M., & Morgan, D. O. (2007). Finishing mitosis, one step at a time. *Nature Reviews. Molecular Cell Biology*, *8*(11), 894–903. http://doi.org/10.1038/nrm2276

Sullivan, N. L., Marquis, K. A., & Rudner, D. Z. (2009). Recruitment of SMC by ParB-parS Organizes the Origin Region and Promotes Efficient Chromosome Segregation. *Cell*, *137*(4), 697–707. http://doi.org/10.1016/j.cell.2009.04.044

Sundin, O., & Varshavsky, a. (1981). Arrest of segregation leads to accumulation of highly intertwined catenated dimers: dissection of the final stages of SV40 DNA replication. *Cell*, *25*(3), 659–669. http://doi.org/10.1016/0092-8674(81)90173-2

Sundin, O., & Varshavsky, A. (1980). Terminal stages of SV40 DNA replication proceed via multiply intertwined catenated dimers. *Cell*, *21*(1), 103–114. http://doi.org/10.1016/0092-8674(80)90118-X

Symeonidou, I.-E., Taraviras, S., & Lygerou, Z. (2012). Control over DNA replication in time and space. *FEBS Letters*, *586*(18), 2803–2812. http://doi.org/10.1016/j.febslet.2012.07.042

Takeuchi, Y., Horiuchi, T., & Kobayashi, T. (2003). Transcription-dependent recombination and the role of fork collision in yeast rDNA. *Genes and Development*, *17*(12), 1497–1506. http://doi.org/10.1101/gad.1085403

Tanaka, S., & Araki, H. (2013). Helicase activation and establishment of replication

forks at chromosomal origins of replication. *Cold Spring Harbor Perspectives in Biology*, *5*. http://doi.org/10.1101/cshperspect.a010371

Tangye, S. G., & Tarlinton, D. M. (2009). Memory B cells: Effectors of long-lived immune responses. *European Journal of Immunology*. http://doi.org/10.1002/eji.200939531

Tark-Dame, M., Jerabek, H., Manders, E. M. M., Heermann, D. W., & van Driel, R. (2014). Depletion of the Chromatin Looping Proteins CTCF and Cohesin Causes Chromatin Compaction: Insight into Chromatin Folding by Polymer Modelling. *PLoS Computational Biology*, *10*(10), e1003877. http://doi.org/10.1371/journal.pcbi.1003877

Tedeschi, A., Wutz, G., Huet, S., Jaritz, M., Wuensche, A., Schirghuber, E., … Peters, J.-M. (2013). Wapl is an essential regulator of chromatin structure and chromosome segregation. *Nature*, *501*(7468), 564–8. http://doi.org/10.1038/nature12471

Tetsu, O., Ishihara, H., Kanno, R., Kamiyasu, M., Inoue, H., Tokuhisa, T., … Kanno, M. (1998). mel-18 negatively regulates cell cycle progression upon B cell antigen receptor stimulation through a cascade leading to c-myc/cdc25. *Immunity*, *9*(4), 439–448. http://doi.org/S1074-7613(00)80627-5 [pii]

Theodoratos, A., Wilson, L. O. W., Gosling, K. M., & Fahrer, A. M. (2012). Splice variants of the condensin II gene Ncaph2 include alternative reading frame translations of exon 1. *The FEBS Journal*, *279*(8), 1422–32. http://doi.org/10.1111/j.1742-4658.2012.08530.x

Therizols, P., Illingworth, R. S., Courilleau, C., Boyle, S., Wood, A. J., & Bickmore, W. A. (2014). Chromatin decondensation is sufficient to alter nuclear organization in embryonic stem cells. *Science*, *346*(6214), 1238–1242.

Thompson, S. L., & Compton, D. a. (2010). Proliferation of aneuploid human cells is limited by a p53-dependent mechanism. *The Journal of Cell Biology*, *188*(3), 369–81. http://doi.org/10.1083/jcb.200905057

Torres, E. M., Williams, B. R., & Amon, A. (2008). Aneuploidy: Cells losing their balance. *Genetics*, *179*(2), 737–746. http://doi.org/10.1534/genetics.108.090878

Tropberger, P., Pott, S., Keller, C., Kamieniarz-Gdula, K., Caron, M., Richter, F., … Schneider, R. (2013). Regulation of transcription through acetylation of H3K122 on the lateral surface of the histone octamer. *Cell*, *152*(4), 859–872.

http://doi.org/10.1016/j.cell.2013.01.032

Uemura, T., Ohkura, H., Adachi, Y., Morino, K., Shiozaki, K., & Yanagida, M. (1987). DNA Topoisomerase II Is Required for Condensation and Separation of Mitotic Chromosomes in S . pombe. *Cell*, *54*(6), 917–925.

Uhlmann, F., & Nasmyth, K. (1998). Cohesion between sister chromatids must be established during DNA replication. *Current Biology : CB*, *8*(20), 1095–1101. http://doi.org/10.1016/S0960-9822(98)70463-4

Vagnarelli, P., Hudson, D. F., Ribeiro, S. a, Trinkle-Mulcahy, L., Spence, J. M., Lai, F., … Earnshaw, W. C. (2006). Condensin and Repo-Man-PP1 co-operate in the regulation of chromosome architecture during mitosis. *Nature Cell Biology*, *8*(10), 1133–42. http://doi.org/10.1038/ncb1475

Vagnarelli, P., Morrison, C., Dodson, H., Sonoda, E., Takeda, S., & Earnshaw, W. C. (2004). Analysis of Scc1-deficient cells defines a key metaphase role of vertebrate cohesin in linking sister kinetochores. *EMBO Reports*, *5*(2), 167–171. http://doi.org/10.1038/sj.embor.7400077

Vagnarelli, P., Ribeiro, S., Sennels, L., Sanchez-Pulido, L., de Lima Alves, F., Verheyen, T., … Earnshaw, W. C. (2011). Repo-Man Coordinates Chromosomal Reorganization with Nuclear Envelope Reassembly during Mitotic Exit. *Developmental Cell*, *21*(2), 328–342. http://doi.org/10.1016/j.devcel.2011.06.020

van den Engh, G., Sachs, R., & Trask, B. J. (1992). Estimating genomic distance from DNA sequence location in cell nuclei by a random walk model. *Science (New York, N.Y.)*, *257*(5075), 1410–1412. http://doi.org/10.1126/science.1388286

Van Der Lugt, N. M. T., Domen, J., Linders, K., Van Roon, M., Robanus-Maandag, E., Te Riele, H., … Berns, A. (1994). Posterior transformation, neurological abnormalities, and severe hematopoietic defects in mice with a targeted deletion of the bmi-1 proto-oncogene. *Genes and Development*, *8*(7), 757–769. http://doi.org/10.1101/gad.8.7.757

Vitre, B., & Cleveland, D. W. (2012). Centrosomes, chromosome instability (CIN) and aneuploidy. *Current Opinion in Cell Biology*, *24*(6), 809–815. http://doi.org/10.1016/j.biotechadv.2011.08.021.Secreted

Vogelstein, B., Papadopoulos, N., Velculescu, V. E., Zhou, S., Diaz, L. a, & Kinzler, K. W. (2013). Cancer Genome Lanscapes. *Science*, *339*(6127), 1546–1558.

http://doi.org/10.1126/science.1235122.Cancer

Vrouwe, M. G., Elghalbzouri-Maghrani, E., Meijers, M., Schouten, P., Godthelp, B. C., Bhuiyan, Z. a., … Darroudi, F. (2007). Increased DNA damage sensitivity of Cornelia de Lange syndrome cells: Evidence for impaired recombinational repair. *Human Molecular Genetics*, *16*(12), 1478–1487. http://doi.org/10.1093/hmg/ddm098

Waizenegger, I. C., Hauf, S., Meinke, a, & Peters, J. M. (2000). Two distinct pathways remove mammalian cohesin from chromosome arms in prophase and from centromeres in anaphase. *Cell*, *103*(3), 399–410. http://doi.org/10.1016/S0092-8674(00)00132-X

Walczak, C. E., Cai, S., & Khodjakov, A. (2010). Mechanisms of chromosome behaviour during mitosis. *Nature Reviews. Molecular Cell Biology*, *11*(2), 91–102. http://doi.org/10.1038/nrm2832

Wang, J. C. (2002). Cellular roles of DNA topoisomerases: a molecular perspective. *Nature Reviews. Molecular Cell Biology*, *3*(6), 430–440. http://doi.org/10.1038/nrm831

Wang, X., Tang, O. W., Riley, E. P., & Rudner, D. Z. (2014). The SMC condensin complex is required for origin segregation in Bacillus subtilis. *Current Biology : CB*, *24*(3), 287–92. http://doi.org/10.1016/j.cub.2013.11.050

Watrin, E., Cubizolles, F., Osborne, H. B., Le Guellec, K., & Legagneux, V. (2003). Expression and functional dynamics of the XCAP-D2 condensin subunit in Xenopus laevis oocytes. *Journal of Biological Chemistry*, *278*(28), 25708–25715. http://doi.org/10.1074/jbc.M300192200

Weaver, B. A. A., Silk, A. D., Montagna, C., Verdier-Pinard, P., & Cleveland, D. W. (2007). Aneuploidy acts both oncogenically and as a tumor suppressor. *Cancer Cell*, *11*(1), 25–36. http://doi.org/10.1016/j.ccr.2006.12.003

Wertz, I. E., Kusam, S., Lam, C., Okamoto, T., Sandoval, W., Anderson, D. J., … Dixit, V. M. (2011). Sensitivity to antitubulin chemotherapeutics is regulated by MCL1 and FBW7. *Nature*, *471*(7336), 110–4. http://doi.org/10.1038/nature09779

Wijshake, T., Malureanu, L. a., Baker, D. J., Jeganathan, K. B., van de Sluis, B., & van Deursen, J. M. (2012). Reduced Life- and Healthspan in Mice Carrying a Mono-Allelic BubR1 MVA Mutation. *PLoS Genetics*, *8*(12).

http://doi.org/10.1371/journal.pgen.1003138

Wilkins, B. J., Rall, N. a, Ostwal, Y., Kruitwagen, T., Hiragami-Hamada, K., Winkler, M., … Neumann, H. (2014). A cascade of histone modifications induces chromatin condensation in mitosis. *Science (New York, N.Y.)*, *343*(6166), 77–80. http://doi.org/10.1126/science.1244508

Wognum, A. W., & Szilvassy, S. J. (2013). Hematopoietic Stem and Progenitor Cells. *Stemcell Technologies*, *5*(May), 1–8.

Wolfer, A., Wilson, A., Nemir, M., MacDonald, H. R., & Radtke, F. (2002). Inactivation of Notch1 impairs VDJ?? rearrangement and allows pre-TCR-independent survival of early ???? lineage thymocytes. *Immunity*, *16*(6), 869–879. http://doi.org/10.1016/S1074-7613(02)00330-8

Wood, A. J., Severson, A. F., & Meyer, B. J. (2010). Condensin and cohesin complexity: the expanding repertoire of functions. *Nature Reviews. Genetics*, *11*(6), 391–404. http://doi.org/10.1038/nrg2794

Wood, J. L., Liang, Y., Li, K., & Chen, J. (2008). Microcephalin/MCPH1 associates with the condensin II complex to function in homologous recombination repair. *Journal of Biological Chemistry*, *283*(43), 29586–29592. http://doi.org/10.1074/jbc.M804080200

Woodward, A. M., Göhler, T., Luciani, M. G., Oehlmann, M., Ge, X., Gartner, A., … Blow, J. J. (2006). Excess Mcm2-7 license dormant origins of replication that can be used under conditions of replicative stress. *Journal of Cell Biology*, *173*(5), 673–683. http://doi.org/10.1083/jcb.200602108

Worcel, A., & Burgi, E. (1972). On the structure of the folded chromosome of Escherichia coli. *J. Mol. Biol.*, *71*, 127–147.

Xu, Y., Ayrapetov, M. K., Xu, C., Gursoy-Yuzugullu, O., Hu, Y., & Price, B. D. (2012). Histone H2A.Z Controls a Critical Chromatin Remodeling Step Required for DNA Double-Strand Break Repair. *Molecular Cell*, *48*(5), 723–733. http://doi.org/10.1016/j.molcel.2012.09.026

Yamane, H., & Paul, W. E. (2012). Cytokines of the γc family control CD4+ T cell differentiation and function. *Nature Immunology*, *13*(11), 1037–1044. http://doi.org/10.1038/ni.2431

Yokoyama, Y., Zhu, H., Zhang, R., & Noma, K. (2015). A novel role for the condensin II complex in cellular senescence. *Cell Cycle*, (June), 00–00.

http://doi.org/10.1080/15384101.2015.1049778

Yu, F., Kuo, C. T., & Jan, Y. N. (2006). Drosophila Neuroblast Asymmetric Cell Division: Recent Advances and Implications for Stem Cell Biology. *Neuron*, *51*(1), 13–20. http://doi.org/10.1016/j.neuron.2006.06.016

Zachariae, W., Schwab, M., Nasmyth, K., & Seufert, W. (1998). Control of Cyclin Ubiquitination by CDK-Regulated Binding of Hct1 to the Anaphase Promoting Complex. *Science*, *282*(5394), 1721–1724. http://doi.org/10.1126/science.282.5394.1721

Zechiedrich, E. L., Khodursky, A. B., & Cozzarelli, N. R. (1997). Topoisomerase IV, not gyrase, decatenates products of site-specific recombination in Escherichia coli. *Genes and Development*, *11*(19), 2580–2592. http://doi.org/10.1101/gad.11.19.2580

Zhang, J., Socolovsky, M., Gross, A. W., & Lodish, H. F. (2003). Role of Ras signaling in erythroid differentiation of mouse fetal liver cells : functional analysis by a flow cytometry – based novel culture system. *Differentiation*, *102*(12), 3938–3946. http://doi.org/10.1182/blood-2003-05-1479.Supported

Zhou, B.-R., Jiang, J., Feng, H., Ghirlando, R., Xiao, T. S., & Bai, Y. (2015). Structural Mechanisms of Nucleosome Recognition by Linker Histones. *Molecular Cell*, *59*(4), 628–638. http://doi.org/10.1016/j.molcel.2015.06.025